Wind Field and Trajectory Models for Tornado-Propelled Objects

EPRI

EPRI NP-748
Project 308
Final Report
May 1978

Keywords:
Tornado
Wind Field Model
Missile Aerodynamics
Trajectory Model

Prepared by
California Institute of Technology
Pasadena, California
(JPL PUBLICATION 78-57)

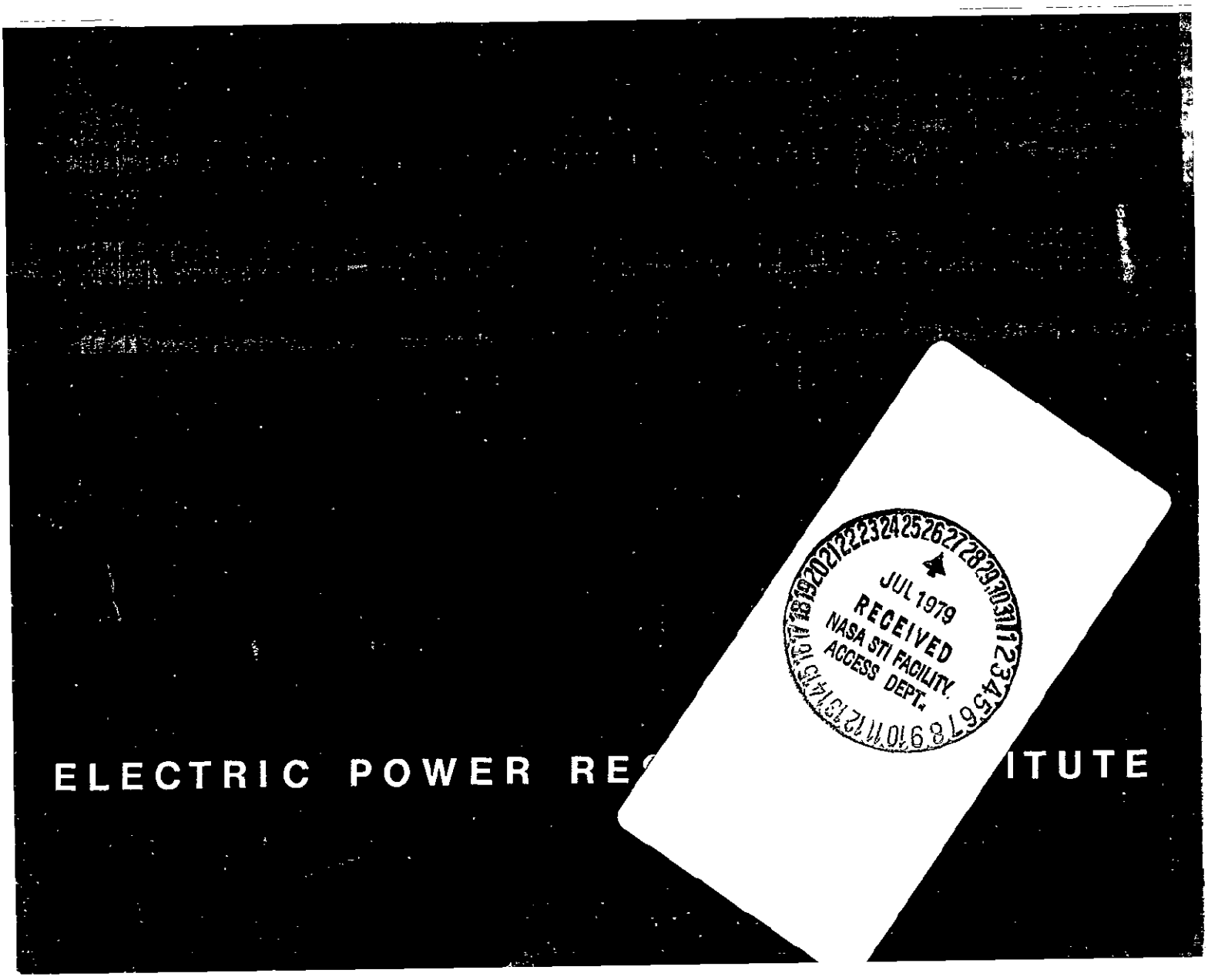

Wind Field and Trajectory Models for Tornado-Propelled Objects

NP-748
Research Project 308

Final Report 2, May 1978

Prepared by

Jet Propulsion Laboratory
CALIFORNIA INSTITUTE OF TECHNOLOGY
Pasadena, California

Principal Investigators
Gunther H. Redmann
John R. Radbill
Jack E Marte
Paul Dergarabedian
Francis E. Fendell

Prepared for

Electric Power Research Institute
3412 Hillview Avenue
Palo Alto, California 94304

EPRI Project Manager
George Sliter
Nuclear Power Division

EPRI PERSPECTIVE

The objective of this project is to provide a method to realistically predict the trajectories of tornado-generated missiles. This report contains the results of the second phase of the project which uses the "worst case" tornado defined in the initial phase, a theoretically consistent wind model, measured aerodynamic coefficients, and a six-degree-of-freedom trajectory code to compute maximum credible tornado-missile speeds. Of special importance are the results for postulated 12-inch-diameter-pipe and automobile missiles, which currently have the most influence on nuclear plant design. Because the aerodynamic coefficients for these missiles are based on full-scale wind-tunnel test data, the maximum speeds for these missiles presented in this report merit a high degree of confidence. In addition, three-degree-of-freedom coefficients were developed for use in simplified methods.

The next phase of the project will focus on the near-ground wind field and injection mechanisms to address the question of whether objects can become airborne. A user-oriented guide for applying the six-degree-of-freedom model in design will also be prepared.

The EPRI project manager, while the research in this report was being performed, was Conway Chan.

George Sliter
EPRI Project Manager

ABSTRACT

This report contains the results of the second phase of a research program which has as its objective the development of a mathematical model to predict the trajectory of tornado-borne objects postulated to be in the vicinity of nuclear power plants. An improved tornado wind field model satisfies the no-slip ground boundary condition of fluid mechanics and includes the functional dependence of eddy viscosity with altitude. Sub-scale wind tunnel data are obtained for all of the missiles currently specified for nuclear plant design. Confirmatory full-scale data are obtained for a 12-inch pipe and automobile. The original six-degree-of-freedom trajectory model is modified to include the improved wind field and increased capability as to body shapes and inertial characteristics that can be handled. The improved trajectory model is used to calculate maximum credible speeds, which for all of the heavy missiles are considerably less than those currently specified for design. Equivalent coefficients for use in three-degree-of-freedom models are developed and the sensitivity of range and speed to various trajectory parameters for the 12-inch diameter pipe is examined.

ACKNOWLEDGMENTS

Special acknowledgment is given to Anatol Roshko, Professor of Aeronautics, California Institute of Technology, for his suggestions in the development of coefficients and for reviewing the formulations in the near-ground wind field. Special acknowledgment is also given to George Carrier, Professor of Applied Mathematics, Harvard University, for his participation in formulating and analyzing the surface in-flow layer and turn-around region of the low-level tornado wind field.

Gunther Redmann*, John Radbill and Jack Marte are members of the technical staff of the Jet Propulsion Laboratory, Caltech. Paul Dergarabedian and Francis Fendell are members of the Technical staff at TRW systems, Redondo Beach, California, and are consultants to the project in tornado wind field definition.

*Mr. Redmann has left Caltech and is now a principal in the consulting firm of Botan and Redmann, Inc.

CONTENTS

CONTENTS (Cont'd)

CONTENTS (Cont'd)

CONTENTS (Cont'd)

FIGURES

FIGURES

FIGURES

CONTENTS (Cont'd)

FIGURES

TABLES

TABLES

TABLES

TABLES

TABLES

SUMMARY

The effects of the impact produced by postulated tornado-propelled objects continues to be a factor in the design of nuclear power plants. For this reason a research program was initiated to develop a mathematical model of the tornado wind field which had the capability of bounding, by means of verifiable experimental data, the impact characteristics of tornado-propelled objects potentially hazardous to nuclear power plants. This report describes the second phase of the program.

In Phase I of the program (Redmann, Radbill, Marte, Dergarabedian, and Fendell 1976)[1], the basic mathematical model for predicting six-degree-of-freedom (6 DOF) trajectories in the wind field of a tornado was developed; a worst-case tornado was defined and its associated wind field modelled; a survey of available aerodynamic data on potential missile configurations was conducted and, because of the lack of available data, wind tunnel tests of a cylindrical configuration were carried out. Significant areas requiring additional research were identified. In this Phase II of the program those areas have been addressed with the following results:

NEAR-GROUND TORNADO WIND FIELD ANALYSIS

The Phase I tornado wind field model was improved by the introduction of modifications that allow all velocity components to reach zero at the ground; the no-slip boundary condition of fluid mechanics is satisfied. The spatially constant eddy viscosity approximation used in Phase I has been replaced by eddy viscosity as an explicit function of altitude through a specified analytic form which permits assignment of two empirical parameters and a value at the ground. This functional dependence of eddy viscosity on altitude was derived on the basis of intuitively reasonable assumptions based on observed behavior. It is this form that is currently employed in the wind field model and the one which was used to obtain the trajectory results presented herein. Since it is ultimately desirable to avoid the inherently heuristic nature of this approach, a unified wall-layer defect layer eddy viscosity formulation is developed (Appendix A), in which the eddy viscosity becomes an explicit function of the velocity field and hence an implicit function of height above ground. Assigned parameters are

[1] Complete references are listed alphabetically at the end of each section.

then functions only of observed data for turbulent flow. Further analytical work is required before this more basic formulation can be incorporated into the wind field model and used to obtain trajectory results. An example of the modified velocity profiles are shown in Fig. 1-2.

TRAJECTORY MODEL

The original trajectory model was modified to include the improved wind field and the additional aerodynamic data. A new option was added to the model to permit treatment of non-cylindrical bodies with three perpendicular planes of symmetry as well as offset center of gravity and nonzero products-of-inertia. This allows modeling of beams and the approximate modeling of automobiles. Revisions were made to the code to enhance its portability so that the programs can be run on IBM370 and other machines as well as on the Univac 1108.

MISSILE AERODYNAMICS

Because of the lack of existing data on static aerodynamic coefficients extending over the complete range of configuration attitudes for shapes of interest to this project, sub-scale wind tunnel tests were conducted in the GALCIT[1] 10-ft Wind Tunnel to obtain this information. Data taken in free air and at various heights above a ground plane are presented in tabular form for the following shapes:[2,3]

1) A schedule-40, 12-in diameter by 15 ft long pipe (open-end right circular cylinder, length/diameter of 14.1).
2) A 1-in. diameter by 3-ft long reinforcement rod (closed-end right circular cylinder, length/diameter of 36.0).
3) A 4 x 12 x 144-in. wood plank (rectangular parallelepiped with overall dimensions in the ratio 1:3:36).
4) A nominal sedan-type automobile.
5) A nominal van-type truck.

---

[1] Graduate Aeronautical Laboratories, California Institute of Technology.

[2] Coefficients suitable for use for the 6-in pipe and utility pole configurations were obtained during Phase I of this project. See EPRI 308, Tech Rept 1, Feb. 1976.

[3] English units, traditional in tornado missile work, are used in most of this report. A table for conversion to SI metric units appears in Appendix F. Metric units will be used in subsequent reports of this program.

Because of the dependence of aerodynamic data for circular cylinders normal to the flow on Reynolds number, an additional test was conducted on a full-scale 12-in. diameter schedule-40 pipe in the Lockheed-Georgia Low Speed Wind Tunnel at supercritical and transitional Reynolds numbers. An example of the results of this test is shown in Figure 3-17. These data are presented in tabular form as well as in plotted form showing the effects of Reynolds number on some of the coefficients. Also shown in plotted form are the effects of the presence of the ground on the aerodynamic coefficients of the short cylinder which appear to be insignificant.

To confirm the subscale car test data, a full-scale automobile test series was run on a 1974 Dodge Dart in the 30-ft. by 30-ft. wind tunnel of the Low Speed Laboratory of the National Research Council, Ottawa, Canada. Tests were conducted in free air and in the vicinity of the ground, but were limited to rotation about the vertical axis. Although the full-scale and subscale configurations differed somewhat in shape and support conditions, the drag coefficient from both tests was essentially the same. The sizeable differences which were measured for the lift, side force and rolling moment coefficients did not lead to significant differences in the important auto trajectory parameters.

In an attempt to experimentally determine random tumbling coefficients for comparison with static coefficients from wind tunnel tests, a short series of drop tests from a building roof was conducted. The aerodynamic resistance of small, light-weight, freely falling, and tumbling models was obtained from motion pictures of the models during the equilibrium portion of the drops. For the 12-in. pipe model and the automobile, good agreement in terms of the flight parameter was obtained between these measurements and a method utilizing the static drag coefficients from the wind tunnel tests. In the case of the car, a value of 2.8 (referred to frontal area) was obtained for the tumbling drag coefficient.

The flight parameter (drag coefficient times its reference area divided by weight) for the automobile obtained by all of the testing in this program was

less than half of the value used in the flight trajectories of Simiu and Cordes 1976. (A lower value of the flight parameter indicates a poorer flight characteristic.)

APPLICATIONS OF TRAJECTORY MODEL

With a view toward determining more realistic initial conditions for use with the mathematical model, an analysis of missile injection has been made in terms of aerodynamic, ramp, and "explosive" modes. In the case of the aerodynamic injection mode, the commonly used approximation of a constant impulse force acting over an arbitrary effective time need no longer be employed since the mathematical model is capable of evaluating the time dependent integrals involved. Only the initial location and orientation of the missile has to be specified. No justification could be found for assuming high ramp velocities in the vicinity of a nuclear plant construction site, so this injection mode is not presented here. Explosive injection was found to have little effect on trajectories so it is also not included in detail. A consistent rationale for initial conditions and injection modes for each missile configuration was developed and used in the trajectories presented in this report. These sets of initial conditions represent logical possibilities rather than worst cases.

The tornado-generated missiles with initial conditions for the trajectory specified by the U.S. Nuclear Regulatory Commission (NRC) (NUREG 75/087) were also examined. Special consideration was given to the automobile because of the attention drawn to it by Simiu and Cordes 1976, as a potential critical missile configuration. Experimentally determined aerodynamic coefficients and realistic areas instead of conservative approximations to both quantities used by Simiu and Cordes lead to considerably reduced horizontal velocities. Comparison of maximum horizontal velocities for the automobile in the three regional design tornadoes, shown in Table 4-12, indicates that the velocities from a 6-DOF analysis are 54%, 38% and 15% of those of Simiu and Cordes, the reduction being greater for weaker tornadoes. Velocities using an equivalent 3-DOF approach were even smaller.

Similar comparisons of JPL 6-DOF maximum velocities for the remaining Spectrum II (NUREG 75/087) missiles with the 3-DOF results of Simiu and Cordes in Table 4-12 show that the JPL values are considerably less with the exception of the reinforcing bar where the results are identical for the two larger tornadoes. In general, the reduction is greatest for the weaker tornadoes.

The sensitivity of range and speed to various trajectory parameters was examined for the 12-in. dia. pipe because it appeared to be potentially the most important missile (with possible exception of the automobile). The maximum swirl velocity and the storm center translational speed produced the maximum sensitivity whereas the sensitivites to storm eye radius were small for eyes greater than 0.1 mile. The range was particularly sensitive (it varied by a factor of 4) to injection location relative to the storm center and its direction of travel. Examination of sensitivity to sub and supercritical Reynolds number aerodynamic data indicated that the subcritical aerodynamic assumption is conservative. All cylindrical missiles but the reinforcing bar are supercritical over most of their trajectories. Thus, supercritical coefficients were used for all cylindrical configurations with the exception of the reinforcement rod.

Derivation of "tumbling coefficients" for 3-DOF trajectory computations by computing average values of drag coefficient from 6-DOF trajectories was examined based on the assumption that each missile configuration has a quasi-stable orientation relative to the wind which is approximately independent of initial conditions. Range and speed for a typical pair of 6-DOF and 3-DOF trajectories for the car missile differ by about 20%. The tumbling coefficients derived for the 12-in. pipe missile agree well with values derived from model drop tests.

REFERENCES

Redmann, G. H., Radbill, J. R., Marte, J. E., Degarabedian, P. and Fendell, F. E., Feb. 1976, Wind Field and Trajectory Models for Tornado-Propelled Objects, EPRI 308, TR-1 Electric Power Research Institute, Palo Alto, California.

Simiu, E. and Cordes, M., April 1976, Tornado-Borne Missile Speeds, NBSIR 76-1050, United States Nuclear Regulatory Commission, Washington, D.C.

Nuclear Regulatory Commission Standard Review Plan, Rev. 1 (NUREG-75/087), Nov. 24, 1975.

SECTION I

NEAR-GROUND TORNADO WIND FIELD ANALYSIS

A. INTRODUCTION

Improvements are introduced for the tornado wind field model as described by Redmann et al., 1976.* Specifically, modifications are introduced which allow all velocity components to go to zero at the ground (z=0). These modifications also lead to a set of equations whose parameters can be varied in a consistent way to match any new improved field data if and when available. The eddy viscosity, ν, which was fixed at a constant value, is now treated as a function of altitude above the ground and the resulting analytical form for ν includes two parameters which can be varied. The resulting forms for the velocity components u (radial), v (azimuthal), and w (axial) are presented in Section I-B. The major shortcoming of this approach is in the heuristic nature of selecting an eddy viscosity behavior which appears to be in reasonable agreement with observed behavior. Finally, in Section I-C and Appendix A, a fully unified theory is presented which will be more fully developed in Phase III, in which this shortcoming is overcome by allowing the eddy viscosity to become an explicit function of the velocity field and hence an implicit function of distance above the ground. The parameters, in this approach, are a function of observed data for turbulent flow. Further analytical work remains to be done in order to use the results of Section I-C to define the wind field model. Thus the results of Section I-B represent the current wind field model as used in this study to determine the behavior of tornado-generated missiles.

B. IMPROVED NEAR-GROUND TORNADO WIND FIELD MODEL

In Redmann et al., 1976, equations (2-8) and (2-9) were derived for the azimuthal and radial velocity components as

$$rv = \Psi \left[1 - \exp\left(- \sqrt{\frac{5\Omega}{3\nu}}\,(z + 270)\right)\right]$$

*Complete references are listed alphabetically at the end of each section.

and

$$ru = -\Psi \left\{ 1 - \left[1 - \exp\left(- \sqrt{\frac{5\Omega}{3\nu}} \; (z + 270) \right) \right]^2 \right\}^{1/2}$$

These results are consistent with the constraint that

$$\Psi^2 \equiv r^2 V^2 = r^2 u^2 + r^2 v^2$$

where V is the azimuthal or swirl velocity far removed from the ground boundary, that is, $V = v(\infty)$. Now the normal form for the velocity v should be

$$rv = \Psi \left[1 - \exp\left(- \sqrt{\frac{5\Omega}{3\nu}} \; z \right) \right] .$$

which correctly predicts zero velocity at ground level. However, with the value of $\nu = 1$ ft^2/sec for the eddy viscosity adopted in the Phase I work, the decrement in v from its asymptotic value V is much too large at rather larger distances from the ground. For purposes of modifying the equations to match observed data that $u \approx v/2$ near the ground, a value of 270 feet was added to z in the equations. This meant that u and v are not zero at $z = 0$. This is not physically reasonable; however, it does approximate the real-world situation of large velocities within a few feet of the ground. Since a constant eddy viscosity is being used in essentially the laminar differential equations of motion, the effect of introducing the 270 feet added to z is to have an eddy viscosity which is large at large z but becomes zero at $z = 0$. The resulting expression for $\nu(z)$ is

$$\nu(z) = \nu_\infty \left(\frac{z}{z + 270} \right)^2$$

The relatively large value for ν_∞ of 1 ft^2/sec is smaller than the value of approximately 50 ft^2/sec which is used for general atmospheric turbulence (though much larger than the laminar value, $\nu_{lam} = 1.7 \times 1.0^{-4}$ ft^2/sec); it is felt that the well-organized, rapidly rotating, flow in a tornado system could well suppress vertical momentum transport by turbulent diffusion.

In the present discussion a modification is proposed which permits the eddy viscosity to approach and equal the laminar value for air as $z \to 0$, together with suitable modifications to the expressions for u and v.

The following expression is proposed for $\nu(z)$:

$$\nu(z) = \nu_\infty \left[\frac{z}{(z + 270)\left(1 - e^{-z/\alpha}\right)} \right]^2$$

where α is a scale height with dimensions of ft.

This expression has the following behavior:

$$\nu \rightarrow \begin{cases} \nu_\infty, & z \rightarrow \infty \\ \nu_\infty \left(\frac{\alpha}{270}\right)^2, & z \rightarrow 0 \end{cases}$$

Thus if we want $\nu_\infty = 1$ ft^2/sec and $\nu(0) = \nu_{lam}$ ($=1.7 \times 10^{-4}$ ft^2/sec), then we have $\alpha = 3.5$ feet.

Figure 1-1 is a plot of the expression for $\nu(z)/\nu_\infty$ for the case of flow past a smooth surface at $z = 0$. The behavior of the curve is such that $\nu(z) \approx \nu_{lam}$ up to a height on the order of 3 ft, then increases approximately linearly up to a height of the order of about 300 feet, and then asymptotically approaches the value of $\nu_\infty = 1$ ft^2/sec as z increases above 300 feet. Of course, the actual values result from the particular choices for the constants (i. e., $\nu_\infty = 1$ ft^2/sec).

This development employs the fluid mechanical equations of laminar theory in which ν_{lam} is replaced by an eddy viscosity. A more general form for $\nu(z)$ can be expressed as

$$\nu(z) = \nu_\infty \left[\frac{z}{(z + \beta)\left(1 - e^{-z/\alpha}\right)} \right]^2$$

where β is a second scale height (ft) where, instead of particular values for α, β, and ν_∞, other values can be used. Thus, instead of the nominal values of $\nu_\infty = 1$ ft^2/sec, $\beta = 270$, and $\nu(0) = \nu_{lam} = 1.7 \times 10^{-4}$ ft^2/sec, leading to $\alpha = 3.5$, one can pick other values. Thus for a rough surface $\nu(0)$ may have a higher value. Also different values for β will increase or lower the "knee" of the curve for $\nu(z)$, etc. At this point, it is not possible to give reasonable

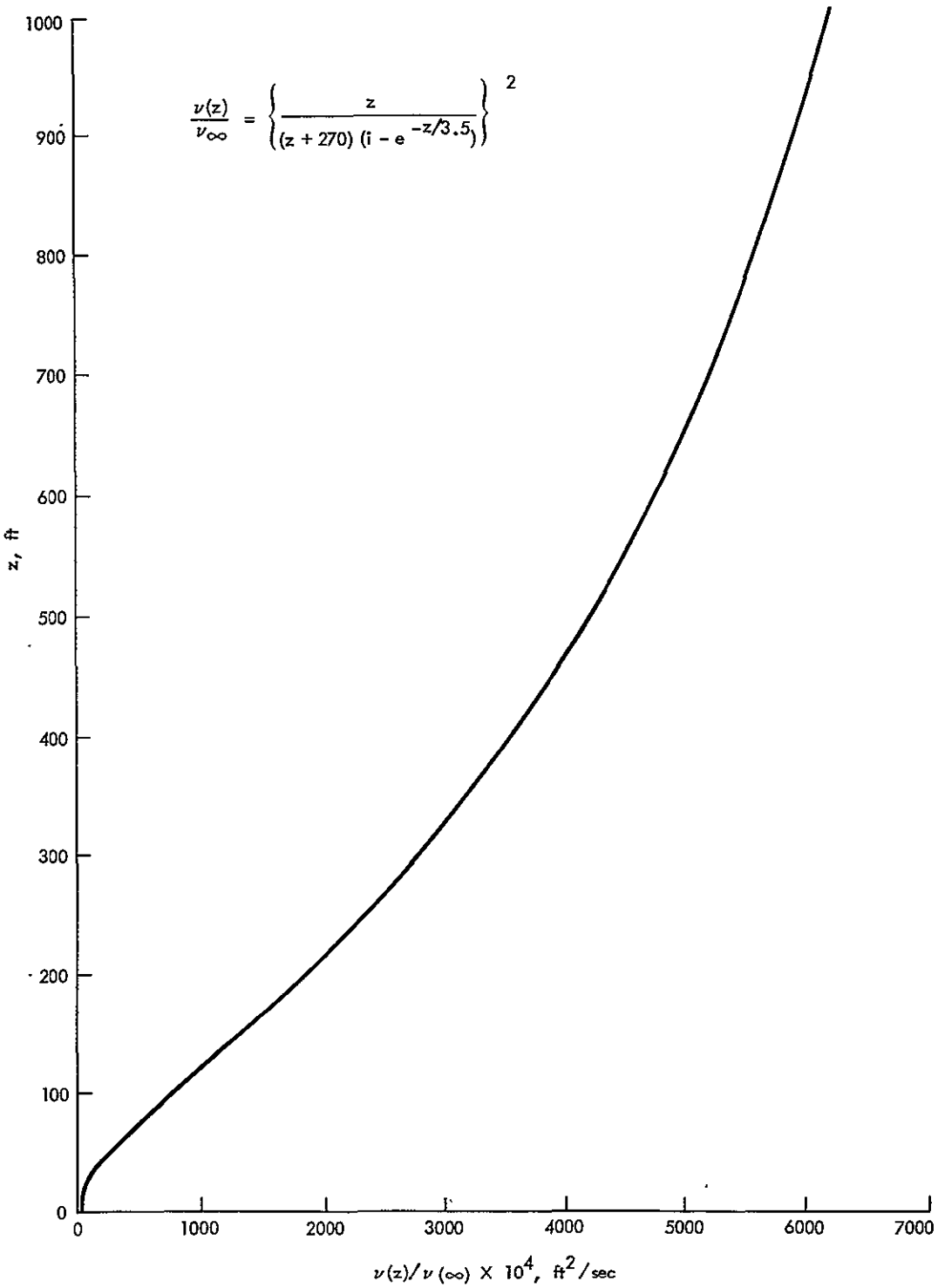

Figure 1-1. Plot of functional dependence of eddy viscosity with height

bounds for these parameters, but the formulas are general enough to vary the values. Field data on well-tracked tornados will be obtained during Phase III and should be of use in fixing more realistic values for these parameters.

As discussed in Redmann, et al., 1976, the layer nearest the ground up to an elevation of the order of 1,000 ft represents the "inertial" boundary layer within which $V^2 \approx u^2 + v^2$ down to within a few feet from the ground where frictional effects predominate. At the ground, all velocity components go to zero. In the intermediate region the behavior of $u^2 + v^2$ can be described as follows:

$$u^2 + v^2 = v^m V^n$$

where $m + n = 2$, $0 < m < 2$, and $n > 0$ such that

$$u^2 + v^2 \to V^2 \quad \text{as } z \to \infty \text{ (i.e., 1000 ft)}$$

and

$$u^2 + v^2 \to 0 \quad \text{as } z \to 0$$

For the present, the following behavior is postulated:

$$u^2 + v^2 = vV \text{—(i.e., } m = n = 1)$$

As the elevation increases $vV \to V^2$ quite rapidly, the exact elevation at which equality occurs depends on the choice of the other parameters. Also, $u^2 + v^2 \to 0$ as $z \to 0$; thus, both boundary conditions are satisfied. The choice, $m = n = 1$ is the simplest satisfying the relationship, $m + n = 2$ and, although a heuristically reasoned choice, there is some physical evidence, discussed later in the section, to support it. This behavior will be examined during Phase III in a more rigorous fashion. The general form for v to be used in Phase II is

$$rv = \Psi F(z)$$

where

$$F(z) \equiv \left[1 - \exp\left(- \sqrt{\frac{5\Omega}{3\nu}} (z+\beta) (1 - e^{-z/\alpha}) \right) \right]$$

and, since Ψ has been defined as equal to r^2v^2, and $u^2 + v^2 = vV$,

$$ru = -\Psi \left\{ F(z) - (F(z))^2 \right\}^{1/2}$$

or

$$r^2u^2 + r^2v^2 = \Psi^2 F(z)$$

where

$$F(z) \to 1, \quad z \to \infty$$

$$F(z) \to 0, \quad z \to 0$$

The interesting behavior to observe is that with no viscous effects (i. e., $\nu = 0$), the radial velocity component, u, and hence the axial velocity component, w, both go to zero and we have only v by the cyclostrophic balance. As ν increases, v decays near the ground, resulting in an increase in u and hence w.

To determine the axial (or vertical updraft) velocity component, w, we utilize the continuity equation

$$rw_z + (ru)_r = 0$$

Since

$$ru = -\Psi \left\{ F(z) - (F(z))^2 \right\}^{1/2}$$

we have from continuity,

$$w_z = \frac{\Psi_r}{r} \left\{ F(z) - (F(z))^2 \right\}^{1/2}$$

or

$$w(r, z) = \frac{\Psi_r}{r} \int_0^z \left\{ F(x) - (F(x))^2 \right\}^{1/2} dx$$

In order to obtain a simple closed-form solution for w, we break up the expression $\left(1 - e^{-z/\alpha}\right)$ in F(z) into two relationships, one valid for $z/\alpha \ll 1$

and one valid for $z/\alpha \gg 1$. We then use the appropriate relationship for the regions $0 \leq z/\alpha \leq 1$ and $1 \leq z/\alpha$, respectively. We note that

$$\left(1 - e^{-z/\alpha}\right) \rightarrow 1, \text{ as } z/\alpha \rightarrow \infty$$

and

$$\left(1 - e^{-z/\alpha}\right) \rightarrow z/\alpha, \text{ as } z/\alpha \rightarrow 0$$

Thus if we introduce the following definitions

$$Z \equiv \frac{z}{\alpha}, \qquad \gamma \equiv \sqrt{\frac{5\Omega}{3\nu}}, \quad \alpha\gamma \equiv \delta$$

and $\beta/\alpha \equiv K$, the result is that (since $\beta/\alpha \gg Z$ for $Z \leq 1$)

$$F(Z) \approx 1 - e^{-\delta K Z}, \text{ for } Z \leq 1$$

and

$$F(Z) \approx 1 - e^{-\delta(Z+K)}, \text{ for } Z \geq 1$$

Hence we have (using the continuity equation)

$$w(r, Z) = \frac{\Psi_r}{r} \int_0^Z \left\{F(x) - (F(x))^2\right\}^{1/2} dx$$

$$= \frac{\Psi_r}{r} \int_0^Z \left\{e^{-\delta K x} - e^{-2\delta K x}\right\}^{1/2} dx$$

for $Z \leq 1$, and

$$w(r, Z) = \frac{\Psi_r}{r}\left[\int_0^1 \left\{e^{-\delta K x} - e^{-2\delta K x}\right\}^{1/2} dx + \int_1^Z \left\{e^{-\delta(K+x)} - e^{-2\delta(K+x)}\right\}^{1/2} dx\right]$$

for $Z \geq 1$.

Integrating these results, we have

$$w(r,z) = \frac{4\alpha\ r_0^2 \nu\gamma}{5\beta\ r_1^2} \left\{ \frac{\pi}{4} - \left[e^{-\gamma\beta z/\alpha} - e^{-2\gamma\beta z/\alpha} \right]^{1/2} \right.$$

$$\left. - \frac{1}{2} \sin^{-1} \left[2e^{-\gamma\beta z/\alpha} - 1 \right] \right\}, \qquad \text{(I-1)}$$

for $z \leq \alpha$, $0 \leq r \leq r_1$, and

$$w(r, z) = w_1(r, \alpha) + \frac{4\alpha\ r_0^2 \nu\gamma}{5\beta\ r_1^2} \left\{ \left[e^{-\gamma(\alpha+\beta)} - e^{-2\gamma(\alpha+\beta)} \right]^{1/2} \right.$$

$$+ \frac{1}{2} \sin^{-1} \left(2e^{-\gamma(\alpha+\beta)} - 1\right)$$

$$- \left[e^{-\gamma(z+\beta)} + e^{-2\gamma(z+\beta)} \right]^{1/2}$$

$$\left. - \frac{1}{2} \sin^{-1} \left(2e^{-\gamma(z+\beta)} - 1\right) \right\}, \qquad \text{(I-2)}$$

for $z \geq \alpha$, $0 \leq r \leq r_1$. (Note that $w_1(r, \alpha)$ is calculated from $w(r, z)$ using the form $w(r, z)$ valid in the region $z \leq \alpha$).

Recall that the nominal values for α and β are $\alpha = 3.5$ feet and $\beta = 270$ feet; with these values $w_1(r, \alpha)$ is quite small. Also, since $\beta >> \alpha$ will almost always be the case, the results obtained with $\alpha = 0$ in the expression for $w(r, z)$ are sufficiently accurate. However, the more general expression can be used for more general results with greater accuracy.

Using the approximations for $(1-e^{-z/\alpha})$ given above, the expressions for $\nu(z)$ are given by

$$\nu(z) \approx \nu_\infty \left[\frac{\alpha}{z+\beta}\right]^2, \quad z \leq \alpha$$

$$\approx \nu_\infty \left[\frac{z}{z+\beta}\right]^2, \quad z \geq \alpha$$

which produce numerical values close to those obtained from the original expression for $\nu(z)$ (which holds over the entire z domain) given by

$$\nu(z) = \nu_\infty \left[\frac{z}{(z+\beta)(1-e^{-z/\alpha})}\right]^2$$

Thus, in summary, the three velocity components are given by

$$rv = \dot{\Psi}\left[1 - \exp\left(-\sqrt{\frac{5\Omega}{3\nu}}\,(z+\beta)(1-e^{-z/\alpha})\right)\right]$$

$$= \Psi F(z)$$

$$ru = -\Psi \left\{F(z) - (F(z))^2\right\}^{1/2}$$

and w is given by the forms derived above (Eqs. I-1 and I-2).

Figure 1-2 shows a plot of u and v with $\beta = 270$ ft and $\alpha = 3.5$ ft. It can be observed that $u = v = 225/2 = 112.5$ ft/sec at $z \approx 1.3$ ft. Recall that in the expression

$$u^2 + v^2 = v^m V^n$$

we selected $m = n = 1$. This yields the result $u \approx v \approx V/2$, near the ground. Observed photos of some waterspouts indicate spiral paths intercepting concentric circles about the axis of the waterspout at about 45°: hence these values seem about right. For values of $m < 1$, u would have higher values near $z = 0$; hence, the intercept angle would tend to be larger. While it is difficult,

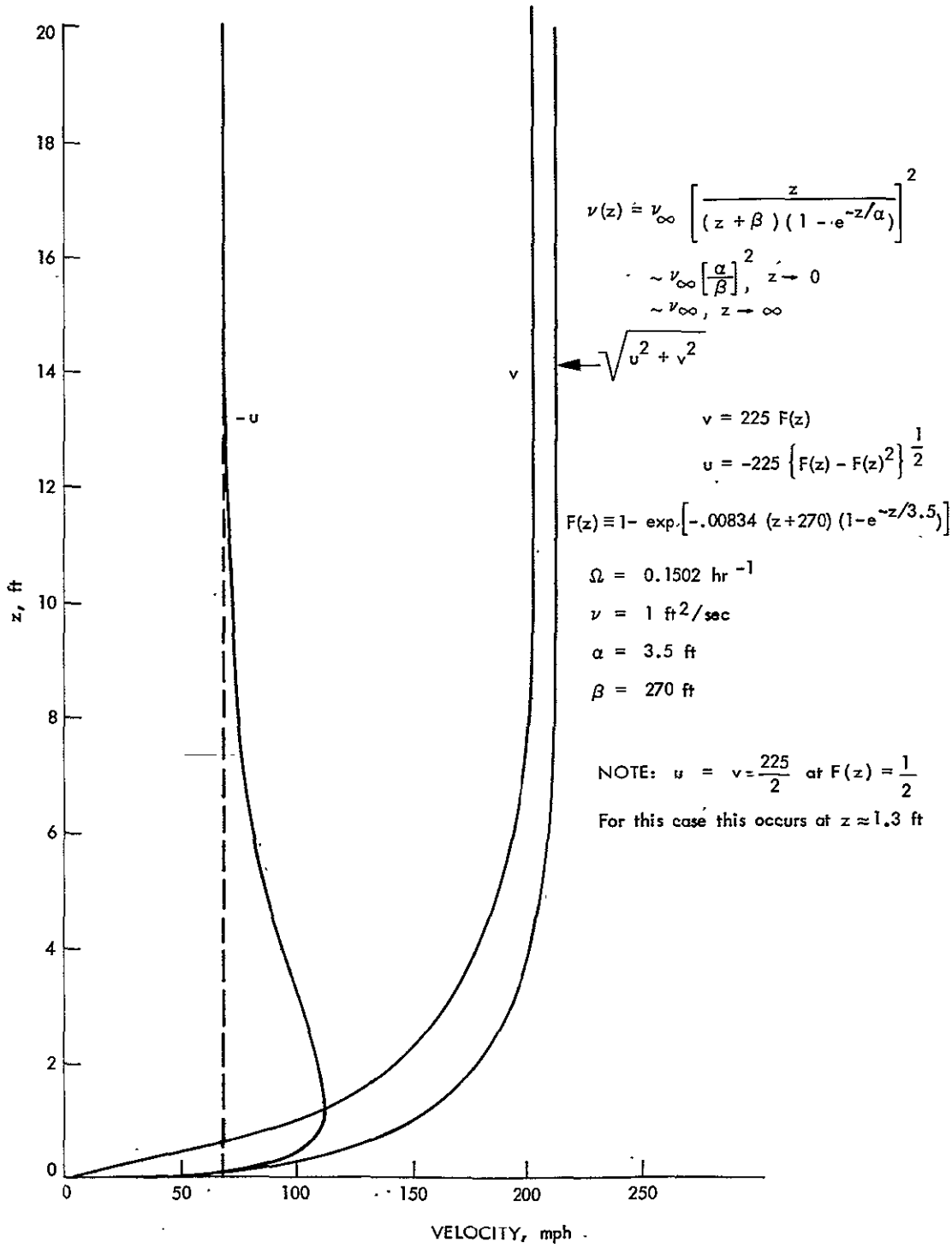

Figure 1-2. Velocity profiles at r = 0.1 mile for radial (u) and azimuthal (v) components

at this time, to pinpoint the correct value for m, the choice of m = 1 looks reasonable. Again, the examination of the physical tornado data planned for Phase III of this program may provide a firmer basis for the evaluation of this parameter.

In part C of this section, which follows, a more rigorous approach is discussed which should lead to a wind field model that is consistent both physically and analytically with the level of knowledge of turbulent rotating flow above a fixed boundry.

C. UNIFIED THEORY OF EDDY VISCOSITY FORMULATION

The results of the heuristic model just discussed utilized a modification of the behavior of the eddy viscosity $\bar{\nu}(z)$ in order to cause all velocity components to go to zero at the ground and to adjust the magnitude and height above the ground for which the radial velocity component is a maximum. This adjustment was based on observed data (Dinwiddle, 1959). The formulation discussed in this section and the analysis in Appendix A paragraph E for a spatially varying eddy viscosity do not rely on the use of such observations to obtain the analytical results. However, the reliability of both approaches would benefit from the availability of more observational data. Such data will be sought during Phase III of this project.

Plots of the resulting velocity field derived from the analysis show similar behavior to the results in Section II (see Figures 2-1, 2-2, and 2-3). Departing from the definition of the previous sections the total viscosity is taken as

$$\nu = \nu_m + \nu_e$$

where ν_m is the molecular viscosity and ν_e is the eddy viscosity taken as

$$\nu_e = \begin{cases} k_1 z^2 \left(u_z^2 + v_z^2\right)^{1/2} & , \text{ in the wall layer}^1 \\ k_2 V \delta^* & , \text{ in the defect layer} \end{cases}$$

(u_z and v_z are partial derivatives with respect to z) where δ^* is the displacement thickness defined as

$$V\delta^* = \int_0^\infty (V - v)\, dz$$

and k_1 and k_2 are physical constants described in Appendix A. The value for V is taken at or near the maximum swirl-velocity point (i. e., $r \approx r_1$) where $V = V_{max} \approx 225$ mph. The relationships for $\nu = \nu_m + \nu_e$ are then incorporated in the equations of motion together with the continuity equation and suitable boundary conditions. Incompressible axisymmetric flow is assumed as in Section I. B. By introduction of self-similar forms for u, v and w, the system of equations is transformed from parabolic partial differential equations to ordinary differential equations.

The resulting formulation, although requiring numerical analysis, is far more tractable than the original set of equations with variable ν. It is believed that with further effort the results of Appendix A will lead to a satisfactory description of the tornado wind field which is suitable for engineering application. In particular, the evaluation of field data from actual tornados during Phase III may produce information bearing on the near-ground velocity components which will add significantly to the usefulness of the refined analysis.

---

[1] The boundary layer under an intense vortex is discussed in detail in sections D and F of Appendix A and shown schematically in Figure A-12. Briefly, the wall layer (also termed the viscous sublayer) is that part of the flow adjacent to the ground in which the turbulence is damped and the laminar viscosity of the medium plays a significant role in shaping the variation of horizontal velocity with height. The defect layer is that part of the flow between the wall layer and free stream in which the horizontal component of velocity is less than its local free stream value.

D. REFERENCES

Dinwiddle, Frank B., 1959, "Waterspout-Tornado Structure and Behavior at Nags Head, North Carolina, August Twelfth, 1952", Monthly Weather Review, Vol. 87, pp 239-250.

Redmann, G.H., Radbill, J.R., Jr., Marte, J.E., Dergarabedian, P., and Fendell, R.E., Feb. 1976, Wind Field and Trajectory Models for Tornado-Propelled Objects, EPRI 308, T. R. 1, Electric Power Research Institute, Palo Alto, California.

E. NOMENCLATURE FOR SECTION I

K	. . . .	$\equiv \beta/\alpha$
k_1	. . . .	square of von Karman constant or $(0.41)^2$; see Appendix A.
k_2	. . . .	Clauser constant or (0.016); see Appendix A.
r	. . . .	radius from center of the tornado.
u	. . . .	radial velocity component of tornado
V	. . . .	azimuthal velocity far from ground
v	. . . .	azimuthal velocity component of tornado
w	. . . .	axial velocity component of tornado
x	. . . .	dummy variable
z	. . . .	height above ground
Z	. . . .	$\equiv z/\alpha$
α	. . . .	scale height
β	. . . .	scale height
γ	. . . .	$\equiv\sqrt{\frac{5\Omega}{3\nu}}$
δ	. . . .	$\equiv \alpha\gamma$
δ^*	. . . .	displacement thickness, $\frac{1}{V}\int_0^\infty (V-v)dz$
ν	. . . .	eddy viscosity
ψ	. . . .	rotational velocity of the tornado
Ω	. . . .	component of the earth's rotational velocity at the edge of the tornado-cyclone ($r = r_0 \simeq 10$ mi.)

Subscripts

o . . . . outer limit of tornado-cyclone

1 . . . . point at which V is a maximum

e . . . . subscript to ν; $\nu_e \equiv$ molecular viscosity

m . . . . subscript to ν; $\nu_m \equiv$ molecular viscosity

∞ . . . . far from ground

SECTION II

TRAJECTORY MODEL

A. INTRODUCTION

This section describes a mathematical model of the inter-related physical processes which govern the flight of tornado-propelled missiles. Some important features of the computer program which implements the model are also described in this section. The model consists of three major parts: first, a tornado wind field, second, missile aerodynamics, and third, missile dynamics.

The model and the associated computer program have a number of features which make them superior to previously published models. These features include: 1) a six degree-of-freedom (6 DOF) simulation of motion, 2) a realistic, physically self consistent near-ground wind field, 3) experimentally derived aerodynamic coefficients for all pitch and yaw angles, 4) theoretically derived rate damping coefficients, 5) a moment of inertia matrix including product of inertia terms with provision for building up the missile from up to ten separate parts, 6) an integration program that changes its order and step size to maintain accuracy at minimum computational cost.

This model's primary improvement over previous models in the literature is in treating the missile motion as having six-degrees-of-freedom rather than three. That is, translation in three directions and rotation about three axes are modeled. Previous studies in this area considered either worst-case drag with the largest area of the missile presented to the relative wind or experimentally unverified "random tumbling" using some empirical weighted average of the drag on all the faces (Lee 1973, 1974 and Iotti 1974). The tumbling of even high aspect ratio missiles is thereby approximated by a probability distribution that is a uniform function of angle. In fact certain orientations are more probable than others in configurations of this type because of the variation of aerodynamic moment with angle. Thus, the average drag is likely to be

somewhere between the worst case and uniform distribution random values. Lift forces cause a more important departure between six-degree-of-freedom and three-degree-of-freedom models since missiles with favorable initial orientation can climb in a 6 DOF model whereas those in a 3-DOF model must always fall unless the drag force due to the vertical relative velocity is sufficiently high to overcome the gravitational force. Six degree-of-freedom trajectories are compared with "equivalent" three-degree-of-freedom trajectories in Section IV below. A method is described there for obtaining average drag coefficients which account for the missile dynamics.

The model and associated computer program (Fortran V) have been written so that all computations are carried out in terms of dimensionless variables and dimensionless groups of reference constants. The nondimensionalization is carried out in order that the computations have consistent units, the variables are scaled for improved computational accuracy, the presentation of results is condensed, and, most importantly, intermediate computations are more easily scanned for errors in checking out the programs.

There are two separate length scales in the tornado-carried missile problem when the orientation of the missile is explicitly followed: the first is associated with the size of the tornado, the eye radius r_1, and the second is associated with the size of the missile, the length of its largest dimension, L.

Let dimensionless quantities be denoted by a bar, for example, $\bar{x}$, and dimensional quantities by the symbol without the bar. Then the components of the position vector of the missile become

$$\bar{x} = x/r_1, \qquad \bar{y} = y/r_1, \qquad \bar{z} = z/r_1$$

The components of the velocity vector are divided by the maximum tangential velocity of the tornado, V_{max}, so that

$$\bar{u} = u/V_{max}, \qquad \bar{v} = v/V_{max}, \qquad \bar{w} = w/V_{max}$$

All forces are divided by the weight of the missile, W.

B. DESCRIPTION OF MODEL

1. Wind Field

The near-ground tornado wind field derived in Section II serves as the driving function for the missile trajectory simulation and thus forms a very important link in the chain of processes drawn from different disciplines which comprises the solution.

The improved near-ground wind field model described in Section I B is used in the trajectory model of this report. The formulas of that section are rewritten here in the form used in the current model which differs from the model used in Redmann et al 1976.

The wind velocity vector, $\vec{v}_w$, for the stationary tornado will be presented in this and the succeeding subsections in terms of radial, azimuthal and vertical components with unit vectors $\vec{u}_r$, $\vec{u}_\theta$, and $\vec{u}_z$ respectively.

$$\vec{v}_w = \begin{cases} \hat{u}(\bar{z})\,\bar{r}\,\vec{u}_r + \hat{v}(\bar{z})\,\bar{r}\,\vec{u}_\theta + \bar{w}(\bar{z})\,\vec{u}_z, & \bar{r} \le 1 \\ \hat{u}(\bar{z})\Psi(\bar{r})\,\vec{u}_r + \hat{v}(\bar{z})\Psi(\bar{r})\,\vec{u} + \bar{w}(\bar{z})\,\vec{u}_z, & 1 < \bar{r} \le \bar{r}_0 \\ 0, & \end{cases}$$

$$\Psi(\bar{r}) = \left(\left(\bar{r}_0^2 - \bar{r}^2\right)\Big/\left(\bar{r}_0^2 - 1\right)\right)^{1/2}\Big/\bar{r}\,, \qquad \bar{r}_o < \bar{r} \qquad \text{(II-1)}$$

The dimensionless outer radius of the storm, $\bar{r}_0$, is

$$\bar{r}_0 = r_0/r_1 = (1.5V_{max}/\Omega r_1)^{1/2}$$

where the local vorticity is given by

$$\Omega = \Omega_e \sin\phi$$

in terms of the earth's rotation Ω_e and latitude ϕ.

The z-dependent factors in the velocity components are

$$\hat{v}(p(\bar{z})) = 1 - \exp(-\bar{\gamma}\, p(\bar{z}))$$
$$\hat{u}(p(\bar{z})) = -(\exp(-\bar{\gamma}\, p(\bar{z}))\, \hat{v}(\bar{z}))^{1/2} \qquad \text{(II-2)}$$

where

$$p(\bar{z}) = (\bar{z} + \bar{\beta})(1 - \exp(-\bar{z}/\bar{\alpha}))$$

and

$$w(\bar{z}) = \begin{cases} (\hat{w}(p_L(\bar{z})) + \pi/(4\bar{\gamma}))\bar{\alpha}/\bar{\beta}\,, & \bar{z} < \bar{\alpha} \\ \hat{w}(p_H(\bar{z})) = \hat{w}(p_H(\bar{\alpha})) + w(\bar{\alpha})\,, & \bar{\alpha} < \bar{z} \end{cases} \qquad \text{(II-3)}$$

where

$$p_L(\bar{z}) = \bar{\beta}\,\bar{z}/\bar{\alpha}$$

$$p_H(\bar{z}) = \bar{z} + \bar{\beta}$$

$$\hat{w}(p(\bar{z})) \equiv (\hat{u}(p(\bar{z})) = \sin^{-1}(\exp(-\bar{\gamma}\, p(\bar{z})) - \hat{v}(p(\bar{z})))/\bar{\gamma}$$

and $p(\bar{z})$ is either $p_L(\bar{z})$ or $p_H(\bar{z})$.

The vertical scale is controlled by

$$\bar{\gamma} \equiv \gamma/r_1 = (5\,\Omega/3\nu_0)^{1/2} \Big/ r_1 \quad \text{and} \quad \bar{\beta} = \beta/r_1$$

In the improved model, ν_o, α, and β are input parameters whereas they were fixed in the previous model. However, values of 1, 3.5 and 270 respectively are provided in the computer program if no values are input. Sample profiles of velocity components u, v, and w are shown in Fig. 2-1 at $\bar{r} = 0.5$, 1., and 1.5 for the above values of the parameters. For purposes of comparison

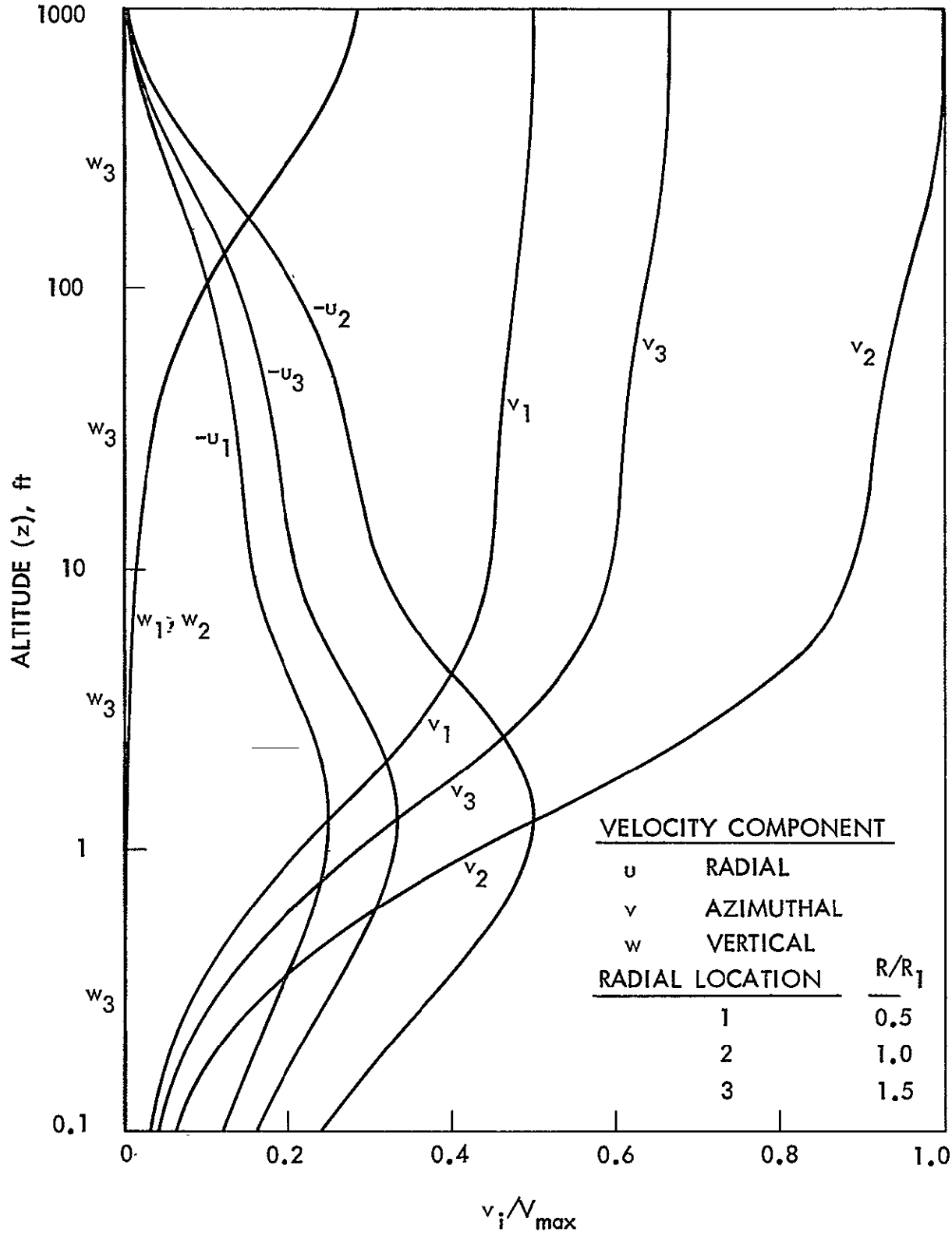

Fig. 2-1. Functional dependence of velocity components with altitude at three radial locations for $\nu_o = 1\ ft^2/sec$, $\alpha = 3.5$, and $\beta = 270$

Figs. 2-2 and 2-3 show results of dividing both α and β by factors of 10 and 100 respectively, to indicate the sensitivity of the profiles to these parameters.

The foregoing model describes the wind fields of stationary symmetric storms. The velocity of the storm center $\vec{v}_{tc}$ is added to the velocity of the stationary storm $\vec{v}_s$, after the latter is transformed to rectangular coordinates (inertial). In order to be consistent with the revised heuristic model, the velocity of the storm center must go to zero at the ground in the same manner. That is, $\vec{v}_{tc}$ is multiplied by the low level approximation to $\hat{v}(P_L(\bar{z}))$

$$\hat{v}(P_L(\bar{z})) = 1 - \exp(\bar{\beta}\,\bar{\gamma}\,\bar{z}/\bar{\alpha})$$

If the angle between the radius from the storm center to the missile location and the positive x-axis is δ, the components, in inertial rectangular coordinates, of the moving storm wind field $\vec{v}_w$ are

$$\begin{aligned} v_{w_1} &= v_{s_1} \cos\delta - v_{s_2} \sin\delta + v_{tc_1} \\ v_{w_2} &= v_{s_1} \sin\delta + v_{s_2} \cos\delta + v_{tc_2} \\ v_{w_3} &= v_{s_3} \end{aligned} \qquad \text{(II-4)}$$

2. Aerodynamics

a. Wind Axis Coordinates

As described in Section III, aerodynamic data used in Section IV were reduced from wind tunnel tests in a wind axis coordinate system, Fig. 2-4, so computation of aerodynamic forces and moments is convenient in this system. The first coordinate is taken in the direction of the wind velocity relative to the moving missile; the second coordinate is taken perpendicular to both the

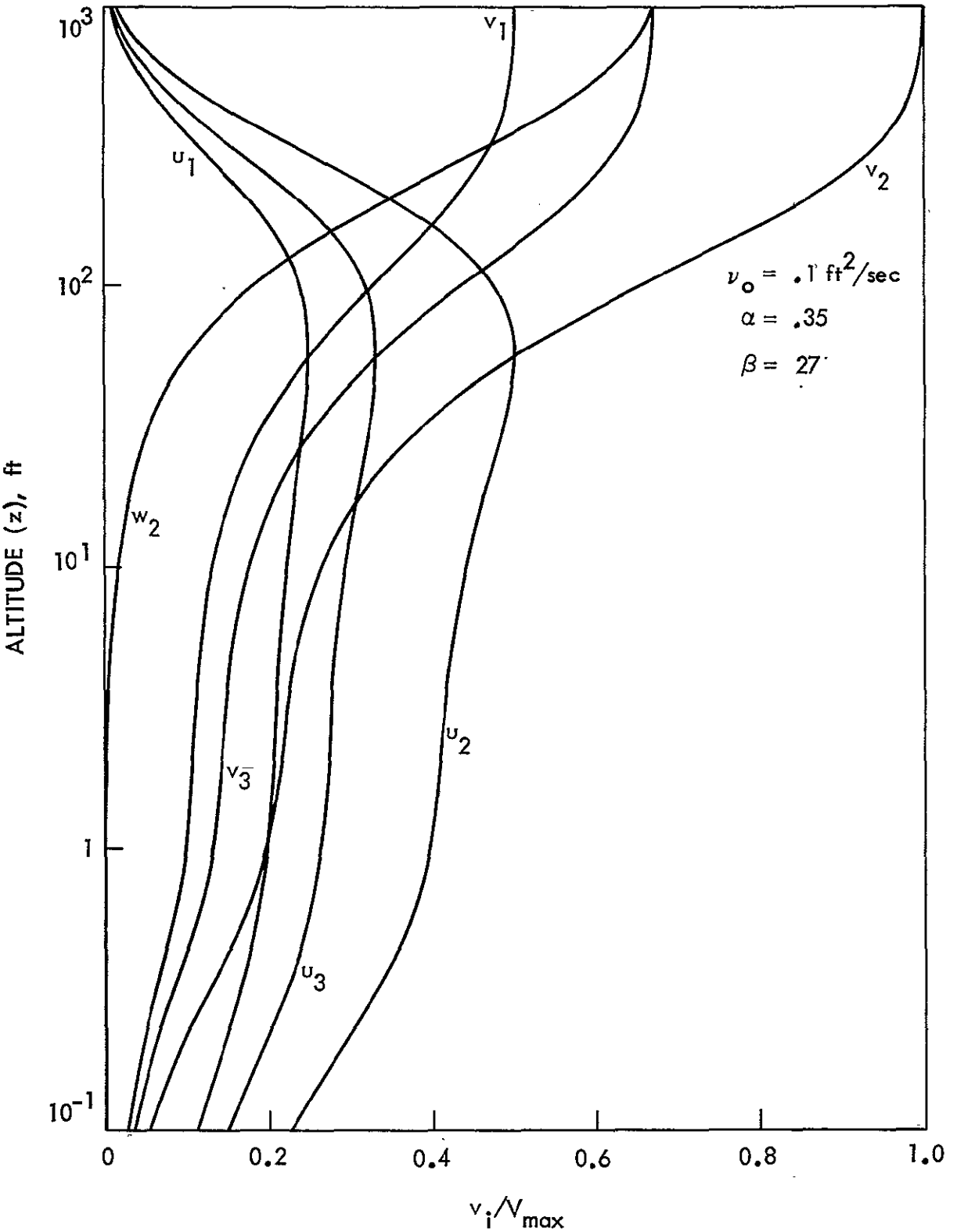

Fig. 2-2. Functional dependence of velocity components with altitude at three radial locations for 0.1 the default values of ν_o, α and β in the computer model

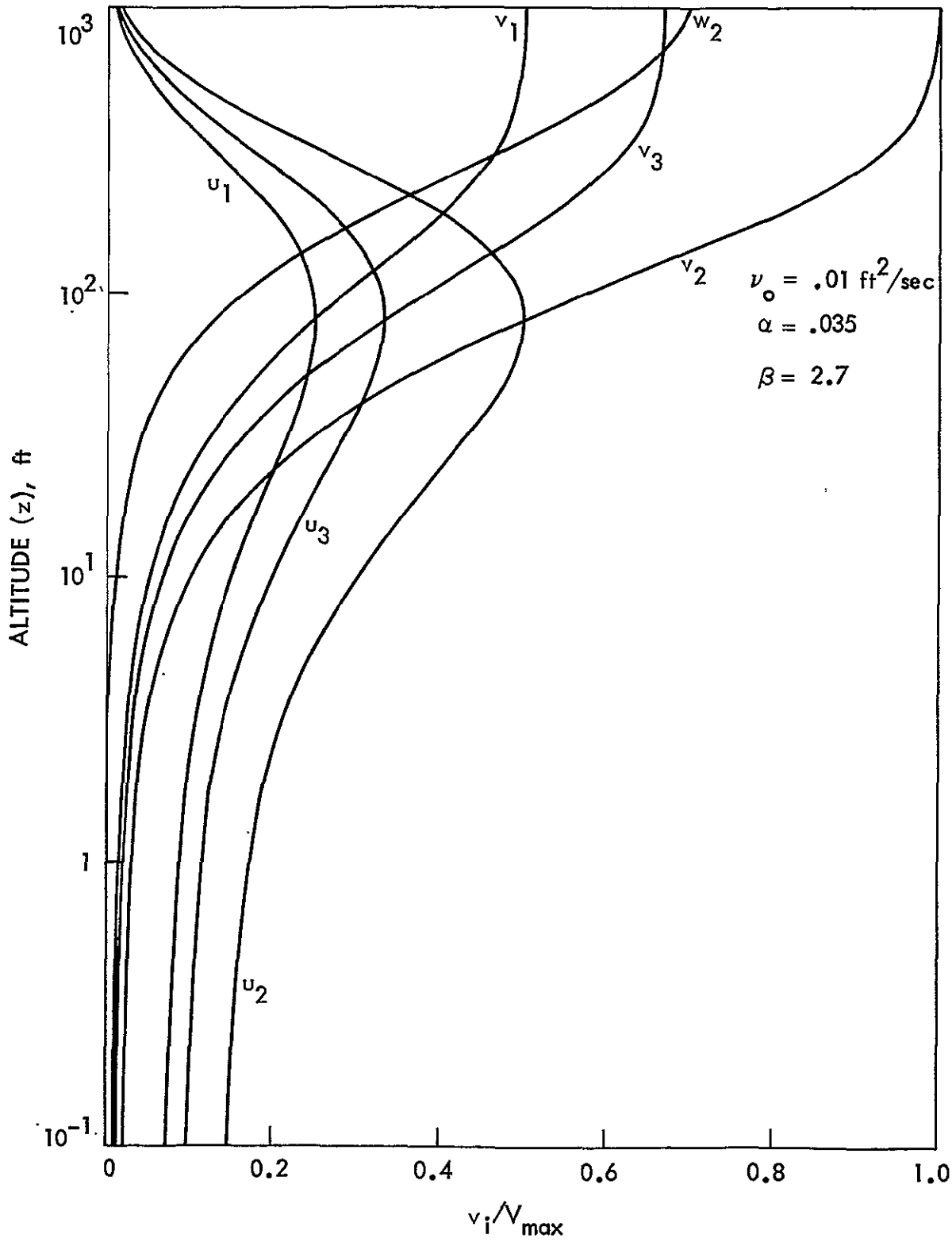

Fig. 2-3. Functional dependence of velocity components with altitude at three locations for 0.01 the default values of ν_o, α and β in the computer model

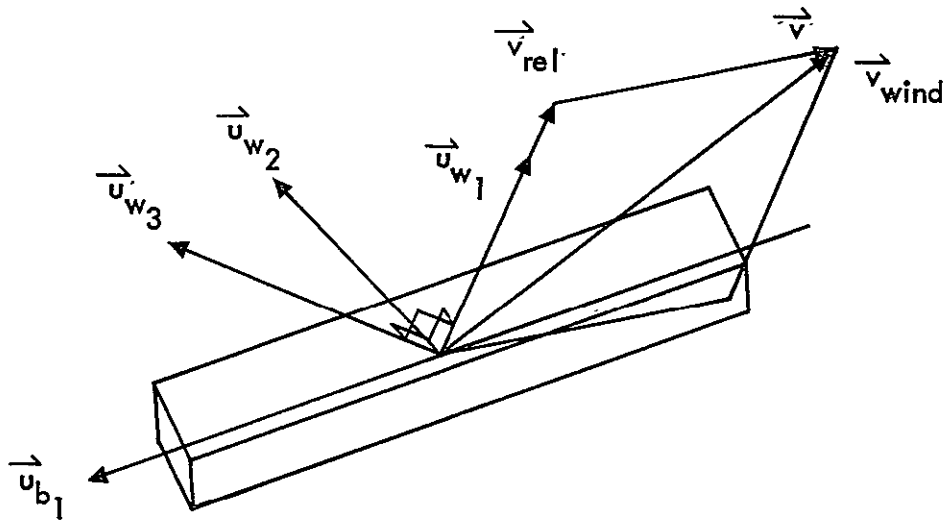

Fig. 2-4. Wind axis coordinates

relative wind vector and the long axis of the missile; and the third coordinate is taken perpendicular to the other two coordinates to form a right-handed system; thus:

$$\begin{aligned} \vec{v}_{rel} &= \vec{v}_w - \vec{v} \\ \vec{u}_{w_1} &= \vec{v}_{rel} / \left| \vec{v}_{rel} \right| \\ \vec{u}_{w_2} &= \vec{u}_{b_1} \times \vec{u}_{w_1} \\ \vec{u}_{w_3} &= \vec{u}_{w_1} \times \vec{u}_{w_2} \end{aligned} \qquad \text{(II-5)}$$

where the symbol $\times$ denotes a vector product.

b. Forces and Moments

In the usual aerodynamic notation, drag force, side force and lift force are in the $\vec{u}_{w_1}$, $\vec{u}_{w_2}$, and $\vec{u}_{w_3}$ directions, respectively, and correspond to wind axis force components F_{w_1}, F_{w_2}, and F_{w_3}, respectively. The dimensionless aerodynamic force components F_{w_i} are given in terms of the coefficients by

$$F_{w_i} = \frac{A_{ref} \rho \left| v_{rel} \right|^2}{2 w g_0} C_{w_i} \qquad i = 1, 2, 3 \qquad \text{(II-6)}$$

where A_{ref} is the reference area for the wind axis aerodynamic coefficients C_{w_i} (A_{ref} = Ld unless otherwise specified), w is the weight of the missile, ρ is the density of the air (taken at sea level standard conditions unless otherwise specified), and g_0 is the constant of proportionality in Newton's second law. The conventional roll, pitch, and yaw moments defined in Section III are about the u_{w_1}, u_{w_2}, and u_{w_3} axes, respectively.

However, since a right-hand screw convention is used for the sign of moments in the model, as opposed to the aerodynamic sign convention as shown in Fig. 3-12, the first and third components of the wind axis aerodynamic moments in the model are equal to the negative rolling and yawing moments defined in Section III, respectively, and the second component is equal to the pitching moment. The dimensionless aerodynamic moment components are given in terms of the coefficient C_{w_i}

$$M_{w_i} = \frac{A_{ref} L_{ref} \rho \left| \vec{v}_{rel} \right|^2}{2wg_0} C_{w_i} \qquad i = 4, 5, 6 \qquad \text{(II-7)}$$

where the symbols are the same as in the force equation and L_{ref} is the longest dimension of the missile.

Rate damping about the two shorter axes of a missile is included in the model. In the case of a cylinder, the damping coefficient C_{m_q} is calculated from experimental data and is inserted as a function of pitch angle. In the more general case of a body with three perpendicular planes of symmetry, rate damping coefficients have been included only about the two shorter axes and only an average value of the coefficients is used. The use of these averaged damping coefficients appears to be justified in most cases, since the average period of rotation is short compared with the missile time of flight and the damping is small compared to the total aerodynamic moment. The relation for the damping moment coefficient for the cylinder is known (Redmann, et al, 1976, pp. 3-10). The relation used in the model for the damping coefficient components for the three axes of the general body are

$$C_{q_1} = 0$$

$$C_{q_2} = \overline{C}_N/6 \qquad \text{(II-8)}$$

$$C_{q_3} = \overline{C}_Y t/(6D)$$

where $\overline{C}_N$ and $\overline{C}_Y$ are average (over pitch and yaw respectively) values of the body axis normal and side force coefficients, respecitvely; t is the missile thickness, and D is the missile width both normal to the long axis. The form of the dimensionless damping moment is

$$M_q = \frac{A_{ref}\rho\left|\vec{v}_{rel}\right|}{2wg_0}\,\frac{L\,C_q}{r_l} \tag{II-9}$$

where C_q stands for C_{m_q} in the cylinder case, and for C_{q_i} in the more general case (i = 1, 2, 3).

Mapping into Coefficient Data Tables

The aerodynamic data for missile shapes are available only over one quadrant of pitch angle θ for cylinders, or over one octant of pitch angle and roll angle ϕ for more general shapes with three planes of symmetry. The remaining portions of the circle or sphere must be covered by mapping into the data tables by means of symmetry arguments. Sign factors are obtained by using the quadrant number of the angle as an index in a short table (the more general case has two factors, and the cylinder, one). An example of a contour map of normalized drag force for all orientations is shown in Fig. 2-5.

3. Rigid Body Dynamics

a. Moment of Inertia

The inertia matrix (tensor) I relates the angular momentum L to the angular velocity $\vec{\omega}$ by

$$\vec{L} = I\vec{\omega} \tag{II-10}$$

The conventional moments of inertia I_{xx}, I_{yy}, I_{zz} and products of inertia P_{xy}, P_{xz}, P_{yz} are easily found for axes through the center of gravity of simple bodies. However, a missile may be composed of several point mass components at

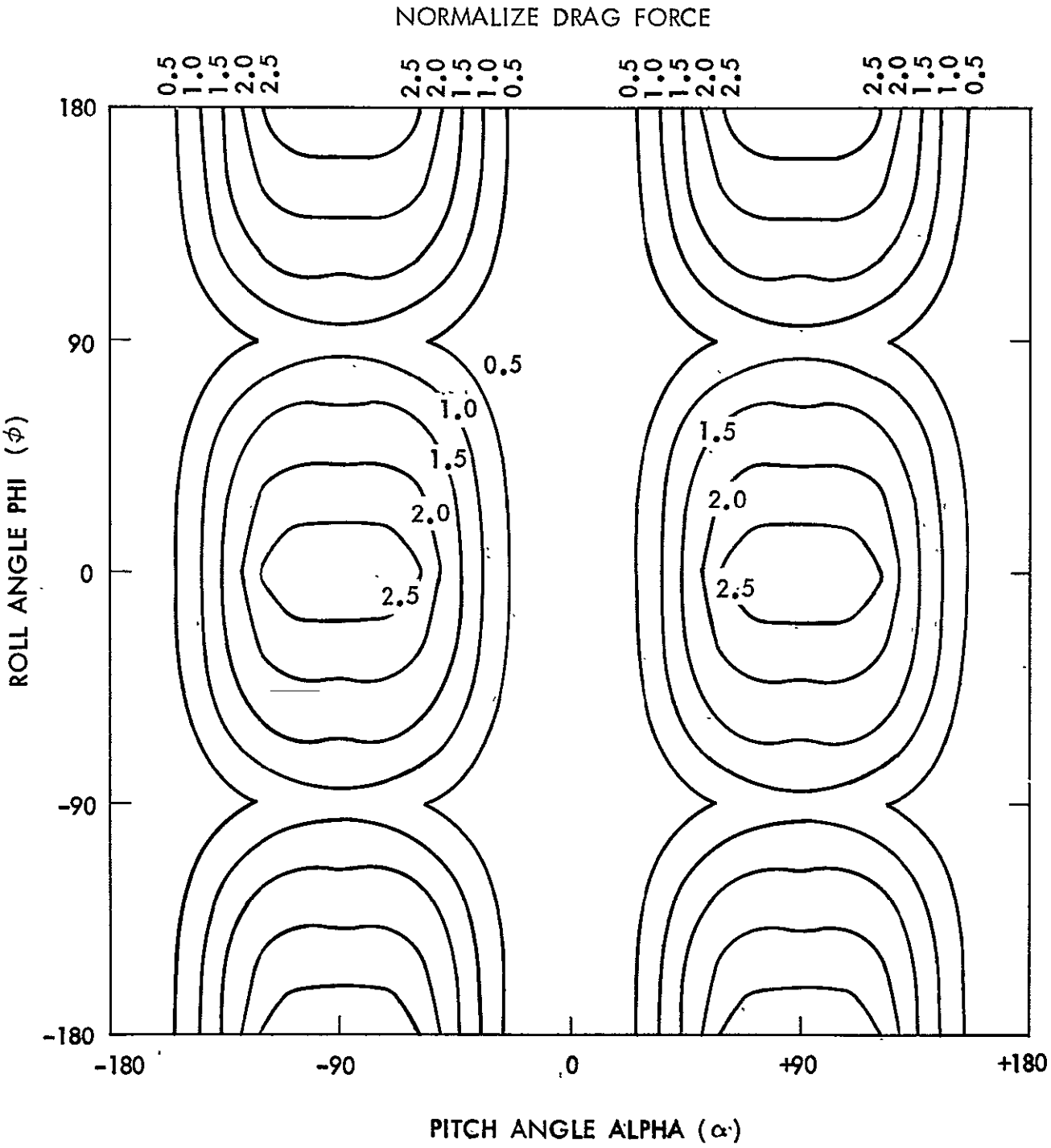

Fig. 2-5. Drag force as a function of missile attitude

various locations (for example, a car is approximated by 6 components), and the origin of the coordinate system to which the aerodynamic data are referenced may be different from the centers of gravity of all of the parts. Thus, the inertia matrix is a sum of terms I_i wherein each particle of mass m_i is transformed to a new origin displaced by r_i by use of the parallel axis theorem,

$$I_i = \begin{Bmatrix} I_{xxcg} + m\left(r_x^2 + r_y^2\right) & -\left(P_{xycg} + mr_x r_y\right) & -\left(P_{xzcg} + mr_x r_z\right) \\ \left(P_{yxcg} + mr_y r_x\right) & I_{yycg} + m\left(r_x^2 + r_z^2\right) & -\left(P_{yzcg} + mr_y r_z\right) \\ -\left(P_{zxcg} + mr_z r_x\right) & -\left(P_{zycg} + mr_z r_y\right) & I_{zzcg} + m\left(r_x^2 + r_z^2\right) \end{Bmatrix}_i \tag{II-11}$$

The model has the capability to handle up to ten components for a missile. Note that "mass particle" components may be used which have no moment or product of inertial about their own centers of gravity. At the same time, the displacement vector $\vec{r}_{cg}$ of the center of gravity of the missile from the center of body coordinates and the total mass of the missile are calculated from

$$m = \sum_i m_i \qquad i = 1, n$$

$$I = \sum_i I_i \tag{II-12}$$

$$r_{cg} = \sum_i m_i r_{cg_i}$$

b. Body Axis Coordinates and Euler Angles

The computation of the change of angular momentum of a missile (rigid body) is most conveniently carried out in a coordinate system fixed in the

missile body, Fig. 2-6. Aerodynamic forces and moments are computed in wind axis coordinates, as has been discussed in Section II-2 a above, and the orientation of the missile is required in inertial coordinates. Thus, the transformation from body to inertial coordinates T (and its inverse, T^{-1}), where

$$\vec{x}_i = T\vec{x}_b \,, \tag{II-13}$$

is needed at every time step in the computation of the missile trajectory. This transformation is defined as being from the current body coordinates to a set of reference inertial coordinates, and consists of a rotation from $\vec{x}_b$ to $\vec{x}_i'$ and a translation from $\vec{x}_i'$ to $\vec{x}_i$. The reference orientation is with the body axes coincident with inertial coordinate axes. In general, there is a rotation from the inertial orientation to the reference orientation for the trajectory. The x-axis is taken positive through the front of the missile (generally the long axis); the y-axis is taken positive through the left side of the missile (generally the second longest axis) and the z-axis positive upward through the top. This definition is different from the usual aerodynamic definition given in Section III, which is a left-handed system with the y-axis positive out the right side of the missile.

Orientation of the missile relative to the reference orientation is specified by three Euler angles ψ, θ, and ϕ, which measure successive rotations in yaw, pitch and roll respectively Fig. 2-7. The Euler angles are used to describe the inertial orientation, the orientation in the output printed at a specified time interval and at the termination of the trajectory. However, the Euler angles are not used in the actual trajectory computation, after the transformation matrix has been initialized, as will be discussed below.

c. Computation of Transformation from Body to Inertial Coordinates

The transformation matrix T from body to inertial coordinates defined by

$$\vec{x}_i = T\vec{x}_b \tag{II-14}$$

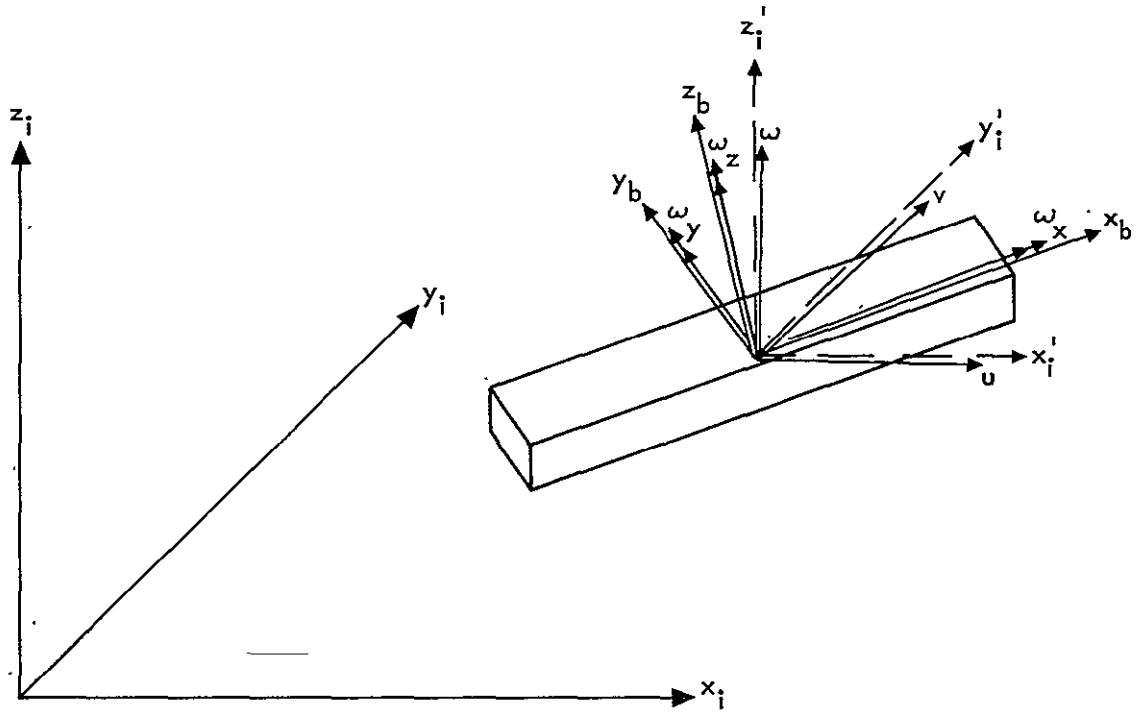

Fig. 2-6. Inertial and body axis coordinate systems

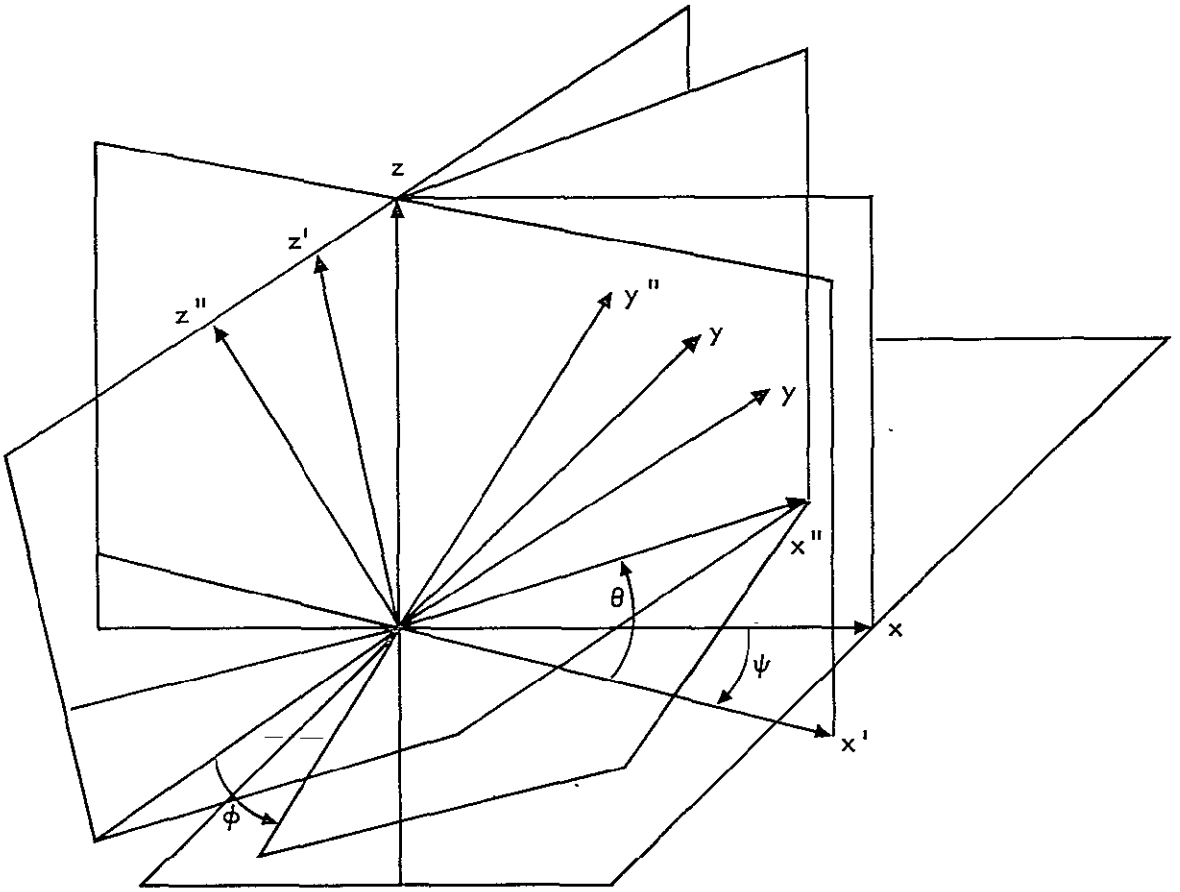

Fig. 2-7. Euler angles

is obtained initially from the Euler angles as described in Appendix B (Equations B-1 to B-3) (Goldstein 1950).

The columns of the transformation matrix T are unit vectors in inertial coordinates in the directions of the three body axes. The inverse matrix T^{-1} of a rotation matrix T is simply equal to its transpose T^t, which has the body axis unit vectors as its rows. Since the elements of a matrix are stored in column order in the FORTRAN computer language, working with the transformation from body to inertial coordinates is more convenient than the inverse because the unit vector elements are stored contiguously.

Quaternions, rather than Euler angles, are used to obtain the inverse transformation matrix in the trajectory calculation once the matrix has been initialized. Quaternions, q, are four component hypercomplex numbers, which have convenient properties for representing finite rotations (Aleksandrov 1963). In particular, the first component of the quaternion represents the cosine of half the angle of rotation and the last three components represent a (vector) axis about which the rotation has been made. Quaternion components are initialized from elements of the transformation matrix T from body to space coordinates (Equations B-4) and the time derivatives are computed from current values of the quaternion and the velocity (Equation B-5). The transformation matrix is computed from the integrated quaternion at each time (Equation B-6).

The relations between the transformation matrix and the quaternion components are derived on the assumption that the quaternion is normalized to unit magnitude (as if it were a four component vector). Owing to errors in integration, the departure from unit magnitude may become important after a number of time steps and will cause problems in evaluation of the Euler angles at output points. The quaternion components are renormalized after every step to avoid this problem.

d. Equation of Motion

The linear acceleration of the missile $\ddot{\bar{x}}_i$ is computed in inertial coordinates and the time derivative of angular momentun, $\dot{\bar{L}}$ is computed in

body coordinates. The aerodynamic force $\vec{F}$ is transformed to inertial components $\vec{F}_i$:

$$\vec{F}_i = T_{wi}\vec{F}_w \tag{II-15}$$

and the missile weight, the only nonaerodynamic force, is added. Since all forces are normalized to the missile weight, the linear equation of motion becomes

$$\ddot{\vec{x}}_i = G(\vec{F}_i - \vec{u}_{i3})$$

where

$$G = g_0\ r_1/V_{max}^2 \tag{II-16}$$

Accelerations are integrated directly to displacements in the model to take advantage of the increased accuracy in integrating second-order differential equations (Krogh 1976). Double integration cannot be applied to the rotational equations of motion since Euler angles are not integrals of the angular velocities.

The time derivative of the angular momentum vector $\dot{\vec{L}}$ is computed in a nonrotating coordinate system that instantaneously coincides with the moving-body coordinate system (Milne-Thompson 1955; Goldstein 1960). The rotation of the body axis system can be shown to add a cross-product term to the moment expressed in the body-axis coordinate system,

$$\dot{\vec{L}} = C_T(\vec{M}_b + \vec{L}\times\vec{\omega}) \tag{II-17}$$

where

$$C_T = (r_1/L)\left(g_0\ r_1/V_{max}^2\right) \tag{II-18}$$

is a factor arising from the nondimensionalization, and

$$\vec{\vec{M}}_b = T^{-1}\, T_{wi}\, \vec{\vec{M}}_w + \vec{\vec{r}}_{cg} \cdot \vec{u}_{b_3} \qquad \text{(II-19)}$$

where the first term is the aerodynamic moment transformed from wind axis to body coordinates and the second term is the moment of the weight about the center of coordinates.

4. Features of the 6 DOF Computer Program

Aspects of the model which are closely connected to its implementation in the computer program are discussed in this section.

a. Initial and Final Conditions

Provision is made in the model for injection of a missile into the wind field at specified linear and angular velocities as well as at a given height above ground. The location of the initial point of the trajectory as well as the initial location of the tornado center are also specified.

Trajectory calculations are terminated either when the origin of the body axis coordinate system passes through z = 0 or when the trajectory has been followed for a specified number of seconds, whichever occurs first. The program can easily be modified to terminate when the trajectory crosses a fixed envelope in space representing a building, but the capability is not implemented at present.

b. Input and Output

Input and output data for the computer program are described in detail in the User's Manual, which is presented as Appendix D. In general, the input is organized by section within the model; for example, the wind field data is in one section, and only the data that are changed need be input after the first series of cases. All the data used in each case are printed out.

Computer values of the state of the missile (velocity, position, Euler angles, etc.) are printed at specified intervals of simulated time along the

trajectory, and additional internal variables, such as relative wind velocity and instantaneous aerodynamic coefficients can be printed if desired. These computer values may also be saved on a FORTRAN file (on tape or disc) for use by plotting programs to be run after the termination of the trajectory program. The same variables which are printed at the uniform time step are also printed (and written to the file) at the termination of the trajectory.

c. Integration - Control of Solution

The study of missiles which are picked up and carried by a tornado leads to an initial value problem. The problem is described by a set of ordinary differential equations which can be solved by integrating forward in time from prescribed initial conditions until the missile has impacted on the ground plane or reached some other prescribed terminal condition. In this model, the process of solution is controlled by an integration subroutine from the JPL mathematical subroutine library called SODE (Krogh 1976). This integrator changes the step size and integration order as the integration proceeds to obtain a solution within the prescribed error bounds with minimal computation time. Among the useful features of the integrator are its abilities to compute different variables to different accuracies and stop on nontemporal terminal conditions. The integrator can also integrate second-order differential equations directly, with a resulting increase in accuracy.

An important feature of this integrator is that its source code contains instructions in the form of comments for specializing it for different computer systems. The integrator program has been specialized for and compiled on a number of computer systems including the Univac 1108, IBM 360/370, and MODCOMP IV. Since the integrator is the largest computer program which has been taken from the JPL general purpose computer library rather than written specifically for the trajectory program, it is essential that it can be moved to other computers with little effort.

d. Software Design

The computer program that implements the trajectory model has been written in FORTRAN V on the Univac 1108 computer and has been run under the EXEC-8 operating system. However, most of the code is written in a subset of FORTRAN V, which corresponds to ASA FORTRAN IV, in order to make the program portable. A portable program is one that can be compiled and run on another computer system without requiring changes. An earlier version of the program corresponding to the Phase I report model but with altered code for portability, was compiled and run on an IBM 370 Model 158. Actually, restriction to ASA FORTRAN IV is more stringent than are requirements for conversion from the 1108 to the 370. There are a number of useful non-ASA language features, such as NAMELIST, that are available on the Univac 1108, IBM 360/370, and several other common machines.

Since the trajectory model has undergone a large number of changes in the development process during Phases I and II of the project, a modular structure for the computer program has been used to localize the effects of the changes. An attempt has been made to make each subroutine module perform a simple identifiable function so that the code is easier to follow and hence easier to modify.

A user manual for the computer program is included in Appendix D. Input parameters are defined and input and output formats are described. Complete information is given on how to set up a card deck to run one or many trajectory cases through the FORTRAN program. System control cards are not given because they are dependent on the user's computer system whereas the FORTRAN program is portable between systems. Listings of the FORTRAN program are given in Appendix E.

C. TRAJECTORY MODEL REFERENCES

Aleksandrov, A. D., Kolmogorov, A. M., and Lavrent'ev, M. A., Eds. 1963, Mathematics, Its Content, Methods, and Meaning, Trans. by K. Hirsch, The M.I.T. Press, Cambridge, Mass., Vol. 3, p. 320.

Goldstein, H., 1950, Classical Mechanics, Addison-Wesley Press, Cambridge, Mass., pp. 143-158.

Iotta, R. C., 1974, Velocities of Tornado Generated Missiles. Report ETR-1103, Ebasco Services Inc., no city.

Krogh, F. T., 1975, Preliminary Useage Documentation for the Variable Order Integrators, SODE and DODE. JPL Section 914 Computing Memorandum 399, Pasadena, California.

Lee, A. J. H., 1973, A General Study of Tornado Generated Missiles. Gilbert Associates, Inc., Reading, Pennsylvania.

Lee, A. J. H., 1974, Design Parameters for Tornado Generated Missiles. Gilbert Associates, Inc., Reading Pennsylvania.

Milne-Thomson, L. M., 1955. Theoretical Hydrodynamics. 3rd Ed., The Macmillan Co., New York, pp. 496-502.

Redmann, G. H., Radbill, J. R., Marte, J. E., Dergarabedian, P., and Fendell, F. E., 1976, Wind Field and Trajectory Models for Tornado-Propelled Orjects, EPR1 308, T. R. 1, Electric Power Research Institute, Palo Alto, California.

D. NOMENCLATURE FOR SECTION II

A_{ref} ..... reference area for aerodynamic coefficients

C_{m_q} ..... damping coefficient

$\bar{C}_N$ ..... average normal force coefficient (body axis)

C_{q1}, C_{q2}, C_{q3} damping moment coefficients for noncylindrical body (eq. II-8)

C_{w_i} ..... aerodynamic coefficients in wind axis coordinates (i=1 through 6)

$\bar{C}_Y$ ..... average side force coefficient (body axis)

$\bar{\bar{C}}_\tau$ ..... proportionality factor (dimensionless) between moment on missile and angular acceleration (eq. II-17)

D ..... missile width (normal to long axis)

$F_{w_1}, F_{w_2}, F_{w_3}$ force components in wind axis coordinates

G ..... proportionality factor (dimensionless) between force on missile and acceleration (eq. II-16)

g_0 ..... constant of proportionality in Newton's second law

I ..... inertia matrix (tensor)

I_{xx}, I_{yy}, I_{zz} moments of inertia about x, y and z axes respectively

L ..... body (missile) length

$\bar{\bar{L}}$ ..... angular momentum vector (eq. II-10)

$M_{w_1}, M_{w_2}, M_{w_3}$ aerodynamic moments in windaxis coordinates

P_{xy} ..... (typical) product of inertia. Moment about x-axis due to angular velocity about y-axis

$P_L(\bar{z})$ ..... $\bar{\beta}\,\bar{z}/\bar{\alpha}$

$P_H(\bar{z})$ ..... $\bar{z} + \bar{\beta}$

q ..... quaternion

$\vec{r}_{cg}$ ..... displacement vector of center of gravity of missile body from center of body coordinates

r_x, r_y, r_z .... components of distance of cg of missile component from cg of missile

r_0 ..... outer radius of tornado

r_1 ..... radius of maximum azimuthal wind velocity

T ..... transformation from body to inertial coordinates

T^{-1} ..... inverse transformation

t ..... missile thickness (in eq. II-8)

u ..... component of missile velocity in x-direction (inertial)

$\vec{u}_r$ ..... radial unit vector

$\vec{u}_{w_1}, \vec{u}_{w_2}, \vec{u}_{w_3}$ unit vectors in wind axis directions

$\vec{u}_\theta$ ..... azimuthal unit vector

$\hat{u}$ ..... z-dependent factor in radial wind velocity

V_{max} ... maximum azimuthal wind velocity

v ..... component of missile velocity in y-direction (inertial)

$\vec{v}_{rel}$ .... velocity relative to missile

$\vec{v}_{w}$ .... wind velocity (vector)

$\hat{v}$ ..... z-dependent factor in azimuthal wind velocity

W ..... weight of missile

w ..... component of missile velocity in z-direction (vertical, inertial)

$\hat{w}$ ..... function in the computation of vertical wind velocity

x ..... cartesian inertial coordinate of missile trajectory

$\vec{x}_{b}$ ..... body coordinate vector

$\vec{x}_{i}$ ..... inertial coordinate vector

y ..... cartesian inertial coordinate of missile trajectory

z ..... cartesian inertial coordinate of missile trajectory (vertical)

Greek

α ..... scale height

β ..... scale height

γ ..... $\sqrt{5\Omega/3\nu_0}$

θ ..... pitch angle (2nd Euler angle)

ν ..... eddy viscosity

ν_0 ..... eddy viscosity at ground level

ρ ..... density of air

ϕ ..... latitude

ϕ ..... roll angle (3rd Euler angle)

Ψ ..... r-dependent factor in radial and azimuthal velocity components (eg. II-1)

ψ ..... yaw angle (1st Euler angle)

Ω ..... component of earth's rotational velocity at edge of tornado-cyclone

Ω_e ..... earth's rotational velocity

$\vec{\omega}$ ..... angular velocity vector

Subscripts

b ..... body

i ..... inertial

w ..... wind

1 ..... maximum azimuthal velocity

Superscripts

$\vec{\ }$	.....	vector quantity
$\dot{\ }$	.....	time derivative ($\dot{x} = dx/dt$)
$\bar{\ }$	.....	over-bar denotes dimensionless quantity made dimensionless by division by r_1

SECTION III
MISSILE AERODYNAMIC COEFFICIENT MEASUREMENTS

The six-degree-of-freedom missile trajectory program requires as input parameters the aerodynamic characteristics of the missile configuration to be studied. In general, this information is required in the form of six static coefficients as a function of attitude relative to the wind (and distance above the ground when near the ground). Since little or no information over a sufficient range of missile attitudes was available in the literature for shapes of interest as missiles, it became necessary to carry out a wind tunnel test program using scale models principally but supplemented by full-scale testing in the case of the cylindrical configurations. In addition, a brief test program was conducted using freely-falling, tumbling sub-scale models.

The use of Reynolds number ($\rho V\ell/\nu$), which is the ratio of inertial to viscous forces, as a scaling parameter is well established in the literature of fluid mechanics. In brief, it can be demonstrated both analytically and experimentally that for geometrically similar shapes, matching the Reynolds number assures matching fields of flow and therefore similar forces and moments are experienced by the shapes. It is this scaling principle which allows for the use of sub-scale models in much experimental work in fluid mechanics. The Reynolds number of the sub-scale test is generally matched to the full-scale value by increasing the density, ρ, or the velocity, V.

For circular cylinders it has long been established that there is a rather abrupt change in the flow field at the so-called "critical Reynolds number". This occurs because, as Reynolds number is increased beyond a critical value, the point at which the flow finally separates from the surface of the cylinder moves rather rapidly rearward from near the point of maximum thickness where it occurs over a range of sub-critical Reynolds numbers. This rearward movement of the separation point results in a much smaller wake behind the cylinder and, because the wake is a major contributor to the drag, the total drag of the cylinder is reduced by a sizable amount. An example of this behavior is shown in Fig. 3-17. The exact value of the critical Reynolds number is dependent on the roughness of the cylinder's surface and turbulence of the flow.

In the case of blunt shapes having sharp edges such as the plank or the car configurations the effect of Reynolds number on the aerodynamics is less because the point of flow separation is usually fixed at a corner regardless of Reynolds number and therefore the wake remains essentially constant in size.

On the basis of these well established facts, aerodynamic coefficients for the plank and motor vehicle shapes were obtained at Reynolds numbers less than full scale but the cylindrical configurations were tested through a range of Reynolds numbers from sub-critical into the supercritical region since for various cylindrical configuration and under various conditions in the tornado flow field both sub-and supercritical Reynolds numbers can occur.

The sub-scale tests were conducted in the GALCIT 10-ft Wind Tunnel (GALCIT TEST 973) and included free-air and ground-plane tests.[1]

Full-scale tests on the 15-ft length of 12-in. dia schedule-40 steel pipe were conducted at the Lockheed-Georgia Low Speed Wind Tunnel (LSWT Test 185) for the purpose of obtaining supercritical Reynolds number data on a cylindrical configuration.

Other full-scale tests (7002) were performed on a 1974 Dodge Dart 4-door sedan at the National Research Council, Ottawa, Canada, using the 30 Foot Wind Tunnel in the Low Speed Laboratory. Free-stream and ground-plane tests were performed to obtain confirmatory data for the GALCIT sub-scale model tests.

The scale model drop tests were conducted from the roof of a building at JPL which allowed for 126 ft of free fall. Their purpose was to obtain experimental tumbling data for comparison with both the empirical formulas appearing in the literature and a synthetic tumbling coefficient generated from the experimental static coefficients of this report.

[1] Data from ground plane tests which show the effect of the presence of the ground on the coefficients is presented in this report but has not been used in the computer runs because the capability of varying aerodynamic coefficients as a function of elevation is not currently a part of the computer program.

A. SCALE-MODEL WIND TUNNEL TESTS

1. Test Conditions

Except for the utility pole shape which was tested during Phase I of this program and presented in Redmann, et al, 1976, all of the missile shapes from the NRC tornado missile shape list were tested in the sub-scale tests at the GALCIT 10-ft Wind Tunnel. In this report, data are presented for five additional missile configurations:

1) Right circular cylinder, length/diameter of 14.1
2) Right circular cylinder, length/diameter of 36.0
3) Rectangular parallelepiped with linear dimensions in the ratio 1:3:36
4) Nominal sedan-type automobile
5) Nominal van-type truck

The shorter fineness ratio cylinder represents a 12-in. schedule-40 steel pipe, 15-ft in length while the longer cylinder has the geometry of a steel reinforcement rod 1-in. in diameter by 3 ft in length. Cylinders of intermediate length-to-diameter ratios representing a utility pole (13.5 in. in diameter and 35 ft long) and a 6-in. diameter, 15-ft long, schedule-40 pipe were also tested but are not reported here because of the relatively minor effect of length-to-diameter ratio, in the range tested, on the aerodynamic characteristics of circular cylinders, i.e., the cylinder data presented here can be used for those shapes at the appropriate Reynolds number. The rectangular parallelepiped represents a wood plank 4 in. x 12 in. x 12 ft. Figures 3-1 and 3-2 show the shapes and basic dimensions of the car and van, respectively. The van was added to the original list of candidate missiles because its basic shape was somewhat representative of such configurations as school busses, house trailers, and semitrailers, and because it represents a motor vehicle with a higher value of the flight parameter, $C_D A/W$, than an automobile.

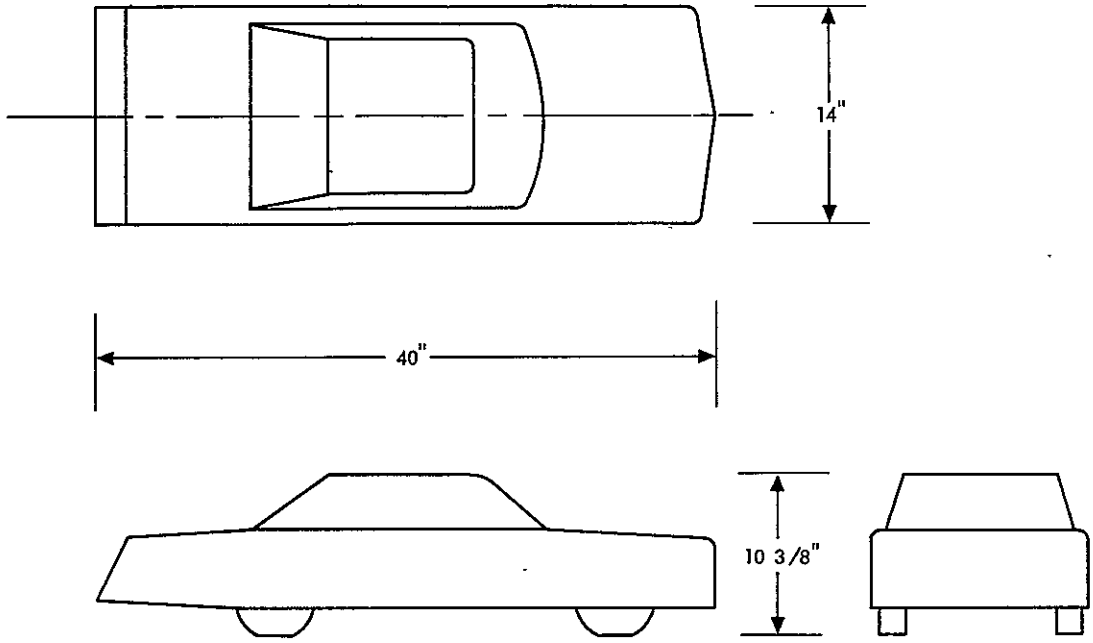

Fig. 3-1. Configuration of test automobile model

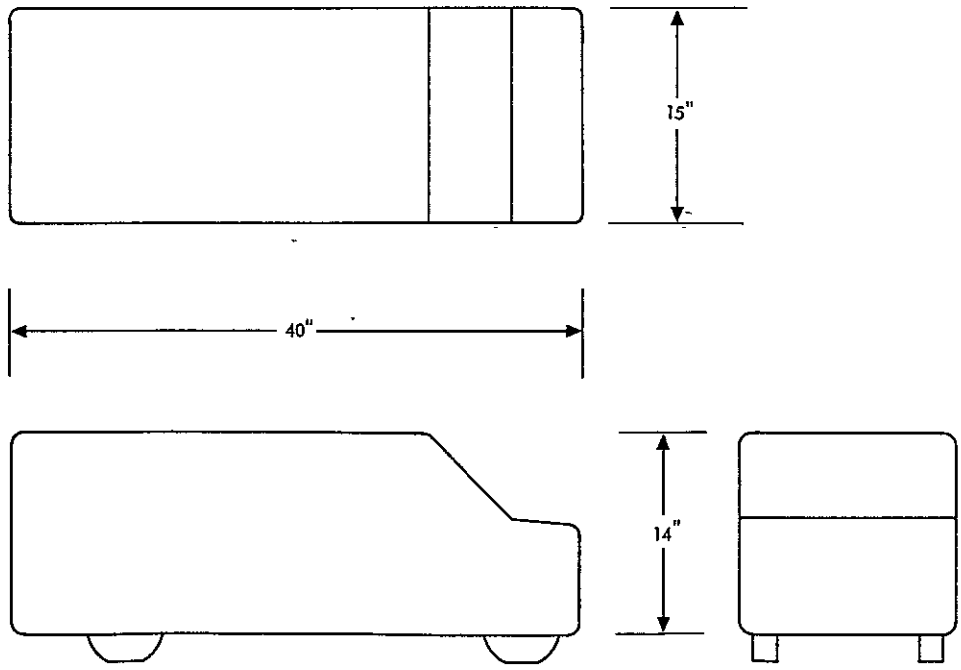

Fig. 3-2. Configuration of test van model

The data from the GALCIT test were obtained at a dynamic pressure of 25 lb/ft^2 which corresponds to a Reynolds number of 0.834 x 10^6/ft and a wind tunnel free-stream velocity of 112.7 mph (165.3 ft/sec). In terms of the diameter (2.50 in.) the Reynolds number for the cylinder models was 1.74 x 10^5, which falls into the sub-critical (high drag) region for a smooth cylinder normal to the flow. It should be used only when subcritical Reynolds number data are required.

2. Model and Test Installation

The cylindrical models were constructed of 0.25-in. wall-thickness seamless aluminum tubing with an outside diameter of 2.50 in. and lengths of 90 in. (L/d = 35) and 35.3 in. (L/d = 14.1). These models were considered to be aerodynamically smooth (but were not polished), and were fitted with removable end caps. They were tested with open ends and with closed ends to represent the utility pole configuration. The closed-end data confirmed the earlier data in Redmann, et al. The cylindrical models were rigidly attached at their midpoints to a support of circular cross-section extending from the roof of the tunnel test section. This support was mounted at its upper end to an external, six-component balance system. It was shielded from wind loads by means of a nonmetric (isolated from the balance) symmetrical airfoil fairing extending to within 0.25 in. of the cylinder surface which was designed to minimize the support-interference effects (Figure 3-3).

The support had the capability of rotating about a vertical axis (yaw) through 54°. The full 100° range of the test was obtained by reorienting the model relative to the balance at the 45° yaw point. An internal mounting plug was required at the midpoint of the cylinders because the wall thickness was not sufficient to carry the steady and unsteady air loads at all dynamic pressures of the test. The plug was designed with six 0.25-in. diameter holes drilled parallel to the cylinder axis of rotation in order to allow internal flow when the end caps were removed. End on ($\psi \simeq 0^\circ$), it probably represented some impediment to the internal flow through the open cylinder but at higher angles of yaw this flow is diminished and the plug has little effect. A view of the schedule 40 pipe model mounted in the wind tunnel is shown in Figure 3-3.

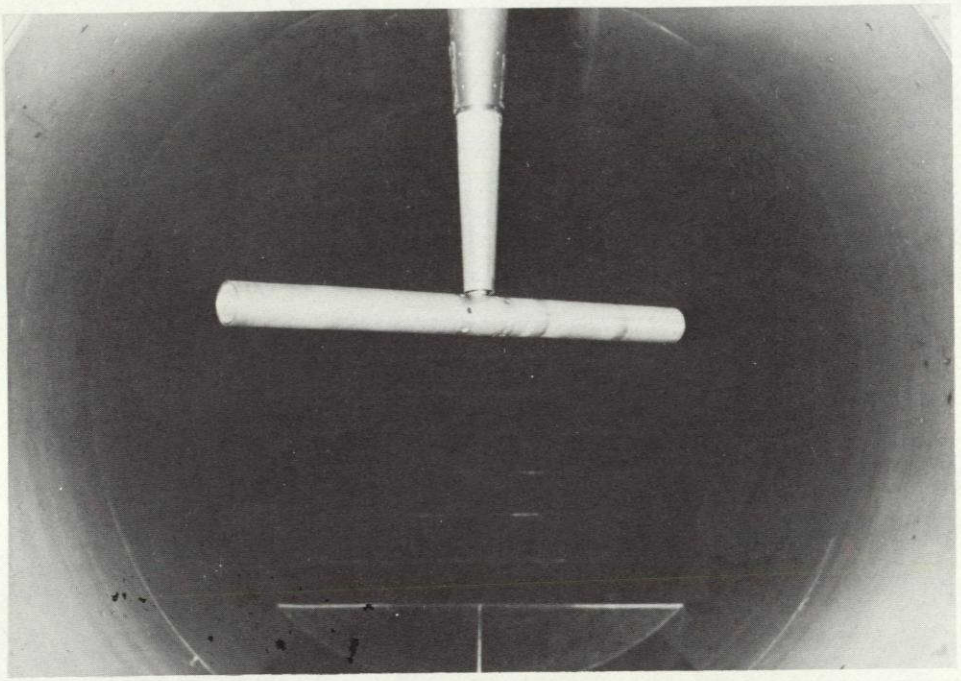

Fig. 3-3. Installation of 12 in., schedule 40 pipe model in GALCIT wind tunnel

The model of the plank which had the shape of a rectangular parallelepiped with the dimensions 2 x 6 x 72 in. (half-scale) was constructed in three sections in order to meet strength requirements without excessive weight. The two end-sections were constructed of plywood faced with Formica and fitted to an aluminum center section by means of a 2-in. wide tongue and groove joint. The sections were joined with five flush bolts on each side. Figure 3-4 shows the model installed in the tunnel. The aluminum center section provided a metal-to-metal fit to the wind tunnel balance as well as an attachment point for adapters which provided settings of 0°, 30°, 60°, and 90° in roll about the longitudinal axis of the plank.

The car and van models were constructed from clear sugar pine, using a hollow box-like interior to reduce weight and provide space for the aluminum support structure. The support was made from 2-in. square tubing and welded such that a support opening was provided in the roof, side, and rear. To this was bolted the inside bottom of the car or van and the shape built up around it.

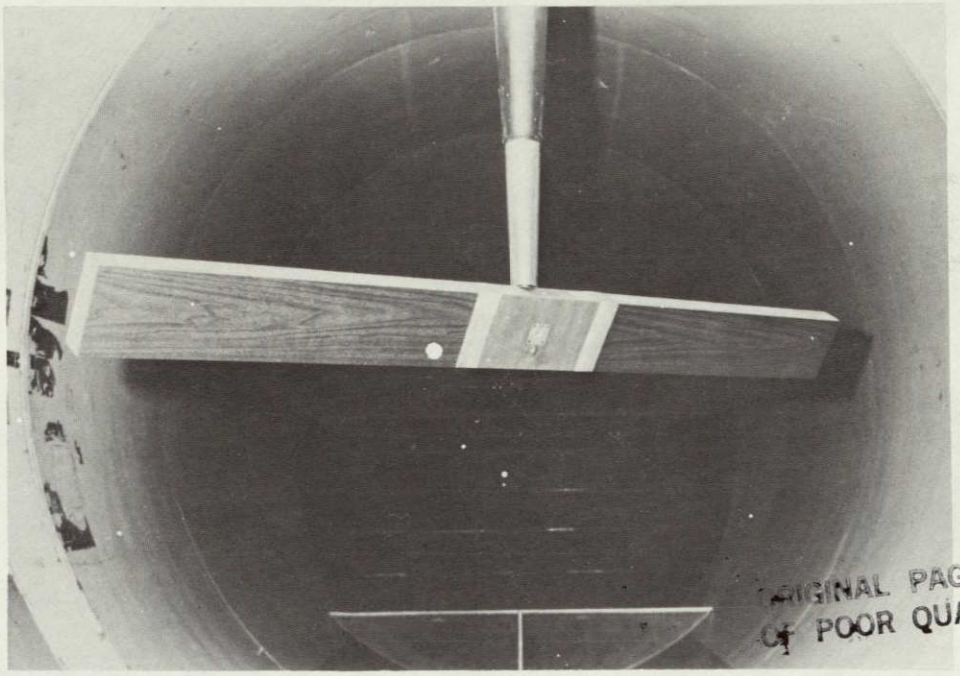

Fig. 3-4. Installation of plank model in GALCIT wind tunnel

Figures 3-5, 3-6, and 3-7 show the car and van installed in the GALCIT wind tunnel with examples of the three mount positions. Both models were approximately 0.20-scale. This scale was chosen as the largest at which tunnel blockage effects could be acceptably removed from the data.

To determine the effects on the aerodynamic coefficients of the presence of the ground, some configurations were tested at various distances above a ground plane which was installed in the test section of the tunnel. This so-called "ground effect" results from the constraining effects of a solid boundary on the flow. The effect decreases as distance from the solid boundary increases. In the ground-plane tests the ground plane spanned the test section and was about 10 ft long. The leading edge was shaped so as to insure smooth flow over the surface. Three-quarter inch plywood arranged in from 9 to 16 panels, necessary to span the circular cross-section at different heights, made up the surface. A substructure supported on four adjustable-length struts cradled the panels. Two screw jacks attached to the ground plane centerline at

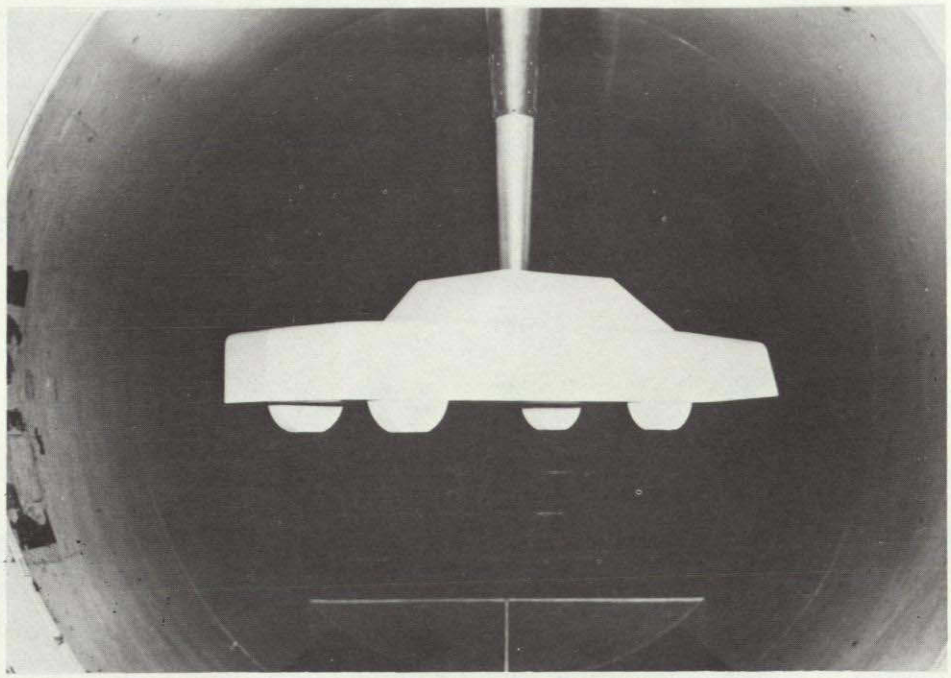

Fig. 3-5. Installation of test automobile model in GALCIT wind tunnel; top mount

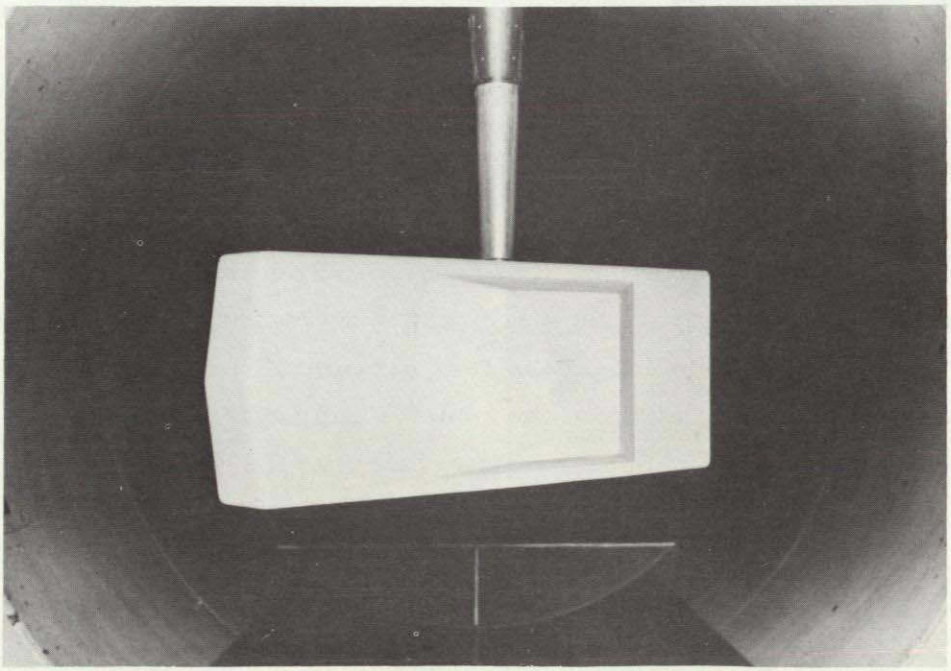

Fig. 3-6. Installation of test automobile model in GALCIT wind tunnel; side mount

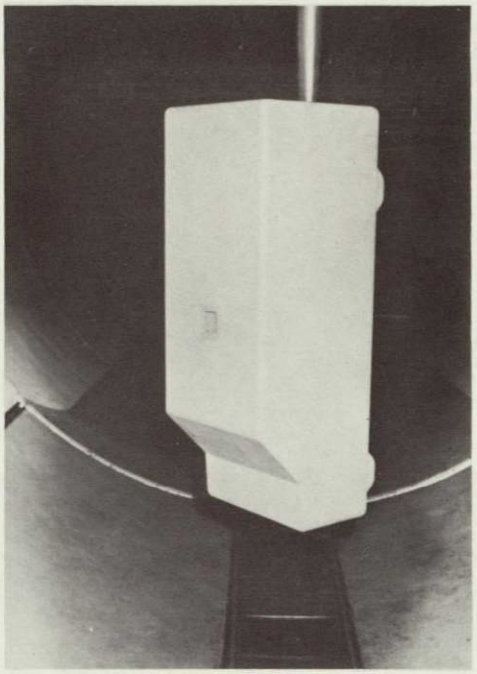

Fig. 3-7. Installation of test van model in GALCIT wind tunnel; rear mount

approximately the 20% and 80% chord positions assisted in adjusting the various heights. Ground-plane height was varied manually and only specific height positions could be used readily. A view of the ground plane with the pipe model at $\psi = 0^{o}$ and a tunnel survey probe (not present during data runs) is shown in Fig. 3-8, a side view of the ground plane with the plank at 0.25 in. above it is shown in Fig. 3-9.

Data from GALCIT tests are reported in Section III-C along with data from full-scale tests described below.

B. FULL-SCALE WIND TUNNEL TESTS

1. Steel Pipe - 12 in. dia by 15 ft long

a. Test Conditions

Because of geometric and tunnel performance constraints in the GALCIT Wind Tunnel, it was not possible to test the cylindrical configurations in their

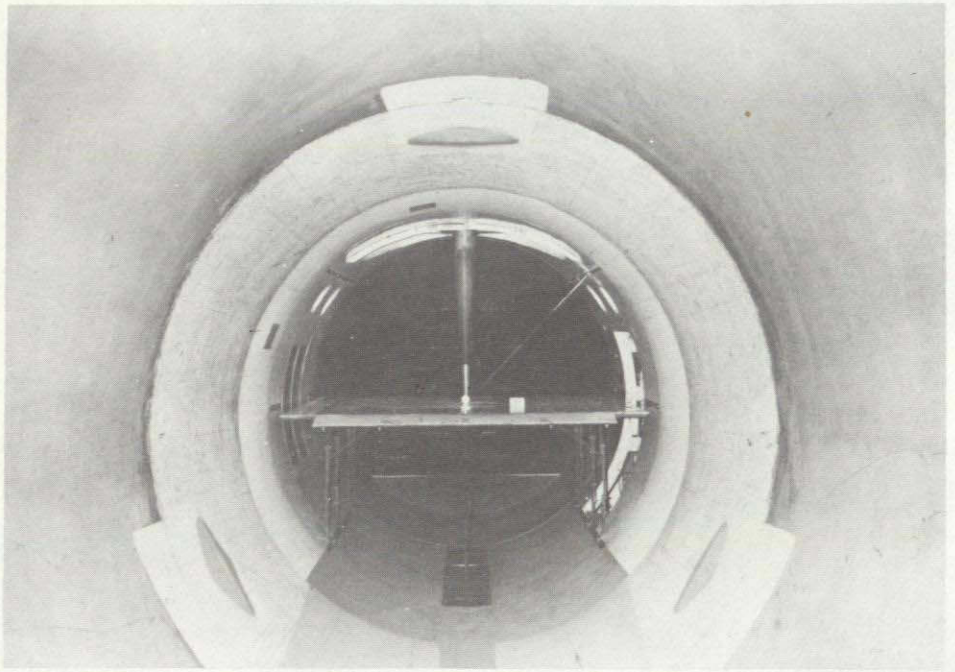

Fig. 3-8. Installation of cylinder model ($\Psi = 0^{o}$) and ground plane in GALCIT wind tunnel, looking downstream

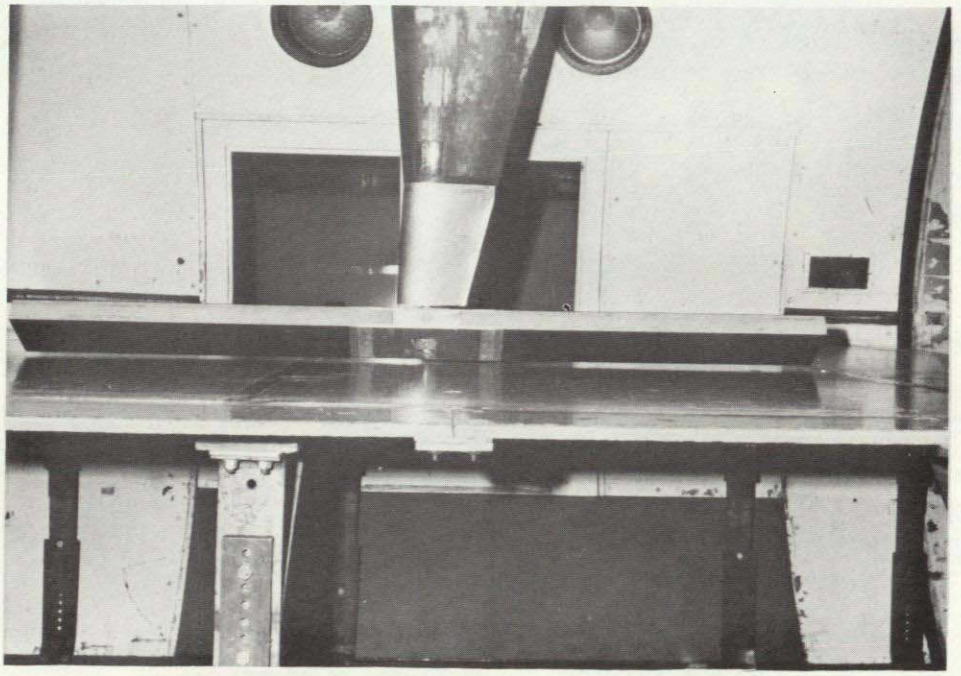

Fig. 3-9. Side view of ground plane installation showing plank model and support with fairing

supercritical Reynolds number regime, i.e., $Re_d > 0.4 \times 10^6$. Since the drag of a cylinder with its longitudinal axis normal to the flow is known to be dependent on the Reynolds number regime, it was deemed expedient to carry out a short test on a full-scale pipe at a supercritical Reynolds number. By using an actual pipe, surface roughness, which exerts a small but significant effect on drag, was also matched exactly.

The model was a 15-ft length of 12-in diameter schedule-40 steel pipe in field condition, i.e., the ends were flame cut and the cylindrical surface of the pipe was tested as it came from an outdoor storage area. Only the open-end pipe and a few runs with the ends closed were tested because the effects of Reynolds number on blunt or sharp-edged configurations, such as the beam and car, are usually small or nonexistent in the range of Reynolds number which will occur during a tornado.

Eleven runs (total) were made at the Lockheed-Georgia Low-Speed Wind Tunnel in the 16.25 x 23.25 ft test section. Most of the runs were made at a nominal free stream velocity of 130 mph ($q = 40$ lb/ft^2) which results in a Reynolds number, based on diameter, of 1.17×10^6. Test data at higher velocities were unreliable because the large unsteady forces resulting from asymmetric vortex shedding caused large shifts in the balance air-off zero readings.

b. Installation

The 12-inch pipe was supported in the wind tunnel as shown in Fig. 3-10 by a 57-in. length of 5-in. OD by 0.5-in. wall Shelby tube, which was butt-welded to the midpoint of the pipe. When the pipe was in test position in the test section, this tube extended through the floor, without contact, into a 17-in. length of 5-in. ID pipe, which was mounted to the wind tunnel balance. Attachment of the Shelby tube to the balance support pipe permitted testing of the model at four heights above the test section floor. The support tube was shielded from air loads by means of a symmetric airfoil-shaped fairing (4-in. thickness by 24-in. chord), which was mounted to the floor but did not touch the model or its support. The fairing (see Fig. 3-11) was constructed of a series of vertical

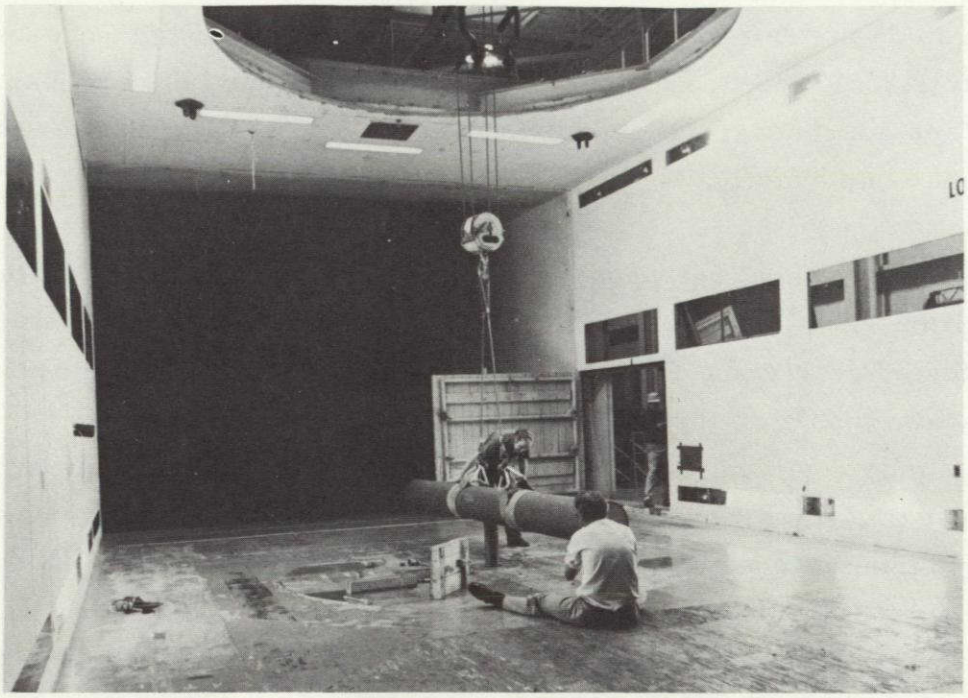

Fig. 3-10. Prototype 15-ft, 12-in. diameter, schedule 40 pipe being installed in Lockheed-Georgia Low Speed Wind tunnel

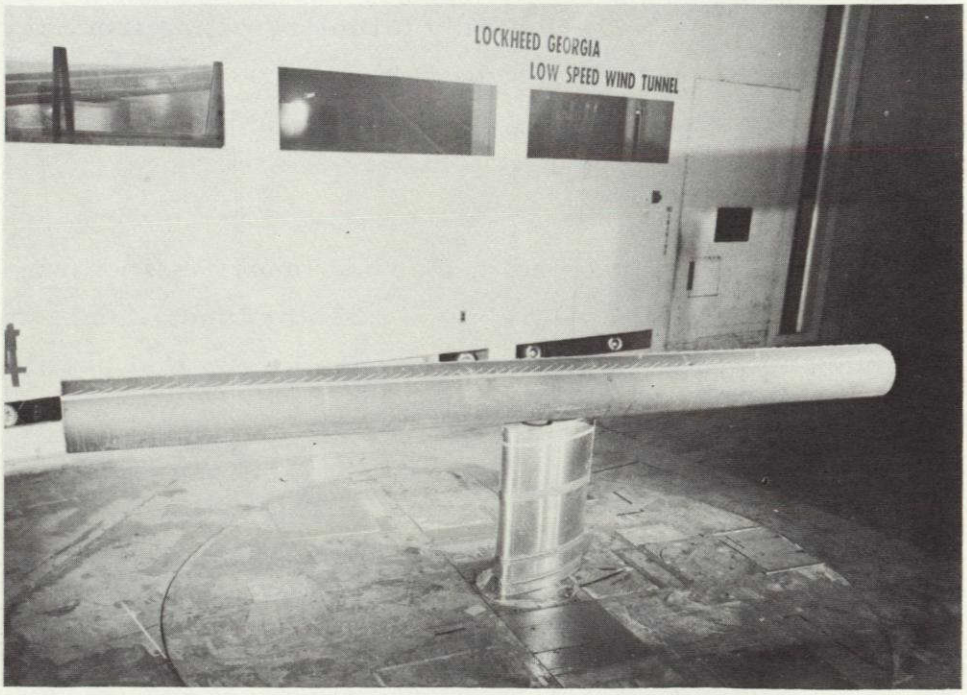

Fig. 3-11. Prototype 15-ft, 12-in. diameter, schedule 40 pipe during testing. Note tufts (used only during flow-visualization run) and support fairing

sections to accommodate the various heights of the model above the wind tunnel floor. At the support position nearest the floor (0.069 diameter or 0.875-in. distance between floor and lowest point on pipe), no fairing was used. The model, together with the support and balance to which it was rigidly attached, could be remotely rotated through the yaw range from -5° to 95°, over which data were taken while the fairing remained aligned with the airstream.

2. Automobile - 1974 Dodge Dart

a. Test Conditions

Wind tunnel tests were performed on a 1974 Dodge Dart 4-door sedan with dimensions approximately 16.7 ft long, 5.8 ft wide and 4.3 ft high. The 30 ft by 30 ft Wind Tunnel in the Low Speed Laboratory of the National Research Council, Ottawa, Canada was used for the tests which included measurements both in free air and in the presence of a ground plane.

The following tests were performed:

1. Vehicle in Free Air (Center of tunnel) - 50 and 70 mph
   a. Roll angle, 0°; yaw angle, -5° to 95°

2. Vehicle on Tunnel Floor (Ground plane) - 50 and 70 mph)
   Roll angle, 0°; yaw angle, -5° to 95°; pitch angle, 0°
   -5° to 15°; 5°
   -5° to 15°; 10°
   Note: Rotation about rear bumper for pitch angle.

3. Reynolds Number Runs - 30 - 120 mph
   Vehicle in center of tunnel: roll angle, 0°; yaw angle, 0°
   90°
   Vehicle on floor : roll angle, 0°; yaw angle, 0°
   90°

The listed free air and ground plane tests were sufficient to provide data for comparison with the GALCIT sub-scale model car tests.

Both wind-on tares (support structures) and static tares have been subtracted from the reported forces and moments. The flow interference effects between the vehicle and the support structures were ignored.

b. Installation

For the free air tests the vehicle was mounted on the two main struts which are normally used for aircraft testing. Bayonets made from 4 in. O. D. tubing positioned the car on tunnel centerline and connected the car to the struts. See Figure 3-12.

The engine, transmission and gas tank were removed from the vehicle and replaced with styrofoam to simulate original shape. Channels and struts were installed on the frame of the car for the bayonet connections and the suspension system was "locked" so that no changes of the vehicle attitude in relation to its wheels could occur during the tests.

The fairings which covered the two main struts always remained aligned with the windstream during the yaw tests. No fairings were used on the bayonet connections.

Special mounting pads and fairings were designed for the ground plane tests to hold the vehicle at the desired angles of attack (5° and 10° rotated about the rear bumper). See Figure 3-13. The vehicle was positioned on the pads, using 4" high wood chocks behind each wheel, and the pads were bolted to the turntable. The pads and fairings were 6 in. wide and the heights were 4.27 in. and 8.61 in. rear and 14.0 in. and 27.9 in. front respectively for the 5° and 10° angle of attack tests. See Figure 3-14. The fairings were not designed to maintain wind alignment because of the limited yaw angle (15°) for the tests.

C. WIND TUNNEL TEST RESULTS

1. Definition of Aerodynamic Coefficients

The tabulated and plotted data from both sub-scale and full-scale wind tunnel tests are presented in the next subsection in terms of wind-axis coefficients. The wind-axis system is one which remains aligned with the relative wind, independent of the attitude of the body. The sign conventions (Fig. 3-15),

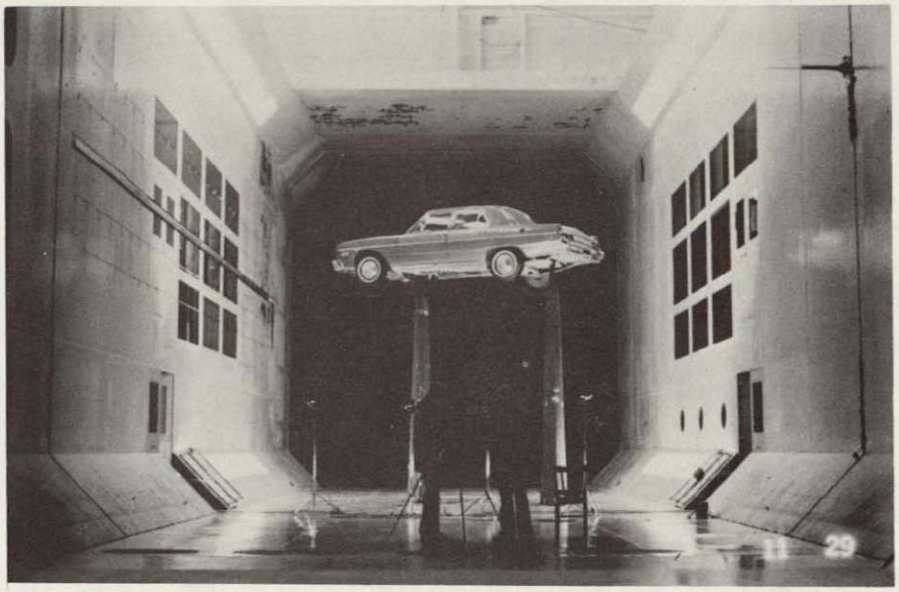

Fig. 3-12. Installation of 1974 Dodge Dart for free air test in the 30 ft by 30 ft Wind Tunnel at National Research Council, Ottawa, Canada

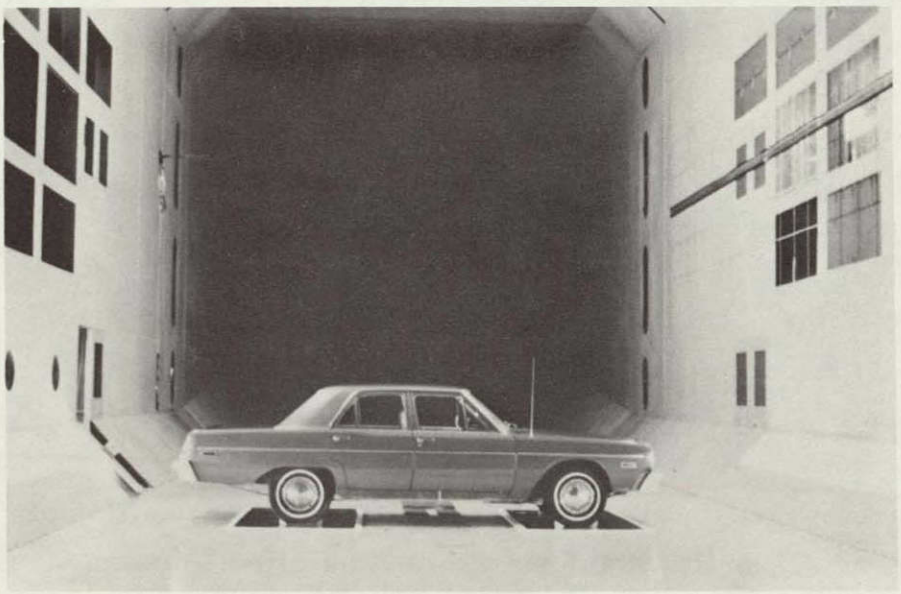

Fig. 3-13. Installation of 1974 Dodge Dart for ground plane tests in the 30 ft by 30 ft Wind Tunnel at National Research Council Ottawa, Canada

Fig. 3-14. Installation of 1974 Dodge Dart for ground plane tests at angle of attack in the 30 ft by 30 ft Wind Tunnel at National Research Council, Ottawa, Canada

are as follows: left side up is positive rotation about the X- (or longitudinal) axis; nose to the right is positive rotation about the Z- (or vertical transverse) axis; and nose up is positive rotation about the Y- (or horizonatal transverse) axis.

The angle of attack α is the angle between the wind vector and the body centerline projected on a vertical plane through the wind vector. The yaw angle ψ is the projection of that angle on a horizontal plane through the wind vector. The roll angle ϕ is the angle between the initially horizontal lateral axis of the body and the horizon.

Forces are defined as positive to the rear, to the right, and upward, for the X-, Y- and Z-axis, respectively.

Given below are definitions for the six wind-axis coefficients as used in this section and Appendix C. These are the definitions commonly used in wind tunnel testing; however, for convenience in writing the trajectory program some of the coefficients have been defined with opposite signs. These changes are explained in Section II.

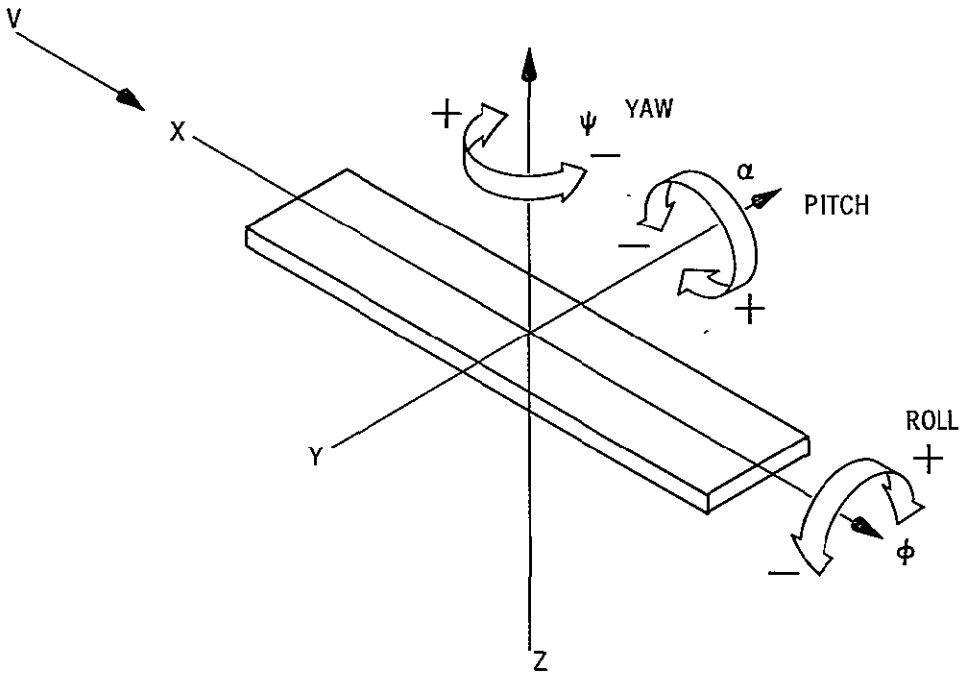

Fig. 3-15. Sign conventions used with aerodynamic coefficients

Lift coefficient	$C_L = \frac{F_Z}{Aq}$
Drag coefficient	$C_D = \frac{F_X}{Aq}$
Side force coefficient	$C_S = \frac{F_Y}{Aq}$
Pitching moment coefficient	$C_m = \frac{M_Y}{A\bar{L}q}$
Yawing moment coefficient	$C_n = \frac{M_Z}{A\bar{L}q}$
Rolling moment coefficient	$C_\ell = \frac{M_X}{A\bar{L}q}$

$F_{()}$ or $M_{()}$ is the aerodynamic force or moment about the axis indicated in the subscript; S is the reference area[1]; L is the reference length; and q is the dynamic pressure, given by the expression

$$q = 1/2\rho V^2$$

where ρ is the density of the air, and V is the relative velocity between air and the center of gravity of the body.

The moment reference center is the cylinder centerline at the nose for the cylindrical configurations and is the corner formed by the nose and bottom of the body in the vertical plane of symmetry for the motor vehicles.

In addition to the six wind-axis coefficients, three body-axis coefficients (C_Y, C_N and C_p) are used to obtain the center of pressure locations. These coefficients are related to the body-axis system, which is tied to the body and moves with it. In the body-axis system, the X-axis is the longitudinal axis of the body and the Y- and Z-axes are, respectively, those which are transverse horizontal and transverse vertical to the X-axis when the body is at zero angle of roll, attack and yaw. The center of pressure is the point through which the aerodynamic forces on the body pass. The expression used to obtain the center of pressure (X_{cp}), non-dimensionalized by the body length, is

$$\frac{X_{cp}}{L} = \frac{C_p}{C_N}$$

where C_p and C_N are, respectively, coefficients of the moment about, and the force along, the Y-body axis. At yaw angles near zero, C_p becomes small and the ratio method of obtaining center of pressure becomes unreliable, especially if support-interference effects are present. Interference effects which are usually not troublesome in determining the individual coefficients may become so due to the small value of the denominator in the ratio. This appeared to be

[1] Reference areas and lengths as well as moment center locations for the various test configurations are given in Table C-1 (Appendix C).

the case for the cylindrical configurations, but not for the shapes with corners, such as the plank. For more reliable values for the location of the cylindrical centers of pressure, minor supplemental tests were conducted using 17-in. and 18-in. long cylinders (of varying diameters) for the L/d = 14.1 and the L/d = 36.0 configurations, respectively, in a small, low-speed JPL wind tunnel at subcritical Reynolds number. In these test the center of pressure was determined as the pivot point farthest aft from the nose at which the small cylindrical models would weathervane into the flow with the flat circular face forward. Data was obtained in this fashion for yaw angles of 0^{o} and 13^{0} for the L/d = 14.1 cylinder, and at 0^{o} only for the L/d = 36.0 configuration (Fig. 3-16). Since these data points are considered more reliable at small yaw angles than those obtained by forming the ratio of the moment and force coefficients (or their slopes), the fairings were extended to them, and the faired values, included in the tabulations. In Fig. 3-16 the points which decrease sharply as the zero yaw angle is approached were obtained by the ratio method while the flagged points in the vicinity of $X_{cp}/L = 0.45$ through which the fairings pass were obtained from the supplemental test.

Although the moment center used in reducing the coefficients is, in the cases of the cylinders and the plank, the center of the body along the longitudinal axis, the values given in the tables in Appendix C have for convenience been referenced to the nose for all configurations.

2. Interpretation of Test Results

Before proceeding to a detailed discussion of the results it will be useful to mention the limitations of the data and the rationale used in fairing the plotted data and tabulating the smoothed results. The models were sized to the tunnel test sections so that standard wind tunnel corrections for blockage and horizontal buoyancy could be and were used in reducing the data. One of the conventional support systems available in each of the tunnels was used throughout these tests, along with external, six-component balance systems. It is well known by experienced aerodynamicists that this support system introduces an interference effect to the flow over the model which varies with the attitude of the model. Indeed, any system of physical support for the model will introduce interference effects, although the magnitude of each system may

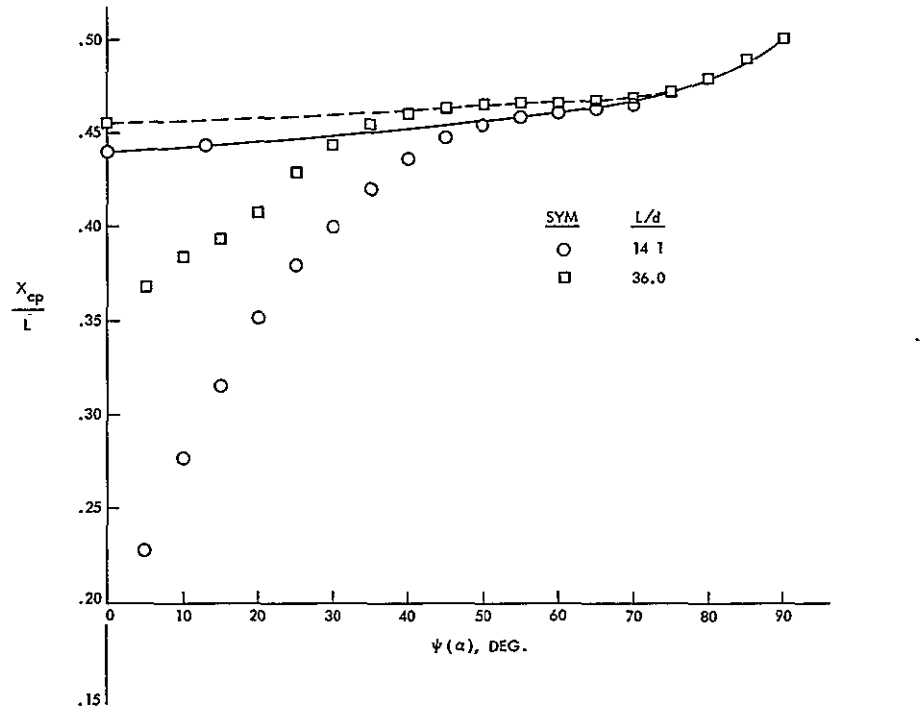

Fig. 3-16. Center of pressure location as a function of yaw angle for open circular cylinders of length-to-diameter ratios equal to 14.1 and 36.0

vary at a given model attitude. Even a model which spans the tunnel can be said to suffer from a form of interference because of the tunnel wall boundary layer and because end effects due to a finite length are not present. Through the design of specialized supports and by testing the same model with alternate support systems it should be possible to evaluate the support interference and to correct it to a limited degree, but a great deal of wind tunnel time and fiscal resources would be needed since each configuration would require a separate evaluation. No such course of action was attempted in this test program because the use for which the data are intended does not require the level of accuracy which would be needed to proceed with a detailed analysis of the flow field in the vicinity of each model. Instead, engineering judgment was a guide in the generation of the faired curves used to produce the tabulated data. For example, where coefficients were known to be zero because of flow field symmetry, the faired curves were forced through the zero points. In other cases where support interference was suspected but not demonstrable, judgment was used in the construction of the fairing.

Summary plots are presented in Figs. 3-14 through 3-17 and discussed in detail below. Tabulated smoothed data which were used in the trajectory calculations are given in Tables C-2 through C-34, Appendix C. All orientations of all models were not tested because of balance mounting points, physical interference with the ground plane, and limited test time.

a. Cylindrical Body Results

Figure 3-17 shows the effect of variation in Reynolds number due to change in the velocity of the air flow on the full-scale pipe free air drag coefficient at $\psi = 90^{o}$. The upper limit of velocity (and Reynolds number) was determined to be that beyond which good data could not be obtained because the fluctuating forces normal to the flow caused by unsteady wake effects led to unreliable results. The lower limit was set by the reduced level of the steady drag force and the balance system sensitivity (accuracy of data reached the limits of acceptability). It is clearly evident that the test Reynolds number of the Lockheed-Georgia full-scale test is in the supercritical regime, which, in this case, occurs for $Re_d > 0.4 \times 10^6$. However, even in the supercritical regime the drag coefficient is shown to be a function of Reynolds number. The shape of the curve in the supercritical region is similar to two-dimensional results obtained by Achenbach, 1971. The Reynolds number range for the 12-in pipe (neglecting gusts) which can occur in a tornado having 225 mph rotational and a 70 mph translational velocity at its center is shown in Fig. 3-17. The maximum value can occur only when the pipe is stationary relative to the ground and is less at all other points in the trajectory because the pipe is moving with the wind. Because of the uncertainty and variability of the Reynolds number of a pipe missile during its trajectory in the tornado and because the Reynolds number effect is smaller or nonexistent at lower values of yaw angle, it appears reasonable that data as obtained from the maximum Reynolds number of the full-scale test be directly used for the 12- and 6-in. pipes in trajectory calculations. Also shown in Fig. 3-17 are two subcritical values of C_D at $\psi = 90^{o}$ for a smooth pipe of the same length-to-diameter ratio obtained during the GALCIT wind tunnel test. Because of its smaller diameter, the Reynolds number of reinforcement rod will fall in this range during its entire trajectory.

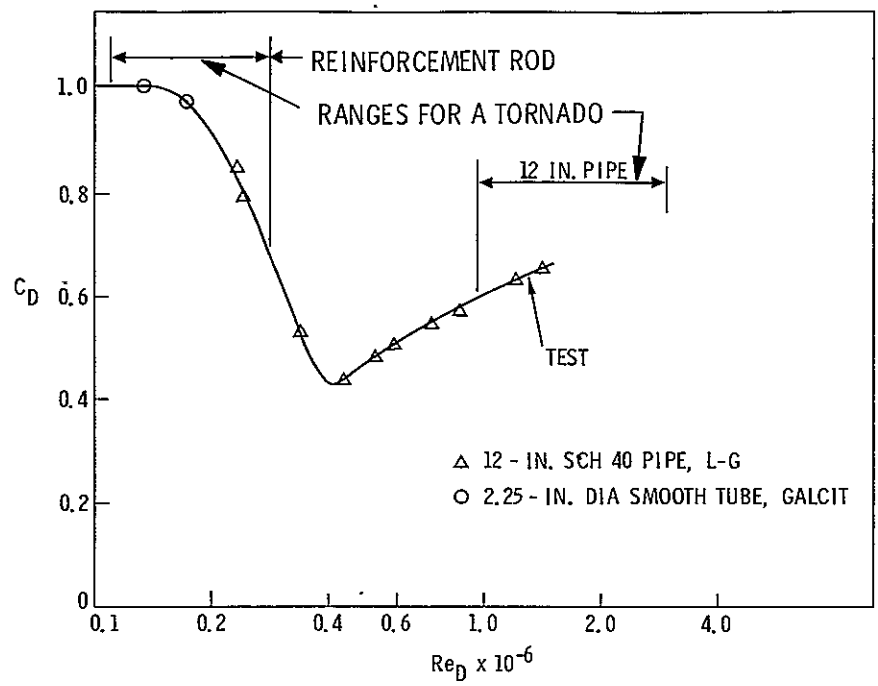

Fig. 3-17. Drag coefficient as a function of Reynolds Number for open circular cylinder, axis normal to flow, length-to-diameter ratio of 14.1, from sub- to supercritical regimes

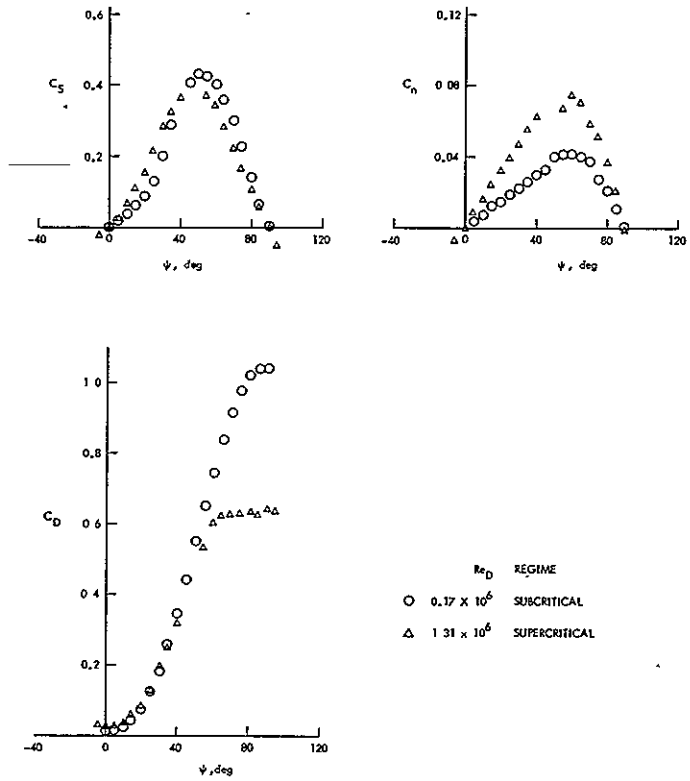

Fig. 3-18. Significant aerodynamic coefficients of open circular cylinder (length/diameter = 14.1) in subcritical and supercritical Reynolds Number regimes

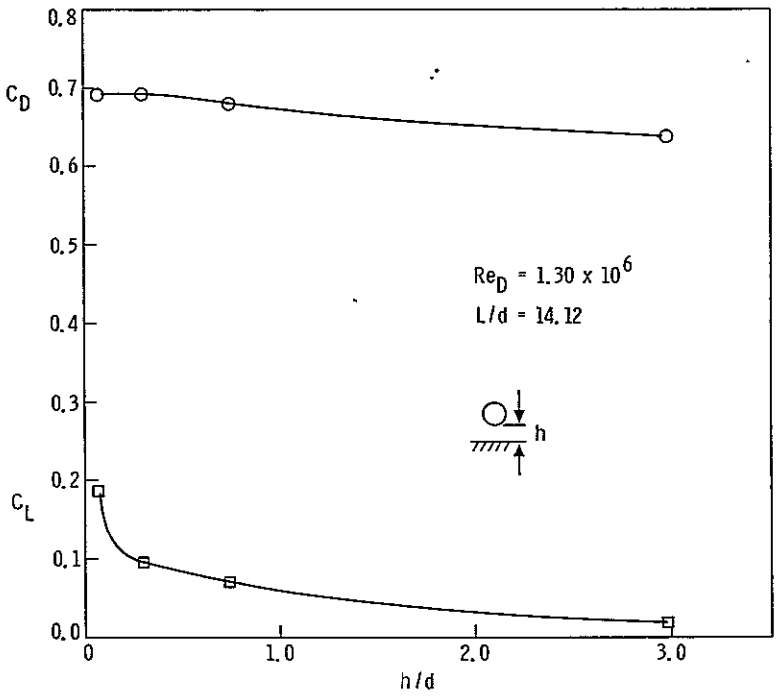

Fig. 3-19. Effect of distance from ground plane on the drag and lift coefficients of open circular cylinder (length/diameter = 14.1) normal to flow ($\psi = 90^{\circ}$) in supercritical Reynolds Number regime

In Fig. 3-18 this comparison between the GALCIT test at subcritical Reynolds number and the Lockheed-Georgia test at supercritical Reynolds number is extended to three wind-axis coefficients over a full quadrant in yaw for an open-ended pipe having a length-to-diameter ratio of 14.1 (the 12-in., schedule-40 pipe). The most important effect of the Reynolds number regime is on C_D, and even there is significant only for $\psi > 60^{\circ}$ although the effect on C_n is also important. In the trajectory calculations the supercritical aerodynamics coefficients were used for the 12-in. and 6-in. pipes and the subcritical values were used with the reinforcement rod.

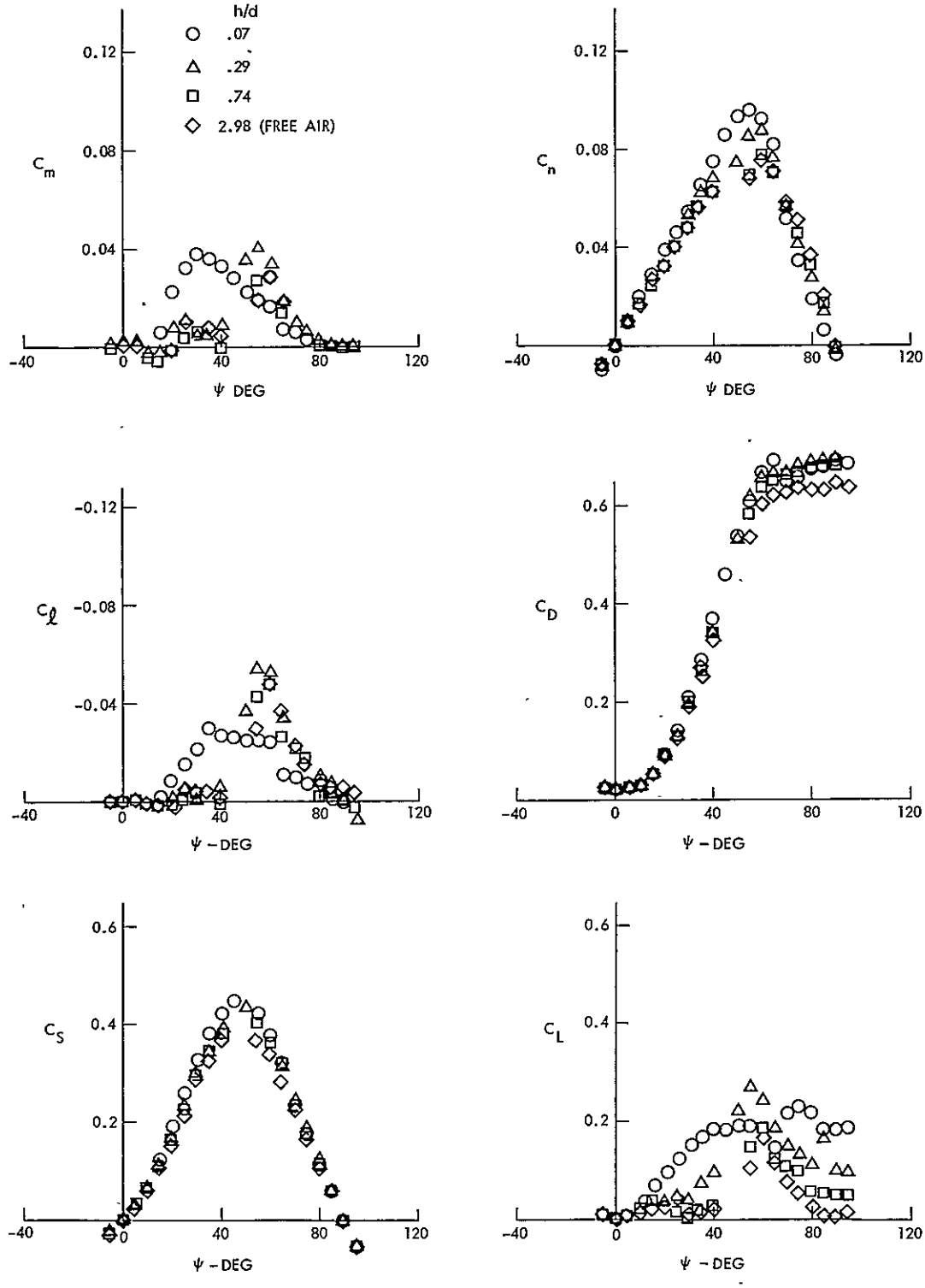

Fig. 3-20. Effect of distance from ground on the aerodynamic coefficients of an open circular cylinder (length/diameter = 14.1) as a function of yaw angle in the supercritical Reynolds Number regime.

The effect of the presence of the ground on the lift and drag coefficients of the pipe at $\psi = 90^{\circ}$ where the effect is greatest for the supercritical Reynolds number regime is shown in Fig. 3-19 and tabulated in Tables C-11 through C-13. The shapes of the curves are similar to those shown in Roshko, Steinolfson, and Chattoorgoon (1975), but the levels are lower because in the cited work the cylinder was two-dimensional and the Reynolds number subcritical. In both cases, the boundary layer thickness was approximately half the diameter of the cylinder. The most significant difference is the fact that in the three-dimensional case, the drag coefficient did not drop abruptly at a ground clearance of 0.5 diameter, as occurred in the two-dimensional case just cited but instead remains slightly above the free stream value, to the smallest value of h/d tested. The test values of h/d were 0.07, 0.29, 0.75 and 2.98. In the two-dimensional case (Roshko, Steinolfson, and Chattoorgoon 1975), free stream values of C_L and C_D were measured for h/d > 2.0; therefore, the h/d value at 2.98 may be considered as free of ground effects. The small positive value of C_L remaining at that height may be regarded as a support-interference effect.

In Fig. 3-20, the ground effect on the full-scale pipe as a function of yaw angle is shown for the six wind-axis coefficients. The drag coefficient C_D shows no ground effect up to a yaw angle of 35°. At higher angles the effect gradually increases up to the values at $\psi = 90^{\circ}$ shown in the previous figure. The ground effects on the side force coefficient C_S are relatively minor but appear to be greatest in the vicinity of $\psi = 45^{\circ}$, where the force is greatest. Some points at the higher ground clearances are missing in the $\psi = 45^{\circ}$ region because the unsteady forces were greatest there and considered dangerous to the wind tunnel balance system. Variation in the lift coefficient curves begins at yaw angles as low as $\psi = 10^{\circ}$ and the ground effect increases to its first maximum at $\psi = 40^{\circ}$; it then decreases up to $\psi = 65^{\circ}$ where it again increases to the second maximum from $\psi = 75^{\circ}$ to 90°. In the case of the pitching moment C_m the steady state free-air value should be zero over the entire quadrant due to the symmetry of the configuration. The small values measured are believed to be support interference effects. The ground effects are greatest at $20^{\circ} \leq \psi \leq 70^{\circ}$. For yawing moment C_n, the ground effects are largest in the same

mid range of yaw angles as they were for side force. This is not surprising since C_n is the sum of the moments induced by the side force and drag. The ground effect is not large for ψ near 90^o even though the effect on drag is greatest in that region because the moment arm approaches zero as ψ approaches 90^o. Again with the rolling moment C_ℓ, the free-air value should be zero due to symmetry, and the values shown are a combination of support interference and ground effects. The shape of the C_ℓ curve at h/d = 0.07 is quite different from all the others in the mid portion of the yaw range; this indicates that the ground effect on this coefficient is quite pronounced near the ground.

b. Full-scale Automobile Results

Figure 3-21 shows a comparison of the full-scale auto wind tunnel data with the sub-scale test data on the model automobile from the GALCIT test. This model had the overall proportions of the full-scale Dodge Dart but was in no sense a model of the actual vehicle. While the C_D, C_m and C_n curves show quite close agreement, the C_L, C_S and C_ℓ curves show a wider variation. These variations are believed to be due principally to differences in the two configurations but may also be caused partially by differences in support-interference effects. The many differences in details between the model (Figs. 3-5 and 3-6) and the full-scale car Fig. 3-12, 3-13, and 3-14 have apparently led to the sizeable differences in C_L in the middle range of yaw angles where the value for the model is near zero and in the vicinity of 0.6 for the full-scale car. The model support on the roof of the model may also have contributed to the difference by spoiling part of the flow over the roof of the model. In the case of C_S, the difference between model and full-scale results is in the opposite direction. No significant Reynold number-effects were observed in either the full scale or sub-scale tests.

Additional ground-effect data were obtained during the wind tunnel test of the full-scale Dodge Dart. Tables C-28 through C-31 present smoothed data for the vehicle with wheels on the tunnel floor ($\alpha = 0^o$) and at five and ten degrees angle of attack.

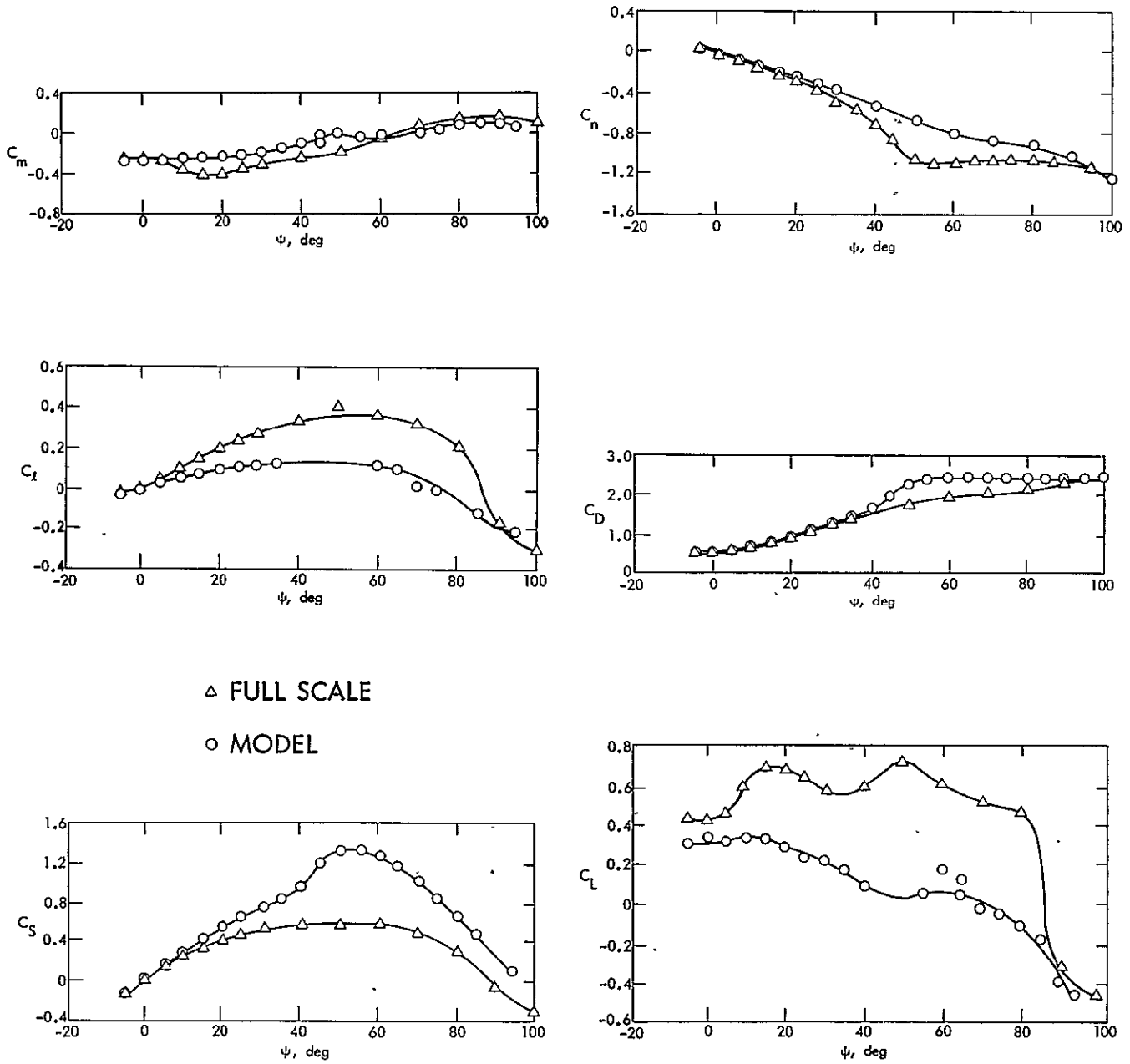

Fig. 3-21. Comparison of six-component aerodynamic data from 1974 Dodge Dart with data from 20%-scale generalized automobile model at $\alpha = 0°$ in free air

D. SCALE MODEL DROP TESTS

Analysis of motion picture data from 31 drops made from the roof of JPL Building 183 to the ground, a distance of 126 ft, produced the following results:

A circular cylinder, L/d = 14.1, was determined to have a tumbling resistance coefficient of 0.42 based on the reference area (length times diameter), with the variation of 7%. This coefficient represents the effective aerodynamic resistance of a tumbling body.* This variation is based on estimated equilibrium velocities for three drops, one each with initial axes of rotation at 0°, 45°, and 90° relative to horizontal. The initial rotational rate was about 108°/sec. The initial rotational mode (about a transverse axis) damped to a falling-leaf mode before returning to the rotational mode. The equilibrium velocity measured, therefore, resulted from motion in a combination of rotating and oscillating modes. In spite of this, the equilibrium velocity varied only from 29.0 to 30.0 ft/sec for the three drops with the various initial conditions described above.

No useful tumbling data were obtained from those cylinders having an L/d greater than 14.1 because rotational damping was too great. Even though moment of inertia was maximized by constructing the cylinders of styrofoam with weights at the tips, it was limited by the maximum weight which could reach equilibrium for an appreciable part of the 126-ft drop distance. The reduction of nonequilibrium data from the film was not feasible in these tests because the velocity did not vary smoothly with time due to its functional dependence on model attitude. Therefore, acceleration could not be determined with sufficient accuracy to be of use in determining the tumbling coefficient.

In the case of the car and van models which have only a single plane of symmetry, an additional complication occurred. The equilibrium velocity was a function of the angle between the longitudinal axis of the vehicle and the direction of motion. Models were launched with initial rotational velocity about the longitudinal axis which was horizontal. The axis of rotation would slowly precess, toward a nose downward direction, due mainly to the location of the center of gravity approximately 42% aft of the vehicle nose. Referenced to frontal

*Similar measurements on full-scale 12-in. pipes have been made by Costello and Stephenson 1978.

area, values of C_D = 3.18 and 2.49 were obtained (two drops) for the car and C_D = 2.74 for the van. An approximate value of 2.8 might be used for both vehicles. These coefficients are based on frontal area of the vehicles.

Although some drops were made with beam models, the photographic data were not reduced because all the models went into an autorotational mode of motion during the drop. As previously discussed by Billingsley and Brunk 1975 and in earlier work by Zipfel, it can be shown that dynamically similar motion for a scaled rotor can exist in the presence of a gravitational field only when ML = 1, and, in the presence of gyroscopic coupling (i.e., nonplane trajectory), only when M = 1, where M is the mass ratio between prototype and model, and L is the ratio of comparable linear dimensions. Since both of the above scaling laws can be satisfied only when L = 1, completely general scaling cannot be accomplished. Even for planar flight which occasionally occurred, the product of M and L can be made equal to unity only by making the model of material that is much more dense than the wood of the full-scale plank. In that case, equilibrium velocity would not have occurred within the drop distance of the test. Although no quantitative data could be obtained on the plank configuration, the tests were useful in that they indicated the possibility of an autorotational mode of motion for the plank configuration, with resultant gliding flight characteristics which are quite different from those usually assumed in the literature.

The drag coefficients obtained for the L/d = 14.1 cylinder and the motor vehicles are compared to values obtained by other methods in the "results" section (IV).

E. MISSILE AERODYNAMICS REFERENCE

Achenbach, E., 1971, Influence of Surface Roughness on the Cross-flow around a Circular Cylinder, J. Fluid Mech., Vol. 46, pp. 321-325.

Billingsley, J. and Brunk, J., July 1975, Autorotating Magnus Rotor Aero Design Handbook, Von Karman Gas Dynamics Facility, Arnold Engineering Development Center, Air Force Systems Command, Arnold Air Force Station, Tennessee, AEDC-TR-75-24, AFATL-TR-75-67.

Costello, J. and Stephenson, A., April 1978, Free Fall of Large Pipes, ASCE Proceedings J. of Engineering Mechanics.

Iotta, R. C., 1974, Velocities of Tornado Generated Missiles, ETR 1003, Ebasco Services, Incorporated

Redmann, G. H., Radbill, J. R., Marte, J. E., Dergarabedian, P., and Fendell, F. E., Feb. 1976, Wind Field and Trajectory Models for Tornado-Propelled Objects, EPRI 308, T. R. 1, Electric Power Research Institute, Palo Alto, California.

Roshko, A., Steinolfson, A., and Chattoorgoon, V., June, 1975, Flow Forces on a Cylinder Near a Wall or Near Another Cylinder, Proceedings of Second U.S. National Conference on Wind Engineering Research, IV-15-1 and 2, Fort Collins, Colorado.

Simiu, E. and Cordes, M., April 1976, Tornado-Borne Missile Speeds, NBSIR 76-1050, United States Nuclear Regulatory Commission, Washington, D.C.

Zipfel, P. (no date), Scaling of Vortex Gliders, MD Study No. 133, Munitions Development Division, Department of the Army, Fort Detrick, Maryland.

F. NOMENCLATURE FOR SECTION III

A	reference area
C_D ...	drag coefficient (wind axis)
C_L ...	lift coefficient (wind axis)
C_ℓ	rolling moment coefficient (wind axis)
C_m ...	pitching moment coefficient (wind axis)
C_N ...	normal force coefficient (body axis)
C_n ...	yawing moment coefficient (wind axis)
C_p ...	pitching moment coefficient (body axis)
C_S ...	side force coefficient (wind axis)
C_Y ...	side force coefficient (body axis)
d	body diameter
h	distance from ground to bottom of body
L	body length
q	dynamic pressure $(1/2\,\rho V^2)$
Re_D ...	Reynolds number, $\frac{\rho V d}{\mu}$
V	free stream air velocity
w	weight
X_{cp} ...	center of pressure
α	angle of attack
μ	air viscosity
ρ	free stream air density
ϕ	roll angle
ψ	angle of yaw

SECTION IV

APPLICATIONS AND RESULTS OF TRAJECTORY MODEL

A. INJECTION MODES AND INITIAL CONDITIONS

Injection modes are defined as the physical phenomena by which objects enter into the flow field of a tornado. It is the injection modes which determine the initial conditions of the tornado-missile flight. In the 6-D. O. F. trajectory program it is necessary to specify the initial values of the missile attitude and rotational velocity in addition to those which are also required for 3-D. O. F. trajectories, i. e., elevation, initial velocity of the center of gravity, and location relative to the storm center. Specification of the initial conditions in a rational manner is an important step toward predicting realistic missile trajectories for use in nuclear plant design. In this section a wide variety of injection modes is discussed and the rationale used to prescribe initial conditions for subsequent trajectory calculations is described.

In general, an object will become airborne when the net vertical force acting on the object is upward. The widely accepted characterization of the modes of missile injection as ramp, aerodynamic, or explosive appears to be adequate. However, recognition should be given to the fact that in many, if not most, instances a combination of the various modes may contribute to the initial conditions of injection. For the purposes of this report the three modes of injection are defined as follows.

1. Modes of Injection

In the ramp mode a part of the kinetic energy generated by the horizontal portion of the wind velocity vector, i. e., the radial and azimuthal components of the tornadic wind, is converted to a vertical orientation by means of a slope or ramp, up which a tumbling or rolling missile is propelled by the horizontal wind components until the end is reached and the missile is launched into the tornado flow field at some initial height with initial vertical, horizontal and rotational velocity components. The forces exerted on many of the missile configurations due to the horizontal components of the flow field can be considerable even for missiles which are initially at rest at ground level.

C-2

Injection from an above ground location such as from an elevated platform or truck or crane can be included under this mode of injection as a special case.

The principal force in the aerodynamic injection mode is lift; i. e., the aerodynamic force normal to the wind velocity resulting from the reduced pressure due to higher velocities over the upper surface. The pressure difference is the result of body shape or of proximity to the ground.

Another contributor to injection of the missile into the main flow field of the tornado is the aerodynamic force due to the vertical component of the wind. However, although this component is significant over much of the trajectory of some of the missile configurations, it must be zero at the ground and is negligible for any missile of concern here which is initially at rest on the ground.

The explosive mode of injection is related to the aerodynamic mode in that the vertical motion is imparted by a pressure differential; it differs in terms of the physical phenomenon imposing the differential. In the older concept of the "explosive" mode, the force was thought to be produced by the very rapid decrease in atmospheric pressure as a tornado moves across a hollow structure such as a building. The external pressure drop was believed to be sufficiently rapid so that the internal pressure of the structure was unable to remain in equilibrium, and a pressure differential was thereby created which led to disintegration of flimsy structures into numerous pieces, some of which resembled the missile configurations under consideration. Because many structures such as buildings have an appreciable leak rate to atmosphere, either by design or due to the nature of the construction, the full pressure differential between normal atmospheric pressure and the reduced atmospheric pressure of a point in the tornado is seldom realized. Bates and Swanson (1967) suggest that a pressure impulse equal to 0.1 of the full pressure differential may be an appropriate value for use in computing the effects of explosive injection. More recent work (Minor et. al., 1976) suggests that wind-induced forces are the principal cause of the "explosion effect" since outward acting forces exist on four of the five sides of a rectangular structure exposed to a linear wind. The following paragraphs explain how these injection modes are treated in trajectory calculations made in this program.

In both the explosive and aerodynamic injection modes the effective upward force acts only for a very short period of time and can be considered as an impulsive force. If one neglects any structural retaining forces, the vertical force balance can be written.

$$\frac{W}{g_0}\frac{dw}{dt} = F(t) - W \qquad \text{(IV-1)}$$

where W is the weight; w, the vertical velocity; and g_0 the constant in Newton's second law. Equation (IV-1) can be solved for the resulting vertical velocity:

$$w(t) = \frac{g_0}{W}\int_o^t F(t)dt - gt \qquad \text{(IV-2)}$$

After the missile has risen from the ground, a vertical component of the tornadc wind field which varies with height, and therefore time, acts and the expression for the total impulse can be expanded to

$$\int_o^t F(t)dt = \int_o^t F_1(t)dt + \int_o^t F_2(t)dt \qquad \text{(IV-3)}$$

where the vertical wind force is

$$F_2 = \frac{1}{2}\rho_a V_z^2 C_D A \qquad \text{(IV-4)}$$

where ρ_a is atmospheric density, C_D is coefficient of drag, V_z is the vertical component of velocity, A is the reference area, and F_1 represents either the impulsive force due to the rapid pressure reduction (explosive injection mode) or the impulsive lift due to the horizontal wind (aerodynamic injection mode). In the former case,

$$F_1 = \Delta p(t)A \qquad \text{(IV-5)}$$

and in the latter,

$$F_l = \frac{1}{2} \rho_a (u^2 + v^2) C_L A \qquad \text{(IV-6)}$$

where C_L is the coefficient of lift.

The aerodynamic coefficients, C_D in eq (IV-4) and C_L in eq (IV-6) are, in general, functions of the missile attitude but are usually approximated as constants in injection calculations in the literature because of the short times involved. However, because the details of the near-ground flow field are included in this fluid-dynamic model of the tornado and because the aerodynamic coefficients for the configurations have been experimentally measured, it is not necessary to approximate the integrals of eq (IV-3) for aerodynamic injection by a constant force acting over some arbitrary effective time as was necessary in the past (Paddleford 1969 and Lee 1973). Instead, they can be numerically evaluated within the computer program and the appropriate variation of force components used in the trajectory computation. In the aerodynamic mode the initial conditions are those which immediately precede the onset of the tornado.

For cases which consider the ramp or explosive mode of injection somewhat more arbitrary assumptions for the injection velocity components based loosely on the geometric and inertial characteristics of the missile configuration must be used. In the explosive ejection cases, the method presented by Paddleford, 1969 is used to estimate an equivalent injection height. This approach analyzes the mode in terms of two processes acting in parallel to reduce the pressure differential applied by the tornado; namely, the flow of air out through openings created by the building reaction and secondly, the increase in contained volume due to building reaction i. e., the movement of the roof and walls. To reduce the degree of approximation, and for greater consistency with the aerodynamic mode of injection, the injection height, which was computed as the result of an impulsive force, is converted to an initial velocity which would result in that height by assuming uniform deceleration due to gravity:

$$w = \sqrt{2gz} \qquad \text{(IV-7)}$$

where z is the injection height and w is the initial vertical velocity. The use

of this simple approach may not be overly realistic but can be expected to produce conservative results (i.e., injection heights or velocities are greater than the real case). For the initial conditions of this report the explosive effect caused an insignificant initial velocity and explosive injection runs are therefore not included in the results.

2. Rationale for Selection of Initial Conditions

The following rationale was used to develop the initial conditions and injection modes for each of the missile configurations. These conditions and modes are consistent with current design criteria. Physical characteristics and initial conditions are given for each configuration in Tables 4-2 through 4-6.

a. Utility Pole

The maximum initial height of 40 ft is assumed to occur while the pole is being carried by a crane prior to emplacement in the ground. The maximum horizontal velocity of 30 mph is taken to be that of a truck carrying the pole. The maximum vertical velocity is taken as the velocity of a pole bouncing along the ground end over end. In terms of orientation, $\alpha = 0^{\circ}$, $\psi = 90^{\circ}$ is a rolling pole or pole on a truck in a cross wind while $\alpha = 45^{\circ}$, $\psi = 0^{\circ}$ is a pole bounding along the ground end over end. The variation of center of gravity offsets allows for the possibility of attachments and simulates to some extent the effects of asymmetric aerodynamics. The offset is assumed to be produced by a point mass located at one end of the configuration which added to the total weight.

In addition to the initial conditions developed for this work, runs were made using the initial conditions of Simiu and Covdes 1967 for purposes of comparison. In those runs the initial height of 40 m (131.2 ft) was greater than what is referred to as maximum initial height in this section.

b. 12-in. Pipe

Initial height could be as high as the top floor of the highest structure in the plant (taken as 100 ft). The initial assumed maximum angular velocity of 10 rpm could be generated either by tumbling end for end in the manner of the

utility pole, or by a wind-assisted flip as it rolls off an upper floor. The maximum initial conditions for the horizontal and vertical velocity components of 40 and 20 mph, respectively occur in bouncing along the ground with a center of gravity offset of 10%.

c. 6-in. Pipe

The same rationale for initial height and velocity components developed for the 12-in. pipe applies. The initial angular velocity was increased to 15 rpm because of the smaller moment of inertia in tumbling.

d. Reinforcement Rod

Again, the same rationale for initial height and velocity components as was used for the 12-in. pipe applies. No offset of the center of gravity is considered, and angular velocity as great as 30 rpm may occur, because of the much smaller moment of inertia in tumbling.

A few preliminary runs using the explosive injection equations and a pressure differential well beyond what would be expected in even the most severe tornado produced an effect equivalent to an initial height of only 15 feet which had a negligible effect on the trajectory so the explosive injection mode was not considered further in the results section.

e. Wood Plank

For the aerodynamic injection cases the same rationale for height, linear velocities and center of gravity offset used for the 12-in. pipe is again employed. The higher rotational velocity results from the lower moment of inertia. Explosive injection was also considered for this configuration under the assumption that the plank was part of the structural support for the roof of a warehouse type of building having linear dimensions of 90-ft and experiencing a pressure differential of 0.15 pis. By use of the method of Lee 1973, the explosive injection height proved to be on the order of one foot, as would occur with an initial vertical velocity of 5 mph. Again, the effect on the trajectory was negligible and explosive modes are not included in the results.

f. Automobile

For purposes of comparison with Simiu and Cordes 1976, an initial height of 40 m (131.2 ft) and zero initial velocity is used for some of the automobile trajectories. In other trajectories we have chosen to assume the case of a car on the ground running away from the tornado at 30 and 60 mph as well as a stationary case.

Some consistent sets of initial conditions which result from the above rationales have been used as initial conditions in the trajectories contained in this section. These cases may not always represent worst cases but they are at least self-consistent and have been logically evolved. Many other scenarios could be postulated which would lead to other sets of self-consistent initial conditions but the resultant trajectories should not differ greatly from those computed in this report. This approach avoids the problem which can arise in a more systematic variation of initial parameters; namely, that the worst case trajectories may result from logically inconsistent sets of initial conditions. For example, a car at a 130 ft. initial height which might represent a multi-story parking structure would not logically also be moving at 60 mph.

Detailed results of trajectory calculations are given below using both the initial conditions of Simiu and Cordes and the initial conditions discussed in Section IVA for each of the Spectrum II missile types.

B. SIX-DEGREE-OF-FREEDOM MISSILE TRAJECTORIES

Because the missile trajectory characteristics derived in Simiu and Cordes 1976 have been used as the basis for the Spectrum II missiles in the N.R.C. Standard Review Plan, Revision 1 (NUREG-75/087), a detailed comparison of their findings with results using the data and methods of this report has been conducted. Comparisons are made between Simiu and Cordes' results and the results obtained using the methods of this report with the Simiu and Cordes

tornado types[1] 1, 2, and 3, henceforth referred to as the Region I, II and III tornadoes and the JPL tornado[2]. The results in terms of maximum horizontal velocity are summarized in Table 4-1.

In general, the comparison shows that the JPL values for maximum velocity for the 6 D. O. F. trajectories which use experimental values of aerodynamic coefficients varying with attitude are considerably less than the 3 D. O. F. trajectory values of Simiu and Cordes. Of special importance are the comparisons for the 12-inch pipe and automobile. For the 12-inch pipe the JPL results give maximum horizontal velocities which are 53%, 54% and 57% of those obtained by Simiu and Cordes for the Region I, II, and III design tornadoes, respectively. For the automobile, initially perpendicular to the storm center direction, the JPL values are 54%, 38%, and 15% of the Simiu and Cordes values.[3] The last two columns of Table 4-1 give results for the JPL tornado with 3 D. O. F. trajectories based on the flight parameter values of Simiu and Cordes and with 6 D. O. F. trajectories. Comparison of these columns with results for the Region II tornado, which is closest in swirl velocity to the JPL tornado, shows that they are approximately equal or less in all cases.

1. Cylindrical Shapes

Effects of the release mechanisms which were postulated in Part A of this section are given in Tables 4-2 through 4-5 which summarize a large number of computer runs. The dimensions and weights of the missiles are given in the respective table headings. All runs presented in this section use the default values of wind field eddy viscosity parameters (ν=1 ft^2/sec, α=3.5 ft, β=270 ft).

These tables also include the cylindrical configurations of the Spectrum II missiles which were run for comparison with Simiu and Cordes using Region I, II and III tornadoes and the same initial conditions except for specification of an

---

[1] These correspond to the interim regional design tornadoes as given by Markee, Beckerly and Sanders 1974 for Regions I, II and III, respectively.

[2] JPL maximum probable tornado: V_{max} = 225 mph, U_{tc} = 30 mph, R_1 = 0.1 mile.

[3] For an initial orientation parallel to the storm direction the JPL values are 41%, 29%, and 24% of the Simiu and Cordes values.

Table 4-1. Comparison of maximum horizontal velocity between the results of Simiu and Cordes and of this report for Spectrum II missiles. Initial height of 131.23 ft (40 m) and initial velocity of zero. Initial orientation long axis perpendicular to storm direction

Missile	Mass (kg)	Dimensions (m)	Maximum Horizontal Velocity (m/s)							
			Region I		Region II		Region III		JPL Tornado	
			S&C	JPL	S&C	JPL	S&C	JPL	S&C	JPL
A. Wood Plank	52	JPL: 0.102 x 0.305 x 3.66 S&C: 0.092 x 0.289 x 3.66	83	63	70	58	58	51	70	55
B. 6-in Sch. 40 Pipe	130	0.168D x 4.57	52	24	42	15	10	5	35	17
C. 1-in. Steel Rod		0.0254D x 0.914	51	51	40	40	38	6	33	18
D. Utility Pole	510	0.343D x 10.62	55	53	48	44	26	14	39	21
E. 12-in Sch 40 Pipe	340	0.324D x 4.57	47	25	28	15	7	4	29	13
F. Automobile[1]	1810	JPL: 5.15 x 1.77 x 1.37 S&C: 5.00 x 2.01 x 1.31	59	32	42	20	41	7	46	23

[1] Proportions taken from an actual automobile were used for the JPL test model.

Table 4-2. Utility Pole, 35 ft x 1.12 ft O. D., 1495 lb (1124 lb runs 8-12), super critical Re

Run	CG Offset % Total Length	Height z ft	Velocity u_0 mph	Velocity w_0 mph	Angular Velocity w_{y0} rpm	Pitch Deg	Yaw Deg	Roll Deg	Injection Mode	V_{max} mph	u_{tc} mph	r_1 mile	x_{tco} mile	y_{tco} mile	z_{max} ft	Speed max fps	Height @ max speed	Range ft
1	0	40	0	0	0	0	90	0	crane, aero	225	30	0.1	0	0.0999	40.0	113.0	0.0	106
2	0	40	0	0	0	45	180	0	crane, aero	225	30	0.1	0	0.0999	44.8	128.0	0.0	151
3	0	10	30	20	10	45	180	0	bouncing, aero	225	30	0.1	0	0.0999	36.4	129.6	0.0	268
4	+10	10	30	20	10	45	180	0	bouncing, aero	225	30	0.1	0	0.0999	35.5	120.7	0.0	250
5	-10	10	30	20	10	45	180	0	bouncing, aero	225	30	0.1	0	0.0999	30.0	103.4	0.0	163
6	+15	10	30	20	10	45	180	0	bouncing, aero	225	30	0.1	0	0.0999	34.1	114.3	0.0	232
7	-15	10	30	20	10	45	180	0	bouncing, aero	225	30	0.1	0	0.0999	28.7	96.1	0.0	153
8	0	10	60	0	0	0	90	0	truck, aero	290	70	0.0284	0.0284	0	288.2	196.0	2.9	948
9	0	131.2	0	0	0	0	90	0	aero S&C	240	60	0.0284	0.0284	0	149.3	168.7	1.3	429
10	0	131.2	0	0	0	0	90	0	aero S&C	190	50	0.0284	0.0284	0	132.0	73.5	0.0	51
11	0	131.2	0	0	0	0	3DOF	0	aero S&C	225	30	0.1	0.0999	0	131.2	146.3	0.8	334
12	0	131.2	0	0	0	0	90	0	aero S&C	225	30	0.1	0.0999	0	131.2	108.3	0.0	148

Note: The 1124-lb weight is used by Simiu and Cordes who took it from (NUREG-75/087).
The 1495-lb weight was common in the literature at the time runs 1-7 were made

Table 4-3. 12-inch pipe, 15 ft x 1.06 ft O. D., 743 lbs, super critical Re

Run	CG Offset %	Height ft	Velocity u_0 mph	Velocity w_0 mph	Angular Velocity ω_0 rpm	Pitch Deg	Yaw Deg	Roll Deg	Injection Mode	V_{max} mph	u_{tc} mph	r_1 mile	x_{tco} mile	y_{tco} mile	Δ_{max} ft	Speed max fps	Height @ max speed ft	Range ft
1	0	6	0	0	0	45	180	0	aero, pile	225	30	0.1	0	0.0999	6.4	54.9	0	29
2	0	20	0	0	0	45	180	0	aero, pile	225	30	0.1	0	0.0999	20.9	82.2	0	58
3	0	40	0	0	0	45	180	0	aero, pile	225	30	0.1	0	0.0999	41.1	106.2	0	89
4	0	100	0	0	0	45	180	0	aero, pile	225	30	0.1	0	0.0999	101.6	135.6	0	201
5	0	6	0	0	-10	45	180	0	aero, pile	225	30	0.1	0	0.0999	6.1	47.5	0	20
6	0	20	0	0	-10	45	180	0	aero, pile	225	30	0.1	0	0.0999	20.3	73.9	0	43
7	0	100	0	0	-10	45	180	0	aero, pile	225	30	0.1	0	0.0999	100.5	128.7	0	160
8	0	6	0	40	0	45	180	0	aero, bouncing	225	30	0.1	0	0.0999	62.7	134.6	0	281
9	0	20	0	40	0	45	180	0	aero, bouncing	225	30	0.1	0	0.0999	86.0	143.4	0	321
10	0	100	0	40	0	45	180	0	aero, bouncing	225	30	0.1	0	0.0999	166.9	175.3	0	477
11	0	100	40	0	-10	45	180	0	aero, bouncing	225	30	0.1	0	0.0999	100.0	157.5	0	269
12	0	100	40	0	-10	45	90	0	aero, rolling	225	30	0.1	0	0.0999	100.0	157.4	0	263
13	10	100	40	20	-10	45	180	0	aero, bouncing	225	30	0.1	0	0.0999	118.2	157.6	0	365
14	0	80	0	0	0	45	180	0	aero, pile	225	50	0.1	0	+0.0999	82.5	139.8	0	186
15	0	60	0	0	0	45	180	0	aero, pile	225	50	0.1	0	+0.0999	62.2	131.6	0	141
16	0	30	0	0	0	45	180	0	aero, pile	225	50	0.1	0	+0.0999	31.8	106.5	0	84
17	0	60	0	0	-10	45	180	0	aero, pile	225	50	0.1	0	+0.0999	60.8	124.0	0	108
18	0	80	0	0	-10	45	180	0	aero, pile	225	50	0.1	0	+0.0999	80.9	132.8	0	144
19	0	40	0	0	-10	45	180	0	aero, pile	225	50	0.1	0	+0.0999	40.7	107.1	0	77
20	0	30	0	0	-10	45	180	0	aero, pile	225	50	0.1	0	+0.0999	30.7	95.0	0	63
21	0	32	0	0	0	45	180	0	aero, pile	225	50	0.1	0	+0.0999	33.9	180.8	0	88
22	0	35	0	0	0	45	180	0	aero, pile	225	50	0.1	0	+0.0999	36.9	112.3	0	93
23	0	60	0	0	-10	45	180	0	aero, pile	225	30	0.1	0	+0.0999	60.4	113.8	0	95
24	0	80	0	0	-10	45	180	0	aero, pile	225	30	0.1	0	+0.0999	80.5	123.5	0	126
25	0	40	0	0	-10	45	180	0	aero, pile	225	30	0.1	0	+0.0999	40.4	97.0	0	69
26	0	30	0	0	-10	45	180	0	aero, pile	225	30	0.1	0	+0.0999	30.3	56	0	86
27	0	60	0	0	0	45	180	0	aero, pile	225	30	0.1	0	+0.0999	61.3	121	0	122
28	0	80	0	0	0	45	180	0	aero, pile	225	30	0.1	0	+0.0999	81.5	129.6	0	159
29	0	30	0	0	0	45	180	0	aero, pile	225	30	0.1	0	+0.0999	31.0	95.2	0	74
30	0	33	0	0	0	45	180	0	aero, pile	225	30	0.1	0	+0.0999	34.0	88.8	0	78
31	0	35	0	0	0	45	180	0	aero, pile	225	30	0.1	0	+0.0999	36.0	101.1	0	81
32	0	6	0	0	0	45	180	0	aero, pile	225	30	0.1	0	0	6.4	54.8	0	29
33	0	131.2	0	0	0	0	90	0	aero S&C	290	70	0.0284	0.0284	0	136.6	118.2	0	156
34	0	131.2	0	0	0	0	90	0	aero S&C	240	60	0.0284	0.0284	0	131.2	80.2	0	66
35	0	131.2	0	0	0	0	90	0	aero S&C	190	50	0.0284	0.0284	0	131.2	78.2	0	38
36	0	131.2	0	0	0	3DOF			aero S&C	225	30	0.1	0	0.0999	131 2	123 8	0	217
37	0	131.2	0	0	0	0	90	0	aero S&C	225	30	0.1	0	0.0999	131 2	97.4	0	81

Table 4-4. 6-inch pipe, 15 ft x 0.521 ft O. D., 285 lb, super critical Re

Run	CG Offset % Total Length	Height ft	Velocity u_0 mph	Velocity w_0 mph	Angular Velocity ω_{yo} rpm	Pitch Deg	Yaw Deg	Roll Deg	Injection Mode	V_{max} mph	u_{tc} mph	r_1 mile	x_{tc}	y_{tc} mile	z_{max} ft	Speed max fps	Range ft
1	0	100	40	0	-15	45	180	0	aero, bouncing	225	30	0.1	0	0.0999	100.6	173.6	432
2	0				-15	0	90	0	aero, rolling	225	30	0.1	0	0.0999	100	187.0	393
3	10	100	40	20	-15	45	180	0	aero, bouncing	225	30	0.1	0	0.0999	130.6	170.6	505
4	-10	100	40	20	-15	45	180	0	aero, bouncing	225	30	0.1	0	0.0999	118.7	163.4	397
5	15	100	40	20	-15	45	180	0	aero, bouncing	225	30	0.1	0	0.0999	128.5	162.2	479
6	-15	100	40	20	-15	45	180	0	aero, bouncing	225	30	0.1	0	0.0999	117.4	159.6	363
7	0	131.2	0	0	0	0	90	0	aero S&C	290	70	0.0284	0.0284	0	143.5	120.2	135
8	0	131.2	0	0	0	0	90	0	aero S&C	240	60	0.0284	0.0284	0	134.5	86.3	72
9	0	131.2	0	0	0	0	90	0	aero S&C	190	50	0.0284	0.0284	0	131.2	74.6	52
10	0	131.2	0	0	0		3DOF		aero S&C	225	30	0.1	0	0.0999	131.2	136.8	282
11	0	131.2	0	0	0	0	90	0	aero S&C	225	30	0.1	0	0.0999	131.2	99.7	114

Table 4-5. Reinforcement Rod, 3 ft x 0.0833 ft O.D., 8 lb, subcritical Re

Run	CG Offset % Total Length	Height ft	Velocity u_0 mph	Velocity w_0 mph	Angular Velocity ω_{yo} rpm	Pitch Deg	Yaw Deg	Roll Deg	Injection Mode	V_{max} mph	u_{tc} mph	r_1 mile	x_{tco} mile	y_{tco} mile	z_{max} ft	Speed max fps	Height @ max speed ft	Range ft
1	0	100	40	0	-30	45	180	0	bouncing, aero	225	30	0.1	0	0.0999	100.3	182.3	0	314
2	0	100	40	0	-30	9	90	0	rolling, aero	225	30	0.1	0	0.0999	100.0	228.4	0.2	497
4	0	45	0	0	-30	0	90	0	rolling, aero	225	30	0.1	0	0.0999	45.0	158.0	0.4	206
5	+10	45	0	0	-30	0	90	0	rolling, aero	225	30	0.1	0	0.0999	45.0	128.5	0	138
6	-10	45	0	0	-30	0	90	0	rolling, aero	225	30	0.1	0	0.0999	45.0	131.7	0	176
7	0	10	40	0	0	0	90	0	rolling, aero	225	30	0.1	0	0.0999	10.0	116.9	0	70
8	+15	45	0	0	-30	0	90	0	rolling, aero	225	30	0.1	0	0.0999	45.0	122.3	0	122
9	-15	45	0	40	-30	0	90	0	rolling, aero	225	30	0.1	0	0.0999	45.0	112.3	0	122
10	0	131.2	0	0	0	0	90	0	aero S&C	290	70	0.0284	0.0284	0	164.9	187.0	0	571
11	0	131.2	0	0	0	0	90	0	aero S&C	240	60	0.0284	0.0284	0	135.7	149.3	0	171
12	0	131.2	0	0	0	0	90	0	aero S&C	190	50	0.0284	0.0284	0	131.2	68.0	0	65
13	0	131.2	0	0	0		3DOF		aero S&C	225	30	0.1	0	0.0999	131.2	131.7	0	255
14	0	131.2	0	0	0	0	90	0	aero S&C	225	30	0.1	0	0.0999	131.2	107.5	0	113

initial orientation (worst case) not required by the 3 DOF of Simiu and Cordes. Table 4-1 shows the direct comparisons in terms of maximum horizontal velocity. The difference is greatest for the weaker tornadoes. An interesting exception to the general rule is the 1 in. dia. steel rod where identical results were obtained for the Region I and II tornadoes. In both bodies of work this configuration was considered to fly at subcritical Reynolds number. All other cylindrical configurations were considered to be in the super-critical regime throughout their trajectories by both groups.

a. Utility Pole

Utility pole trajectories are tabulated in Table 4-2. The bouncing/aerodynamic cases have the greatest range (268 ft) and velocity (130 fps). Although the crane cases, runs 1 and 2, have the greatest initial height and the truck case, runs 3-7 have the greatest initial horizontal velocity, a combination of initial horizontal and vertical velocity seems to be most effective in producing speed and range. In all cases examined, the effect of offsetting the center-of-gravity of the pole by adding weight at one end is to reduce the speed and range. Orientation is seen to be important for the same shift in c.g..

b. 12-inch Pipe

Twelve inch schedule 40 pipe trajectories are collected in Table 4-3 for the initial conditions postulated in Part A of this section. Three types of aerodynamic injection mechanisms are represented: 1) injection from a pile, 2) bouncing injection, and 3) rolling injection. The greatest ranges and speeds were attained by bouncing cases injected from a 100 ft structure. Initial angular velocity, which was evaluated in a number of cases appears to reduce both impact speed and range.

c. 6-inch Pipe

Six-inch pipe trajectories are summarized in Table 4-4. The six-inch pipe generally flies farther and faster than the 12-in. pipe, as has been stated above, but since the 12-in. pipe is more than twice as heavy, it has a much larger terminal momentum for the same impact speed. The bouncing/

aerodynamic injection cases are interesting because of the large difference in the range of the 10 percent offset initial conditions for opposite orientation although the speed is only slightly affected.

d. Reinforcement Rod

Reinforcing rod trajectories are summarized in Table 4-5. The speeds and ranges are generally less for the reinforcing rod than for the 6-in. pipe (the other small cylindrical missile) for the same wind field and initial conditions. Because of the small diameter of the bar, subcritical Reynolds number aerodynamic coefficients were used in these computations making the difference smaller than it would have been if both missiles had the same Reynolds number range. Note that as in other missiles considered above the initial orientation of an asymmetric missile has an important effect on its speed and range.

2. Plank

Plank trajectories are summarized in Table 4-6 where the dimensions and weight are given. The computations for the plank missle are unique because the plank is the only noncylindrical shape for which a complete set of aerodynamic coefficients is available at roll angles of 30° and 60° as well as 0° and 90°. This is important because some of the coefficients peak at intermediate values of roll angle.

Trajectories for the plank exhibit the longest ranges and highest velocities of any of the trajectories considered. Examination of the complete output (not given in this report) for run 3 which shows the longest range (818 ft) shows higher angular velocities about the long axis (about 4 revolutions per second) during most of the trajectory. Autorotational effects are a function of this angular velocity but were not considered in this run. The speed also oscillates during most of the time of the trajectories. This missile was considered because it was included in the NRC list, however, the speed and range are probably academic because the wooden missile can be expected to disintegrate into splinters on impact.

3. Automobile

Because of the attention drawn to the automobile as a potential critical

Table 4-6. Plank, 12 ft x 1 ft x 0.333 ft, 200 lb (runs 13-17 115 lb)[1]

Run	CG Offset % Total Length	Height z ft	Velocity u_0 mph	Velocity w_0 mph	Angular Velocity ω_{yo} rpm	Pitch Deg	Yaw Deg	Roll Deg	Injection Mode	V_{max} mph	u_{tc} mph	r_1 mile	x_{tco} mile	y_{tc} mile	z_{max} ft	Speed max fps	Height @ max speed	Range ft
1	0	100	40	0	-15	45	180	0	bouncing, aero	225	30	0.1	0	0.0999	102.9	243.3	4.3	642
2	0	100	40	0	-15	45	180	60	bouncing, aero	225	30	0.1	0	0.0999	101.9	224.3	21.0	486
3	0	100	40	0	-15	45	180	90	bouncing, aero	225	30	0.1	0	0.0999	102.5	232.7	66.4	818
4	0	100	0	0	0	45	180	0	aero	225	30	0.1	0	0.0999	106.4	208.0	10.5	573
5	0	100	0	0	0	45	180	60	aero	225	30	0.1	0	0.0999	104.8	215.4	1.2	408
6	0	100	0	0	0	45	180	90	aero	225	30	0.1	0	0.0999	104.9	237.2	7.0	678
7	0	100	0	0	-15	45	180	0	aero	225	30	0.1	0	0.0999	102.0	215.2	2.5	550
8	0	100	0	0	-15	45	180	60	aero	225	30	0.1	0	0.0999	103.3	215.3	12.8	447
9	0	100	0	0	-15	45	180	90	aero	225	30	0.1	0	0.0999	129.9	259.7	118.2	1175
10	-30	100	0	0	-15	45	180	0	aero	225	30	0.1	0	0.0999	102.5	162.3	0	279
11	-30	100	0	0	-15	45	180	60	aero	225	30	0.1	0	0.0999	104.9	192.5	1.8	447
12	-30	100	0	0	-15	45	180	90	aero	225	30	0.1	0	0.0999	101.1	172.7	0.3	462
13	0	131.2	0	0	0	0	90	90	aero S&C	290	70	0.0284	0.0284	0	504.5	227.1	301.3	1800
14	0	131.2	0	0	0	0	90	90	aero S&C	240	60	0.0284	0.0284	0	361.7	197.0	327	1142
15	0	131.2	0	0	0	0	90	90	aero S&C	190	50	0.0284	0.0284	0	232.9	170.2	215	651
16	0	131.2	0	0	0		3DOF		S&C 3DOF	225	30	0.1	0	0.0999	138.4	228.3	135.2	985
17	0	131.2	0	0	0	0	90	90	S&C 6DOF	225	30	0.1	0	0.0999	131.2	187.5	0.6	532

Note: The 115 lb weight is used by Simiu and Cordes who took it from (NUREG-75/087).
The 200 lb weight was common in the literature at the time runs 1-12 were made.

missile configuration in Simiu and Cordes, 1976, special consideration has been given to the configuration. In the current work the availability of experimental measurements and the use of an improved wind field model together make possible more realistic trajectory computations.

The capability of the trajectory program to handle non-cylindrical bodies is illustrated by the following computation of the trajectory of a compact car. The trajectory program treats objects which have three perpendicular planes of symmetry. In reality, the car has only one plane of symmetry, but since the wind tunnel data are available in only one octant of the unit sphere, symmetry has been specified to approximate the unavailable data. In order to enforce the symmetry, the wind tunnel data had to be modified on the boundaries of symmetry. For example, C_L was made to pass through zero at zero pitch angle so that positive pitch angle data could be mapped into negative pitch angles. The pitching moment was also set zero at zero pitch for the same reason.

Aerodynamic coefficients tabulated for the car in Appendix C are referenced to the three sting (mount) orientations. These were mapped into one consistent coordinate system for use in the computer program and transformed to a set of axes through the centroid of the volume. The orientations are specified relative to the wind vector by a pitch angle α followed by a roll angle ϕ. The transformed modified coefficients are given in Table 4-7. The moments and products of inertia of the car were estimated by assuming it to be made up of seven pieces: chassis and wheels, two sides, top, engine and transmission, gas tank, and differential. The properties of these components are given in Table 4-8 and the resulting inertia matrix in the Table 4-9. The center of gravity is 0.2 ft in front of the centroid of the volume and 0.9 ft below. Note from Table 4-9 that there are nonzero products of inertia terms.

As discussed in Section III, full-scale car aerodynamic data were obtained, but only for a sweep on yaw angle. Therefore, the pitch angle sweep data had to be supplied from the subscale wind tunnel tests. The lift coefficient displayed the greatest difference between the full scale and model data. However, the lift coefficient in the yaw sweep data is not used in the computer program due to the symmetry requirements enforced by mapping aerodynamic data from one octant of the unit sphere onto the whole sphere. The neglected lift force is perpendicular to the plane formed by the wind vector and the car longitudinal axis and would not increase the tumbling rate.

Table 4-7. Transformed Aerodynamic Coefficients for Car from Subscale Data

ϕ (deg) = 0 α (deg)	C_D	C_S	C_L	C_l	C_n	C_m
0.	0.4970	0.0000	0.0000	0.0000	0.0000	0.0000
5.	0.5400		0.1840		0.1109	
10.	0.6900		0.5670		0.1983	
15.	0.8830		1.0160		0.2646	
20.	1.1690		1.4120		0.3473	
25.	1.4700		1.7630		0.4096	
30.	1.8300		1.9960		0.4369	
35.	2.2640		2.1760		0.5682	
40.	2.6410		2.3500		0.5103	
45.	3.0300		2.4510		0.5497	
50.	3.3180		2.4340		0.5562	
55.	3.6150		2.3450		0.5649	
60.	3.6040		2.2100		0.5768	
65.	3.9450		2.0280		0.5357	
70.	4.5420		1.9980		0.4666	
75.	4.8840		1.8950		0.4732	
80.	5.0220		1.3600		0.3954	
85.	5.0400		0.7630		0.2750	
90.	5.0500	0.0000	0.0000	0.0000	0.0000	0.0000
ϕ (deg) = 90 α (deg)	C_D	C_S	C_L	C_l	C_n	C_m
0.	0.4970	0.0000	0.0000	0.0000	0.0000	0.0000
5.	0.5220		0.1600		0.0010	
10.	0.6300		0.2940		0.0300	
15.	0.7500		0.4550		0.0734	
20.	0.9100		0.5800		0.1041	
25.	1.0830		0.6820		0.1274	
30.	1.2100		0.7650		0.1291	
35.	1.3800		0.8480		0.1326	
40.	1.5700		0.9780		0.1384	
45.	1.9190		1.2090		0.1861	
50.	2.2360		1.3340		0.2044	
55.	2.3530		1.3600		0.2595	
60.	2.3700		1.2790		0.2797	
65.	2.3800		1.1660		0.2811	
70.	2.3700		1.0340		0.2624	
75.	2.3600		0.8750		0.2339	
80.	2.3500		0.6880		0.1986	
85.	2.3400		0.4880		0.1558	
90.	2.3300	0.0000	0.0000	0.0000	0.0000	0.0000

Table 4-8. Inertial Properties of Car Components

Part No.	Component Name	Weight lb	Location x ft	Comp. y ft	CG z ft	Comp. I about own CG		
						I_{xx} lb_m-ft^2	I_{yy} lb_m-ft^2	I_{zz} lb_m-ft^2
1	Chassis and Wheels	1130.	-0.8	0.0	-1.5	2355.	24116.	26470.
2	Side	870.	0.0	2.9	-1.0	609.	19160.	18550.
3	Side	870.	0.0	-2.9	-1.0	609.	19160.	18550.
4	Top	348.	0.0	0.0	1.1	464.	725.	1188.
5	Engine and Trans.	522.	5.7	0.0	-0.7	0.	0.	0.
6	Gas Tank and Diff	261.	-4.8	0.0	-1.5	0.	0.	0.

Table 4-9. Inertia matrix lb_m-ft^2

24293.	0.	-1099.
0.	92224.	0.
-1099.	0.	103225.

The flight parameter, $(C_D A/W)$, which is also occasionally called the inverse ballistic coefficient, is the most important of the missile configuration parameters used as inputs in the trajectory program. In the 6-DOF trajectories which make up most of the cases presented in this report, the flight parameter is a function of time since the drag and the effective area change with the attitude of the missile relative to the wind as it tumbles during its flight. In the 3-DOF approximation, the flight parameter remains constant during the entire trajectory. The literature is replete with empirical methods of either averaging the drag coefficient to obtain a "random tumbling coefficient" as discussed in Section III of this report or of obtaining some average area for use with a drag coefficient based on flow normal to a surface.

In this report two independent methods, both based on experimental results, have been used to obtain values of the flight parameter for use in comparison with equivalent 6-DOF trajectories and to compare with other 3-DOF trajectory results in the literature such as those in Simiu and Cordes, 1976. In the first method, the value obtained for $C_D A$ from analysis of motion pictures made during the drop tests on a tumbling automobile model as described in Section III is used directly. In the second, the drag coefficient values of a 6-DOF trajectory were averaged over the time of flight. These values result from tables of experimentally obtained static coefficients that have been an input to the 6-DOF trajectory program. They are functions of the missile attitude as described in Section III. The reference area used with this averaged drag coefficient is the frontal cross-section area of an actual automobile having the proportions of the wind tunnel model from which the drag coefficients were obtained. Table 4-10 shows the values of the flight parameter obtained from the two methods just described along with equivalent values from Simiu and Cordes 1976, Iotta 1974, and Beech and Hobbs 1975. Note that the two independent experimental methods used in this report are in good agreement with each other and result in values which are less than half of that given for the flight parameter by Simiu and Cordes. (A smaller value of the flight parameter results in a shorter trajectory.) The reason for this discrepancy is two-fold. Measured values of drag coefficient and area are used in this report. Simiu and Cordes used a very high drag coefficient of 2.0 and additionally assumed that this C_D acted on the average of the rectangular areas defined by

Table 4-10. Comparison of Flight Parameter ($C_D A/W$) for automobiles

Source	$C_D A/W$ ft^2/lb	Height ft	Width ft	Length ft	Weight lb	Remarks
Sub-scale data	0.012	4.5	5.8	16.9	4000	Avg. C_D from 6-D. O. F. trajectory Actual A = 21.7 ft^2
Full-scale data	0.015	4.5	5.8	16.9	4000	Avg. C_D from 6-D. O. F. trajectory Actual A = 20 ft^2
Drop tests	0.015	4.5	5.8	16.9	4000	$C_D A$ from drop tests
Simiu and Cordes	0.0343	4.3	6.6	16.4	4000	Max C_D, Max A
Iotta	0.018	4.0	7.0	17.0	4000	Equation from Bates and Swanson, 1967
Beech and Hobbs	0.0099	4.0	5.0	15.0	4000	Average of $C_D A$ on all surfaces

the overall dimensions of the vehicle rather than on actual vehicle areas. This leads to a maximum value for $C_D A/W$ which we believe to be less realistic than the results obtained in this report. The values from Iotta and Beech and Hobbs are included as examples of other empirical values in the literature. The equations used in these references are somewhat similar to that used by Simiu and Cordes but the assumptions for C_D are less conservative, i.e., smaller. The car dimensions used are also included in the table. Although not identical they are quite similar and have little effect on the relative magnitudes of the flight parameter except in the case of Beech and Hobbs where an increase in the dimensions would serve to move the value into closer agreement with this report. The dimensions used in this report are those of a real American automobile and are consistent with the weight of 4,000 lbs.

Three series of automobile trajectory runs were conducted. As indicated in Table 4-11*, the first series, runs 1 through 9 and 26 through 28, used the same initial conditions as in Simiu and Cordes and the same tornado parameters

*Overall dimensions and weight are given in the table header.

Table 4-11. Automobile, 16.7 ft x 5.21 ft x 3.58 ft, 4000 lb

Run	Missile	Initial Conditions						Tornado					Final Conditions					Maxima (if different from final)			
		z(0) ft	u(0) mph	v(0) mph	Yaw deg	Roll deg	C_DA/W ft^2/lb	V_{max} mph	u_{tc} mph	l ft.	X_{tc} ft.	Y_{tc} ft.	t sec	R ft	Speed ft/sec	V_{xy} ft/sec	V_z ft/sec	Z_{max} ft.	R_{max} ft.	S_{max} ft/sec	$V_{xy\ max}$ ft/sec
1	CAR	131.23	0	0	90	0	- -	290	70	150	-149.4	0	6.3	213	137.0	106.1	86.6	147.8	-	-	-
2	CAR	131.23	0	0	90	0	-	240	60	150	-149.4	0	5.2	62	101.8	66 9	76.7	.37.7	63	-	-
3	CAR	131.23	0	0	90	0	0	190	50	150	-149.4	0	4.1	59	79.2	19.1	76.8	131.8	-	-	22.2
4	CAR	131.23	0	0	3 DOF		0.0131	290	70	150	-149.4	0	5.2	55	110.0	77.6	78.1	132.2	80	-	-
5	CAR	131.23	0	0	3 DOF		0.0119	240	60	150	-149.4	0	4.2	51	79.9	37.4	70.6	131.2	72	-	-
6	CAR	131.23	0	0	3 DOF		0.0123	190	50	150	-149.4	0	3.6	69	76.6	7.0	70 6	131.2	26	-	-
7	CAR	131.23	0	0	3 DOF		0.0343	290	70	150	-149.4	0	8.0	335	142.9	105.7	96.2	242.6	-	-	105.8
8	CAR	131.23	0	0	3 DOF		0.0343	240	60	150	-149.4	0	7.2	197	123.5	87.0	87.6	187.4	-	-	87.2
9	CAR	131.23	0	0	3 DOF		0.0343	190	50	150	-149.4	0	6.0	86	100.1	66.8	74 5	134.2	124	-	66.9
10	CAR	3.	0	0	0	0	-	225	30	528	-527.5	0	0.44	3	17.6	11.2	13.6	3.0	-	-	-
11	CAR	3.	0	0	0	0	-	225	50	528	-527.5	0	0.44	3	16.9	9.9	13.6	3.0	-	-	-
12	CAR	3.	0	0	0	0	-	225	70	528	-527.5	0	0.44	3	16.3	8.9	13.6	3.0	-	-	-
13	CAR	3.	0	0	0	0	-	225	30	528	0	-527.5	0.44	2	16.1	8.6	13.6	3.0	-	-	-
14	CAR	3.	0	0	0	0	-	225	30	528	+527.5	0	0.44	4	19.9	14.5	13.6	3.0	-	-	-
15	CAR	3.	0	0	0	0	-	225	30	528	0	-527.5	0.44	2	16.9	10.0	13 6	3.0	-	-	-
16	CAR	3.	0	0	90	90	-	225	30	528	-527.5	0	0.44	3	18.0	11.8	13.5	3.0	-	-	-
17	CAR	3.	0	0	90	90	-	225	70	528	-527 5	0	0.44	1	14.9	6.3	13.5	3.0	-	-	-
18	CAR	3.	0	0	3 DOF		0.0100	225	30	528	-527.5	0	0.44	2	16.3	8.8	13.7	3.0	-	-	-
19	CAR	3.	0	0	3 DOF		0.0066	225	70	528	-527 5	0	0.43	1	14.6	4.8	13.8	3.0	-	-	-
20	CAR	3.	30	0	0	0	-	225	30	528	-527.5	0	0.44	19	46.0	43.9	13.5	3.0	-	-	44.1
21	CAR	3.	30	0	0	0	-	225	70	528	-527.5	0	0.44	19	46.6	44.6	13.6	3.0	-	-	44.9
22	CAR	3.	60	0	0	0	-	225	30	528	-527.5	0	0.44	38	86.6	85.5	13.5	3.0	-	88.0	88.0
23	CAR	3.	60	0	0	0	-	225	70	528	-527.5	0	0.44	38	87.8	86.8	13.5	3.0	-	88 0	88.0
24	CAR	131.23	0	0	3 DOF		0.0343	225	30	528	-527.5	0	4.0	443	161.5	147.5	65.6	131.2	-	-	149.4
25	CAR	131.23	0	0	90	0	-	225	30	528	-527.5	0	3.6	160	111.0	74.1	82 7	131.2	-	-	74 3
26	CAR	131.23	0	0	0	0	-	425	103	150	-149.0	0	6.0	96	119.2	78.9	89.3	143.1	-	-	-
27	CAR	131.23	0	0	0	0	-	352	88	150	-149.0	0	5.0	26	90.0	49.8	75.0	131.2	84.2	-	-
28	CAR	131.23	0	0	0	0	-	279	73	150	-149.0	0	4.1	78	69.4	13.4	68.1	131.2	80.5	-	32.1
29	CAR*	131.23	0	0	0	0	-	425	103	150	-149.0	0	6.1	176	130.4	97.8	86.2	147.2	-	-	-
30	CAR*	131.23	0	0	0	0	-	352	88	150	-149.0	0	5.1	56	99.4	63.8	76.2	137.5	63.9	-	-
31	CAR*	131.23	0	0	0	0	-	279	73	150	-149.0	0	4.1	59	77.9	17.5	75.9	131.7	-	-	22.0
32	CAR*	131.23	0	0	0	0	-	425	103	150	-149.0	0	5.9	78	113.0	71.9	87.2	140.5	86.8	-	-
33	CAR*	131.23	0	0	0	0	-	352	88	150	-149.0	0	5.0	31	86.8	45.1	74.1	131.2	83.3	-	-
34	CAR*	131.23	0	0	0	0	-	279	73	150	-149.0	0	4.0	78	70.4	9.6	69.8	131.2	79.9	-	31.6
35	CAR*	131.23	0	0	0	0	-	225	44	528	-527.5	0	3.6	144	106.7	66.8	83.2	131.2	-	-	-
36	CAR*	131.23	0	0	0	0	-	225	44	528	-527.5	0	3.3	168	111.7	81.0	76.9	131.2	-	-	81.2
37	CAR	131.23	0	0	0	0	-	225	44	528	-527.5	0	3.4	178	114.1	84.0	77.2	131.2	-	-	-

*Full scale aerodynamic data complemented with sub-scale data.

(i. e., maximum tangential velocity, eye radius, and storm center speed) although the wind fields still differed because the tornado models were different. In the second series, runs 10 through 23 and 37, the JPL tornado parameters were used to study sensitivity of trajectory parameters to variations in some of the initial conditions. The initial orientation of the car was specified as wheels down, car long axis perpendicular to the direction of storm center travel ($\psi' = 90$).

Runs 26, 27, and 28 were made with the long axis of the car parallel to the direction of the storm center travel ($\psi' = 0$ deg). The runs with $\psi' = 90$ deg resulted in somewhat larger maximum horizontal velocities for the stronger tornados (Regions I and II), and runs with $\psi' = 0$ resulted in larger horizontal velocity for the region III tornado and the JPL tornado. In order to have a consistent set, $\psi' = 90$-deg runs were used in Table 4-1. The initial orientation condition does not exist in the 3 DOF trajectory of Simiu and Cordes but is required for the 6 DOF representation of this report. In the third series, runs 29-36, full-scale car data (complemented with subscale data) were used for comparison with 6 DOF runs made with subscale wind tunnel data. Results for both initial orientations, ψ', are shown ($\psi' = 0^{\circ}$ parallel to storm center direction $\psi' = 90^{\circ}$ perpendicular to storm center direction). The full-scale results are close to the subscale results for both orientations and for all the sets of tornado parameters; maximum difference is 15 percent.

The small difference between the trajectories based on aerodynamic data for the model and the full-scale car, which were similar in general configuration, but different in detail, leads to the conclusion that the model data should be adequate for any standard passenger car shape. Part of this effect was probably caused by the symmetry assumptions required by the incomplete data set.

An important difference between the 6 DOF trajectories in this report and 3 DOF trajectories is Simiu and Cordes is that in the 6 DOF case the flight parameter varies with the missile attitude; it is therefore a function of time and cannot be specified as a constant as in a 3 DOF program. Another significant point of difference between the two bodies of work is that the aerodynamic inputs used in the trajectory calculations of this report are based on experimental wind tunnel results as described in Section III.

In the case of the automobile configuration this leads to considerably lower values of aerodynamic resistance (and therefore of the flight parameter) than the conservative approximate values of both drag coefficient and area used by Simiu and Cordes. This subject is discussed in greater detail elsewhere in this section. The comparative results, as presented in Table 4-12, show that for similar initial conditions the results from this report (Runs 1, 2, and 3) indicate maximum horizontal velocities which are 54%, 38% and 15% of those obtained by Simiu and Cordes for the Regions I, II and III design tornadoes, respectively.

Runs 32, 33, and 34, are included in Table 4-11 to reiterate the small difference between results with subscale and full-scale aerodynamic coefficients.

Runs 4, 5 and 6 of Table 4-11 are a 3-DOF version of runs 1, 2 and 3 respectively using the method of time averaging the drag coefficients over the 6-DOF trajectory as described elsewhere in this section. The results, as shown in Table 4-12, are even lower than for the 6-DOF runs. Note that JPL values for the flight parameter as given in Table 4-10 average out to 36% of the value of 0.0343 used by Simiu and Cordes. These runs are the most direct comparison between the two sets of results; however, the 6-DOF results of runs 1, 2 and 3 are believed to be the more accurate than the 3-DOF version.

Table 4-12. Comparison of maximum horizontal velocities, V_{xy} (m/s), of an automobile under matching initial conditions between Simiu and Cordes results and those of this report. Initial height was 131.23 ft (40 m) and initial velocity was zero.

Model			Regions of Design Tornados			Run Number
Wind Model	Flight Parameter	Trajectory Model	I	II	III	
S&C	S&C	S&C 3DOF	59	52	41	—
JPL	JPL 6DOF (Subscale)	JPL 6 DOF	32	20	7	1, 2, 3
JPL	JPL 6 DOF (Full scale)	JPL 6DOF	30	19	7	32, 33, 34
JPL	JPL 3DOF	JPL 3DOF	24	11	2	4, 5, 6
JPL	S&C	JPL 3DOF	32	27	20	7, 8, 9
S&C	JPL 3DOF	S&C 3DOF	37	12	5	—

Runs 7, 8 and 9 are identical to runs 4, 5 and 6 except that the flight parameter value used by Simiu and Cordes was substituted for the JPL values used in the earlier runs in order to investigate the sensitivity of horizontal velocity (V_{xy}) to this parameter. The comparison indicates the larger flight parameter values result in values for V_{xy} that are 1.36, 2.33 and 9.54 times the values obtained in runs 4, 5 and 6 for the Region I, II and III design tornadoes. The effect of the larger flight parameter appears to be much greater for the weaker tornadoes. Also noteworthy are the effects of the larger flight parameter on maximum height (Z_{max}) and range (R). Using the JPL aerodynamic coefficients, the automobile does rise as much as six feet above the height of origin during the trajectory for the Region I tornado (Table 4-11, run 1) but when the drag coefficient and areas of Simiu and Cordes are used with the JPL wind field model the effect is to cause the car to rise by more than 111 feet above the injection point. This causes the range to be increased by 122 feet or 57% over that in run 1.

The final comparison of results shown in Table 4-12 was made to investigate the effect of using the Simiu and Cordes tornado wind field model in place of the JPL wind field model. This was accomplished by using the flight parameter values of runs 4, 5 and 6 together with Figure 3 of Simiu and Cordes which is a plot of maximum horizontal speed as a function of flight parameter for the various tornadoes. Comparisons with runs 4, 5 and 6 show that the differences in the wind field models, rather than the tornado parameters, was important for both the Type I and Type III tornadoes.

In summary, the detailed comparison of the results from Simiu and Cordes with the results from this report for the automobile trajectory indicates that the use of experimentally determined aerodynamic coefficients and realistic areas instead of the conservative approximations to both quantities used in Simiu and Cordes leads to considerably smaller values of maximum horizontal velocity. The effect is greater for the weaker tornadoes but significant in all cases.

In a second series with the automobile runs 10 through 23 in Table 4-11, the sensitivity of the trajectory parameters to variations in some of the initial conditions are presented. The JPL tornado parameters were used throughout this series (V_{max} = 225 mph; r_1 = 528 ft) and the automobile was assumed to be

at ground level (Z(o) = 3 ft) initially. The following initial conditions and their ranges were investigated: tornado linear velocity, U_{tc}(0, 30, 50, 70 mps); initial position relative to the center of the tornado, X_{tc} and Y_{yc}, (east, west, north and south 1/2 foot inside the radius of V_{max}); vehicle orientation (side to wind and bottom to wind for 6 D.O.F. and 3 D.O.F. programs; and car speed (0, 30 and 60 mph with the wind). Because of the fact that the car was initially on the ground and never lifted off in any of the cases studied, the variations in the trajectory parameters should not be considered as significant. (The program terminates when the height of the center of gravity reaches ground level.) The result that the car never lifted from the ground in any of the runs is, itself, of considerable significance.

Run number 2 in Table 4-11 was used as the sample run to illustrate the details of a car trajectory which will be discussed below. The car was injected into a 260 mph tornado of 150 ft radius which was moving East at 60 mph. This storm, except for its direction which is arbitrary along the positive x-axis, is the intermediate of the three storms (Region II) studied by Simiu and Cordes 1976 and is closest to the storm used in this report for much of the sensitivity analysis. The injection point is chosen infinitesimally inside the radius of maximum velocity of the storm (eye) such that the missile is directly in the path of the storm. Initial elevation is 40 meters (131.23 ft) with zero initial horizontal and vertical velocity components of the car "missile". Initial orientation of the car is with its long axis perpendicular to the direction of the storm and wheels on the ground.

The trajectory of the car during its 5.16-second flight is described by Fig. 4-1 where three components of displacement, range, velocity, Euler angles, angular velocities, absolute and relative wind velocity components, and aerodynamic coefficients are shown. From the first part of the figure, the car can be seen to climb a few feet due to its favorable orientation and high relative velocity during the first second before it begins to fall. The y-component of the range first increases then decreases as the relative position of the "missile" moves around the center toward the rear of the tornado. Speed has a plateau between 1 and 3 seconds corresponding to the x and y components of the wind velocity passing through zero.

Euler angles, yaw, pitch and roll are somewhat difficult to follow because

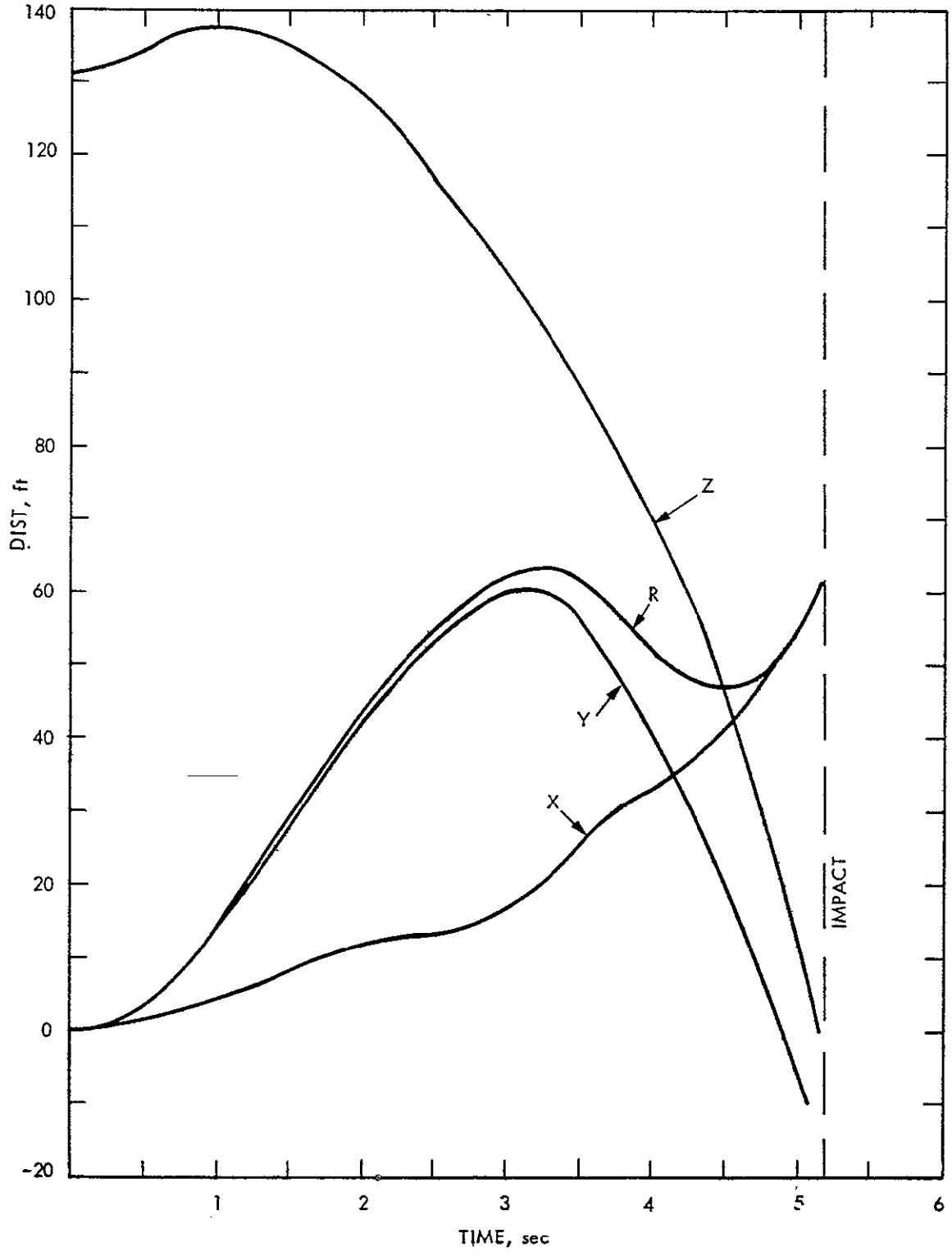

Fig. 4-1. Trajectory details for a car

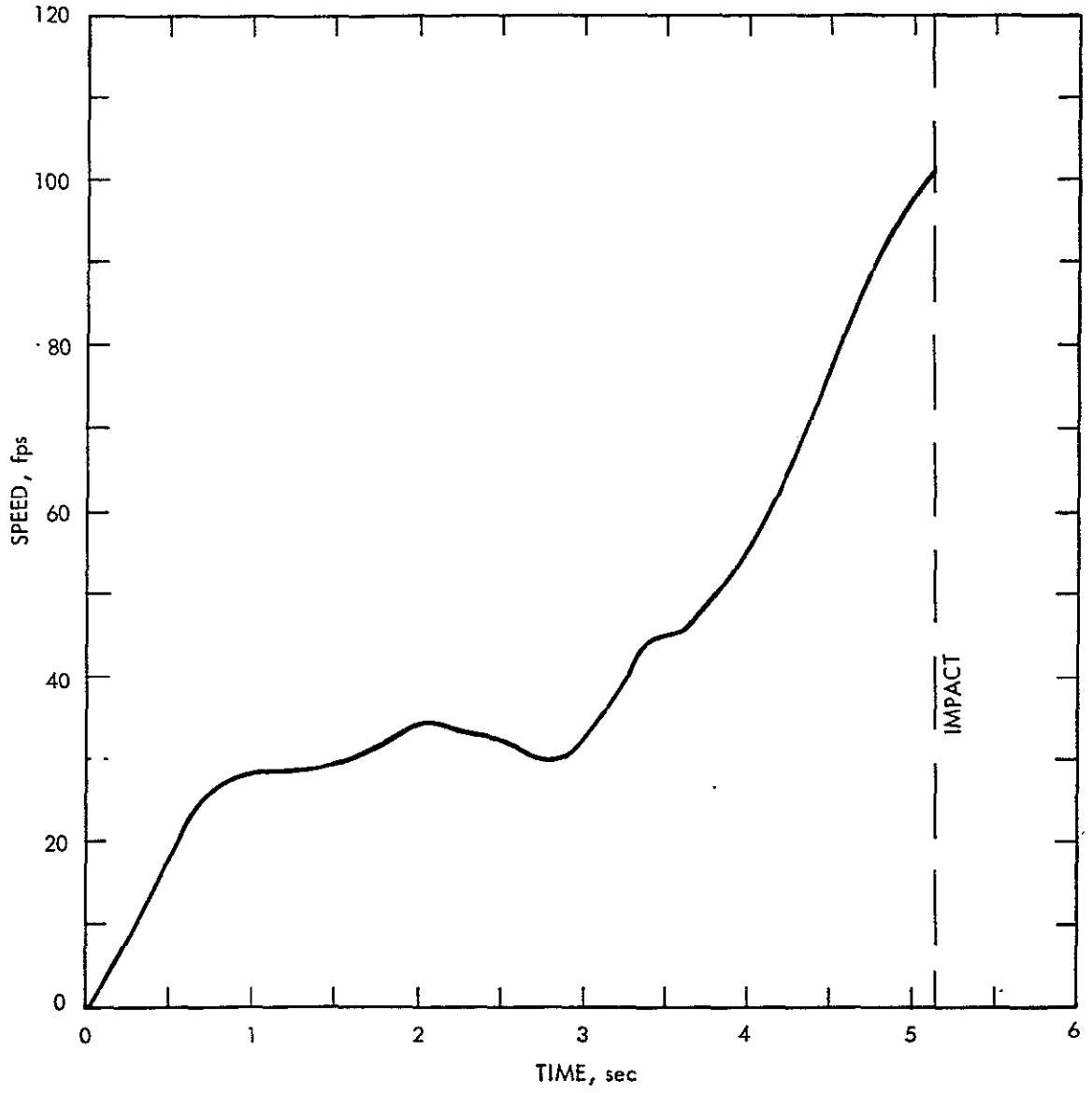

Fig. 4-1. Trajectory details for a car (continued)

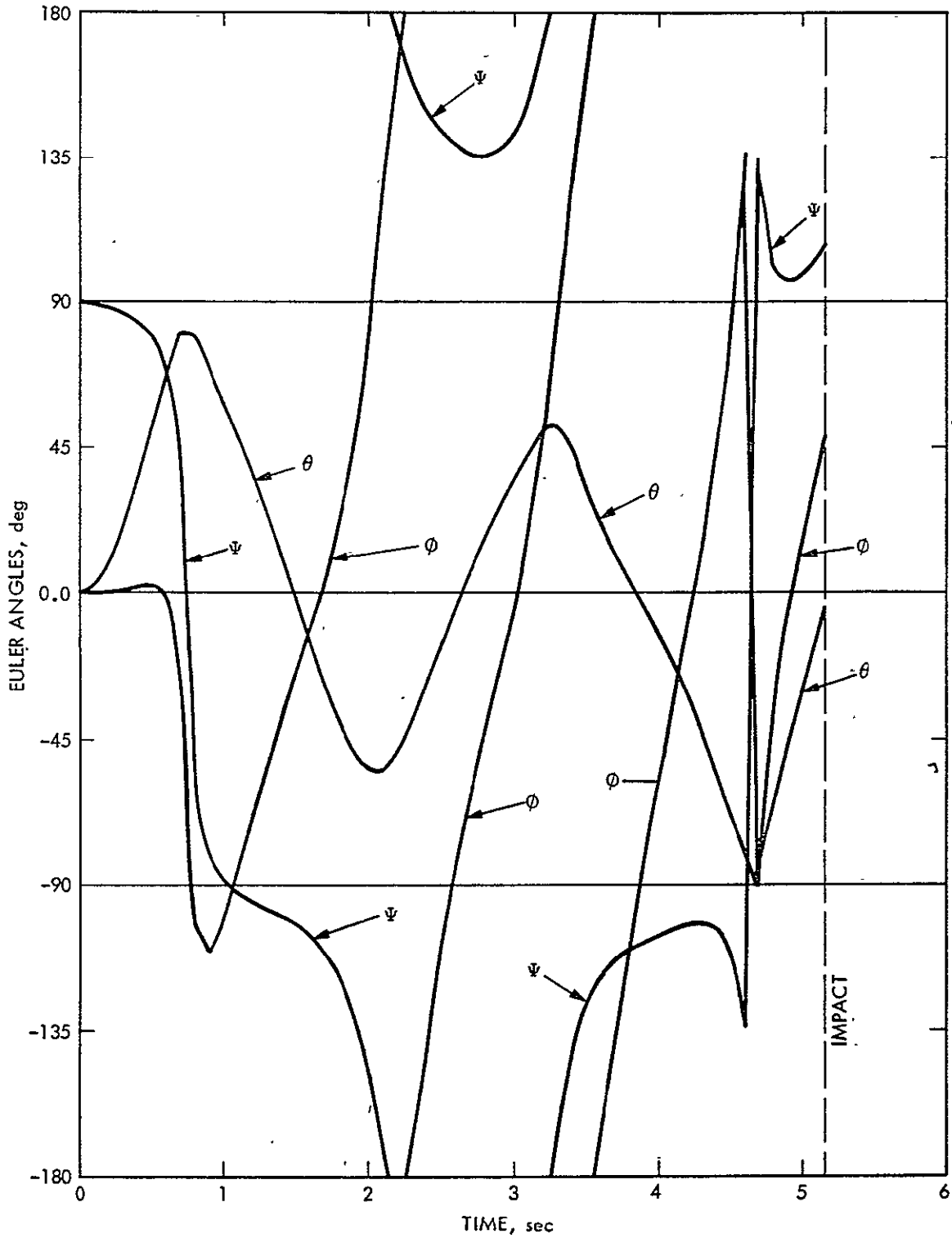

Fig. 4-1. Trajectory details for a car (continued)

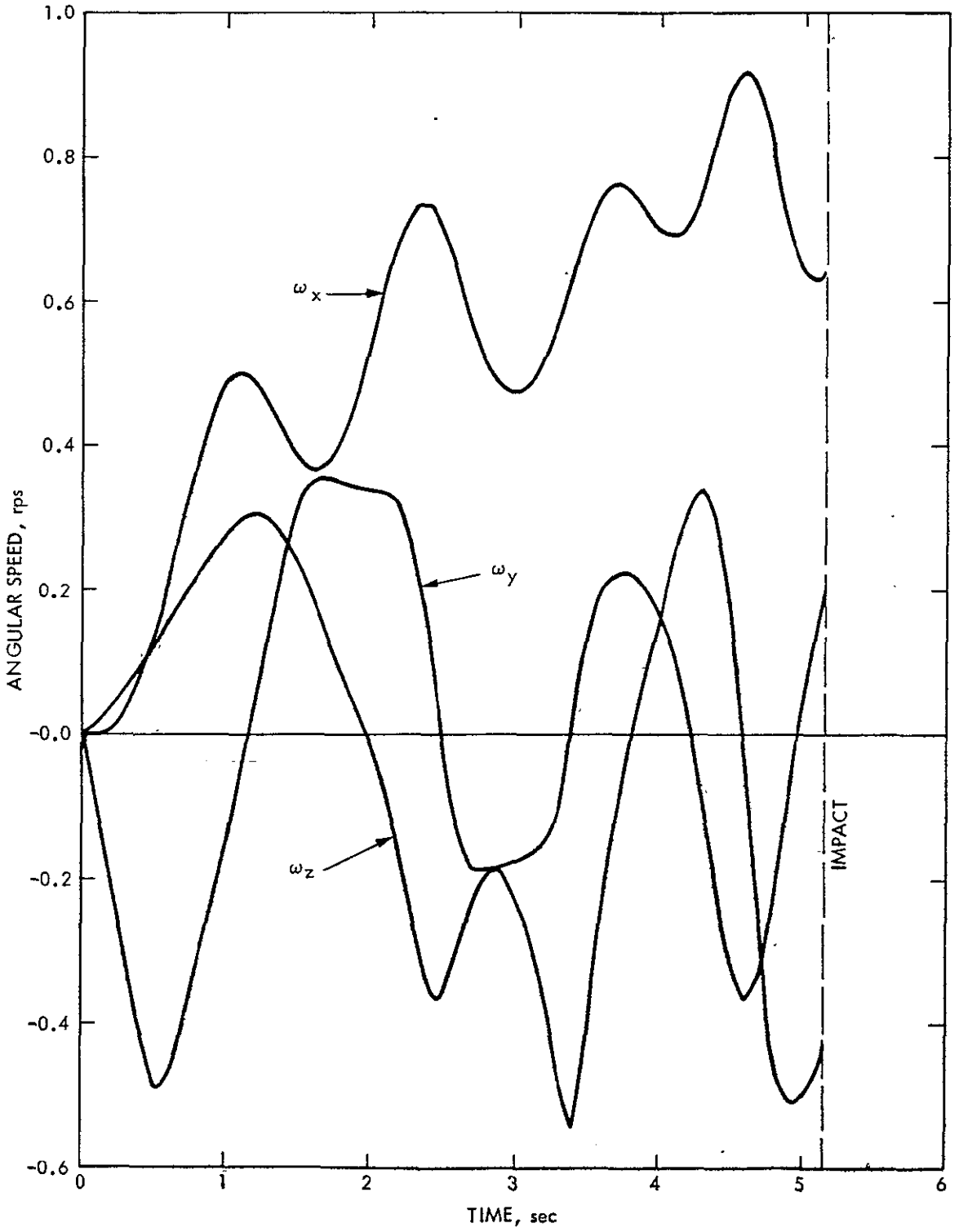

Fig. 4-1. Trajectory details for a car (continued)

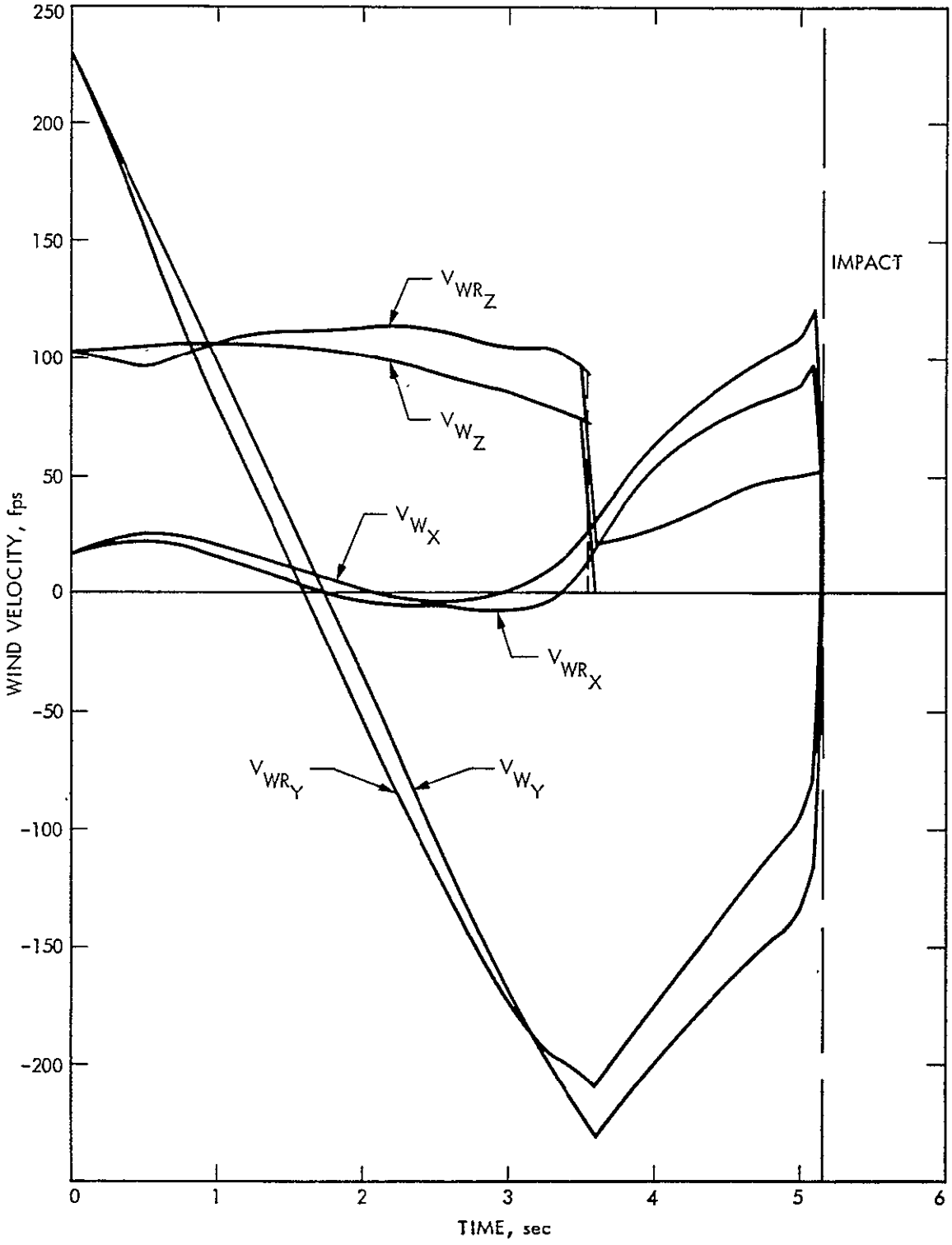

Fig. 4-1. Trajectory details for a car (continued)

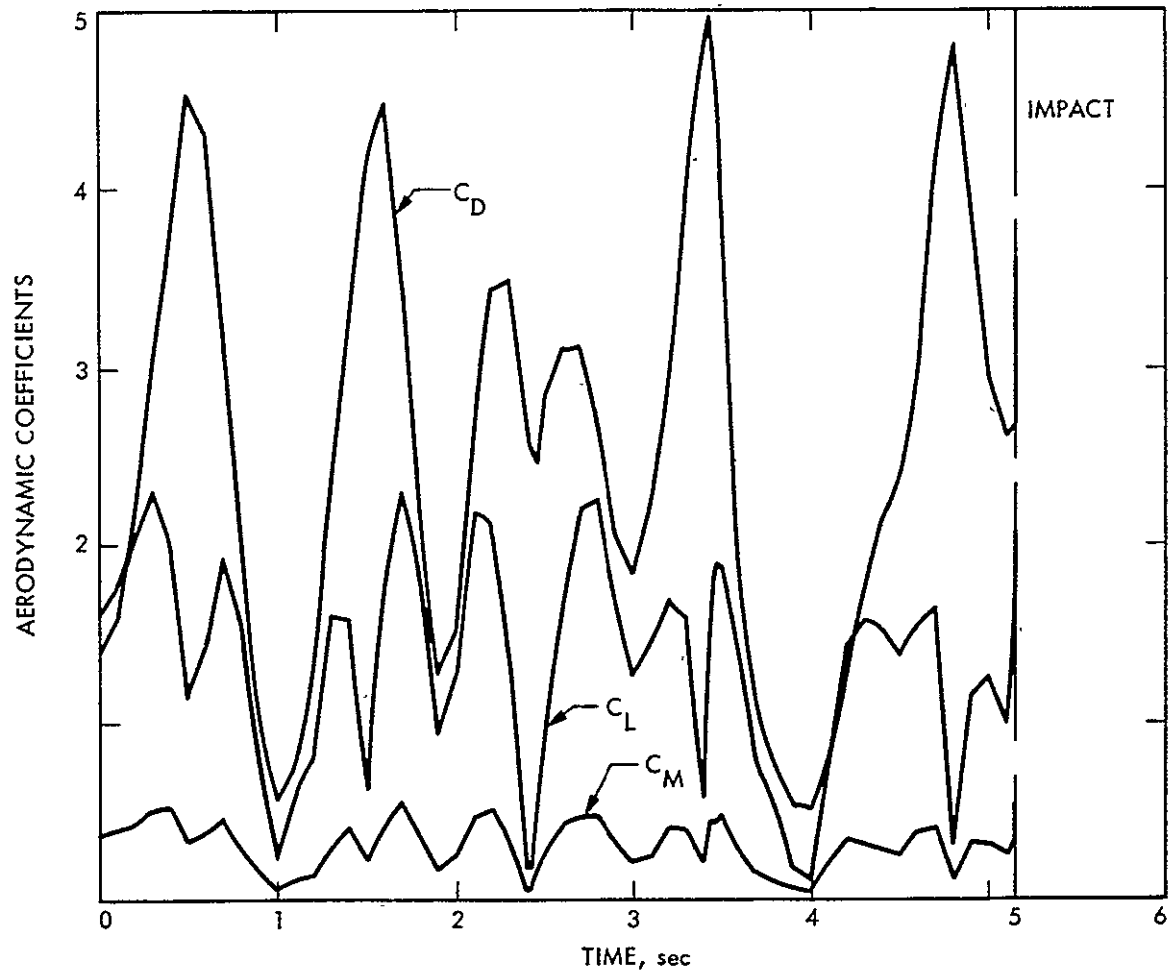

Fig. 4-1. Trajectory details for a car (continued)

the first and last are defined to be in the range ± 180 degrees and the second to be in the range ± 90 degrees. Attitude is more easily understood by simultaneous reference to angular velocity and Euler angles. Roll velocity, ω_x, oscillates about a steadily increasing trend whereas the pitch velocity, ω_y, and the yaw velocity, ω_z, oscillate about nearly zero means.

Wind velocity z-component is seen to change discontinuously at about 3.5 seconds corresponding to the missile passing out of the eye of the storm. Reference to section I shows that the formulas for wind velocity change at radius r_1. The change in wind velocity at r_1 causes a sharp change in the lift and moment coefficients, but the sudden change in the drag coefficient is less noticeable because the coefficient is already changing rapidly.

The drag coefficient (based on frontal area) oscillates over a range from 0.5 to 5.0 with a period between one and two seconds. The peaks of the oscillations are very narrow as only a small portion of the total time is spent near the extremes. There are approximately five cycles in the drag coefficient oscillation so that the average value 2.808 of the coefficient may be expected to be meaningful. The use of averaged coefficients will be discussed in subsection C. below.

4. Sensitivity Analysis

In this subsection, the sensitivity of missile trajectories to tornado parameters, initial conditions, and aerodynamic parameters will be examined. That is, the effects of variation of individual parameters will be examined with other parameters held constant. We attempt to understand the relative importance of various factors in influencing missile trajectories and to understand how we may infer trajectories for sets of parameters which are close to ones for which we have solutions. To the extent that the dependence on the individual parameters is largely decoupled, that is, that the speed, range, etc., are approximately products of functions of single variables the sensitivities will have broad utility.

The sensitivity analyses of this section are based primarily on runs assuming a ramp injection mode which are not included in the tables. However, the magnitude of the sensitivities are believed to be applicable to a wide class of initial conditions.

Parameters to be varied for the sensitivity analysis are divided into three classes: wind field, initial condition, and aerodynamics. The wind field parameters are maximum tangential velocity, V, radius of maximum tangential velocity, r_1, storm center velocity, u_{tc}, and azimuth of storm center from release point. The initial condition parameters are injection height and initial rotation rate ω_{yo}. The aerodynamic parameter is the Reynolds number range (sub-or supercritical).

The 12-in. diameter, schedule 40, 15-ft long pipe (referred to below as the 12-in. pipe missile) appears to be the most important of the postulated missiles from the standpoint of penetration of reinforced concrete walls (Stephenson, 1976). The sensitivity analysis of a number of parameters used in determining missile trajectories has been concentrated on this missile and some data for the 6-in. pipe (15 ft. in length) has been included for comparison.

The base from which variations are made for sensitivity to tornado parameters is V_{max} = 225 mph, r_1 = 0.1 mile, u_{tc} = 30 mph, h_0 = 10 ft, u_0 = w_0 = 40 mph, $\psi_0 = 90^\circ$, $\phi_0 = 0^\circ$. The release point is just inside the radius of maximum tangential velocity at the azimuth from the center where the tangential velocity and storm center velocity have the maximum vector sum. This would be due south of an eastward-moving storm or a storm center azimuth of 0°. Aerodynamic coefficients for a supercritical Reynolds number have been used for these sensitivity calculations.

The sensitivity of maximum speed and range of the 12-in. and 6-in. pipes to maximum tangential wind velocity is shown in Figs. 4-2. The speed ranges from 90 fps at 50 mph to 235 fps at 300 mph with a slope of 0.64 fps/mph at V_{max} = 225 mph for the 12-in. pipe. Range varies from 233 feet at 50 mph to 630 feet at 300 mph with a slope of 1.8 feet range per mile per hour of tangential velocity at 225 mph. The speed and range curves for the 6-in. pipe are slightly above and nearly parallel to those for the 12-in. pipe.

Sensitivity of maximum speed and range to radius of maximum tangential wind velocity (eye wall radius) is shown in Fig. 4-3 for the same configurations. Speed ranges from 170 fps at 0.05 mile radius to 177 fps at 0.2 mile radius.

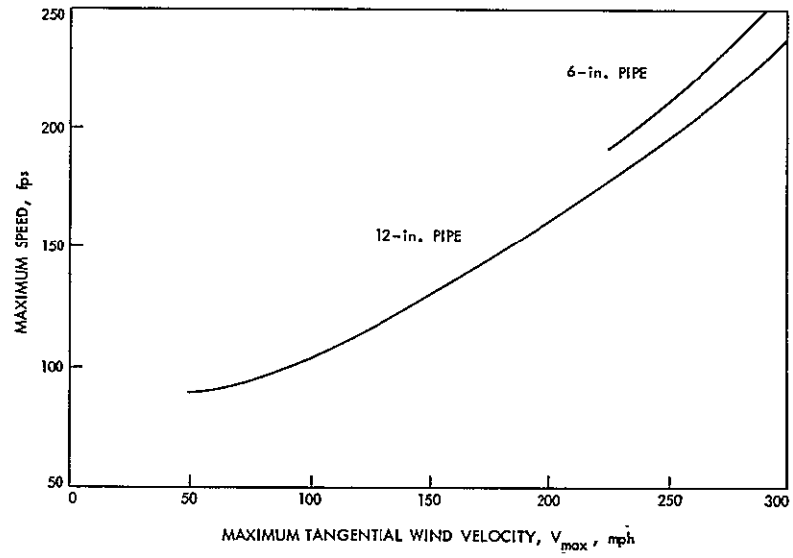

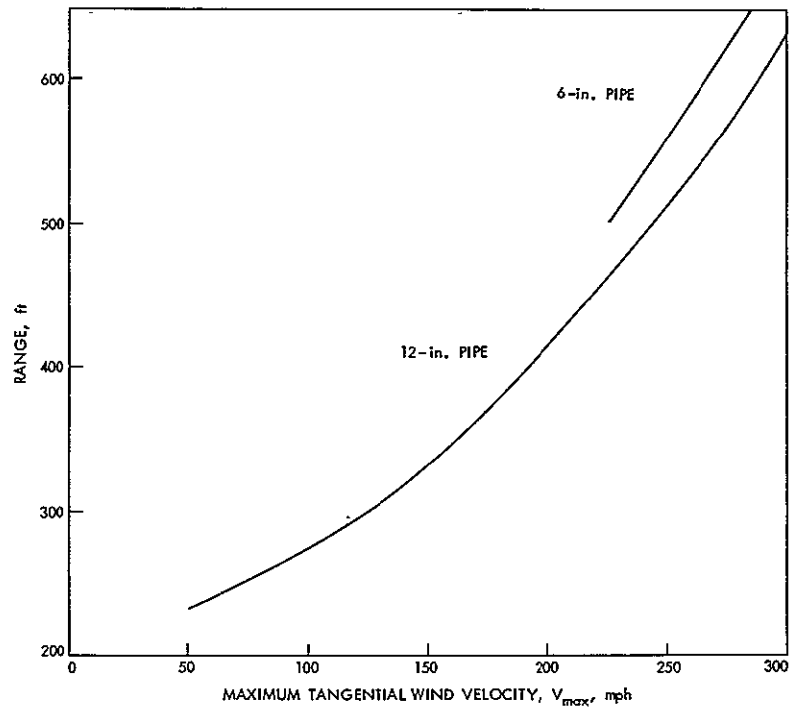

6-in. PIPE,
12-in. PIPE, Schedule 40, 15-ft long

$u_0 = w_0 = 40$ mph

SUPERCRITICAL Re

$u_{tc} = 30$ mph, $h_0 = 10'$, $r_1 = 0.1$ mile

$\psi_0 = 90^\circ$, $\theta_0 = 0^\circ$

Fig. 4-2. Sensitivity of maximum speed and range to maximum tangential wind velocity for 6-in. and 12-in. pipe .

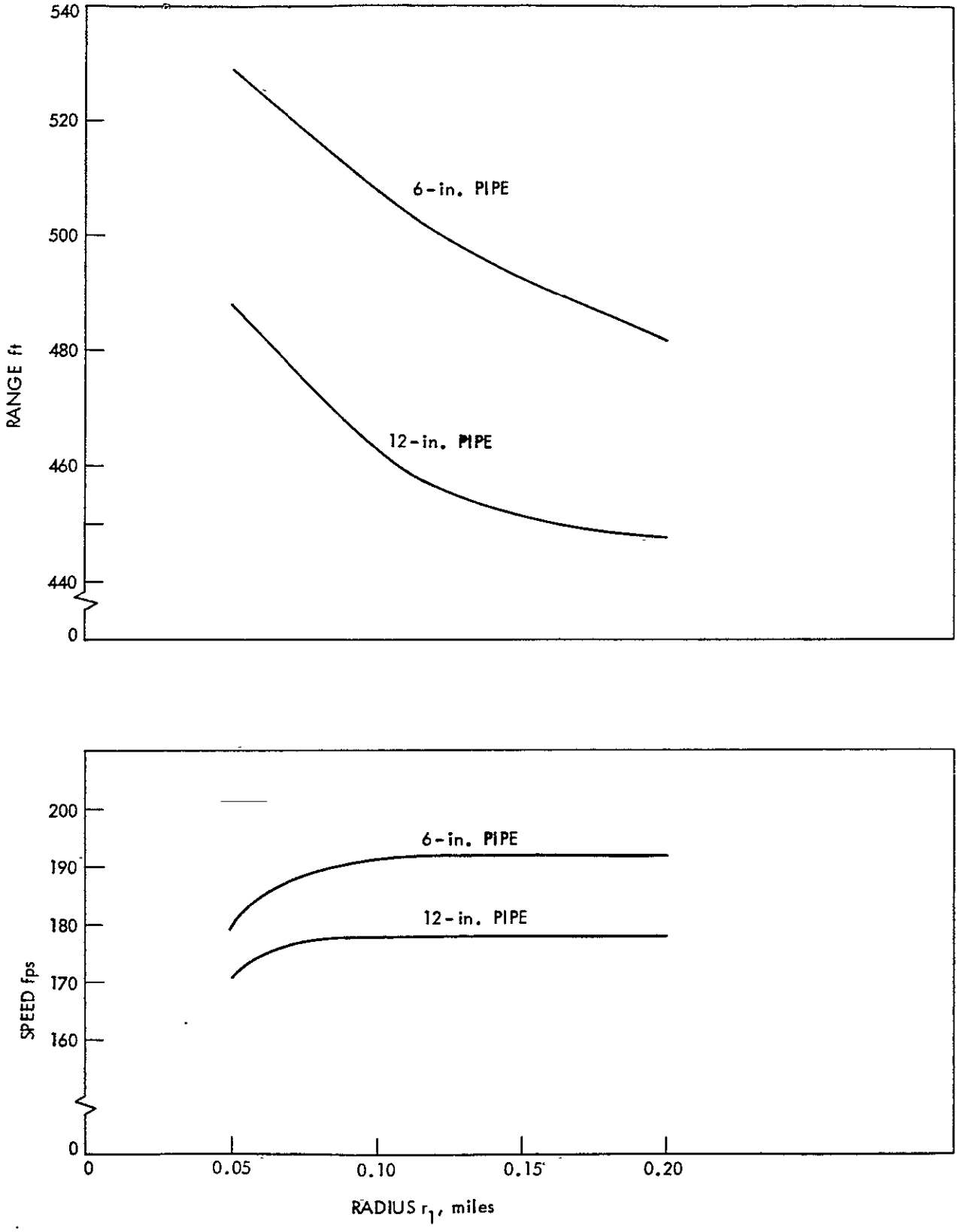

Fig. 4-3. Sensitivity of maximum speed and range to tornado radois fpr 6-in. and 12 in. pipe

Range varies from 484 ft at 0.05 mile radius to 444 ft at 0.2 mile radius with a negative slope. Neither the speed or the range are strongly influenced by the radius of the storm. (The fact that range decreases with storm size is a little surprising. This appears to be due to two factors: first, the vertical wind velocity is higher for the smaller storm, second, the yaw angle decreases more rapidly for the missile in the larger storm decreasing the drag in the downrange direction.) The 6-in. pipe curves are again above the 12-in. pipe curves.

Sensitivity of maximum speed and range to the translational speed of the tornado center is shown in Fig. 4-4 over a range of 15 mph to 90 mph. At 30 mph the slopes are 1.46 fps per mph and 1.80 ft per mph. As would be expected, each mph of storm speed adds approximately one mph of missile speed over most of the range.

Azimuth of the storm center from the release point affects the maximum speed along the trajectory and the range as shown in Fig. 4-5. The independent variable is cyclic so the left and right edges of the plots are coincident. The minimum range occurs near 180° where the tangential velocity of the storm is reduced by the colinear translational velocity vector. The speed has two distinct local minima: one near 180° and the other near 90° where the wind velocity vector makes a small angle with the pipe axis at release so the initial acceleration is small. Later the pipe yaws in the wind so the drag force increases and the range is not as strongly affected as the maximum speed.

The sensitivity plots (Fig. 4-6) show the effect of initial height on maximum speed and range as well as the effect of initial rotation; i.e., curves are shown for conditions of no initial rotation and -10 rpm about the y axis. The base case for this comparison differs from the others in this section in that the pipe is initially pitched up 45 degrees into the wind and there is no initial linear velocity. This is the worst case for no initial velocity. The rate of increase of speed with height decreases rapidly, reflecting the exponential decay in the model wind velocity as the ground is approached. Initial rotation of the pipe missile results in a small reduction in maximum speed and a larger percentage reduction in range. These reductions are due to the pipe spending a shorter period of time in a favorable orientation for lift and hence having a shorter time of flight.

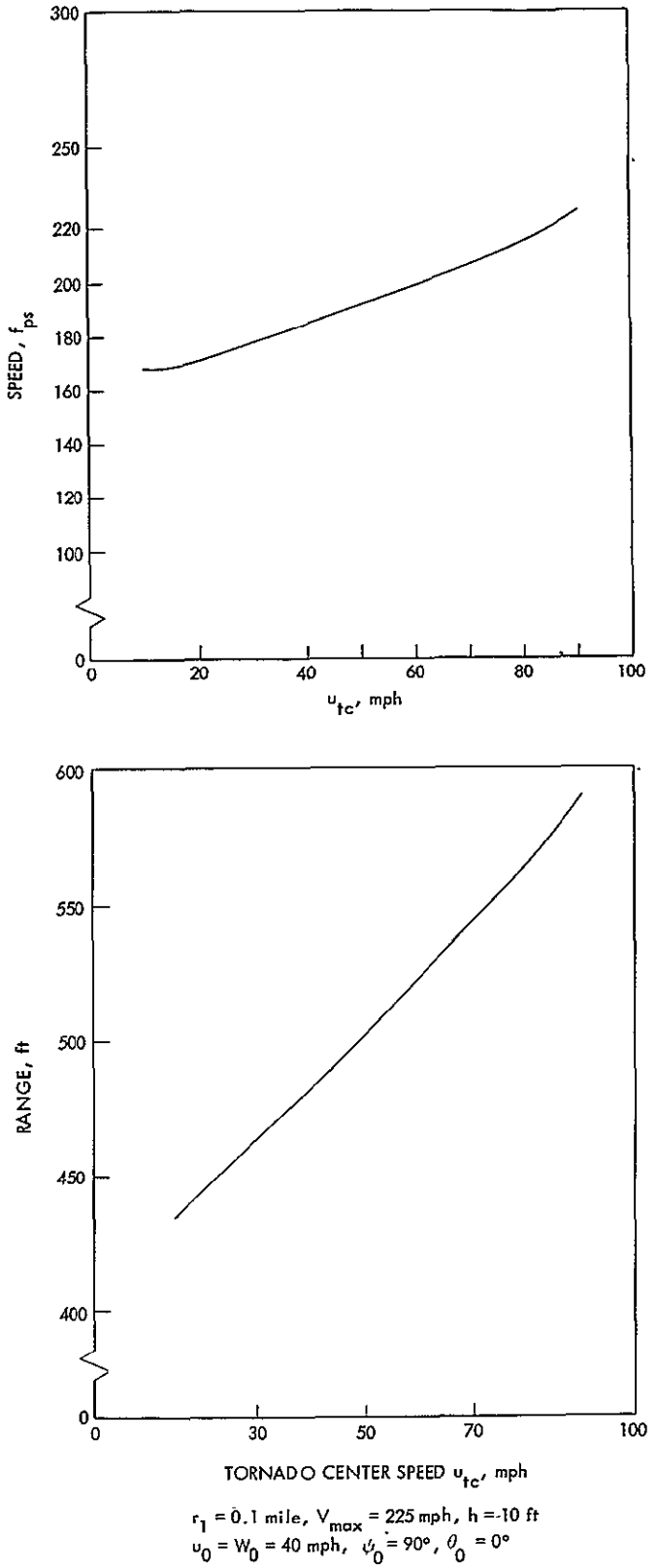

Fig. 4-4. Sensitivity of maximum speed and range to tornado center speed for 12-in. pipe

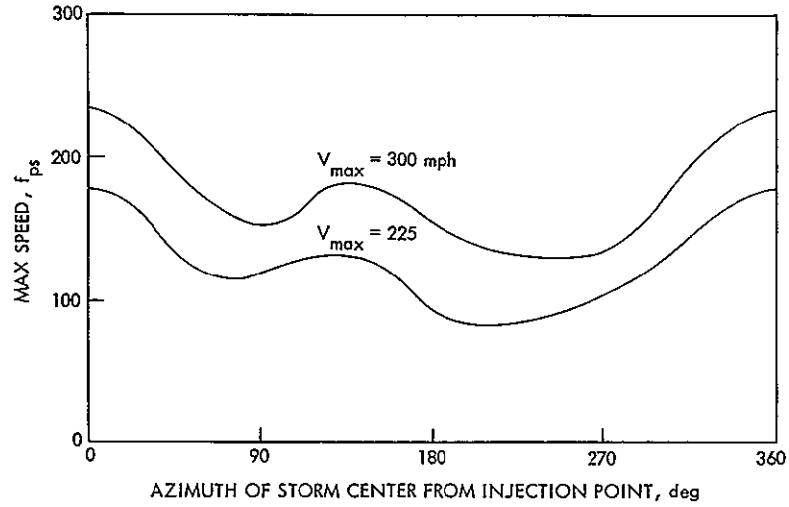

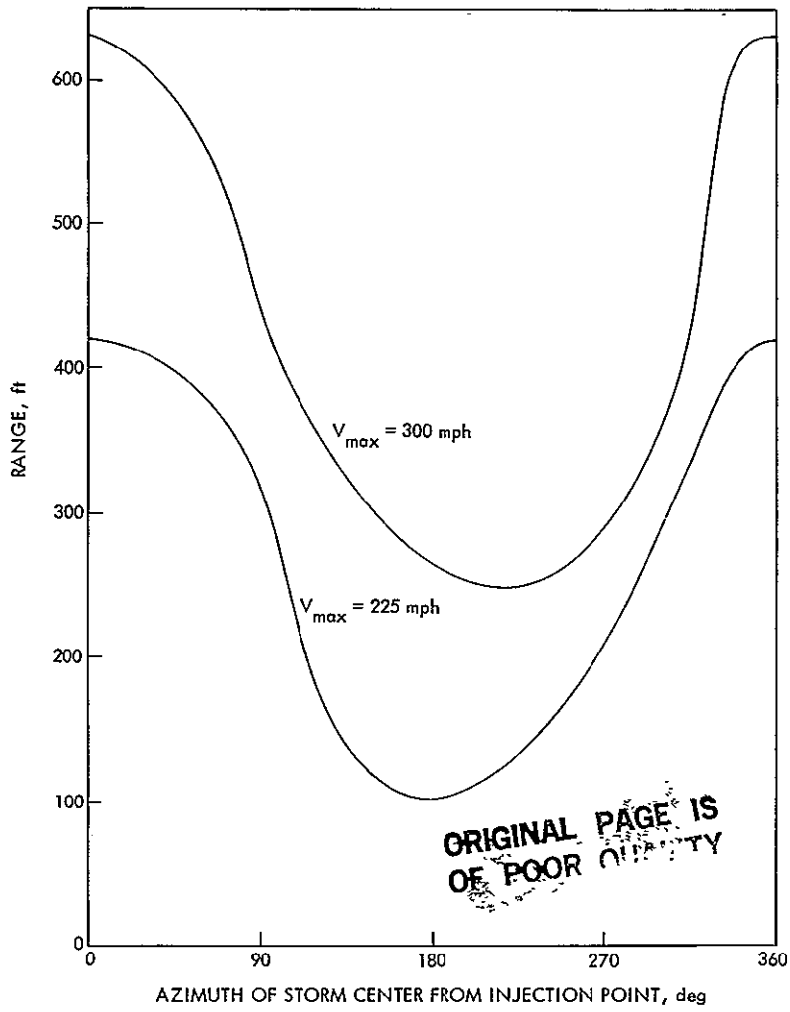

$r_1 = 0.1$ mile, $\psi_0 = 90$, $\theta_0 = 0$
$z_0 = 10$ ft

Fig. 4-5. Sensitivity of maximum speed and range to azimuth of storm center from injection point for an easterly-moving storm for 12-in. pipe

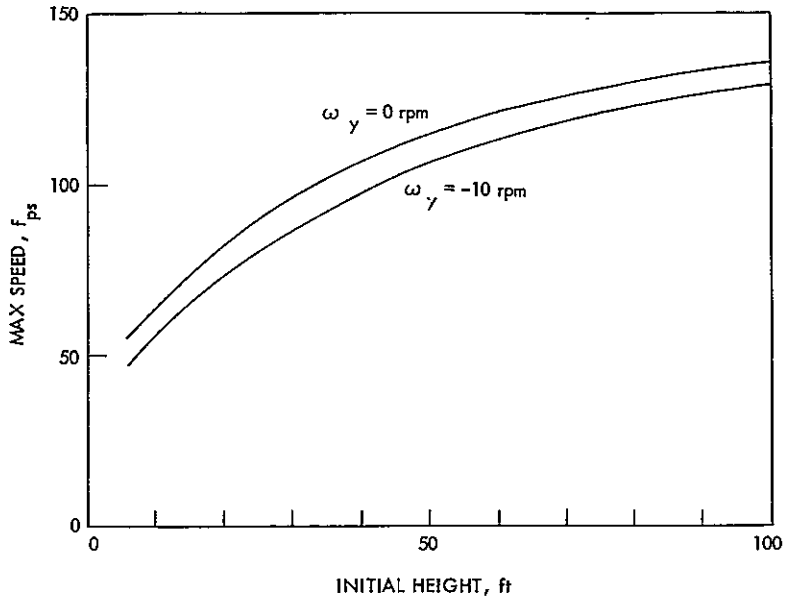

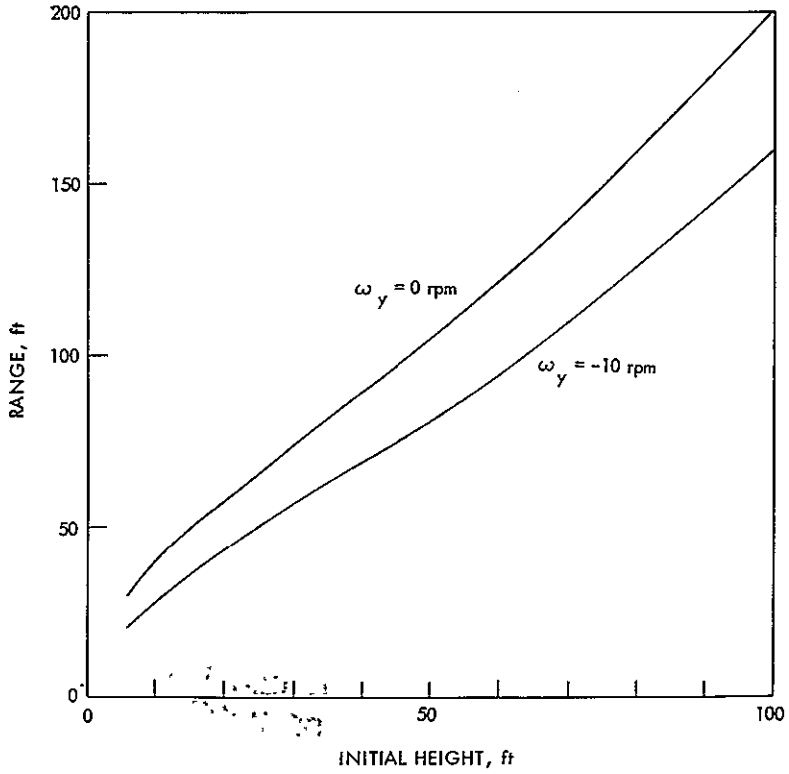

$u_0 = w_0 = 0$, SUPERCRITICAL Re
$u_{tc} = 30$, $V_{max} = 225$ mph, $r_t = 0.1$ mile
$\psi_0 = 180°$, $\theta_0 = 45°$

Fig. 4-6. Effects of initial height and initial rotation on maximum speed and range

Another type of sensitivity is that due to Reynolds number range. Sub- and super-critical Reynolds number effects on a typical trajectory are compared in Fig. 4-7. The use of subcritical Reynolds number data can be seen to be conservative because the speed and the component distances of the trajectory are all larger for the subcritical case (curves labeled 2) than for the supercritical case (curves labeled 1). Refering to Fig. 4-7 shows that although the rotation indicated by yaw, pitch, and roll occurs sooner in the trajectory for the supercritical case the attitude at impact is nearly the same for the two cases. The greater range and speed in the subcritical case is due principally to higher drag at large angles of attack, represented by large pitch and yaw in the 0.5 to 1.0 sec region of the plots. A comparison of the instantaneous drag coefficients along the trajectory is shown in Fig. 4-8.

C. THREE-DEGREE OF FREEDOM MISSILE TRAJECTORIES

1. Coefficient Development

For making engineering estimates of tornado missile velocities for nuclear plant design, a simplified method of computation is desirable. An obvious question is: How may acceptable results be obtained from a simplified method in light of the results of more complete solutions? An approach to simplification is to reduce the 6-DOF solution to an appropriate 3-DOF solution in which the actual orientation of a missile is neglected. Instead, an effective value of drag coefficient is derived from a typical 6-DOF solution that yields nearly the same speeds and ranges given by 3-DOF solutions. The distance traveled in the cross-wind direction can not be computed from the 3-DOF model because there will be no lift or aerodynamic side force acting on the assumed spherical mass and the accuracy of the range may be affected by the absence of lift.

The method consists in running a few typical trajectories with representative sets of initial conditions using the 6-DOF program. Instantaneous values of the drag coefficient are recorded as a function of time as is shown in Fig. 4-8 for 12 inch pipe trajectories using subcritical and supercritical aerodynamic coefficients (c.f. Fig. 4-1 for the car). An average value is computed for the

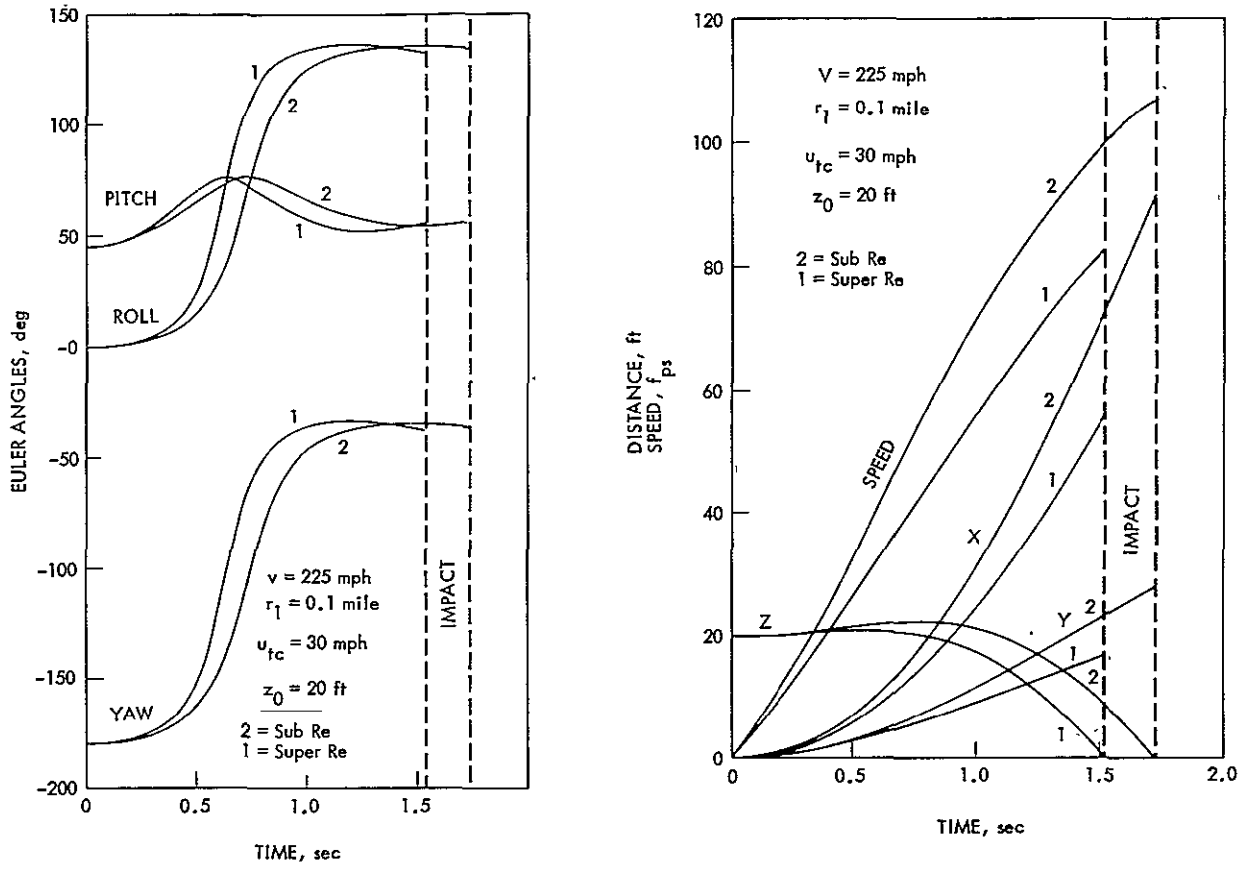

Fig. 4-7. Trajectory components and orientation of 12-in. pipe for subcritical and supercritical Reynolds number aerodynamic coefficients

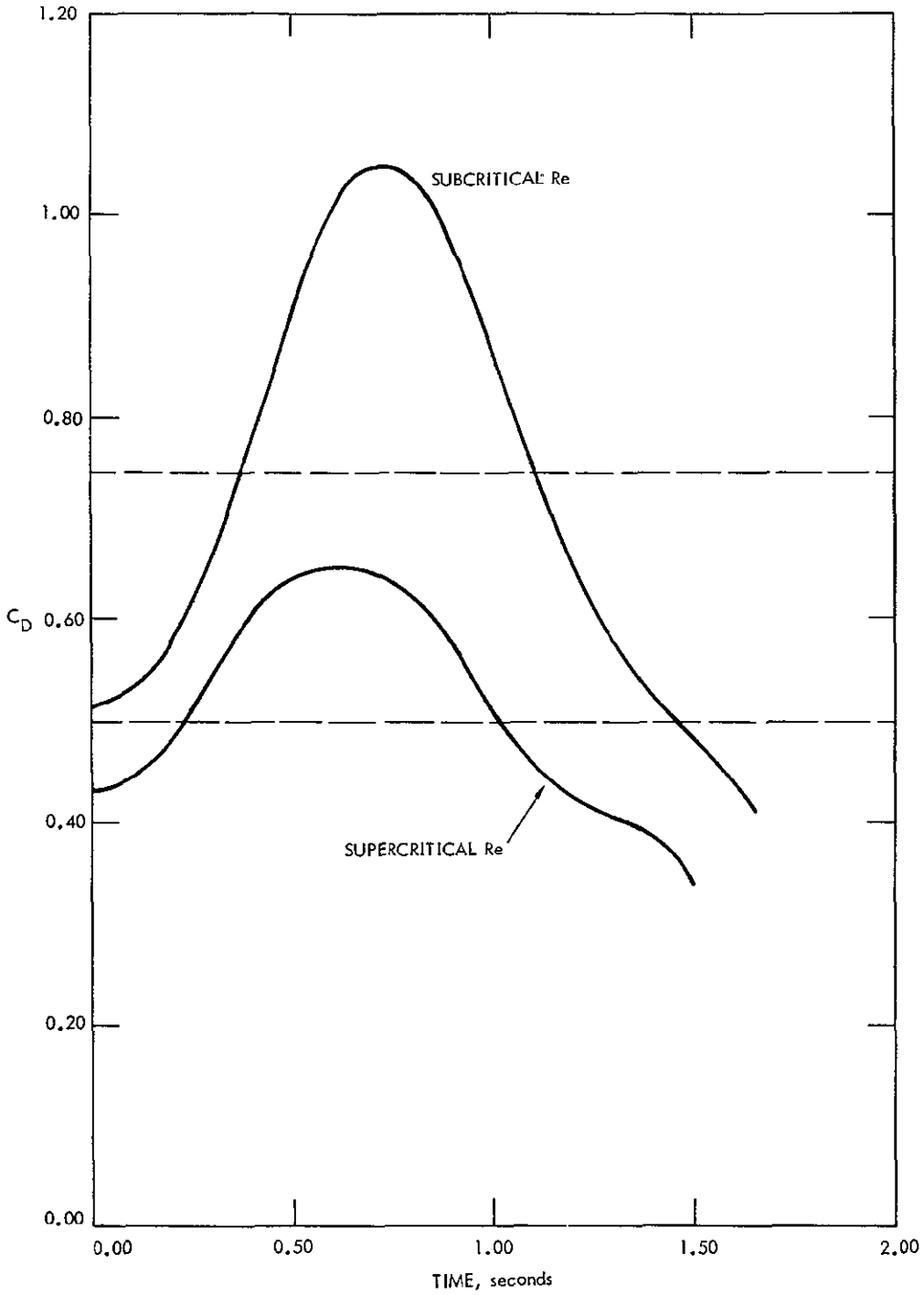

Fig. 4-8. Instantaneous drag coefficient along a trajectory for the 12-in. pipe missile

drag coefficient over the run. This average value is then used for 3-DOF computations. The assumption underlying the method is that each missile configuration has a quasi stable orientation or cyclic mode which is approximated by an average drag coefficient and which is independent of initial conditions if the trajectory is sufficiently long. In addition to using better aerodynamic data than previous investigators, the averaging carried out here uses better weights for the different orientations. Note that this average drag coefficient would be difficult to obtain by any means other than the 6-DOF computer program or the drop tests described in section IIIC above. Values derived by the current method will be compared with the results of these scale-model drop tests below.

2. Trajectory Comparisons

Figure 4-9 compares the speed along the trajectories of the 12-inch pipe for the 6-DOF supercritical solution and the approximating 3-DOF trajectory. Note that the speed is fairly well approximated except that the time of flight for the 6-DOF model is longer due to positive lift in the initial part of the trajectory.

For a blunt shape such as the compact car model the use of a 3-DOF model with an average drag coefficient is a slightly better approximation than for the 12-in. pipe. For the initial conditions considered in Section IVB1, the average of the instantaneous drag coefficient in Fig. 4-1 is 2.5. The 3-DOF trajectory speed run with this drag coefficient Fig. 4-10 differs by 22 fps in 102 fps or 22 percent and the range differs by about 11 ft in 62 ft or 13 percent. These results for compact shapes suggest that the 3-DOF approximation is probably adequate for design purposes, particularly if used with a small safety factor (e.g., 1.5).

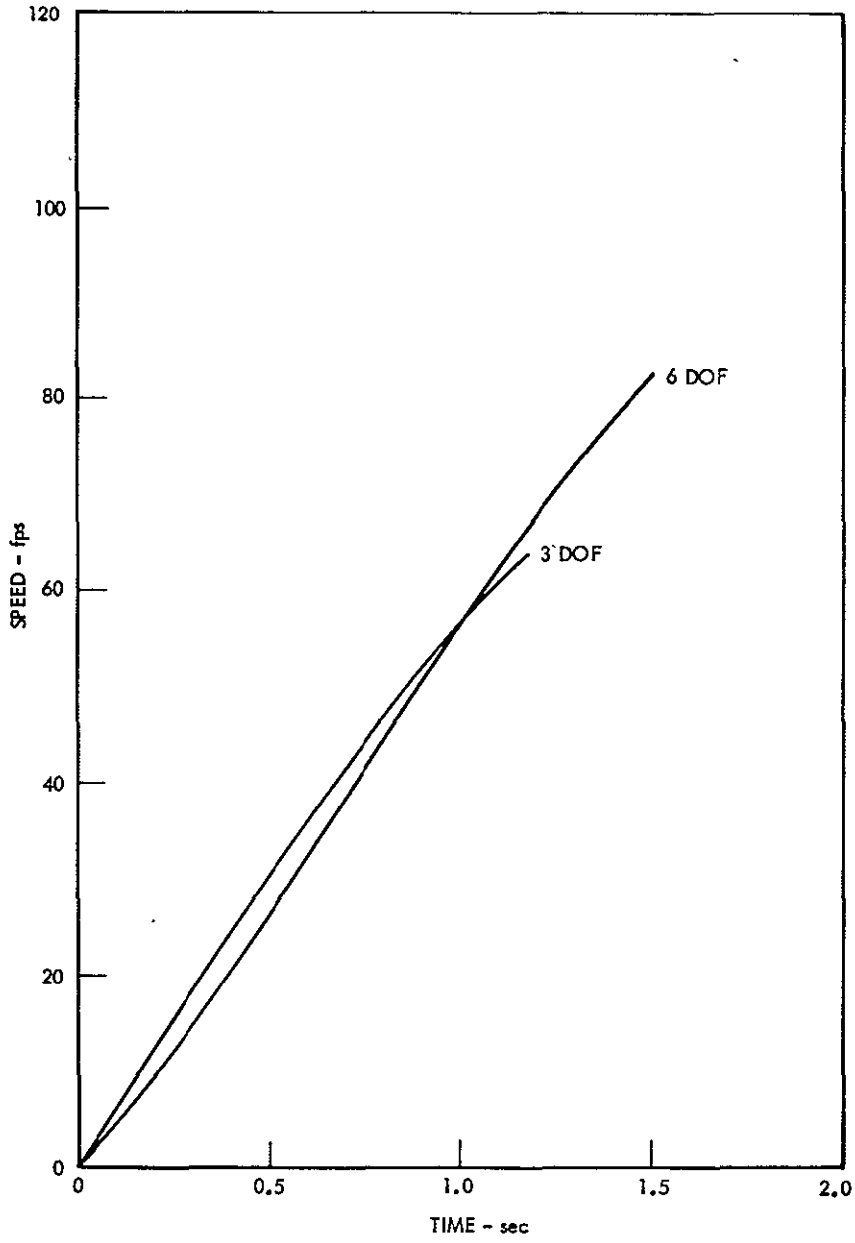

Fig. 4-9. Comparison between 6 DOF and 3 DOF trajectories for the 12-in. pipe

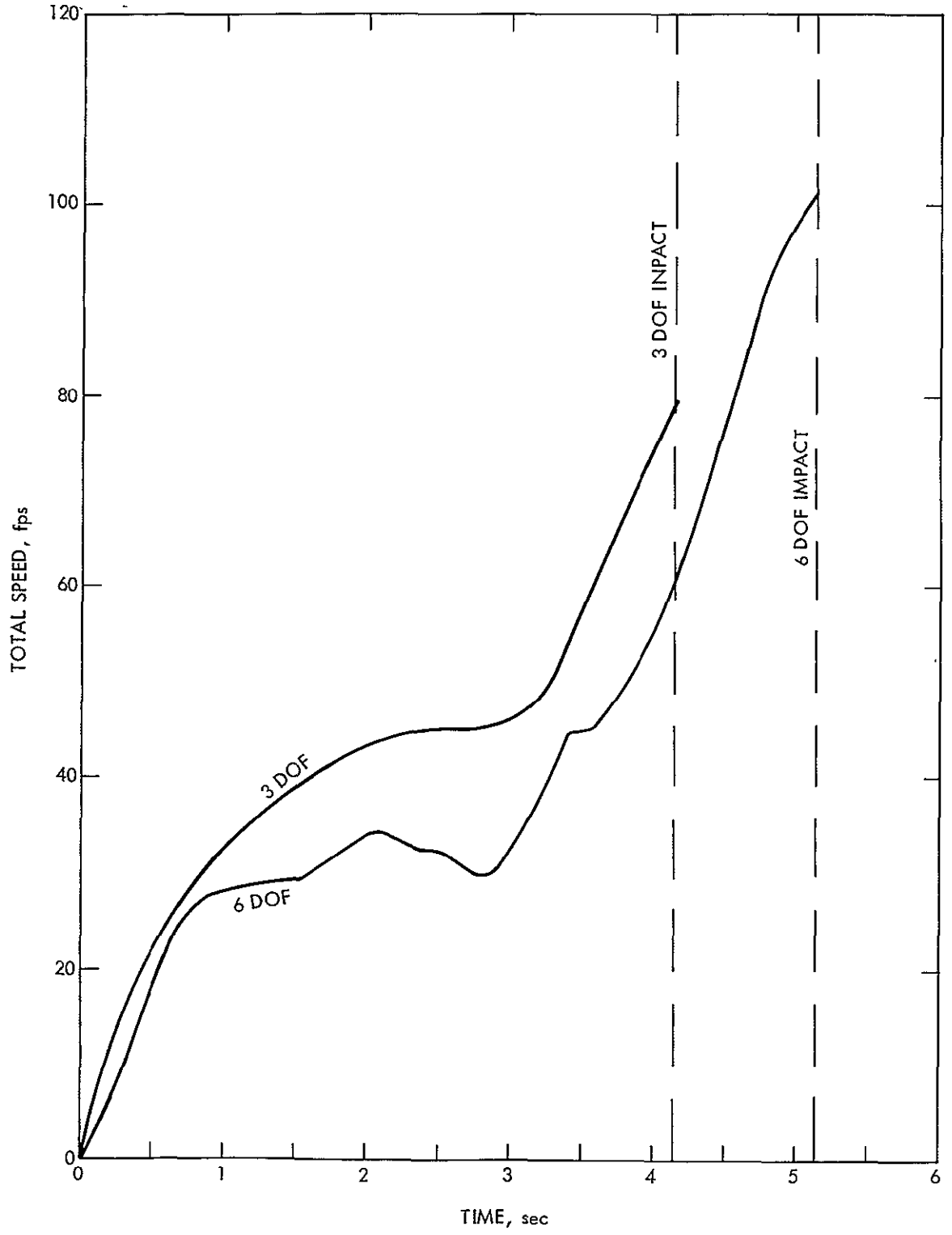

Fig. 4-10. Comparison of 6 DOF and 3 DOF trajectories for the car-missile

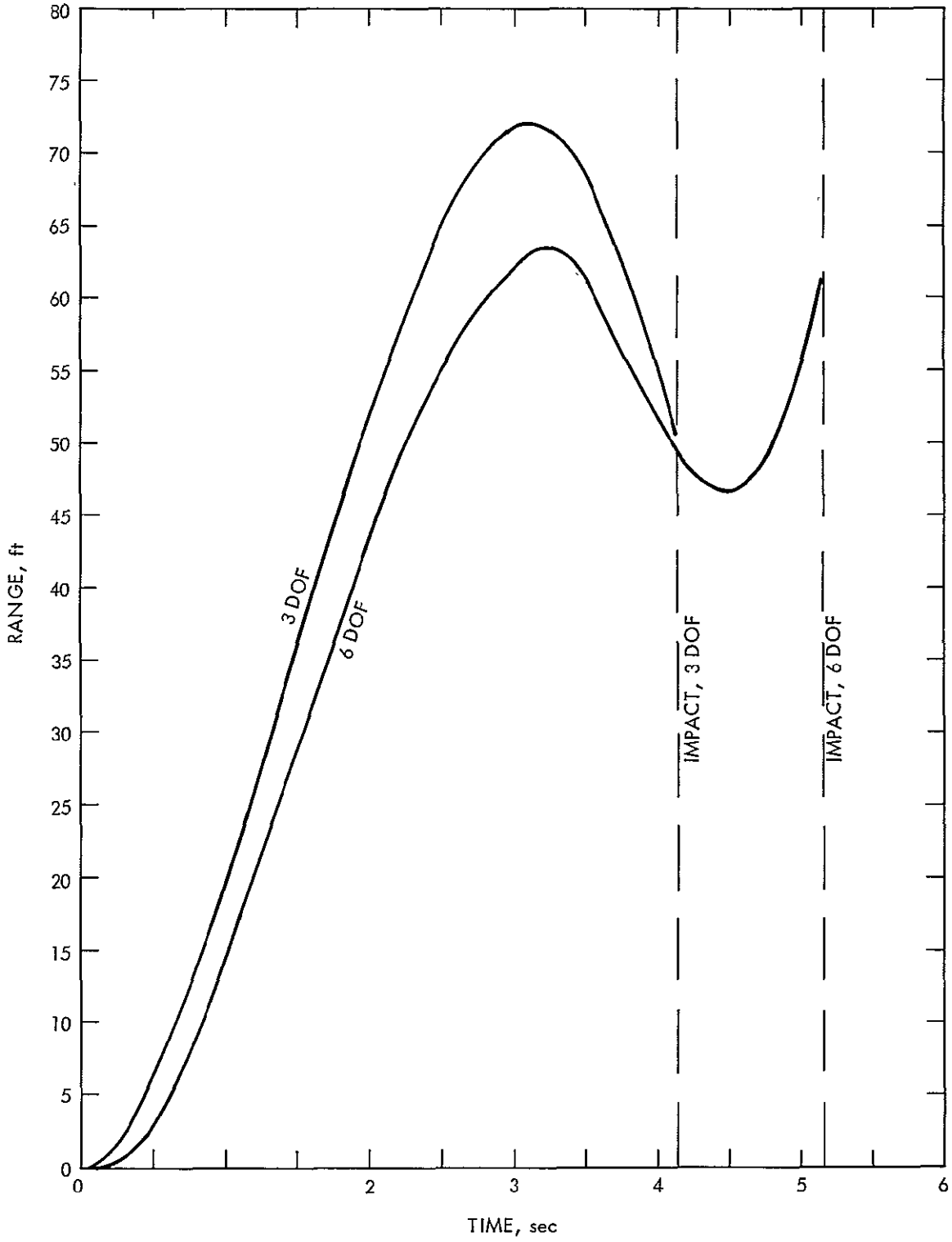

Fig. 4-10. Comparison of 6 DOF and 3 DOF trajectories for the car-missile (continued)

REFERENCES

Bates, F. C. and Swanson, A. E., Nov. 1967, Tornado Design Considerations for Nuclear Power Plants, Trans. of the Am. Nuclear Soc., 10 pp 712-713.

Beech, D. R. and Hobbs, S. E., 1975, Analysis of Tornado Generated Missiles. Topical Report B&R-001, Brown and Root Inc., P. O. Box 3, Houston, Texas 77001.

Iotta, R. C., 1974, Velocities of Tornado Generated Missiles. Report ER-1003, Ebasco Services Inc.

Lee, A. J. H., Dec. 1973, A General Study of Tornado Generated Missiles, ASCE Specialty Conference on Structural Design of Nuclear Power Plant Facilities, Chicago, Illinois.

Markee, E. H., Beckerly, J. G., Saunders, K. E., May 1974, Technical Basis for Interim Regional Tornado Criteria, Wash-1300 (UC-11), U.S. Atomic Energy Commission, Office of Regulation.

Minor, J. E. et al, July 1976, Air Flow Around Buildings as Reflected in Failure Modes, ASHRAE Transitions, Vol. 82, Part I.

Paddleford, D. F., Apr. 1969, Characteristics of Tornado Generated Missiles, TRWCAP-7879, Nuclear Energy Systems, Westinghouse Corp., Pittsburgh, Pennsylvania.

Simiu, E., and Cordes, M., April 1976, Tornado-Borne Missile Speeds, NBSIR 76-1050, National Bureau of Standards, Washington, D.C., prepared for U.S. Nuclear Regulatory Com.

Stephenson, A. E., July 1977, Full-Scale Tornado-Missile Impact Tests, EPRI Final Report NP-440.

NRC Standard Review Plan, Rev. 1 (NUREG-75/087), November 24, 1975.

E. NOMENCLATURE FOR SECTION IV

A	... area of "missile"
C_D	... drag coefficient (wind axis)
C_L	... lift coefficient (wind axis)
C_ℓ	... rolling moment coefficient (wind axis)
C_m	... pitching moment coefficient (wind axis)
C_n	... yawing moment coefficient (wind axis)
C_s	... side force coefficient (wind axis)
$F(t)$	... structural force function restraining injection
F_1	... impulsive force due to rapid pressure drop in injection formulas
F_2	... vertical wind force in injection formulas
g	... acceleration of gravity
g_o	... constant of proportionality in Newton's second law
h_o	... initial height of "missile"
I_{xx}, I_{yy}, I_{zz}	... moments of inertia in x, y, and z directions
p	... pressure
Re	... Reynolds number
r_1	... radius of maximum azimuthal velocity in tornado
t	time
u	... horizontal velocity component of missile
u_{tc}	... speed of storm center
V	... Vertical velocity of injection, missile ground velocity
V_{max}	... maximum azimuthal velocity of tornado
V_{xy}	... horizontal velocity
v	... azimuthal component of velocity

W ... weight of "missile"

w ... vertical velocity of "missile"

x ... distance in direction of storm center velocity

y ... distance transverse to storm direction

z ... height above ground

α ... angle of attack, scale height in wind field model

β ... scale height in wind field model

ν ... eddy (kinematic) viscosity

ρ_a ... density of air

ϕ ... roll angle

ψ ... yaw angle

ψ' ... initial yaw angle relative to storm center direction

$\omega_{x'}$, $\omega_{y'}$ ... rotational velocity components of missile

Subscripts

rel ... relative (to missile)

tc ... tornado center

w ... wind

o ... injection condition

APPENDIX A

ANALYSIS OF THE NEAR-GROUND WIND FIELD OF A TORNADO WITH STEADY AND SPATIALLY VARYING EDDY VISCOSITY*

A. INTRODUCTION

The near-ground flow in a tornado vortex is of primary engineering concern, because it is the portion of the whirlwind to which structures and objects are subjected. The low-level pressure deficit and wind field present a hazard to structures directly, and indirectly through the potential injection and transport of missiles of sundry conceivable shapes, weights, and sizes. Thus, one major motivation for improved low-level tornado modeling is to furnish a more realistic wind field for use in trajectory calculations, which in turn can be used to establish design criteria for structures. Also, from a meteorological point of view, the low-level wind field places a major constraint on the secondary flow field, hence on the entire structure of a tornado, and thus merits close study, especially in the absence of extensive field data. Existing detailed field data concerns particle or cloud tracking on cinematographic records of a few whirlwinds (Hoecker 1960; Golden and Purcell 1975; Golden 1976). These data raise questions of discrepancy between solid particle motion and air motion (Morton 1966), of inconsistencies as a result of the time-compositing of data taken over the lifetime of the whirlwind (Redmann et al. 1976), and of problems with condensation, dust, and debris that often preclude inspection of the interesting central portion of the swirl. More importantly, the field data currently cannot furnish the detail of all three velocity components required for trajectory calculations and for physical insight.

---

*This Appendix is extracted from the final report prepared by TRW for JPL under JPL Contract 954533. The authors were George F. Carrier, Harvard University, Consultant to TRW, and Francis E. Fendell, TRW, Principal Investigator. The report was published as TRW Document 29584-6001-RU-00, 21 May 1976 - 21 January 1977.

Thus the need for modeling persists. The modeling undertaken here is intended to be along an intermediate path between the overly simplified and the overly elaborate. In particular, the turbulent transport of momentum is represented by an explicit, spatially varying eddy viscosity, within a gradient-diffusion representation; such a phenomenology has been shown to be of value in subsonic aerodynamic shear layers near smooth and rough walls under accelerating (favorable) pressure gradients at large Reynolds number (Smith and Cebeci 1968; White 1974), conditions which hold in the geophysical flow of interest. While a constant eddy viscosity has been studied as a preliminary case, the above emphasis on a spatially-varying eddy viscosity seems well warranted and within aerodynamic experience. Also included in the model is a distinction of a wall layer (viscous sublayer) from an outer defect layer.

The use of elaborate simulation appears further unwarranted in that the computation appears overly refined within the limitations of the formulation. The mature intense tornado is invariably idealized as quasi-steady and axisymmetric in modeling. In fact, the maximum swirl speed of the mature tornado changes appreciably and nonmonotonically in time, from interpretation of available funnel-cloud photography (Ferrel 1893; Glaser 1960; Dergarabedian and Fendell 1971a, 1971b, 1973). Also, just as in many turbulent shear flows once believed to be characterized adequately by inhomogeneous small-scale randomness, so also closer inspection of the tornado (Fujita 1975; Forbes 1976; Fujita and Forbes 1976) reveals the apparent existence of recurring large-scale coherent vortical substructure (Davies and Yule 1975; Roshko 1976). The substructure consists of so-called satellite or suction vortices that persist for a few seconds within the confines of the larger identity referred to as a tornado; the suction vortices are sometimes conceived of as symmetrically positioned within an annulus circumscribed by the large tornado. Time-averaged modeling has not, and perhaps inherently cannot, recover such transient nonaxisymmetric substructure; of course, the significance of such substructure to any mean description of the tornado for many engineering purposes is moot, though clearly other departures from the mean (such as gustiness) are probably significant for injection of missiles into the vortical flow field. It should be noted that Coriolis effects and translational wind speeds often interject nonaxisymmetric properties in the outer portions of the tornado wind field, but suction vortices introduce nonaxisymmetric properties into the

whirlwind core. Due to these considerations, the present approach is considered to be more appropriate to the problem.

Here, not only is the mature intense vortex taken as axisymmetric and steady in those portions of interest, but the axis of rotation is taken as vertical. Highly tilted and irregular axes are often indications of a weak (incipient or decaying) vortex (Morton 1966), but exceptions have been cited. Nevertheless, a conventional cylindrical polar coordinate system is adopted here, since the simpler cases deserve treatment before the more complicated cases are undertaken.

B. STRUCTURE OF A TORNADO

The model for the surface inflow layer, in which frictional effects balance with pressure-gradient and inertial effects, may be clarified by first presenting an idealized four-part subdivision (Barcilon 1967; Carrier 1970; Dergarabedian and Fendell 1970) of the entire intense quasi-steady axisymmetric vortex (Figure A-1). In region I there is rapidly swirling air, in which the radial pressure gradient inward is virtually in equilibrium with the centrifugal force (so-called cyclostrophic balance). (The Coriolis acceleration enters at larger radial distances at which the swirl decreases to translational and other ambient wind speeds, such that a gradient wind balance approximates the conservation of radial momentum. However, interest here is on the high-swirl regions in which the Coriolis acceleration, important as it may be during spin-up, plays little role in the intense mature vortex.) In region I there is very little variability with altitude of the dependent variables (aside from hydrostatic stratification); there is virtually no radial inflow, and only a weak downdraft into the surface inflow layer II. The radial profile of the swirl in I is taken to be that of a potential vortex; this is particularly appropriate in the high-speed region if one views spin-up as involving convectively induced advection of (particlewise conserved) ambient angular momentum. The potential vortex is an adequate, if less accurate, profile at larger radial positions.

In region II, the no-slip boundary condition retards the centrifugal force, such that the "favorable" radial pressure gradient of I drives an appreciable

radial influx of swirling air toward the axis of symmetry. The frictional effects at the surface dissipate some of the angular momentum of inflowing air; i.e., in II angular momentum is not conserved. In II, the classical thin-layer approximation of Prandtl is valid, such that parabolic partial differential equations describe the conservation of radial and azimuthal momentum, the radial velocity being comparable to, and even possibly exceeding, the swirl in some limited parts of region II. The (relatively small) vertical velocity component is obtained from continuity, once the swirl and radial velocity components are known.

In region III, there is an eruption of the boundary layer upward, virtually to the tropopause, in an annulus around the central region IV. In region III the hydrostatic approximation may be locally invalid very near the ground owing to rapid upward acceleration, even though the hydrostatic approximation suffices in general. At the inner edge of region III the swirl increases very rapidly with radius, rising from virtually zero at the inner edge to its maximum value. Fluid particles rise rapidly, such that the moist adiabat furnishes a rough approximation to the locus of thermodynamic states. The low-level flow in III may well overshoot its equilibrium, such that the fluid particles move radially inward, then radially outward as they rise; with increasing radial distance from the axis, under conservation of angular momentum, swirl decreases, such that relative to an observer in a noninertial frame of reference, the upper-tropospheric swirl at large radial distances may appear to be reversed in sense from that in the lower troposphere. Thus, the tornado has low-level inflow, inner updraft, and high-level outflow. Region III may well warrant furthur subdivision, but since it is not the matter of principal concern here, the subject is deferred; it seems likely that an adequate treatment of region II, attempted here, must precede treatment of region III, because II furnishes starting spatial conditions for III.

Region IV is a central downdraft of dry virtually nonrotating upper-tropospheric, or, more likely, lower-stratospheric air, that undergoes compressional heating on a dry adiabat as it descends. Thermohydrostatic calculations for tornado-spawning ambient (Dergarabedian and Fendell 1976) indicate that the 100 mb pressure deficits from ambient, compatible with 200 mph peak

swirls implicit in funnel-cloud behavior, are realizable only if there is a two-cell structure to severe tornadoes (Dergarabedian and Fendell 1973). Thus the severe tornado has a nonrotating central core analogous to the eye of a hurricane or typhoon (Carrier, Hammond, and George 1971; Fendell 1974). Because of the smaller radial spatial scale of a tornado, the updraft of the "eyewall" of a tornado (region III) so shears the "eye" (region IV) that a significant recirculation (although still no rotation) can be established in the "eye." This recirculation helps explain how an "eye" may form within a tornado on the order of 10 min, the scale on which a tornado can go from 100 mph to 200 mph. The "eye" may be an oscillatory or transient tornado property that recurringly is established and decays. Finally the existence of a significant "eye" recirculation suggests that absolute upper bounds on achievable pressure deficits cannot be obtained by thermohydrostatic calculations using idealized atmospheric processes; minor corrections owing to additional pressure deficit from ambient from nonhydrostatic effects may need consideration. However, estimation that the thermohydrostatically computed bounds are 100% in error (Lewellen 1976), such that peak swirls may reach 450 mph, seems unsubstantiated.

C. THE FRICTIONAL INFLOW LAYER FORMULATION

Because it is of primary interest here, further attention is now focused on the frictional inflow layer.

Because of the current lack of detailed understanding of how friction occurs in a spinning fluid at large Reynolds number, one introduces eddy viscosity concepts. Such an approximate formulation warrants only an approximate solution, which presents the key information in convenient, readily usable form. Thus, in addition to the already discussed model of an incompressible axisymmetric flow under a potential vortex, with negligible role for Coriolis acceleration, further convenient simplifications of consistent character are introduced. For example, selfsimilar concepts are to be developed as far as possible, so ordinary differential equations, rather than parabolic partial differential equations, require treatment (Burggraf, Stewartson, and Belcher 1971).

A closed system of finite radial extent r_0, is adopted, so there is no radial flow across the outer boundary. Typically, $r_0 = 10\ r_1$, where r_1 is the radius of maximum winds. The boundary layer grows monotonically, but relatively slowly in thickness as one proceeds radially inward from the outer edge of the vortex. Near the outer edge, friction plays a role across the entire vertical extent of the surface inflow layer. However, closer to the axis, the bulk of the radial inflow is described by inviscid analysis; only in a thin layer immediately adjacent to the ground does friction alter the radial velocity component significantly (for enforcement of the no-slip surface boundary condition) (Carrier 1971; McWilliams 1971; Burggraf, Stewartson and Belcher 1971). On the other hand, the azimuthal velocity component profile is shaped significantly by friction across the entire extent of the surface inflow layer, at all radial positions. The precise details of the flow, but not its qualitative character, depend upon the eddy viscosity model. For example, one anticipates a nonoscillatory vertical profile for both the radial and azimuthal velocity components. Whereas the radial velocity component has a larger maximum at smaller radial positions (a maximum that can become as large as the swirl speed above the surface inflow layer), at fixed altitude within the inflow layer the circulation becomes smaller at smaller radial positions. In any case, the assertion (Chi 1975; Lewellen 1976) that the swirl within the inflow layer may appreciably exceed its asympotic value outside the inflow layer, at fixed radial position, is regarded as unlikely.

Under previously discussed approximations, if in cylindrical polar coordinates (r, θ, z) the corresponding velocity components are denoted (u, v, w), the conservation of mass, radial momentum, and angular momentum may be expressed as follows (with subscript r, z denoting partial differentiation):

$$(ru)_r + (rw)_z = 0 \ ; \tag{A-1}$$

$$\frac{(rV)^2 - (rv)^2 - (ru)^2}{r^2} = [\nu(ru)_z]_z - u(ru)_r - w(ru)_z \ ; \tag{A-2}$$

$$[\nu(rv)_z]_z - u(rv)_r - w(rv)_z = 0 \ ; \tag{A-3}$$

the boundary conditions are

$$z - \infty: \quad v \to \psi/r \text{ const.}; \; u \to 0 ; \tag{A-4}$$

$$z = 0 : \; u = v = w = 0 ; \tag{A-5}$$

$$r = r_0: \; u = 0, \; v \text{ specified } (-\psi/r_0) \tag{A-6}$$

Here, r_0 is a given const., and signifies the outer extent. It is anticipated that the formulation is to be applied only in the range $r_1 \leq r \leq r_0$, where r_1 is the (finite) radius of maximum winds. Also,

$$\psi = rV, \text{ const.} \tag{A-7}$$

It may be noted that the cyclostrophic balance has been used to identify the radial pressure gradient in (A-2):

$$\frac{1}{\rho} p_r = \frac{V^2}{r} . \tag{A-8}$$

D. CONSTANT VISCOSITY SOLUTION

If ν is const., either because a laminar flow is under investigation, or because the eddy visocosity is crudely approximated as a constant in turbulent flow, then solution to (A-1) - (A-2) is sought in the form

$$ru = -\psi \beta(r) g'(\eta), \; rv = \psi f(\eta), \; w = W(\eta), \tag{A-9}$$

where

$$\eta = \frac{z}{\sqrt{s(r)}} \left(\frac{\psi}{\nu}\right)^{1/2} \tag{A-10}$$

Here, $s(r)$ and $\beta(r)$ are functions to be identified in solution. One does not expect (A-9) - (A-10) to give an exact solution, but to capture the essence of the functional behavior in a very useful form.

Substitution of (A-9) - (A-10) in (A-1) gives

$$W_\eta = (\nu\psi)^{1/2}\left[\frac{s^{1/2}}{r}\,\beta' g' - \frac{\beta s'}{2r\,s^{1/2}}\,\eta g''\right]$$

$$= (\nu\psi)^{1/2}\left[\frac{s^{1/2}}{r}\,\beta' g' - \frac{\beta s'}{2r\,s^{1/2}}\,(\eta g' - g)'\right];$$

$$W = (\nu\psi)^{1/2}\left[\left(\frac{s^{1/2}\,\beta'}{r} + \frac{\beta s'}{2r\,s^{1/2}}\right) g - \frac{\beta s'}{2r\,s^{1/2}}\,\eta g'\right], \qquad \text{(A-11)}$$

where by (A-5)

$$g(0) = 0\,. \qquad \text{(A-12)}$$

Substitution of (A-9) - (A-10) in (A-2) and (A-3) gives, respectively,

$$\frac{\psi^2}{r^2}\,(1 - f^2 - \beta^2 g'^2) = -\beta\psi^2\left[\frac{g'''}{s}\left(\frac{\beta'}{r} + \frac{\beta\, s'}{2r\, s}\right) gg''\right] - \frac{\psi^2}{r}\,\beta\beta' g'^2\,; \qquad \text{(A-13)}$$

$$\psi^2\left[\frac{f''}{s} - \left(\frac{\beta'}{r} + \frac{\beta s'}{2r\, s}\right) gf'\right] = 0\,. \qquad \text{(A-14)}$$

The terms in (A-13) derive, from left to right, from similarly positioned terms in (A-2). For self-consistency, one must take

$$\frac{s\beta'}{r} + \frac{s'\beta}{2r} = -1\,, \qquad \text{(A-15)}$$

say; also, it is necessary, but not sufficient, to take

$$g'^2 = 1 - f^2 , \tag{A-16}$$

$$\frac{\beta\beta'}{r} = - \frac{1 - \beta^2}{r^2} \tag{A-17}$$

From (A-6), $\beta(r_0) = 0$; hence, from (A-17),

$$\beta^2 = \frac{r_0^2 - r^2}{r_0^2} . \tag{A-18}$$

Equation (A-15) may be written

$$(\beta^2 s)' = -2r\beta \Longrightarrow s = \frac{2}{3} r_0 (r_0^2 - r^2)^{1/2} \tag{A-19}$$

by use of (A-18).

The term in square brackets in (A-13) is $0(\beta\psi^2/s)$, while the other terms are $0(\psi^2/r^2)$; substitution of (A-18) and (A-19) shows that the ratio of the bracketed to unbracketed terms is $0(3r^2/2r_0^2)$, so that for $r \ll r_0$, the bracketed term is negligible. The neglect of the bracketed term gives an inaccurate result where the motion is slow [i.e., where $v = 0(v_{max}/10)$, $u < 0(v_{max}/10)$], and an accurate result where the motion is fast. From (A-19), $s^{1/2} \sim (r_0 - r)^{1/4}$, as $r \to r_0$; this is consistent with the more meticulous analysis of Stewartson, Burggraf, and Belcher (1971). It may be noted that such physical insights into flow details remain totally unexposed in most accounts (Kuo 1971).

The radial momentum equation for $r_0^2 \gg r^2$, so that $\beta \to 1$, becomes a statement that the left-hand side of (A-2) vanishes; i.e., $V^2 = u^2 + v^2$, such that the radial velocity component is inviscidly controlled. The two-point nonlinear third-order boundary-value problem, from (A-13) - (A-18), becomes

$$f''' + gf'' = 0 \; ; \tag{A-20}$$

$$g' = (1 - f^2)^{1/2} \; ; \tag{A-21}$$

$$f(0) = g(0) = 0, \; f(\infty) \to 1. \tag{A-22}$$

The boundary conditions follow from (A-4), (A-5), (A-7), (A-9), (A-10), and (A-12). The problem is readily solved numerically by shooting; one finds

$$f''(0) \doteq 0.7456, \; g(\infty) \doteq 1.941. \tag{A-23}$$

Results are graphed in Fig. A-2, where it is evident that f monotonically increases (so g' monotonically decreases).

Of course, the reduction to third order results from dropping of the frictional term in the conservation of radial momentum (A-13), which has been taken in the inviscid form (A-16). Enforcement of all of (A-5), specifically $g'(\eta = 0) = 0$ so that $u(x, z = 0) = 0$, requires restoration of the frictional term in a thin near-ground sublayer of the inflow layer.

For completeness, a brief sketch of the near-wall sublayer, in which u falls to zero, is developed now. If

$$ru = -\psi\beta(r)h'(\sigma), \; \sigma = \frac{z}{m(r)}\left(\frac{\psi}{\nu}\right)^{1/2}, \; \beta = 1 - (r/r_0)^2 \; , \tag{A-24}$$

then from continuity

$$(rw)_\sigma = m\left(\frac{\nu}{\psi}\right)^{1/2} \left[\beta\psi h' - \beta\psi h'' \left(\frac{m'}{m}\right)\sigma \right] , \tag{A-25}$$

or

$$rw = m\left(\frac{\nu}{\psi}\right)^{1/2} \left[\beta'\psi h - \beta\psi \left(\frac{m'}{m}\right)(\sigma h' - h)\right] \tag{A-26}$$

From the radial momentum equation,

$$-\left(\frac{\beta}{m^2}\right) h''' - \left(\frac{\beta\beta'}{r}\right) h'^2 + \left[\frac{\beta(\beta' + \beta m^{-1} m')}{r}\right] hh''$$

$$= \frac{1}{r^2} - \left(\frac{\beta^2}{r^2}\right) h'^2 - \left(\frac{1}{r^2}\right) f^2 , \qquad \text{(A-27)}$$

where the last term involving f^2 is dropped as negligible. The function m is assigned by demanding

$$\frac{\beta^2 m'}{r\, m} = \frac{1}{r^2} \qquad \text{(A-28)}$$

If attention is concentrated on $(r/r_0) \ll 1$, such that $\beta \to 1$, $\beta' \to 0(1)$, then

$$m \doteq r , \qquad \text{(A-29)}$$

and

$$-h''' + (hh')' \doteq 1 , \qquad \text{(A-30)}$$

where all neglected terms are $0(r^2/r_0^2)$ or smaller. The boundary conditions are

$$h(0) = 0,\ h'(0) = 0,\ h'(\infty) \to 1 ; \qquad \text{(A-31)}$$

these enforce $w(x,\ z = 0) = 0$, $u(x,\ z = 0) = 0$, and matching of the sublayer and outer-layer solutions, respectively. One arrives at a Riccati equation

$$-h' + \frac{h^2}{2} = \frac{\sigma^2}{2} - h''(0)\,\sigma,\ h(\sigma \to \infty) \to \sigma , \qquad \text{(A-32)}$$

where the boundary conditions have been used to assign a constant of integration. The results of Burggraf, Stewartson, and Belcher (1971) assure that a solution exists, and for present purposes

$$h(\sigma) \doteq \sigma + \exp(-\sigma) - 1 \Longrightarrow h'(\sigma) = 1 - \exp(-\sigma) , \tag{A-33}$$

captures its behavior adequately (see Fig. A-3). Hence, a uniformly valid expression for $r^2 \ll r_0^2$ is

$$ru \doteq -\psi\beta(r)\left[h'(\sigma) + h'(\eta) - 1\right] \tag{A-34}$$

where $h'(\sigma)$ is given by (A-32), or, facilely, by (A-33), and $h'(\eta)$ is given by (A-20) - (A-22).

This modification is regarded here as a detail from an engineering point of view; the solution to (A-20) - (A-22) would normally furnish an adequate approximation by itself.

E. THE FLAT-PLATE TURBULENT BOUNDARY LAYER

The purpose of this section is to establish concepts and procedures for Section F, in which the ground frictional layer under a tornado vortex is studied for a spatially varying eddy viscosity. Here, a mean description of the downstream-asymptotic turbulent boundary layer on a smooth flat plate is developed for two-dimensional isobaric constant-density constant-property flow. The initial goal is to develop a simple method leading to simply interpreted results. Explicitly, a uniformly valid representation of the solution is sought for a plausible eddy-viscosity model: a Prandtl mixing-length theory (without the van Driest correction factor) for the viscous sublayer, is patched, at the local transverse position of equal magnitude, to a Clauser form (without the Klebanoff intermittency correction factor) for the defect layer (Smith and Cebeci 1968; Fendell 1972; Bush and Fendell 1972; White 1974). The total viscosity is the sum of the molecular and eddy viscosities.

If (x, z) are the streamwise and transverse coordinates, respectively, and (u, w) are the corresponding velocity components, then continuity and momentum conservation require (subscripts x, z denote partial differentiation):

$$u_x + w_z = 0 \,, \tag{A-35}$$

$$(\nu u_z)_z - u u_x - w u_z = 0 \,, \tag{A-36}$$

where the no-slip boundary conditions and outer condition are ($0 \leq z \leq \infty$):

$$u(x, 0) = w(x, 0) = 0; \quad u(x, z \to \infty) \to u_0, \text{ const. (given)} \,. \tag{A-37}$$

The total viscosity is taken as

$$\nu = \nu_0 + \nu_e \,, \tag{A-38}$$

where ν_0 is the molecular viscosity and ν_e is the eddy viscosity. Explicitly, then,

$$\nu_e = \begin{cases} k_1 z^2 u_z & \text{in the viscous sublayer} \\ \\ k_2 u_0 \delta^*(x) & \text{in the defect layer,} \end{cases} \tag{A-39}$$

where the velocity displacement thickness

$$\delta^*(x) = \int_0^\infty \frac{u_0 - u}{u_0} \, dz \,. \tag{A-40}$$

The factor $k_1 = \kappa^2$, where the von Karman constant $\kappa = 0.41$; the Clauser constant $k_2 = 0.016$.

The following change of coordinates is introduced:

$$(x, z) \rightarrow (\bar{x}, \eta) \text{ where } \bar{x} = x, \ \eta = z/s(x) , \tag{A-41}$$

and s(x) is to be identified. The motivation behind this change of independent variable is that the solution may be profitably sought initially as a function of η only, i.e., in selfsimilar form. This selfsimilar form may then be simply modified to account for the non-selfsimilar character of the solution.

Accordingly, if subscript η denotes partial differentiation,

$$u(x, z) \equiv u_0 f_\eta(x, \eta) , \tag{A-42}$$

and from continuity (A-35),

$$w_\eta = -su_x$$

$$= -su_0 \left(f_{x\eta} - \frac{s'}{s} \eta f_{\eta\eta} \right) , \tag{A-43}$$

or, from (A-37),

$$w = -su_0(f_x) + s'u_0(\eta f_\eta - f) . \tag{A-44}$$

Use of (A-41) and (A-42) in (A-39) gives

$$\nu_e = \begin{cases} u_0 \, s(x) \, k_1 \eta^2 \, f_{\eta\eta}(x, \eta), & \text{in the viscous sublayer} \\ u_0 \, s(x) \, k_2 \delta^*(x), & \text{in the defect layer,} \end{cases} \tag{A-45}$$

where

$$\delta^*(x) = \int_0^\infty \left[1 - f_\eta(x, \eta) \right] d\eta. \tag{A-46}$$

At any fixed x, the transition between functional forms for ν_e occurs at $\eta_1(x)$, where

$$k_1 [\eta_1(x)]^2 f_{\eta\eta}[x, \eta_1(x)] = k_2 \delta^*(x) . \tag{A-47}$$

Hence it is convenient to write

$$\nu_e = u_0 s(x) \left\{k_1 \eta^2 f_{\eta\eta}(x, \eta)\right\}_* \tag{A-48}$$

where, with $\eta_1(x)$ defined by (A-47),

$$\left\{H(x,\eta)\right\}_* \equiv \left\{k_1 \eta^2 f_{\eta\eta}(x,\eta)\right\}_* = \begin{cases} k_1 \eta^2 f_{\eta\eta}(x,\eta) , & 0 \leq \eta \leq \eta_1(x) \\ \\ k_1 \eta_1^2 f_{\eta\eta}(x,\eta_1), & \eta_1(x) \leq \eta \leq \infty . \end{cases} \tag{A-49}$$

If the inverse of the Reynolds number based on streamwise distance is introduced:

$$\epsilon \equiv \frac{\nu_0}{u_0 s(x)} , \quad 0 < \epsilon << 1 , \tag{A-50}$$

then (A-37) may be written

$$\left\{\left[\epsilon(x) + \left\{H(x,\eta)\right\}_*\right] f_{\eta\eta}\right\}_\eta + s' f f_{\eta\eta} = s(f_\eta f_{x\eta} - f_x f_{\eta\eta}) . \tag{A-51}$$

Tentatively it is taken that

$$s' = 1 \Rightarrow s \doteq x . \tag{A-52}$$

It will later be shown that this is an inadequate representation for s; but it seems advisable for exposition to adopt this simple form, demonstrate the need for improvement, and thus motivate better representation.

One may now write, if $E \equiv \ell n\ \epsilon$,

$$\left\{ \left[\epsilon(x) + \left\{ H(x,\eta) \right\}_* \right] f_{\eta\eta} \right\}_\eta + f_\eta f_{\eta\eta} = f_{\eta\eta} f_E - f_\eta f_{\eta E} , \tag{A-53}$$

$$f(x,0) = f_\eta(x,0) = f_\eta(x, \eta \to \infty) - 1 = 0 . \tag{A-54}$$

Clearly the source of explicit x dependence in f is owing to $\epsilon(x)$, so one may write

$$f(x,\eta) \to f\left[\epsilon(x), \eta \right] \tag{A-55}$$

Again, $0 < \epsilon(x) << 1$ is of interest in a downwind-asymptotic theory. For the tractability of selfsimilarity, it is tempting to seek a solution for f which is only parametrically dependent on $\epsilon(x)$, in the hope that f varies little with $\epsilon(x)$ for small $\epsilon(x)$. Thus, (A-53) is approximated as

$$\left\{ \left[\epsilon(x) + \left\{ H(\eta) \right\}_* \right] f_{\eta\eta} \right\}_\eta + f\, f_{\eta\eta} \doteq 0, \quad \epsilon = \frac{\nu_0}{u_0 x} , \tag{A-56}$$

subject to (A-54). In solving (A-56), one may assign a sequence of small numerical values to $\epsilon(x)$, and obtain $f(\eta;\epsilon)$. Hence,

$$\left\{ H(\eta) \right\}_* = \begin{cases} k_1\, \eta^2\, f_{\eta\eta}(\eta;\epsilon), & 0 \leq \eta \leq \eta_1(\epsilon) \\ k_1\, \eta_1^2\, f_{\eta\eta}(\eta_1;\epsilon), & \eta_1(\epsilon) \leq \eta \leq \infty, \end{cases} \tag{A-57}$$

where

$$k_1^2[\eta_1(\epsilon)]^2 f_{\eta\eta}(\eta_1;\epsilon) = k_2\sigma(\epsilon) , \tag{A-58}$$

where, in turn, σ is a special designation for δ^*:

$$\sigma(\epsilon) = \int_0^\infty [1 - f_\eta(\eta;\epsilon)]\, d\eta . \tag{A-59}$$

In fact, it will turn out that substitution of the solution to (A-56), subject to (A-54), into (A-53) reveals that the discarded terms on the right-hand side may not be justifiably ignored relative to terms that are retained. The differential dependence on the streamwise coordinate cannot be treated as a purely parametric dependence; i.e., the "local similarity" approximation does not yield high accuracy.

As presently stated, for fixed given ϵ, in numerically solving (A-56), with (A-57) - (A-59), under (A-54), one must apparently guess, say $f''(\eta = 0;\epsilon)$ and $\eta_1(\epsilon)$ to obtain $f(\eta \to \infty;\epsilon)$ and σ. When the obtained $f(\eta \to \infty;\epsilon) \to 1$ and the obtained σ is compatible with (A-58), one has a solution for that ϵ. In fact, there is a standard procedure to reduce this two-degree-of-freedom shooting-type boundary-value problem to a simpler one-degree-of-freedom problem. For this purpose, consider a boundary-value problem for $F(\xi;\epsilon')$, where $0 \leq \xi \leq \infty$, $\epsilon' > 0$:

$$\left\{ [\epsilon' + \{k_1\xi^2 F_{\xi\xi}\}_*]\, F_{\xi\xi} \right\}_\xi + FF_{\xi\xi} = 0, \tag{A-60}$$

where (A chosen)

$$F(\xi = 0;\epsilon') = F_\xi(\xi = 0;\epsilon') = F_{\xi\xi}(\xi = 0;\epsilon') - A = 0 , \tag{A-61}$$

and ξ_1 is chosen, where

$$\left\{k_1 \xi^2 F_{\xi\xi}(\xi;\epsilon')\right\}_* = \begin{cases} k_1 \xi^2 F_{\xi\xi}(\xi;\epsilon'), & 0 \leq \xi \leq \xi_1 \\ k_1 \xi_1^2 F_{\xi\xi}(\xi_1;\epsilon'), & \xi_1 \leq \xi \leq \infty. \end{cases} \tag{A-62}$$

One may now readily calculate $F(\xi;\epsilon')$, where for convenience the notation

$$F_\xi(\xi \to \infty;\epsilon') \to B \tag{A-63}$$

is introduced. For relation of (A-60) - (A-63) to (A-56) - (A-59), one lets

$$\eta = \alpha\xi, \; f(\eta;\epsilon) = c\,F(\xi;\epsilon'), \; \epsilon = c^2\epsilon' , \tag{A-64}$$

where α, c are constants to be identified. The two boundary-value problems are equivalent with respect to boundary conditions at the origin and infinity, and with respect to differential equation if

$$\alpha = 1 \Rightarrow \eta = \xi; \; c = \frac{1}{B} \Rightarrow f(\eta;\epsilon) = B^{-1}F(\eta;B^{-2}\epsilon) . \tag{A-65}$$

However, the η_1, ϵ, f, and σ so obtained will not, in general, satisfy (A-58) - (A-59). Thus one must select another trial value for the transition point in the ξ problem, denoted here ξ_1'; this new trial yields B', hence c' (ϵ' conveniently being held fixed). The new $F'(\eta;\epsilon')$ implies a new function $f'(\eta;\epsilon)$, and hence a new integral value σ'. The procedure of selecting transition points in the ξ problem is continued until results compatible with the requirement of (A-58) are obtained. Thus a one-degree-of-freedom iteration has been identified, albeit an iteration in which one cannot preselect ϵ.

Numerical results for the boundary-value problems posed by (A-54) and (A-56), obtained by use of (A-60) - (A-65), are displayed in Figs. A-4 to A-6 for a physically interesting range of ϵ; the initial data required to "shoot" (A-54) and (A-56) are summarized in Table A-1.

One now considers the value of the right-hand side of (A-53), and the value of the nonlinear convective term of the left-hand side of (A-53), for several values of η for each value of ϵ studied. Simple finite differences between results for a given ϵ under scrutiny, and the results for the next larger value of ϵ for which computations were undertaken, are used to constitute derivatives with respect to $E = \ell n(\epsilon)$. Inspection of the numerical results reveals that the neglected right-hand side is adequately approximated for current purposes as a constant multiple of the left-hand side. In short, in (A-52),

$$s(f_\eta f_{x\eta} - f_x f_{\eta\eta}) = -s' A\, ff_{\eta\eta},\ A \doteq -1/2 . \tag{A-66}$$

If now

$$S = s'(1 + A) \tag{A-67}$$

then (A-51) may be written as (A-56) if $S = 1$, so that

$$s' = 1/(1 + A) . \tag{A-68}$$

Hence, selfsimilar results presented in Figures A-4 to A-6 and Table A-1 as solutions to (A-54) and (A-56) are satisfactory solutions to the nonselfsimilar problem (A-53) and (A-54) if one merely reinterprets s, such that in (A-41), (A-44), (A-45), and (A-50)

$$s = 2x . \tag{A-69}$$

The convenience of the selfsimilar form makes the present development preferable to a direct numerical solution of the partial differential equation. Ultimately a more adequate accounting for the contribution of the nonselfsimilar terms is warranted; of course, a comparison with experimental results is also planned.

F. THE TURBULENT BOUNDARY LAYER UNDER A TORNADO VORTEX

Solution to (A-1) - (A-6) is again sought in the selfsimilar form (A-9):

$$ru = -\psi\beta(r)g'(\eta),\quad rv = \psi f(\eta),\quad w = W(\eta)\ , \tag{A-70}$$

where now

$$\eta = \frac{z}{s(r)}\ . \tag{A-71}$$

The functions $\beta(r)$, $s(r)$ will not be those appropriate to the constant-viscosity problem, but must be determined by an analysis of the same character as that used in the constant-viscosity problem. Specifically, in contrast to the representation in paragraph C, here

$$\nu = \frac{s\psi}{r}\ H(\eta)\ , \tag{A-72}$$

where $H(\eta)$ is to be specified. From the results of paragraph E, it is clear that selfsimilarity is not entirely adequate, and in future investigations, the authors anticipate improving the tentative results which will be given in the following.

Substitution of (A-70) into (A-1) yields, under (A-5),

$$W(\eta) = \psi\left[\left(\frac{s\beta'}{r} + \frac{\beta s'}{r}\right) g - \frac{\beta s'}{r}\ \eta g'\right] \tag{A-73}$$

Substitution of (A-70) into (A-3) gives

$$\frac{1}{sr}\left\{\left[H(\eta)f'\right]' - (\beta s)'\ gf'\right\} = 0\ ; \tag{A-74}$$

consistency leads to the choice

$$(\beta s)' = -1 \Rightarrow \beta s = r_0 - r\ , \tag{A-75}$$

where (A-6) has been used. Hence,

$$(Hf')' + gf' = 0 . \tag{A-76}$$

Substitution of (A-70) into (A-2) gives

$$\frac{\beta}{rs}\left[(Hg'')' + gg''\right] + \frac{\beta\beta'}{r}(g')^2 = \frac{1}{r^2}\left[1 - f^2 - \beta^2(g')^2\right] . \tag{A-77}$$

It is generally expected, and it is appropriate to anticipate here also, that the boundary layer associated with the azimuthal velocity component v thickens faster in the turbulent case than in the laminar case. It may be noted that the pressure gradient plays no role in the conservation of angular momentum (A-76), and hence does not directly enter into considerations concerning the thickness of the swirl boundary layer. One may also expect that the radial-velocity-component "sublayer", in which friction enters as a significant factor, will occupy even less of the swirl-boundary-layer thickness than in the laminar case (paragraph C). Thus, in most of radial-velocity-component boundary layer, especially that portion in which the radial inflow plays a significant convective role, (A-77) degenerates to a balance between acceleration and pressure gradient, without friction; i.e., (A-77) may be approximated

$$\frac{\beta\beta'}{r}(g')^2 = -\frac{1}{r^2}\left[1 - f^2 - \beta^2(g')^2\right] . \tag{A-78}$$

For self-consistency on the right-hand side

$$(g')^2 = 1 - f^2 ; \tag{A-79}$$

then for self-consistency on the left-hand side

$$\frac{\beta\beta'}{r} = -\frac{1 - \beta^2}{r^2} \Rightarrow \beta^2 = 1 - \left(\frac{r}{r_0}\right)^2 , \tag{A-80}$$

from (A-6).

From (A-75) and (A-80), tentatively,

$$s = r_0 \left(\frac{r_0 - r}{r_0 + r} \right)^{1/2} \tag{A-81}$$

From the results of the flat-plate boundary layer study of paragraph D, it is anticipated that ultimately the definition of s must be modified from that given in (A-81) to account for the nonnegligible contributions from nonselfsimilar terms in the conservation of radial and angular momentum.

Hence the boundary-value problem becomes (A-76) and (A-79), with the boundary conditions analogous to (A-22):

$$f(0) = g(0) = 0; \; f(\eta \to \infty) \to 1 \; . \tag{A-82}$$

By analogy again, this time with the flat-plate turbulent boundary layer studied in paragraph E, $\nu = \nu_0 + \nu_e$.

$$\nu_e = \begin{cases} k_1 z^2 \left(u_z^2 + v_z^2 \right)^{1/2} & \text{in the wall layer} \\ \\ k_2 \left(\frac{\psi}{r} \right) \delta^* & \text{in the defect layer} \end{cases} \tag{A-83}$$

where ν_0 is the molecular viscosity; k_1 is the square of the von Karman const., or $(0.41)^2$; k_2 is the Clauser const., 0.016; and δ^* is the angular-momentum-defect thickness.† Again a van Driest-type wall layer correction and an intermittancy-type defect layer correction (Fendell 1972; Bush and Fendell 1972; White 1974) have been omitted as nonessential. In similarity variables, in view of (A-79), (A-83) becomes

$$\nu_e = \begin{cases} \left(\frac{\psi s}{r} \right) k_1 \eta^2 \; \frac{f'}{(1 - f^2)^{1/2}} \left[1 + f^2 (\beta^2 - 1) \right]^{1/2} \\ \\ \left(\frac{\psi s}{r} \right) k_2 \sigma \end{cases} \tag{A-84}$$

† The notation δ^* is used for this quantity for the remainder of the appendix because it is analogous to the displacement thickness defined in eq. A-40.

in the corresponding regions. In the defect layer, use is made of the fact, if σ denotes a constant (to be determined),

$$\delta^* = \int_0^\infty \left(1 - \frac{rv}{\psi}\right) dz = s \int_0^\infty (1 - f)\, d\eta \equiv s\sigma \,. \tag{A-85}$$

Hence, from (A-72), since the molecular viscosity is taken as everywhere additive to the eddy viscosity, in conventional manner, for $r << r_0$ so $\beta \to 1$,

$$\nu = \frac{s\psi}{r} H(\eta),\ H(\eta) = \epsilon + k_1 \left\{ \frac{\eta^2 f'(\eta)}{\left[1 - f^2(\eta)\right]^{1/2}} \right\}_* \,. \tag{A-86}$$

Here, as before, $\{F(\eta)\}_* = \{F(\eta)\}$ for $0 \leq \eta \leq \eta_1$ and $\{F(\eta)\}_* = F(\eta_1)$ for $\eta_1 \leq \eta \leq \infty$, and since $s \cdot r_0$ for $r \ll r_0$,

$$\epsilon = \left(\frac{\nu_0}{\psi}\right) \frac{r}{s} \to \left(\frac{\nu_0}{\psi}\right) \frac{r_{min}}{r_0} \,. \tag{A-87}$$

For consistency with the similarity treatment, r has been taken uniformly constant at its smallest value within the range of interest. At $\eta = \eta_1$, the eddy viscosity switches from its mixing-length form appropriate to the wall layer (viscous sublayer) $0 \leq \eta \leq \eta_1$, to its Clauser form appropriate to the defect layer $\eta_1 \leq \eta \leq \infty$. The eddy viscosity is made continous by defining η_1 such that

$$k_1 \eta_1^2 \frac{f'(\eta_1)}{\left[1 - f^2(\eta_1)\right]^{1/2}} = k_2 \sigma \,. \tag{A-88}$$

In summary, the solution for the functions of (A-70) - (A-71), with β identified in (A-80), s in (A-81), and W in (A-73), is given by

$$(HF') + gf' = 0; \; (g')^2 = 1 - f^2 ;$$

$$H(\eta) = \begin{cases} \epsilon + k_1 \dfrac{\eta^2 f'(\eta)}{\left[1 - f^2(\eta)\right]^{1/2}} & , \; 0 \leq \eta \leq \eta_1 \\ \epsilon + k_1 \dfrac{\eta_1^2 f'(\eta_1)}{\left[1 - f^2(\eta_1)\right]^{1/2}} & , \; \eta_1 \leq \eta \leq \infty \end{cases}$$

where $\epsilon(\ll 1)$ is given, $k_1 = (0.41)^2$, and η_1 is given by ($k_2 = 0.016$)

$$k_1 \eta_1^2 \frac{f'(\eta_1)}{\left[1 - f^2(\eta_1)\right]^{1/2}} = k_2 \sigma ,$$

in which

$$\sigma = \int_0^\infty \left[1 - f(\eta)\right] d\eta .$$

The boundary conditions are

$$f(0) = g(0) = 0, \; f'(\eta \to \infty) \to 1.$$

This is a two degree-of-freedom iteration in that, for example, one must anticipate both $f'(0)$ and η_1, and confirm the validity of the guesses by obtaining σ compatible with (A-88) and $f(\eta \to \infty)$ compatible with (A-82), in a shooting-type method of solution. Reduction to a one-degree-of-freedom iteration is not readily executed. Nevertheless, solution for various values of ϵ is

straightforward, and presented in Figs. A-7 to A-11, with the values required for "shooting" tabulated in Table A-2.

Clearly $g'(0) = 1$, so there exists a very thin near-wall sublayer through which friction acts to enforce the no-slip ground boundary condition on the radial velocity component. The analogy to the sublayer developed in (A-24) - (A-34) for the constant-viscosity model could be developed for the variable viscosity model; pending that development, one may adopt the constant-viscosity results given in (A-24) - (A-34).

G. PRELIMINARY DISCUSSION OF THE TURNAROUND

The eruption of the low-level inflow in region II into the annular updraft of region III (Fig. A-1) is now given very brief consideration.

First, it is recalled from Paragraphs D and F that the boundary layer under an intense vortex has a two-part structure (Fig. A-12). If z again denotes distance normal to the solid bounding surface, $z = a(r)$ denotes the thickness of that portion of the boundary layer in which intense frictional stresses arise. This portion becomes thinner at smaller radial distances from the axis of symmetry, because of acceleration under the positive radial pressure gradient. Conversely, the thickness of the larger layer $z = b(r) - a(r) \doteq b(r)$, in which the defect in the azimuthal velocity component is balanced by an increase in the radial velocity component as the boundary is approached, increases slowly in thickness at smaller radial distances from the axis. Thus, under the most intense part of the vortex, there is a spiral, almost inviscid flow pattern separated from the boundary by a thin (and thinning) viscous layer, in which the motion is almost purely radial. If one very reasonably neglects the sublayer between $z = 0$ and $z = a(r)$, which will lie in the innermost portion of the updraft annulus III, an inviscid theory suffices for III; the gain in tractability far outweighs the small loss in accuracy engendered by such an approximation.

The influx of fluid across a symmetrically situated cylindrical surface in the region where Fig. A-12 applies, is (if, again, r denotes the cylindrical radial coordinate and u, the radial inflow component)

$$Q = 2\pi r \int_0^\infty u \, dz. \tag{A-89}$$

The angular momentum of that batch of fluid is

$$M = 2\pi\rho r^2 \int_0^\infty uv\, dz, \tag{A-90}$$

where, again, v denotes the azimuthal velocity component. The angular momentum per unit mass of the "extruded" fluid,

$$\frac{M}{Q} = \left[r \int_0^\infty uv\, dz \Big/ \int_0^\infty u\, dz \right] << \psi\,, \tag{A-91}$$

where ψ characterizes the potential vortex strength in region I (Fig. A-1). Furthermore, when the boundary layer flow becomes a more nearly vertical flow, the fluid that was in $0 < z < a(r)$, and that possesses very little angular momentum, must occupy the inner portion of the upflow annulus III. Thus, there is either little or no torque exerted by the updraft fluid on the slowly moving fluid in the core, region IV (Fig. A-1).

What are the dynamic balances which permit the radial influx of fluid to accelerate into a nearly vertical annular flow; what is the geometry of the configuration in which this occurs? A very primitive answer may be sought as follows.

In constant-density inviscid axisymmetric steady flow, angular momentum is conserved along the streamlines defined by the secondary (radial and axial) velocity components. The core, region IV, is taken as motionless and isobaric (for the altitudes of interest); the flow just outside the inflow-updraft "channel" has circulation ψ, with radial and axial velocity components effectively zero. The flow in the boundary layer II under the vortex I is specified in simplistic terms, and this permits the geometry of the annulus III to be determined. More particularly, the shape of the streamlines constituting the inner and outer limits of III may be obtained from the conservation of radial and of total momentum.

(An integral of the latter is, of course, Bernoulli's equation.) Especially, the radial distances, at which the streamlines bounding III becomes vertical, so both radial flow and also changes with altitude are small, may be determined. Details are not developed in this preliminary outline, however they will be further treated in the next phase of the program.

REFERENCES

Barcilon, A. 1967 Vortex Decay above a Stationary Vortex. J. Fluid Mech. 27, 155-175.

Brown, R. A., Editor 1976, The Union City Tornado of 24 May 1973. NOAA Technical Memorandum ERL NSSL-80.

Burggraf, O. R., Stewartson, K., and Belcher, R. 1971 Boundary Layer Induced by a Potential Vortex. Phys. Fluids 14, 1821-1833.

Bush, W. B. and Fendell, F. E. 1972 Asymptotic Analysis of Turbulent Channel and Boundary-Layer Flow. J. Fluid Mech. 56, 657-681.

Carrier, G. F. 1970 Singular Perturbation and Geophysics. SIAM Rev. 12, 175-193.

Carrier, G. F., Hammond, A. L., and George, O. D. 1971 A Model of the Mature Hurricane. J. Fluid Mech. 47, 147-170.

Carrier, G. F. 1971 The Intensification of Hurricanes. J. Fluid Mech. 49, 145-158.

Chi, S. W. 1975 Numerical Modeling of Ground Turbulent Boundary Layers of Intense Atmospheric Vortices. In Second U. S. National Conference on Wind Engineering Research, pp. II-4-1-II-4-3. Fort Collins, Colorado: Wind Engineering Research Council, Colorado State University.

Davies, P. O. A. L. and Yule, A. J. 1975 Coherent Structures in Turbulence. J. Fluid Mech. 69, 513-537.

Dergarabedian, P. and Fendell, F. E. 1970 On Estimation of Maximum Wind Speeds in Tornadoes and Hurricanes. J. Astronaut. Sci. 17, 218-236.

Degarabedian, P. and Fendell, F. E. 1971a A Method for Rapid Estimation of Maximum Tangential Wind Speed in Tornadoes. Mon. Wea. Rev. 99, 143-145.

Degarabedian, P. and Fendell, F. E. 1971b Estimation of Maximum Wind Speeds in Tornadoes. Tellus 22, 511-516.

Degarabedian, P. and Fendell, F. E. 1973 One- and Two-Cell Tornado Structure and Funnel-Cloud Shape. J. Astronaut. Sci. 21, 26-31.

Fendell, F. E. 1972 Singular Perturbation and Turbulent Shear Flow near Walls, J. Astronaut. Sci. 20, 129-165.

Fendell, F. E. 1974 Tropical Cyclones. In Advances in Geophysics, Vol. 17, ed. by H. E. Landsberg and J. Van Mieghem, pp. 1-100. New York, New York: Academic Press.

Ferrel, W. 1893 A Popular Treatise on the Winds. New York, New York: John Wiley.

Forbes, G. S. 1976 Photogrammetric Characteristics of the Parker Tornado of April 3, 1974. In Preprints Symposium on Tornadoes: Assessment of Knowledge and Implications for Man. Lubbock, Texas: Texas Tech University.

Fujita, T. T. 1975 New Evidence from April 3-4, 1974 Tornadoes. In Ninth Conference on Severe Local Storms, pp. 248-255. Boston, Massachusetts: American Meteorological Society.

Fujita, T. T. and Forbes, G. S. 1976 Three Scales of Motion Involving Tornadoes. In Preprints Symposium Proc. on Tornadoes: Assessment of Knowledge and Implications for Man. Lubbock, Texas: Texas Tech University.

Glaser, A. H. 1960 On Observational Deduction of the Structure of a Tornado Vortex. In Cumulus Dynamics (Proc. of the First Conf. on Cumulus Convection), pp. 157-166. New York, New York: Pergamon.

Golden, J. H. and Purcell, D. 1975 Photogrammetric Studies for the Great Bend, Kansas Tornado: Accelerations and Asymmetries. In Ninth Conference on Severe Local Storms, pp. 336-343. Boston, Massachusetts: American Meteorological Society.

Golden, J. H. 1976 An Assessment of Windspeeds in Tornadoes. In Preprints Symposium on Tornadoes: Assessment of Knowledge and Implications for Man. Lubbock, Texas: Texas Tech University.

Hoecker, Jr., W. H. 1960 Wind Speed and Air Flow Patterns in the Dallas Tornado of April 2, 1957. Mon. Wea. Rev. 88, 167-180.

Kuo, H. L. 1971 Axisymmetric Flows in the Boundary Layer of a Maintained Vortex. J. Atmos. Sci. 28, 20-41.

Lewellen, W. S. 1976 Theoretical Models of the Tornado Vortex. In Preprints Symposium Proc. on Tornadoes: Assessment of Knowledge and Implications for Man. Lubbock, Texas: Texas Tech University.

McWilliams, J. C. 1971 The Boundary Layer Dynamics of Symmetric Vortices. Ph.D. thesis, Harvard University, Cambridge, Massachusetts.

Morton, B. R. 1966 Geophysical Vortices. In Progress in Aeronautical Sciences, Vol. 7, ed. by D. Kuchemann, pp. 145-194. Oxford, England: Pergamon.

Redmann, G. H., Radbill, J. R., Marte, J. E., Dergarabedian, P., and Fendell, F. E. 1976 Wind Field and Trajectory Models for Tornado-Propelled Objects. Tech. Report 1, EPRI Res. Proj. 308. Palo Alto, California: Electric Power Research Institute.

Roshko, A. 1976 Structure of Turbulent Shear Flows: A New Look. AIAA Paper 76-78, 12 pp. New York, New York: American Institute of Aeronautics and Astronautics.

Smith, A. M. O. and Cebeci, T. 1968 Solution of the Boundary-Layer Equations for Incompressible Turbulent Flow. In Proceedings of the 1968 Heat Transfer and Fluid Mechanics Institute, ed. by A. F. Emery and C. A. Depew. Stanford, California: Stanford University.

White, F. M. 1974 Viscous Fluid Flow. New York, New York: McGraw-Hill.

Table A-1. Properties of the Approximate Selfsimilarity Solution for the Flat-Plate Turbulent-Boundary-Layer Boundary-Value Problem

ϵ_1	$f''(0)$	η_1	σ
1.2295^{-4}	7.3768^{+1}	9.3522^{-3}	1.9036^{-2}
3.2145^{-5}	1.9287^{+2}	6.4557^{-3}	1.1853^{-2}
8.6645^{-6}	5.1987^{+2}	4.8239^{-3}	7.8603^{-3}
2.3825^{-6}	1.4295^{+3}	3.8131^{-3}	5.4872^{-3}
1.6200^{-6}	1.9441^{+3}	3.5820^{-3}	4.9671^{-3}
6.6447^{-7}	3.9868^{+3}	3.1345^{-3}	3.9956^{-3}
1.8740^{-7}	1.1244^{+4}	2.6506^{-3}	3.0136^{-3}
1.2826^{-7}	1.5392^{+4}	2.5313^{-3}	2.7849^{-3}
5.3360^{-8}	3.2016^{+4}	2.2897^{-3}	2.3407^{-3}
1.5333^{-8}	9.1998^{+4}	2.0113^{-3}	1.8635^{-3}
4.6010^{-9}	2.7606^{+5}	1.7713^{-3}	1.5131^{-3}
1.3300^{-9}	7.9798^{+5}	1.5591^{-3}	1.2498^{-3}

Exponents denote the power of ten. Results for the two smallest values of ϵ are less accurate than entries for larger values of ϵ.

Table A-2. Properties of the Approximate Selfsimilarity Solution for the Turbulent Boundary Layer Under a Tornado Vortex

ϵ	σ	η_1	$f'(0)$
10^{-4}	$1.35 \cdot 10^{-2}$	$6.18 \cdot 10^{-3}$	$1.17868 \cdot 10^{2}$
10^{-5}	$6.90 \cdot 10^{-3}$	$3.85 \cdot 10^{-3}$	$6.24682 \cdot 10^{2}$
10^{-7}	$2.88 \cdot 10^{-3}$	$2.395 \cdot 10^{-3}$	$2.56536 \cdot 10^{4}$
10^{-9}	$1.637 \cdot 10^{-3}$	$1.805 \cdot 10^{-3}$	$1.36583 \cdot 10^{6}$
10^{-11}	$1.034 \cdot 10^{-3}$	$1.436 \cdot 10^{-3}$	$9.72465 \cdot 10^{7}$

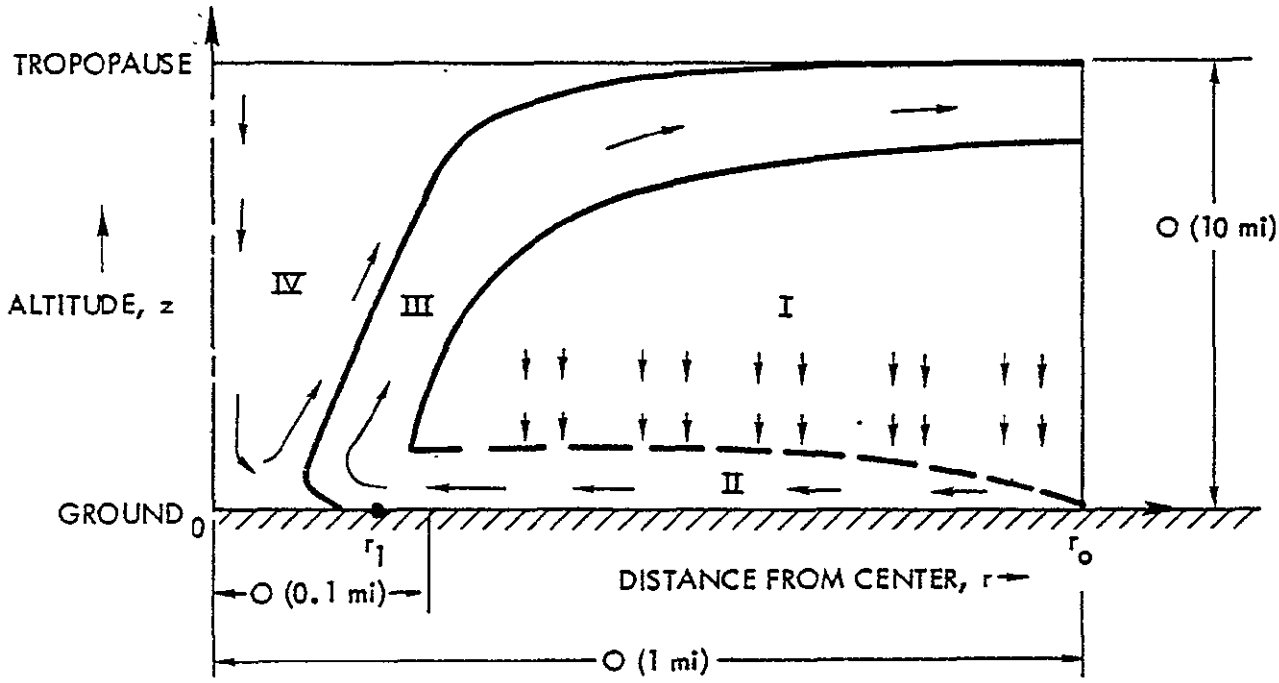

Fig. A-1. A schematic diagram, not to scale, of the postulated four-part structure of an idealized mature severe tornado, here taken conveniently as a vertical closed axisymmetric two-cell system extending from ground to tropopause. Region I is the potential vortex; II, the surface inflow layer; III, the turnaround, slightly sloped updraft, and outflow; IV, the recirculation core, or "eye". In the absence of an "eye", such that III extends to the axis of rotation, the peak swirl is appreciably reduced. The arrows suggest the secondary flow (radial and axial velocity component streamlines). The radius of maximum winds is r_1 and the outer radius is r_0.

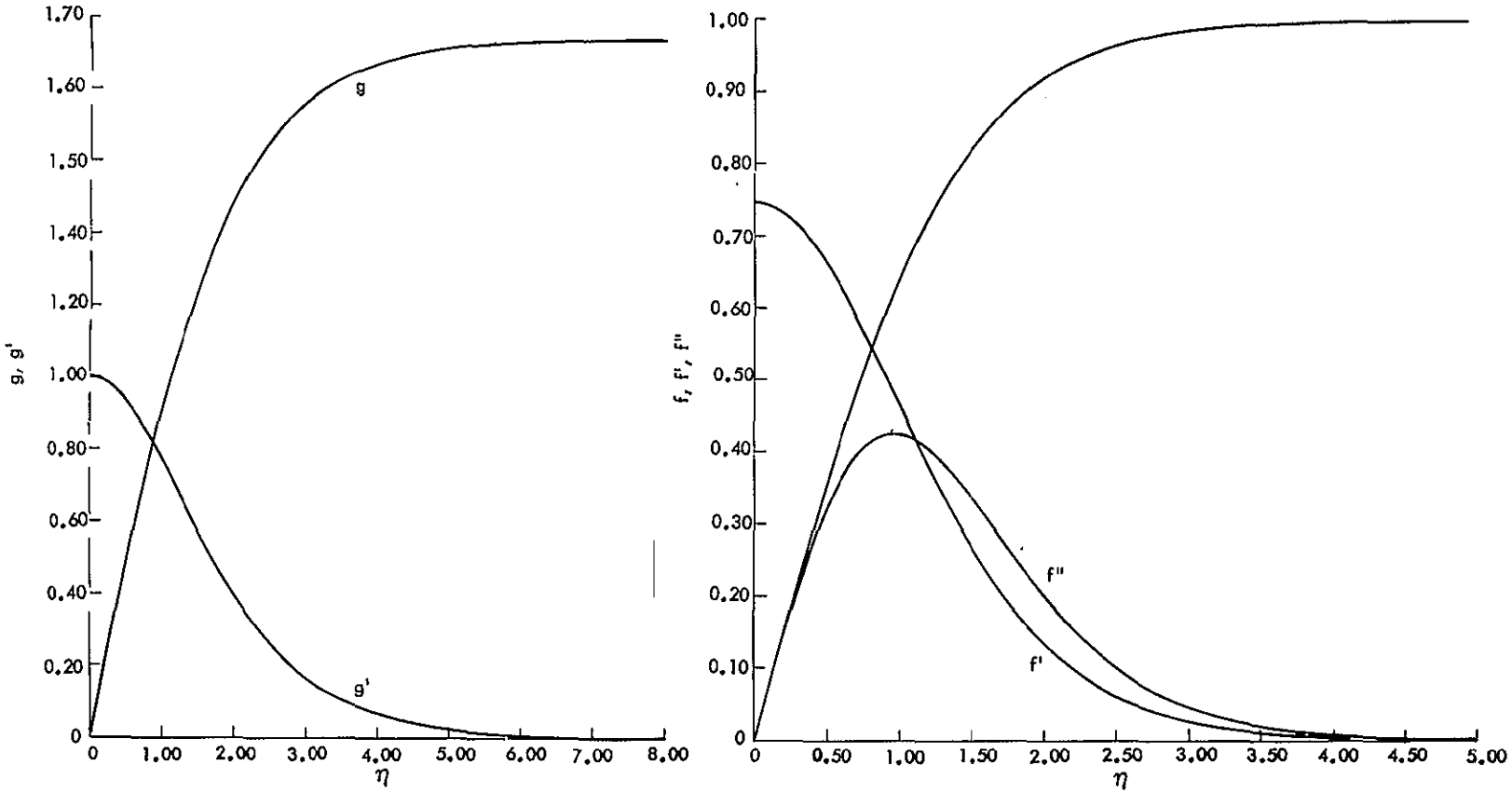

Fig. A-2. For spatially constant viscosity, similarity results for the outer, preponderant portion of the boundary layer under the high-speed portion of an impressed vortex. Left, results related to the radial and axial flow components. Right, results related to the swirl velocity component. The similarity independent variable η is large for large distances normal to the ground or for small radial distances from the outer edge of the vortex system.

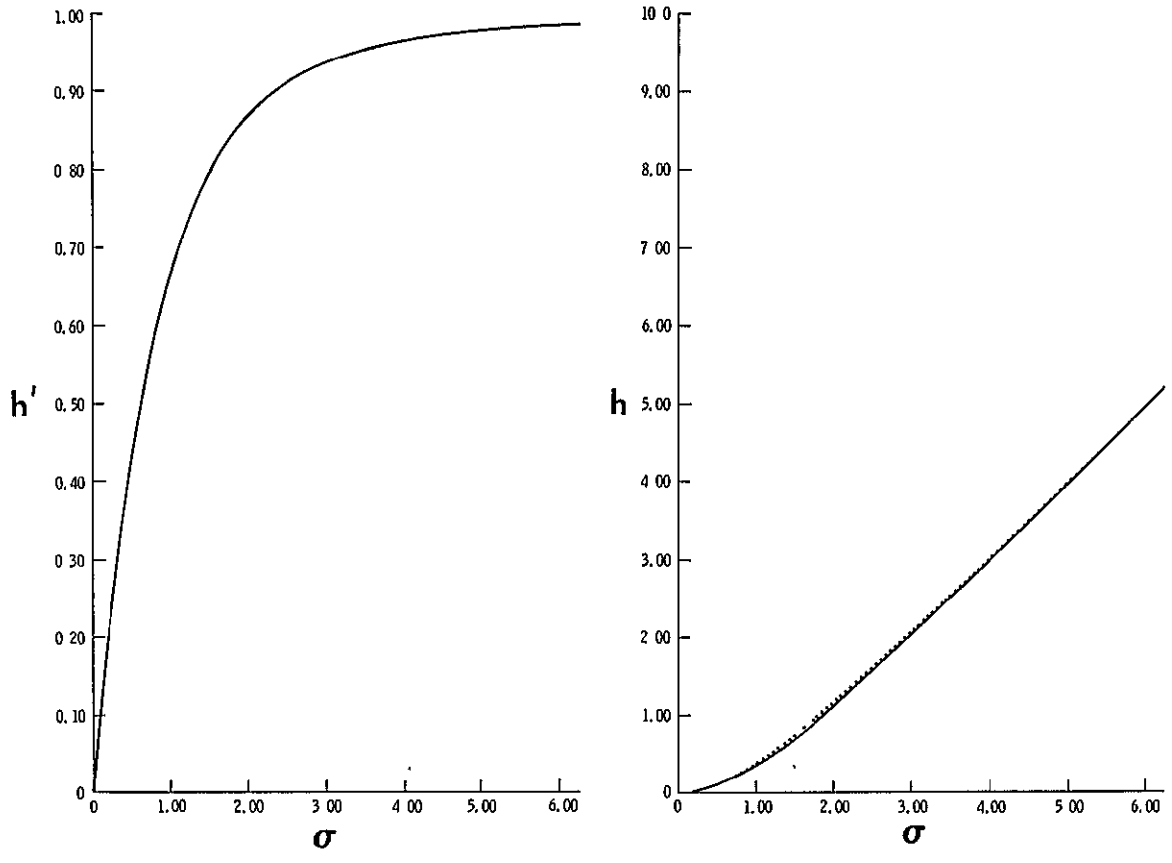

Fig. A-3. For spatially constant viscosity, similarity results related to the radial inflow in the thin, effectively nonrotating sublayer under the high-speed portion of an impressed swirl. Left, $h'(\sigma)$, as computed numerically; right, a comparison of numerically computed (dotted line) and approximate analytic (solid line) results for $h(\sigma)$. The similarity independent variable σ is large for large distances normal to the ground or for small radial distances from the axis of rotation.

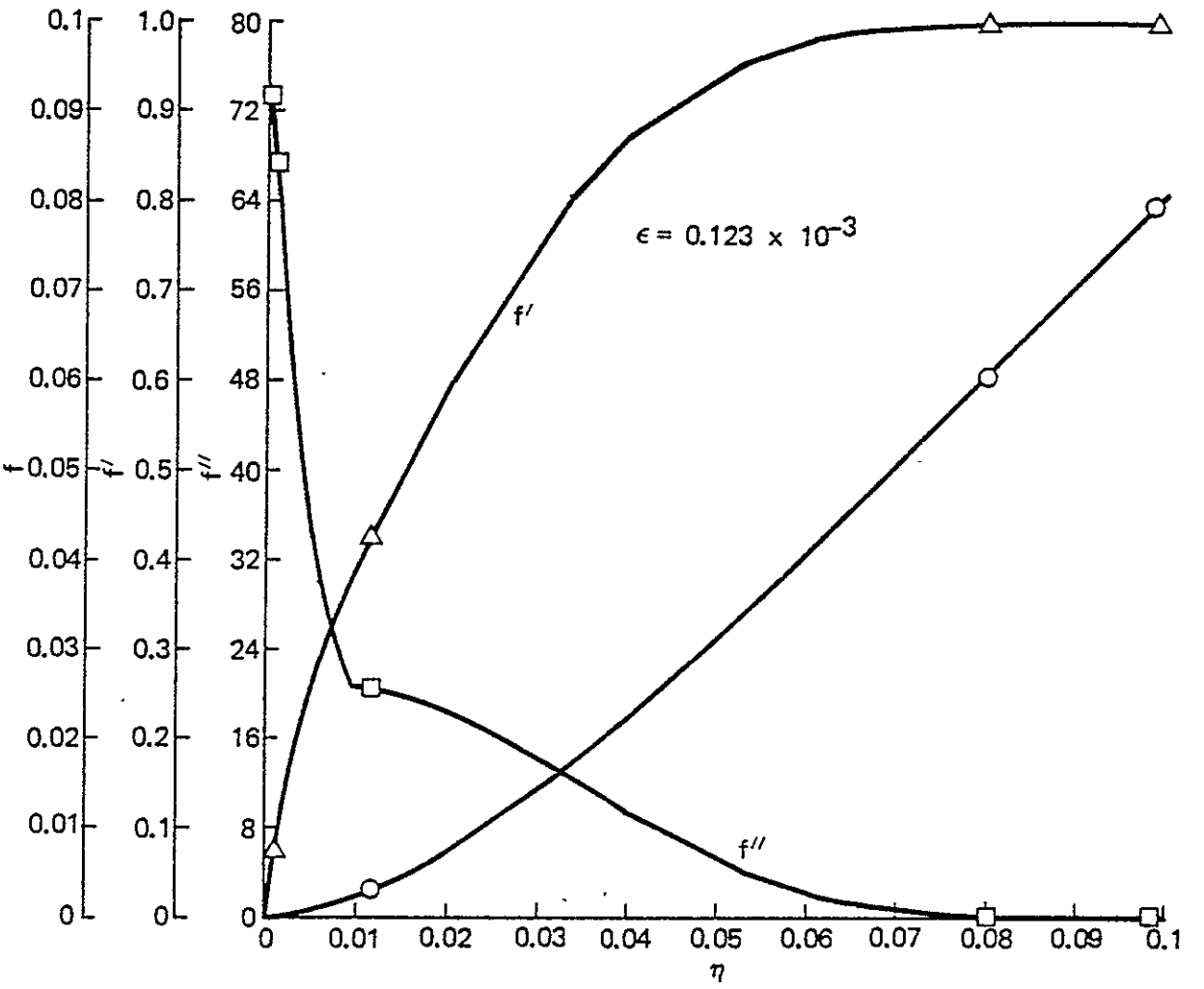

Fig. A-4. Results of flow field computation for the turbulent flat-plate boundary layer with no pressure gradient. Results are based on an approximate self-similarity treatment of an eddy-viscosity model of turbulent diffusion. The value of the inverse Reynolds number ϵ is noted, f' denotes the dimensionless streamwise velocity component, and η is a similarity independent variable that is large for large distance normal to the ground or for short distance downstream.

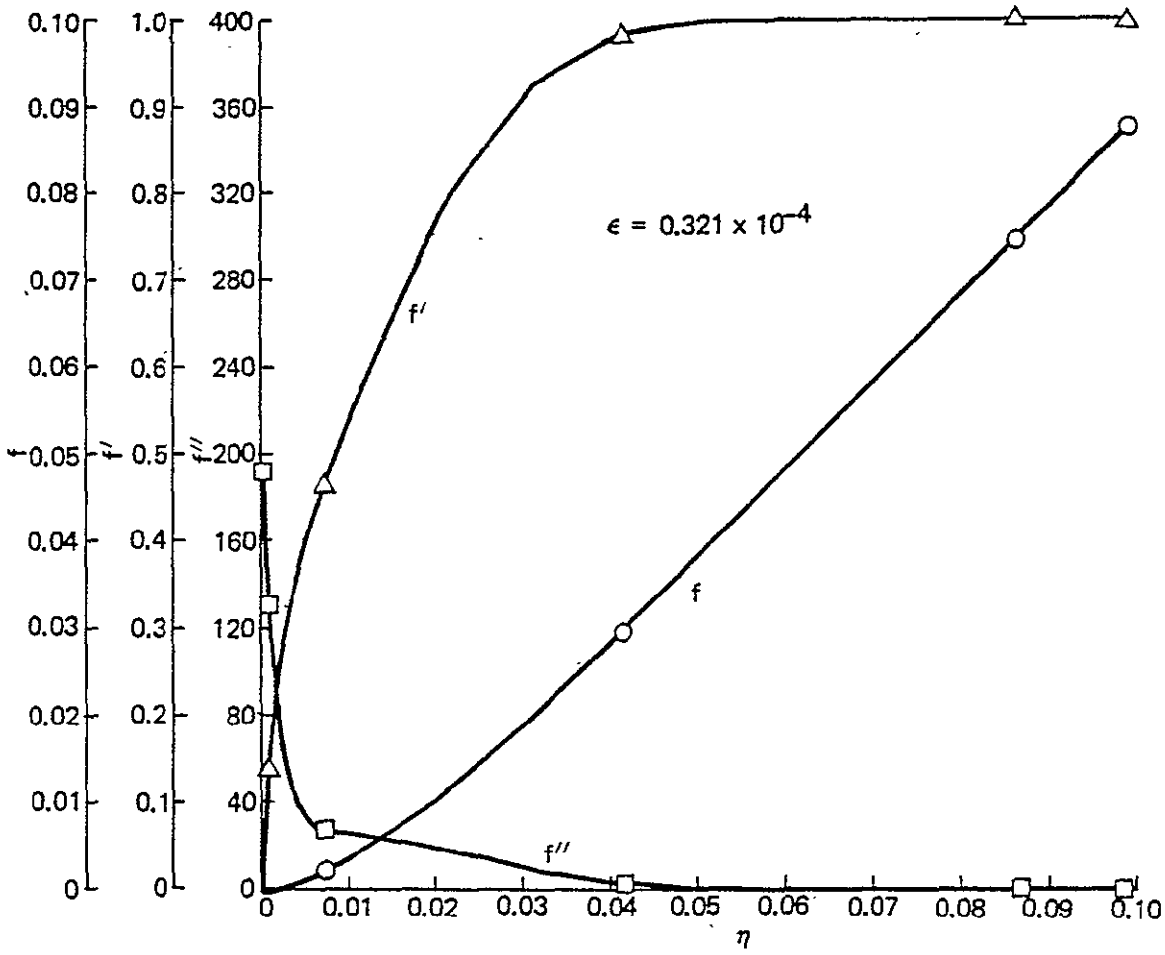

Fig. A-5. Results, for smaller inverse Reynolds number, for the turbulent flat-plate boundary layer.

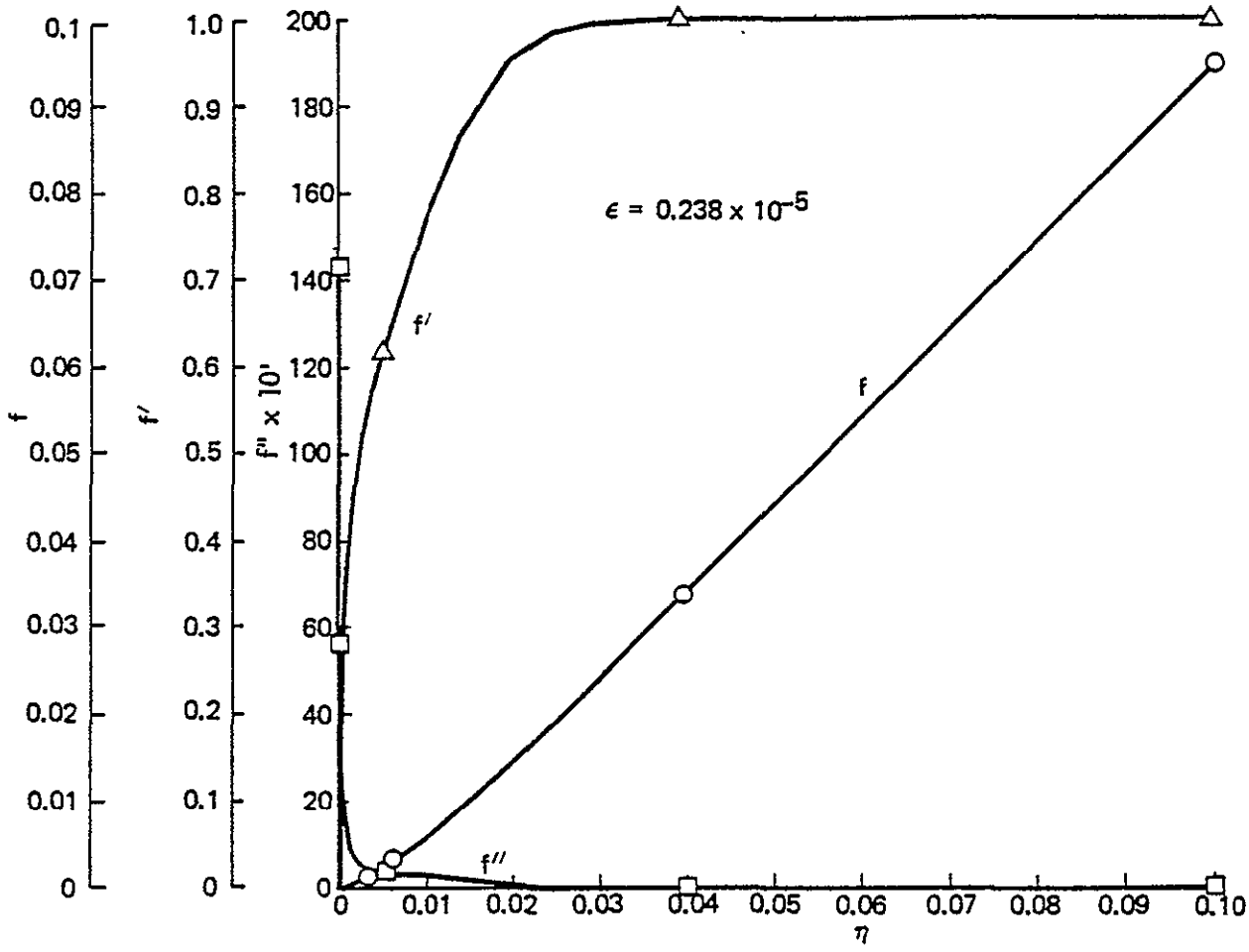

Fig. A-6. Results, for still smaller inverse Reynolds number, for the turbulent flat-plate boundary layer.

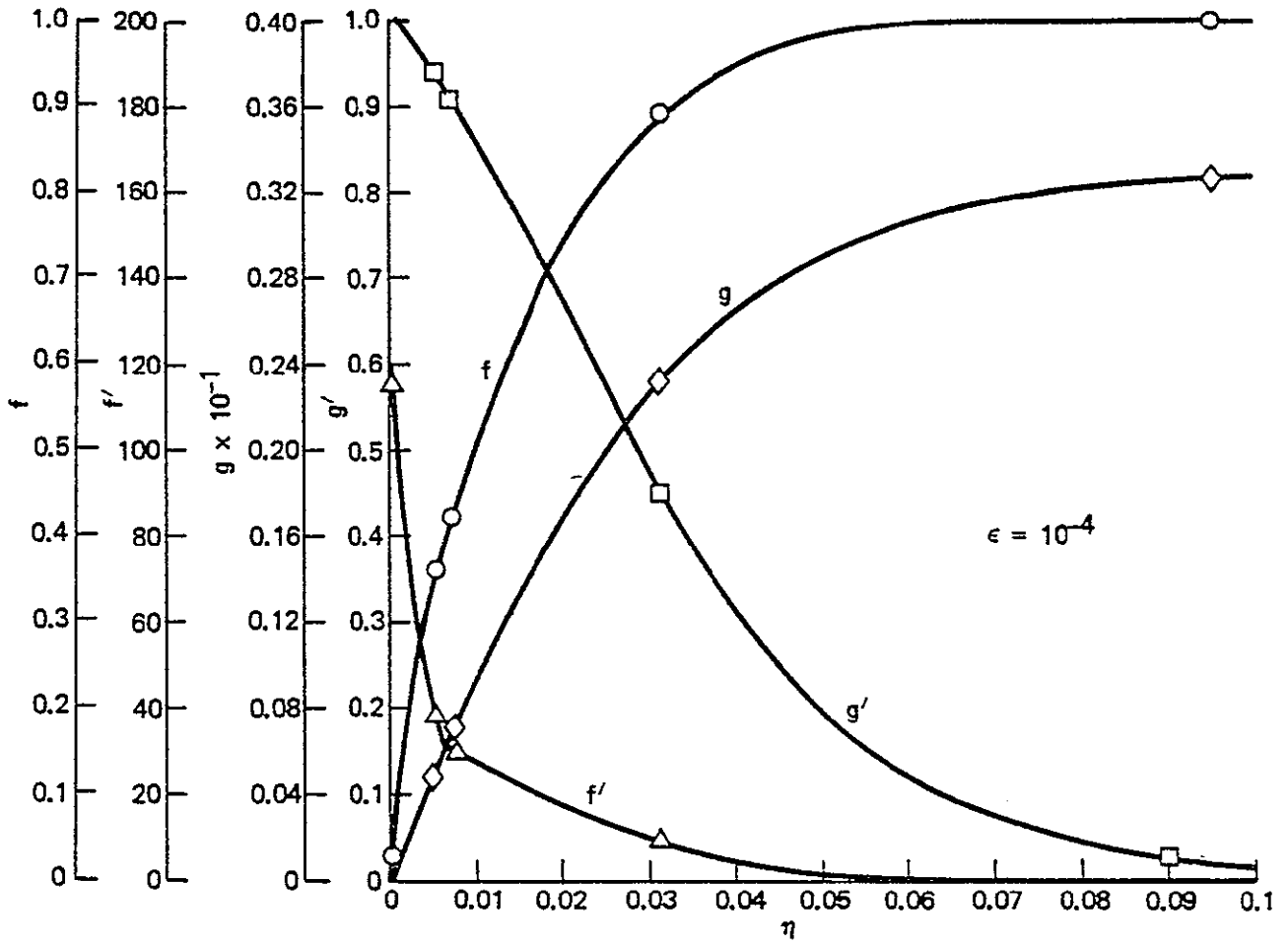

Fig. A-7. Results for the flow field computation for the turbulent boundary layer under the high-speed portion of a tornado vortex. Results are based on an approximate selfsimilarity treatment of an eddy-viscosity model of turbulent diffusion. The value of the inverse Reynolds number ϵ is noted. The variable f is related to the swirl, and the variable g is related to the radial and axial velocity components. The similarity independent variable η is large for large distance normal to the wall or for small radial distance from the outer edge of the vortex system.

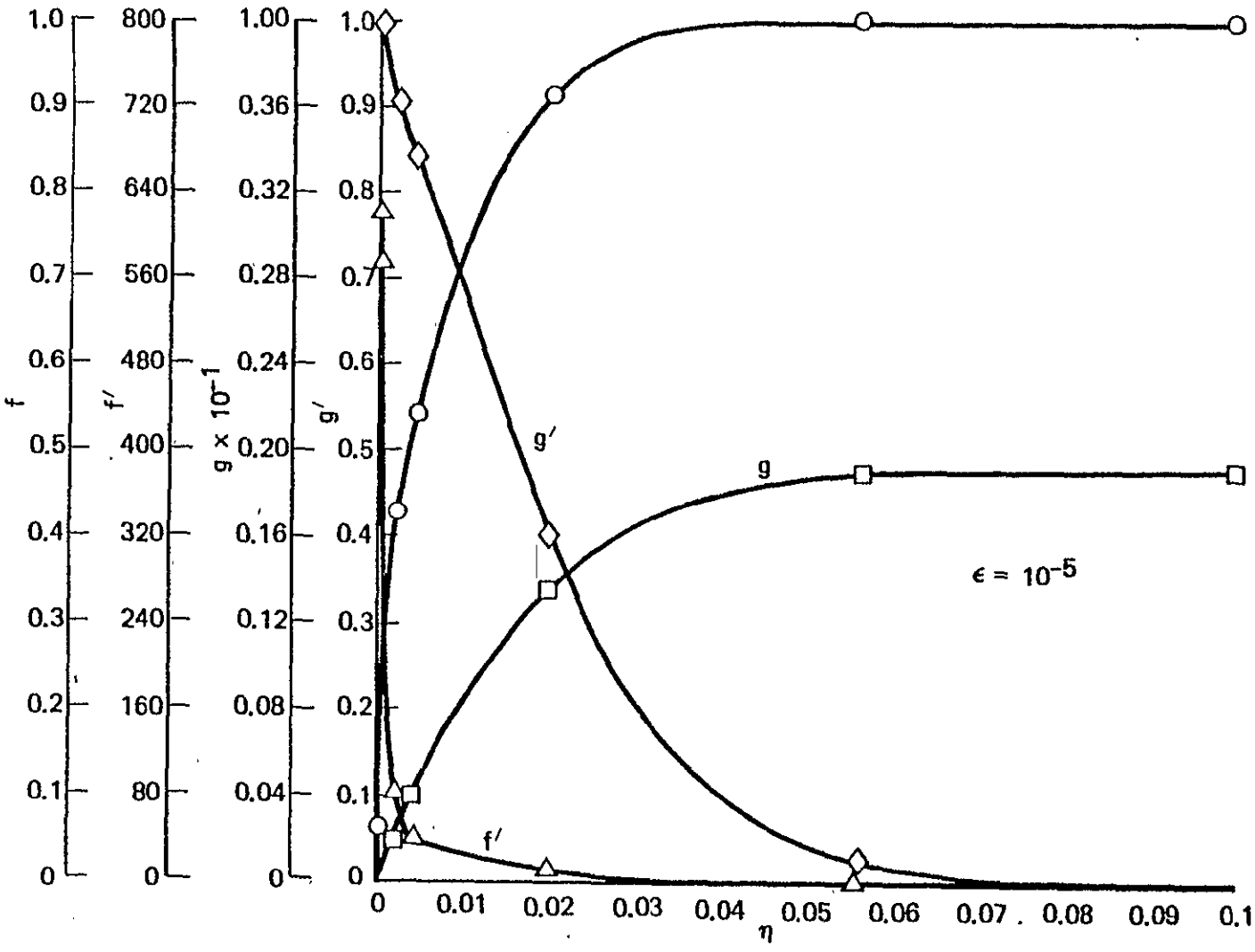

Fig. A-8. Results, for smaller inverse Reynolds number, for the turbulent boundary layer under a tornado vortex.

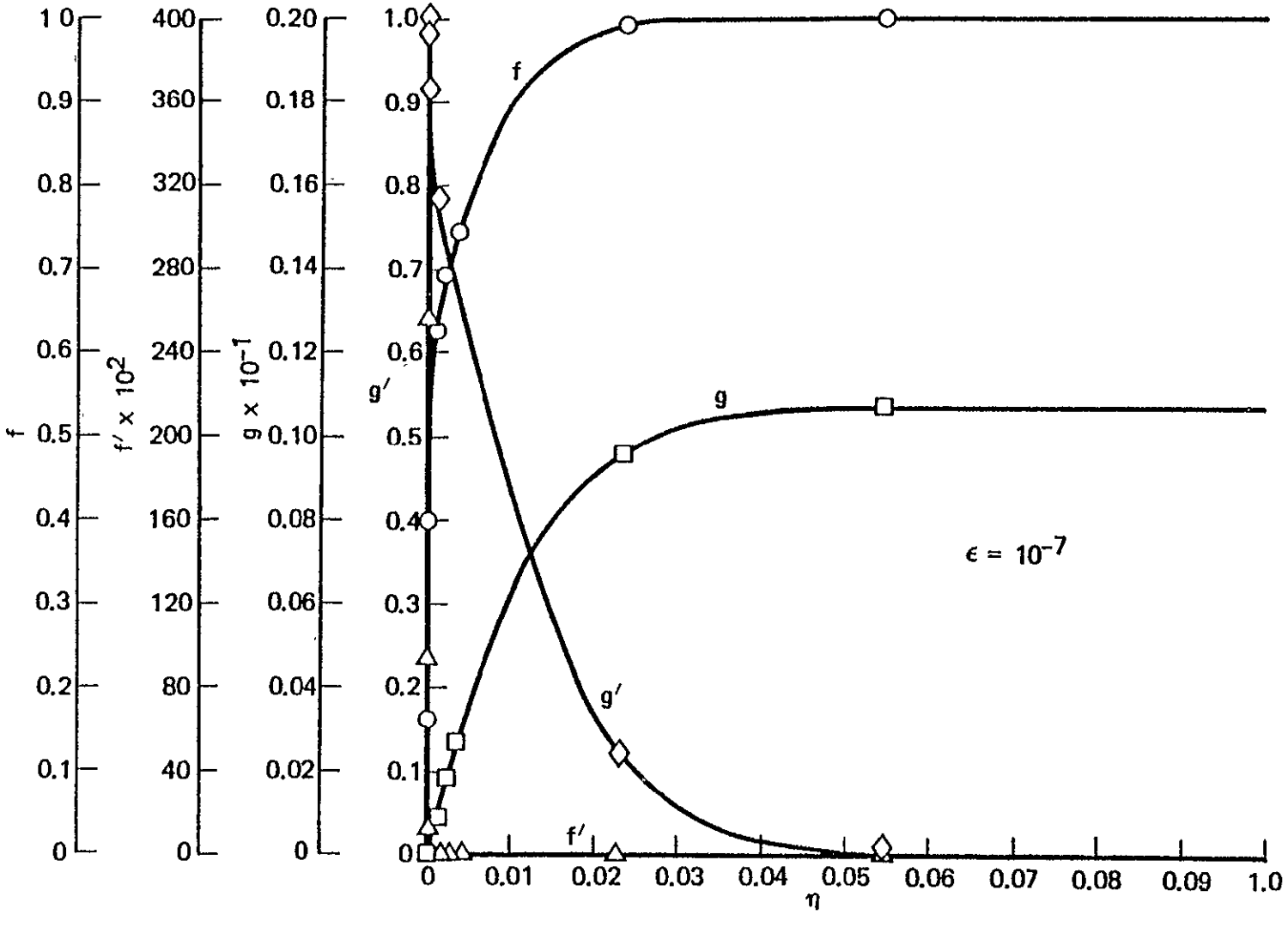

Fig. A-9. Results, for smaller inverse Reynolds number, for the turbulent boundary layer under a tornado vortex.

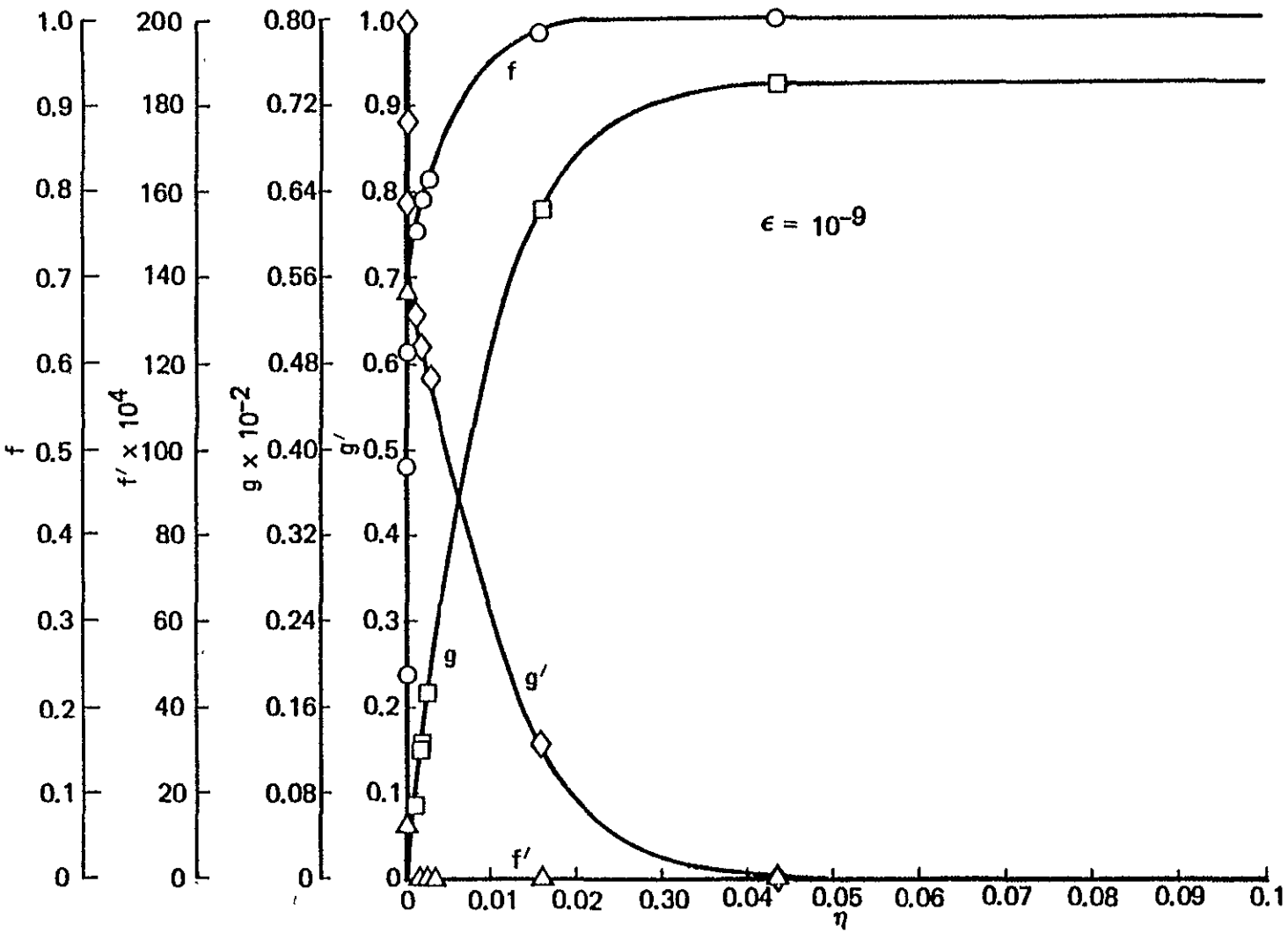

Fig. A-10. Results, for smaller inverse Reynolds number, for the turbulent boundary layer under a tornado vortex.

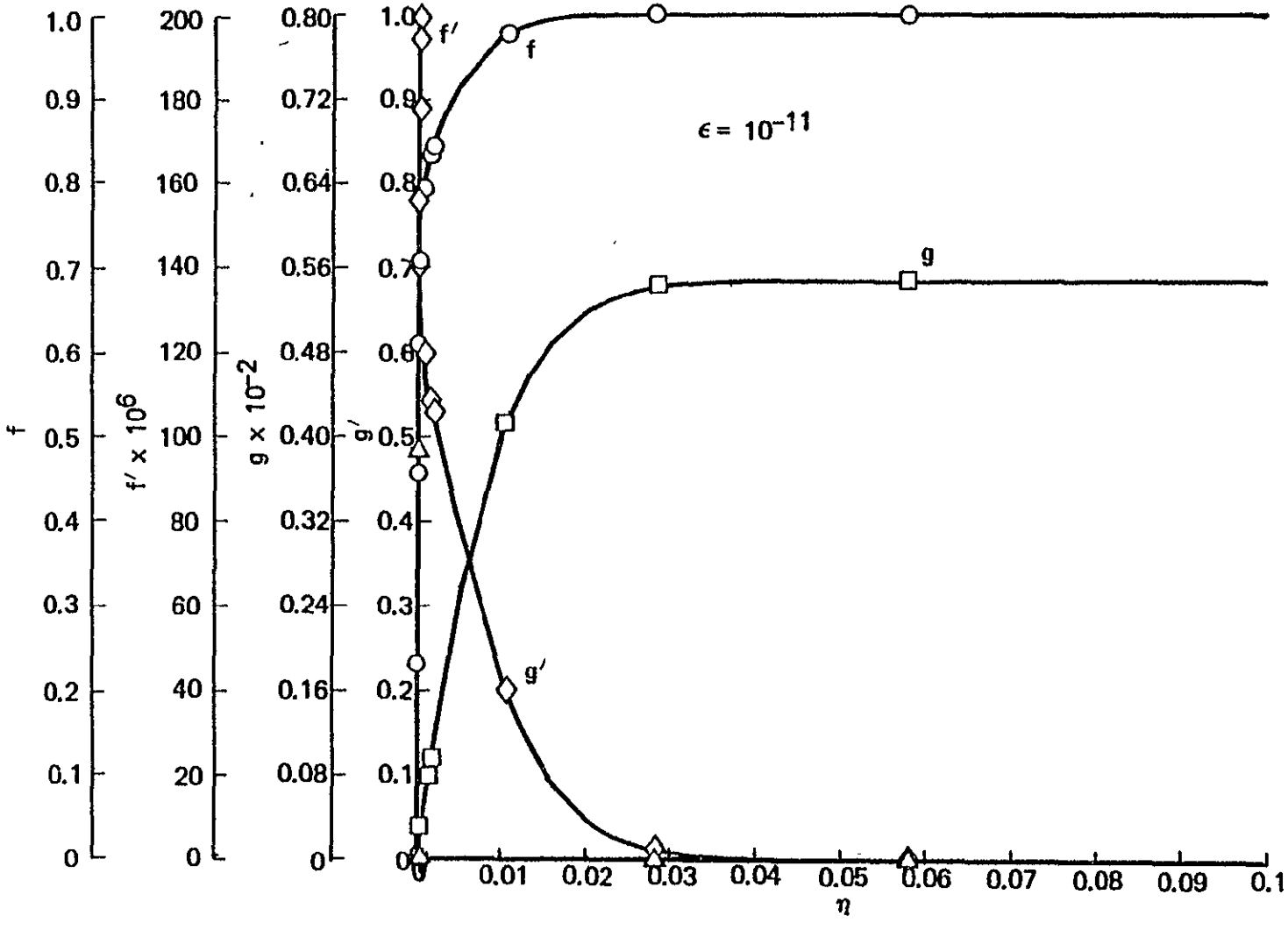

Fig. A-11. Results, for smaller inverse Reynolds number, for the turbulent boundary layer under a tornado vortex.

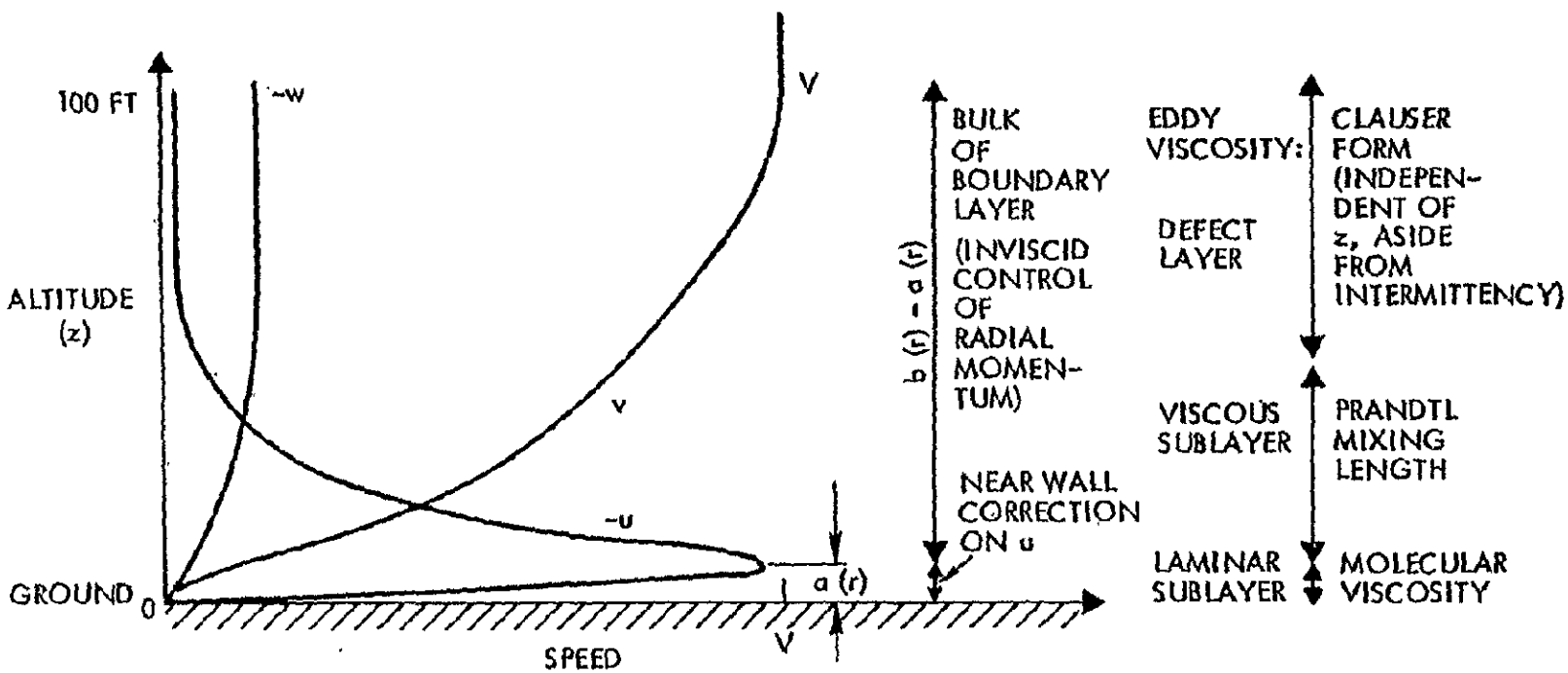

Fig. A-12. A schematic of the axial profile of radial velocity component u, azimuthal velocity component v, and axial velocity component w, at a radial distance r from the center of the vortex, where the impressed swirl V is large.

J. NOMENCLATURE FOR APPENDIX A

r_o	....	radius to edge of system
r_I	....	radius of maximum winds
u	....	radial velocity component in tornado or streamwise velocity component on flat plate
v	....	azimuthal velocity component
w	....	axial velocity component in tornado or transverse (to stream) component on flat plate
ψ	....	rotational velocity
z	....	height above ground
ρ	....	atmospheric density
p	....	atmospheric pressure
V	....	azimuthal velocity component far from ground
ν	....	total viscosity
ν_o	....	molecular viscosity
ν_e	....	eddy viscosity
k_1	....	square of von Karman constant
k_2	....	Clauser constant
u_o	....	transverse velocity component far from surface of flat plate
δ^*	....	velocity displacement thickness, angular-momentum-defect thickness
ϵ	....	inverse Reynolds number

APPENDIX B

TRANSFORMATION OF COORDINATES

Transformation from Body to Inertial Coordinates

The transformation matrix T from body to inertial coordinates is given in terms of the roll, pitch and yaw rotation matrices X, Y, Z by

$$T = ZYX \tag{B-1}$$

where

$$X = \begin{pmatrix} \cos\psi & \sin\psi & 0 \\ -\sin\psi & \cos\psi & 0 \\ 0 & 0 & 1 \end{pmatrix}$$

$$Y = \begin{pmatrix} \cos\theta & 0 & -\sin\theta \\ 0 & 1 & 0 \\ \sin\theta & 0 & \cos\theta \end{pmatrix} \tag{B-2}$$

$$Z = \begin{pmatrix} 1 & 0 & 0 \\ 0 & \cos\phi & \sin\phi \\ 0 & -\sin\phi & \cos\phi \end{pmatrix}$$

so that

$$T = \begin{pmatrix} \cos\psi\cos\theta & -\cos\psi\sin\theta\sin\phi + \sin\psi\cos\phi & -\cos\psi\sin\theta\cos\phi - \sin\psi\sin\phi \\ -\sin\psi\cos\theta & \sin\psi\sin\theta\sin\phi + \cos\psi\cos\phi & \sin\psi\sin\theta\cos\phi - \cos\psi\sin\phi \\ \sin\theta & \cos\theta\sin\phi & \cos\theta\cos\phi \end{pmatrix} \tag{B-3}$$

Quaternion Representation of Transformation

Quaternion components are initialized from the elements of the transformation matrix T from body to space coordinates. The components are usually subscripted 0-3, but they will be subscripted 1-4 below to be consistent with FORTRAN subscripting practice.

$$
\begin{aligned}
q_1 &= (1 + T_{11} + T_{22} + T_{33})^{1/2}/2 \\
q_2 &= (T_{32} - T_{23})/4q_1 \\
q_3 &= (T_{13} - T_{31})/4q_1 \\
q_4 &= (T_{21} - T_{12})/4q_1
\end{aligned}
\qquad \text{(B-4)}
$$

Reference to the expanded form of the transformation matrix from body to inertial coordinates, Eq. 2-8, shows that the relations just given for initializing q cannot be used when yaw is 180° and roll is 0° because q_1 is zero. Instead, components 2-4 are determined directly from the position of the axis of rotation:

$$
\begin{aligned}
q_1 &= 0 \\
q_2 &= \sin(\theta/2) \\
q_3 &= 0 \\
q_4 &= -\cos(\theta/2)
\end{aligned}
$$

The derivatives with respect to time of the quaternion components q_1 are computed from the current values of the quaternion components and the angular velocity components ω_i:

$$
\begin{aligned}
\dot{q}_1 &= (q_2\omega_1 + q_3\omega_2 + q_4\omega_3)/2 \\
\dot{q}_2 &= (-q_1\omega_1 - q_4\omega_2 + q_3\omega_3)/2 \\
\dot{q}_3 &= (q_4\omega_1 - q_1\omega_2 - q_2\omega_3)/2 \\
\dot{q}_4 &= (-q_3\omega_1 + q_2\omega_2 - q_1\omega_3)/2
\end{aligned}
\tag{B-5}
$$

Starting with the initial values, one computes the derivatives of the components by integrating to time t, at which the new transformation matrix components are obtained from

$$
\begin{aligned}
T_{11} &= 1 - 2\left(q_3^2 + q_4^2\right) \\
T_{21} &= 2(q_2q_3 + q_1q_4) \\
T_{31} &= 2(q_2q_4 - q_1q_3) \\
T_{12} &= 2(q_2w_3 - q_1q_4) \\
T_{22} &= 1 - 2\left(q_2^2 + q_4^2\right) \\
T_{32} &= 2(q_3q_4 + q_1q_2) \\
T_{13} &= 2(q_2q_4 - q_1q_3) \\
T_{23} &= 2(q_3q_4 - q_1q_2) \\
T_{33} &= 1 - 2\left(q_2^2 + q_3^2\right)
\end{aligned}
\tag{B-6}
$$

C3

C. NOMENCLATURE FOR APPENDIX B

q_1, q_2, q_3, q_4	.....	components of quaternion
T	.....	transformation matrix
T_{11}, T_{12}	.....	elements of transformation matrix
t	.....	time
X	.....	yaw dependent factor (matrix) of transformation matrix
Y	.....	pitch dependent factor (matrix) of transformation matrix
Z	.....	roll dependent factor (matrix) of transformation matrix

GREEK

θ	.....	pitch angle (2nd Euler angle)
ϕ	.....	roll angle (3rd Euler angle)
ψ	.....	yaw angle (1st Euler angle)
$\omega_1, \omega_2, \omega_3$	.....	components of angular velocity

SUPERSCRIPTS

	.....	time derivative (eg. $\dot{q}_1 = dq_1/dt$)

APPENDIX C

TABLES OF AERODYNAMIC COEFFICIENTS

The tabulated coefficients contained in this appendix are those which have been used in the trajectory model program to obtain the results presented in that section. The coefficients in these tables have been smoothed by plotting the experimentally determined values and fairing with a best fit smooth curve from which the smoothed values were read. Where coefficients were known to be zero because of flow field symmetry, the curves were forced through the zero points. For a further discussion of the aerodynamic coefficients, see Section III.

Table C-1. Coefficient Reference Quantities

Configuration	Area	Length	Moment Center
Cylinders	Length x Diameter	Axial Length	Mid-point on Axis
Plank	Length x Width	Long Dimension	Mid-point on Long Center Line
Car	Frontal, $\psi = 0^{o}$	Overall Length	Lower Front Corner on Lateral Center Line
Van	Frontal, $\psi = 0^{o}$	Overall Length	Lower Front Corner on Lateral Center Line

Table C-2. Smoothed aerodynamic coefficients in the sub-critical Reynolds Number regime for open-end circular (len./dia = 14.1) in free air.

(ψ) Deg	C_D	C_s	C_n	$X_{cp/L}$
0	.049	.000	.000	.440
5	.060	.022	.007	.441
10	.076	.050	.012	.442
15	.098	.083	.016	.444
20	.124	.134	.019	.446
25	.162	.185	.022	.447
30	.218	.243	.025	.449
35	.295	.312	.027	.450
40	.385	.377	.029	.452
45	.487	.430	.031	.454
50	.598	.451	.033	.456
55	.724	.495	.034	.459
60	.800	.422	.035	.461
65	.857	.366	.034	.463
70	.902	.288	.032	.466
75	.937	.212	.028	.472
80	.967	.137	.021	.479
85	.992	.066	.011	.489
90	.997	.000	.000	.500

Table C-3. Smoothed aerodynamic coefficients in the sub-critical Reynolds Number regime for open-end circular cylinder (len./dia = 14.1), h/d = 1.6.

(ψ) Deg	C_L	C_D	C_s	C_n	$X_{cp/L}$
0					
5					
10					
15					
20					
25					
30					
35					
40					
45	.085	.570	.455	.044	.439
50	.125	.700	.488	.049	.443
55	.170	.815	.496	.054	.443
60	.170	.907	.471	.058	.444
65	.135	.970	.420	.059	.444
70	.105	1.000	.338	.055	.448
75	.085	1.100	.293	.049	.455
80	.070	1.100	.155	.039	.464
85	.055	1.100	.071	.026	.476
90	.042	1.100	.000	.000	.500

Table C-4. Smoothed aerodynamic coefficients in the sub-critical Reynolds Number regime for open-end circular cylinder (len./dia = 14.1), h/d = 1.0

(ψ) Deg	C_L	C_D	C_s	C_n	$X_{cp/L}$
0	.005	.049	.000	.000	.425
5	.006	.06k	.030	.005	.427
10	.010	.073	.060	.010	.430
15	.015	.095	.100	.016	.432
20	.024	.127	.150	.022	.433
25	.035	.179	.210	.028	.435
30	.050	.230	.272	.033	.436
35	.070	.310	.335	.037	.437
40	.092	.410	.400	.041	.438
45	.120	.520	.445	.044	.440
50	.165	.670	.470	.047	.444
55	.200	.780	.475	.049	.445
60	.210	.850	.455	.051	.447
65	.165	.910	.390	.051	.450
70	.135	.950	.300	.045	.455
75	.115	.970	.215	.038	.462
80	.100	.980	.135	.030	.470
85	.090	.980	.065	.015	.485
90	.080	.980	.000	.000	.500

Table C-5. Smoothed aerodynamic coefficients in the sub-critical Reynolds Number regime for open-end circular cylinder (len./dia = 14.1), h/d = 0.1

(ψ) Deg	C_L	C_D	C_s	C_n	$X_{cp/L}$
0	.010	.049	.000	.000	.370
5	.013	.052	.031	.010	.371
10	.023	.073	.081	.018	.372
15	.031	.109	.170	.028	.373
20	.044	.157	.215	.036	.375
25	.059	.209	.275	.030	.376
30	.078	.270	.325	.053	.377
35	.105	.339	.388	.061	.378
40	.139	.410	.400	.069	.381
45	.183	.470	.415	.076	.382
50	.227	.560	.407	.085	.383
55	.269	.610	.385	.086	.385
60	.305	.635	.340	.077	.393
65	.340	.645	.275	.065	.405
70	.369	.650	.215	.053	.421
75	.394	.653	.155	.040	.438
80	.412	.656	.100	.027	.457
85	.423	.658	.043	.014	.478
90	.425	.660	.000	.000	.500

Table C-6. Smoothed aerodynamic coefficients in the sub-critical Reynolds Number regime for open-end circular cylinder (len./dia. = 36.0) in free air.

(ψ) Deg	C_D	C_s	C_n	$X_{cp/L}$
0	.025	.000	.000	.455
5	.027	.013	.002	.456
10	.030	.029	.005	.456
15	.049	.050	.007	.457
20	.072	.081	.010	.458
25	.114	.125	.012	.459
30	.168	.187	.015	.460
35	.243	.275	.017	.461
40	.332	.35w	.020	.462
45	.434	.395	.022	.463
50	.550	.417	.024	.465
55	.652	.422	.026	.466
60	.744	.412	.028	.466
65	.816	.366	.030	.467
70	.879	.289	.030	.468
75	.937	.211	.027	.472
80	.973	.136	.021	.479
85	1.014	.067	.011	.489
90	1.025	.000	.000	.500

Table C-7. Smoothed aerodynamic coefficients in the sub-critical Reynolds Number regime for open-end circular cylinder (len./dia. = 36.0), h/d=1.6

(ψ) Deg	C_L	C_D	C_s	C_n	$X_{cp/L}$
0	0	.025	.000	.000	.455
5	0	.029	.017	.003	.456
10	0	.043	.035	.006	.456
15	0	.057	.063	.008	.457
20	0	.081	.100	.012	.458
25	0	.120	.160	.015	.459
30	.007	.190	.265	.005	.460
35	.025	.290	.357	.006	.461
40	.055	.392	.413	.011	.462
45	.085	.495	.465	.014	.463
50					
55					
60					
65					
70					
75					
80					
85					
90					

Table C-8. Smoothed aerodynamic coefficients in the sub-critical Reynolds Number regime for open-end circular cylinder (len./dia. = 36.0), h/d = 1.0

(ψ) Deg	C_L	C_D	C_s	C_n	$X_{cp/L}$
0	.000	.025	.000	.000	.455
5	.000	.029	.020	.003	.456
10	.000	.043	.042	.004	.456
15	.000	.052	.070	.007	.457
20	.005	.076	.105	.010	.458
25	.024	.120	.160	.014	.459
30	.065	.185	.250	.012	.460
35	.100	.260	.320	.015	.461
40	.135	.355	.375	.019	.462
45	.165	.460	.417	.023	.463
50	.185	.565	.439	.027	.465
55	.195	.672	.447	.030	.466
60	.153	.790	.440	.032	.466
65	.120	.885	.416	.033	.467
70	.085	.868	.376	.033	.468
75	.068	1.030	.320	.031	.472
80	.055	1.075	.235	.026	.479
85	.055	1.100	.135	.016	.489
90	.060	1.105	.000	.000	.500

Table C-9. Smoothed aerodynamic coefficients in the sub-critical Reynolds Number regime for open-end circular cylinder (len/dia = 36.0), h/d=0.1

(ψ) Deg	C_L	C_D	C_s	C_m	$X_{cp/L}$
0	.006	.025	.000	.000	.384
5	.013	.029	.020	.002	.385
10	.020	.043	.047	.007	.386
15	.027	.054	.088	.010	.387
20	.040	.083	.130	.016	.388
25	.056	.120	.175	.022	.389
30	.079	.165	.215	.028	.391
35	.107	.210	.248	.036	.394
40	.139	.260	.273	.041	.395
45	.150	.315	.285	.043	.400
50	.210	.370	.280	.042	.407
55	.250	.420	.269	.040	.418
60	.294	.455	.240	.035	.430
65	.335	.485	.207	.028	.445
70	.375	.505	.171	.022	.460
75	.406	.527	.125	.016	.473
80	.425	.541	.080	.010	.485
85	.433	.558	.037	.005	.493
90	.434	.560	.000	.000	.500

Table C-10. Smoothed aerodynamic coefficients in the supercritical Reynolds Number regime for open-end circular cylinder (len/dia =14.1), in free air.

(ψ) Deg	C_D	C_s (C_L)	C_n (C_m)	$X_{cp/L}$
0	.023	.000	.000	.358
5	.026	.027	.009	.358
10	.036	.065	.017	.359
15	.054	.109	.024	.360
20	.082	.156	.032	.361
25	.125	.215	.040	.362
30	.187	.285	.047	.364
35	.251	.329	.056	.367
40	.328	.366	.063	.368
45	.400	.387	.070	.372
50	.462	.388	.075	.376
55	.534	.370	.078	.380
60	.582	.342	.076	.387
65	.615	.285	.071	.396
70	.625	.227	.060	.408
75	.632	.166	.052	.422
80	.635	.110	.037	.442
85	.637	.058	.021	.467
90	.638	.000	.000	.500

Table C-11. Smoothed aerodynamic coefficients in the supercritical Reynolds Number regime for open-end circular cylinder (len/dia = 14.1), h/d = 0.74.

(ψ) Deg	C_D	C_s (C_L)	C_n (C_m)	$X_{cp/L}$
0	.023	.000	.000	.358
5	.026	.030	.010	.358
10	.036	.069	.017	.359
15	.055	.113	.024	.360
20	.085	.165	.032	.361
25	.131	.229	.039	.362
30	.193	.292	.048	.364
35	.259	.340	.057	.367
40	.340	.379	.064	.370
45	.420	.406	.071	.374
50	.475	.412	.076	.378
55	.585	.402	.078	.402
60	.638	.361	.078	.393
65	.652	.302	.070	.403
70	.664	.241	.057	.419
75	.669	.179	.047	.433
80	.674	.117	.033	.452
85	.679	.058	.017	.475
90	.680	.000	.000	.500

Table C-12. Smoothed aerodynamic coefficients in the supercritical Reynolds Number regime for open-end circular cylinder (len/dia = 14.1), h/d = 0.29

(ψ) Deg	C_D	C_s (C_L)	C_n (C_m)	$X_{cp/L}$
0	.022	.000	.000	.358
5	.026	.026	.009	.358
10	.035	.063	.018	.359
15	.055	.113	.026	.360
20	.087	.173	.034	.361
25	.135	.237	.043	.362
30	.198	.303	.053	.364
35	.264	.346	.062	.367
40	.343	.386	.068	.368
45	.450	.424	.076	.372
50	.530	.432	.082	.380
55	.610	.421	.085	.384
60	.637	.372	.087	.392
65	.657	.308	.076	.406
70	.668	.243	.055	.422
75	.679	.182	.041	.441
80	.687	.121	.027	.461
85	.693	.060	.014	.480
90	.694	.000	.000	.500

Table C-13. Smoothed aerodynamic coefficients in the supercritical Reynolds Number regime for open-end circular cylinder (len/dia = 14.1), h/d=0.07

(ψ) Deg	C_D	C_s (C_L)	C_n (C_m)	$X_{cp/L}$
0	.020	.000	.000	.360
5	.024	.030	.010	.360
10	.035	.068	.020	.360
15	.055	.122	.030	.360
20	.091	.189	.038	.360
25	.142	.259	.046	.360
30	.209	.326	.054	.361
35	.287	.383	.066	.362
40	.370	.423	.075	.364
45	.461	.448	.086	.366
50	.521	.446	.094	.368
55	.555	.421	.096	.371
60	.584	.379	.092	.379
65	.610	.322	.082	.395
70	.635	.238	.052	.416
75	.654	.176	.035	.449
80	.672	.118	.019	.472
85	.687	.061	.006	.491
90	.692	.000	.000	.500

Table C-14. Smoothed aerodynamic coefficients for the plank model at 0° roll angle in free air.

(ψ) Deg	C_D	C_s	C_n	$X_{cp/L}$
0	.034	.000	.000	.375
5	.036	.009	.001	.409
10	.038	.021	.002	.426
15	.047	.037	.004	.417
20	.058	.054	.007	.401
25	.071	.071	.009	.404
30	.088	.087	.011	.408
35	.108	.101	.011	.424
40	.133	.115	.012	.431
45	.161	.127	.011	.446
50	.195	.135	.008	.466
55	.231	.138	.007	.474
60	.267	.135	.005	.483
65	.304	.125	.004	.488
70	.337	.108	.003	.492
75	.373	.087	.002	.495
80	.395	.060	.001	.498
85	.409	.030	.000	.500
90	.415	.000	.000	.500

Table C-15. Smoothed aerodynamic coefficients for the plank model at 30° roll angle in free air.

(ψ) Deg	C_L	C_D	C_s	C_m	C_n	C_ℓ	$X_{cp/L}$
0	.000	.034	.000	.000	.000	.000	.375
5	.018	.037	.018	.001	.003	.000	.438
10	.050	.044	.056	.002	.006	.000	.456
15	.126	.067	.113	.003	.010	.000	.459
20	.230	.105	.179	.007	.015	.000	.465
25	.300	.155	.253	.020	.022	-.008	.435
30	.363	.226	.330	.047	.030	-.021	.398
35	.450	.322	.406	.059	.038	-.034	.383
40	.590	.424	.458	.060	.047	-.045	.389
45	.703	.514	.478	.061	.055	-.056	.394
50	.693	.591	.477	.061	.065	-.065	.388
55	.664	.664	.454	.058	.073	-.072	.383
60	.650	.712	.413	.047	.077	-.071	.387
65	.661	.750	.360	.036	.079	-.065	.400
70	.702	.772	.297	.031	.076	-.057	.413
75	.639	.788	.232	.025	.062	-.046	.428
80	.582	.798	.158	.020	.042	-.033	.443
85	.541	.801	.080	.010	.021	-.017	.469
90	.522	.802	.000	.008	.000	.000	.500

Table C-16. Smoothed aerodynamic coefficients for the plank model at 60° roll angle in free air.

(ψ) Deg	C_L	C_D	C_s	C_m	C_n	C_ℓ	$X_{cp/L}$
0	.000	.034	.000	.000	.000	.000	.375
5	.017	.037	.034	.000	.006	.000	.386
10	.038	.050	.096	.001	.013	.000	.394
15	.068	.083	.174	.001	.022	.000	.403
20	.111	.134	.261	.001	.033	.000	.408
25	.171	.209	.354	.002	.045	-.001	.415
30	.244	.316	.449	.002	.057	-.004	.416
35	.323	.470	.578	.006	.060	-.007	.420
40	.437	.612	.667	.010	.084	-.011	.422
45	.492	.722	.703	.014	.097	-.016	-.417
50	.532	.812	.693	.015	.107	-.021	-.412
55	.580	.905	.654	.015	.115	-.026	.410
60	.648	1.010	.600	.016	.120	-.031	.410
65	.720	1.059	.518	.016	.116	-.034	.415
70	.759	1.077	.413	.015	.097	-.035	.429
75	.760	1.084	.305	.012	.072	-.030	.439
80	.761	1.088	.209	.009	.049	-.023	.458
85	.762	1.090	.104	.008	.024	-.017	.474
90	.762	1.092	.000	.008	.000	.000	.500

Table C-17. Smoothed aerodynamic coefficients for the plank model at 90° roll angle in free air.

(ψ) Deg	C_D	C_s	C_n	$X_{cp/L}$
0	.034	0	0	.375
5	.035	.036	.008	.375
10	.048	.101	.017	.375
15	.087	.194	.028	.375
20	.149	.306	.043	.375
25	.235	.418	.059	.376
30	.340	.532	.079	.373
35	.481	.632	.103	.370
40	.639	.715	.121	.374
45	.807	.757	.136	.377
50	.940	.763	.146	.382
55	1.115	.752	.153	.387
60	1.253	.720	.154	.393
65	1.360	.651	.145	.404
70	1.397	.537	.121	.419
75	1.416	.377	.083	.443
80	1.424	.234	.053	.463
85	1.426	.110	.025	.482
90	1.426	0	0	.500

Table C-18. Smoothed aerodynamic coefficients for the plank model at 0^{o} roll angle, 0.725 plank widths above ground plane.

(ψ) Deg	C_L	C_D	C_s	C_n	$X_{cp/L}$
0	.000	.035	.000	.000	.360
5	.004	.037	.012	.002	.375
10	.014	.040	.025	.003	.387
15	.020	.050	.040	.006	.399
20	.024	.062	.057	.008	.409
25	.027	.078	.075	.010	.418
30	.032	.103	.095	.012	.427
35	.036	.130	.118	.012	.436
40	.031	.162	.138	.012	.444
45	.017	.195	.152	.011	.452
50	.000	.230	.162	.011	.458
55	-.025	.270	.165	.010	.465
60	-.052	.310	.157	.008	.473
65	-.090	.350	.145	.007	.480
70	-.140	.390	.126	.005	.486
75	-.205	.420	.105	.003	.492
80	-.260	.443	.075	.002	.496
85	-.290	.460	.040	.001	.498
90	-.304	.465	.000	.000	.500

Table C-19. Smoothed aerodynamic coefficients for the plank model at 0^{o} roll angle, 0.500 plank widths above ground plane.

(ψ) Deg	C_L	C_D	C_s	C_n	$X_{cp/L}$
0	.000	.027	.000	.000	.360
5	.004	.030	.006	.002	.375
10	.014	.035	.019	.003	.387
15	.020	.045	.032	.006	.399
20	.027	.056	.050	.008	.409
25	.040	.074	.068	.010	.418
30	.050	.096	.085	.012	.427
35	.057	.123	.106	.012	.436
40	.057	.152	.120	.012	.444
45	.052	.182	.135	.011	.452
50	.040	.215	.142	.011	.458
55	.013	.250	.144	.010	.465
60	-.035	.285	.138	.008	.473
65	-.110	.324	.132	.007	.480
70	-.173	.360	.112	.005	.486
75	-.230	.388	.090	.003	.492
80	-.272	.410	.070	.002	.496
85	-.305	.425	.040	.001	.498
90	-.327	.430	.000	.000	.500

Table C-20. Smoothed aerodynamic coefficients for the plank model at 0° roll angle, 0.083 plank widths above ground plane.

(ψ) Deg	C_L	C_D	C_s	C_Y	C_n	$X_{cp/L}$
0	.000	.028	.000	.000	.000	.357
5	.005	.030	.005	.010	.002	.370
10	.013	.035	.019	.022	.004	.382
15	.027	.045	.034	.044	.006	.391
20	.051	.055	.050	.067	.009	.400
25	.085	.067	.068	.090	.012	.409
30	.121	.086	.085	.118	.013	.416
35	.160	.109	.105	.145	.014	.424
40	.193	.135	.121	.176	.015	.430
45	.206	.167	.135	.210	.015	.437
50	.210	.200	.142	.240	.014	.443
55	.205	.230	.143	.270	.013	.450
60	.195	.262	.138	.298	.012	.456
65	.177	.298	.127	.324	.011	.464
70	.156	.325	.112	.345	.010	.472
75	.135	.345	.093	.361	.008	.477
80	.125	.365	.070	.374	.006	.484
85	.115	.375	.040	.382	.003	.492
90	.114	.382	.000	.385	.000	.500

Table C-21. Smoothed aerodynamic coefficients for the plank model at 30° roll angle, 2.0 plank widths above ground plane.

(ψ) Deg	C_L	C_D	C_s	C_m	C_n	C_ℓ	$X_{cp/L}$
0	.000	.030	.000	.000	.000	.000	.375
5	.018	.033	.024	.001	.003	.000	.430
10	.060	.047	.065	.002	.006	.000	.450
15	.130	.073	.111	.003	.010	.000	.460
20	.225	.110	.170	.007	.015	-.003	.460
25	.320	.160	.240	.016	.021	-.010	.435
30	.400	.229	.320	.034	.028	-.020	.405
35	.490	.310	.386	.050	.037	-.031	.390
40	.580	.408	.445	.055	.045	-.042	.385
45	.700	.510	.482	.057	.052	-.055	.385
50	.695	.583	.484	.057	.058	-.064	.386
55	.682	.655	.460	.053	.063	-.069	.388
60	.676	.715	.428	.046	.066	-.070	.394
65	.695	.750	.385	.035	.068	-.066	.403
70	.725	.775	.330	.026	.069	-.057	.416
75	.700	.790	.260	.019	.062	-.045	.432
80	.645	.799	.182	.014	.045	-.032	.455
85	.595	.804	.095	.010	.024	-.016	.477
90	.583	.806	.000	.008	.000	.000	.500

Table C-22. Smoothed aerodynamic coefficients for the plank model at 30° roll angle, 0.033 plank widths above ground plane.

(ψ) Deg	C_L	C_D	C_s	C_m	C_n	C_ℓ	$X_{cp/L}$
0	.000	.030	.000	.000	.000	.000	.375
5	.033	.033	.037	.004	.006	.000	.376
10	.103	.047	.087	.011	.012	-.001	.385
15	.205	.075	.146	.020	.018	-.005	.387
20	.316	.120	.225	.033	.025	-.013	.385
25	.442	.185	.320	.050	.033	.024	.380
30	.572	.270	.415	.069	.044	-.040	.375
35	.691	.370	.488	.086	.058	-.060	.365
40	.890	.486	.540	.097	.075	-.087	.357
45	.875	.605	.560	.101	.090	-.105	.355
50	.950	.694	.556	.097	.100	-.116	.358
55	.953	.754	.522	.084	.107	-.119	.367
60	.930	.790	.470	.058	.107	-.107	.381
65	.845	.817	.410	.034	.064	-.071	.395
70	.833	.840	.343	.021	.052	-.057	.414
75	.826	.850	.270	.014	.041	-.045	.432
80	.823	.860	.186	.009	.029	-.032	.455
85	.819	.866	.095	.005	.015	-.016	.477
90	.815	.868	.000	.004	.000	.000	.500

Table C-23. Smoothed aerodynamic coefficients for the plank model at 90° roll angle, 1.71 plank widths above ground plane.

(ψ) Deg.	C_L	C_D	C_s	C_n	$X_{cp/L}$
0	.000	.020	.000	.000	.323
5	.004	.025	.040	.006	.342
10	.010	.040	.110	.016	.360
15	.020	.080	.190	.027	.368
20	.035	.146	.290	.041	.372
25	.047	.238	.400	.059	.372
30	.053	.340	.503	.079	.372
35	.054	.475	.630	.101	.372
40	.051	.632	.718	.122	.373
45	.046	.800	.770	.136	.375
50	.041	.990	.785	.145	.380
55	.032	1.125	.770	.150	.386
60	.020	1.250	.730	.151	.394
65	.014	1.342	.655	.144	.407
70	.007	1.405	.548	.122	.423
75	.004	1.436	.400	.080	.448
80	.001	1.445	.249	.049	.470
85	.000	1.450	.118	.023	.487
90	.000	1.450	.000	.000	.500

Table C-24. Smoothed aerodynamic coefficients for the plank model at 90° roll angle, 0.083 plank widths above ground plane.

(ψ) Deg	C_L	C_D	C_s	C_n	$X_{cp/L}$
0	.005	.018	.000	.000	.280
5	.023	.038	.050	.012	.290
10	.060	.075	.130	.025	.325
15	.076	.135	.240	.038	.360
20	.082	.213	.380	.052	.377
25	.075	.317	.542	.068	.390
30	.042	.459	.739	.087	.396
35	-.022	.640	.895	.122	.393
40	-.060	.830	.941	.155	.376
45	-.075	.981	.940	.175	.370
50	-.091	1.092	.900	.179	.374
55	-.104	1.174	.820	.170	.387
60	-.113	1.225	.721	.091	.425
65	-.120	1.265	.618	.071	.445
70	-.124	1.305	.505	.054	.460
75	-.127	1.338	.390	.040	.473
80	-.129	1.368	.265	.026	.483
85	-.131	1.386	.132	.013	.493
90	-.130	1.390	.000	.000	.500

Table C-25. Automobile model, side mounted in free air.

(Ψ) Deg	C_D	C_s	C_n
0	.497	-.184	.195
5	.540	.184	.089
10	.690	.567	-.037
15	.883	1.016	-.235
20	1.169	1.412	-.406
25	1.470	1.763	-.595
30	1.830	1.996	-.780
35	2.264	2.176	-.964
40	2.641	2.350	-1.147
45	3.030	2.451	-1.315
50	3.318	2.434	-1.449
55	3.615	2.345	-1.561
60	3.804	2.210	-1.625
65	3.945	3.028	-1.711
70	4.542	1.998	-2.069
75	4.884	1.895	-2.232
80	5.022	1.360	-2.279
85	5.040	.763	-2.326
90	5.050	.041	-2.376

Table C-26. Automobile model, roof mounted in free air.

(ψ) Deg	C_L	C_D	C_s	C_m	C_n	C_ℓ
0	.302	.497	.000	-.238	.000	.000
5	.315	.522	.160	-.238	-.060	.011
10	.330	.630	.294	-.238	-.123	.046
15	.320	.750	.455	-.236	-.194	.062
20	.288	.910	.580	-.226	-.270	.078
25	.256	1.083	.682	-.212	-.354	.091
30	.217	1.210	.764	-.186	-.450	.101
35	.167	1.380	.848	-.154	-.558	.102
40	.098	1.570	.978	-.109	-.694	.110
45	.049	1.919	1.219	-.050	-.883	.112
50	.032	2.230	1.334	-.010	-1.045	.110
55	.052	2.353	1.340	-.038	-1.068	.107
60	.072	2.370	1.279	-.052	-1.060	.100
65	.056	2.380	1.166	-.038	-1.048	.078
70	.014	2.370	1.034	.018	-1.040	.027
75	-.043	2.360	.874	.068	-1.038	-.037
80	-.113	2.350	.688	.102	-1.040	-.095
85	-.219	2.340	.488	.120	-1.054	-.156
90	-/350	2.330	.276	.114	-1.078	-.232

Table C-27. Automobile, rear mounted in free air

(Ψ) Deg	C_L	C_D	C_s	C_m	C_n	C_l
0	.435	4.932	.000	2.347	.000	.000
5	.539	4.939	-.200	2.341	.020	.017
10	.548	4.619	-.420	2.128	.013	-.018
15	.425	4.512	-.569	2.126	-.005	-.034
20	.273	4.641	-.658	2.254	-.001	-.053
25	.147	4.653	-.742	2.225	-.009	-.184
30	.047	4.681	-.780	2.248	-.005	-.213
35	-.013	4.622	-.823	2.235	-.020	-.237
40	-.042	4.488	-.835	2.147	-.022	-.259
45	-.037	4.271	-.851	2.046	-.031	-.277
50	0	4.125	-.840	1.936	-.003	-.296
55	.033	3.815	-.826	1.806	.018	-.307
60	.052	3.557	-.719	1.666	.044	-.285
65	.073	3.206	-.555	1.517	.066	-.230
70	.085	2.896	-.326	1.348	.099	-.133
75	.104	2.564	-.001	1.188	.136	.009
80	.199	2.233	.527	1.075	.172	.344
85	.373	2.309	.059	1.043	.164	.409
90	.388	2.287	-.393	1.028	.125	.123

Table C-28. Full-Scale Automobile (1974 Dodge Dart), Bottom Mounted in Free Air

ψ deg	C_L	C_D	C_S	C_m	C_n	C_l
0	.420	0.54	0.020	-.230	.018	-.015
5	.448	0.56	0.158	-.240	.040	.033
10	.588	0.68	0.272	-.325	-.107	.090
15	.690	0.78	0.373	-.390	-.170	.143
20	.682	0.96	0.440	-.385	-.224	.188
25	.649	1.11	0.487	-.340	-.290	.224
30	.578	1.25	0.533	-.282	-.362	.258
35	.553	1.38	0.566	-.246	-.428	.290
40	.587	1.53	0.586	-.220	-.512	.319
45	.656	1.66	0.600	-.200	-.586	.338
50	.710	1.78	0.007	-.164	-.654	.350
55	.672	1.87	0.616	-.102	-.722	.353
60	.606	1.95	0.612	-.035	-.790	.350
65	.555	1.99	0.582	.032	-.836	.332
70	.516	2.01	0.530	.085	-.860	.304
75	.491	2.03	0.452	.137	-.886	.267
80	.457	2.08	0.340	.162	-.917	.202
85	.282	2.15	0.165	.180	-.960	.052
90	-.317	2.28	-0.020	.182	-1.020	-.185

Table C-29. Full-Scale Automobile (1974 Dodge Dart), on Ground
α = 0° bottom mounted

ψ deg	C_L	C_D	C_S	C_m	C_n	C_l
0	0	0.58	0	-.242	0	0
5	.635	0.65	.203	-.255	-.081	.045
10	.790	0.73	.379	-.346	-.144	.100
15	1.106	0.89	.454	-.527	-.197	.168
20	1.100	1.09	.495	-.489	-.245	.236
25	1.150	1.23	.530	-.491	-.312	.314
30	1.264	1.64	.564	-.509	-.383	.393
35	1.404	1.52	.569	-.515	-.474	.475
40	1.570	1.63	.618	-.503	-.568	.572
45	1.740	1.74	.640	-.476	-.683	.687
50	1.865	1.87	.665	-.426	-.800	.770
55	1.718	2.03	.679	-.329	-.903	.689
60	1.508	2.19	.683	-.217	-.990	.604
65	1.350	2.28	.670	-.128	-1.048	.583
70	1.255	2.37	.603	-.044	-1.094	.608
75	1.280	2.43	.436	+.027	-1.140	.660
80	1.304	2.50	.270	+.082	-1.179	.670
85	1.238	2.53	.128	+.136	-1.218	.589
90	1.122	2.55	-.007	+.177	-1.252	.463

Table C-30. Full-scale Automobile (1974 Dodge Dart), on Ground, α = 5° bottom Mounted

ψ deg	C_L	C_D	C_S	C_m	C_n	C_l
0	0.770	0.66	0.000	.317	0.000	0.000
5	0.834	0.72	0.187	.374	0.063	0.030
10	1.102	0.85	0.312	.526	0.113	0.100
15	1.415	1.07	0.394	.667	0.157	0.182

Table C-31. Full-scale Automobile (1974 Dodge Dart), on Ground, α = 10° bottom Mounted

ψ deg	C_L	C_D	C_S	C_m	C_n	C_l
0	1.136	0.86	0.000	.517	0.000	0.000
5	1.255	0.95	0.198	.589	0.056	0.026
10	1.510	1.05	0.369	.727	0.098	0.104
15	1.800	1.19	0.522	.888	0.114	0.235

Table C-32. Van model, roof mount

(ψ) Deg	C_L	C_D	C_s	C_m	C_n	C_l	$X_{cp/L}$
0	.019	.440	.000	-.048	.000	.000	.405
5	-.007	.504	.270	-.032	-.113	.045	.400
10	-.067	.661	.499	.010	-.200	.076	.391
15	-.169	.836	.735	.068	-.326	.097	.390
20	-.279	1.073	.944	.134	-.474	.103	.389
25	-.374	1.282	1.146	.172	-.588	.095	.389
30	-.489	1.497	1.307	.196	-.713	.094	.388
35	-.611	1.803	1.390	.334	-.840	.049	.390
40	-.746	1.981	1.486	.379	-.960	.050	.393
45	-.458	2.015	1.542	.330	-1.026	.117	.400
50	-.272	2.101	1.539	.242	-1.090	.252	.411
55	-.017	2.244	1.536	.236	-1.158	.366	.425
60	.346	2.397	1.534	.134	-1.222	.539	.436
65	.558	2.530	1.510	.188	-1.270	.649	.442
70	.677	2.623	1.452	.260	-1.306	.744	.446
75	.698	2.734	1.345	.330	-1.338	.651	.455
80	.690	2.798	1.194	.388	-1.360	.558	.468
85	.655	2.832	.926	.404	-1.380	.478	.485
90	.627	2.840	.102	.433	-1.386	.371	.500

Table C-33. Van model, side mount

(ψ) Deg	C_D	C_s	C_n
0	.444	.120	-.043
5	.547	.337	-.126
10	.690	.549	-.217
15	.881	.816	-.347
20	1.088	.979	-.445
25	1.249	1.052	-.514
30	1.409	1.076	-.595
35	1.559	1.101	-.664
40	1.702	1.126	-.737
45	1.805	1.148	-.788
50	1.931	1.190	-.843
55	2.114	1.268	-.998
60	2.326	1.334	-1.210
65	2.500	1.338	-1.229
70	2.630	1.297	-1.236
75	2.688	1.118	-1.294
80	2.736	.242	-1.378
85	2.770	-.391	-1.464
90	2.798	-.575	-1.527

Table C-34. Van model, rear mount

(ψ) Deg	C_L	C_D	C_S	C_m	C_n	C_l
0	1 023	2 800	.000	1.813	000	-.000
5	1.066	2 810	-.321	1.813	.045	- 044
10	1.011	2.848	- 317	1 813	.073	-.072
15	.830	2 940	-.308	1.872	112	-.105
20	875	3.064	-.256	1.970	.172	- 118
25	.868	3.235	- 231	2 105	.212	- 125
30	.794	3.312	- 174	2 154	.274	-.120
35	.682	3.323	-.123	2.170	333	-.107
40	622	3 366	-.042	2.152	.392	- 087
45	605	3 372	-.017	2 074	.430	- 052
50	.576	3 287	012	1 926	.483	-.024
55	.534	3.120	.041	1.740	497	.012
60	.441	2 934	.137	1.590	.521	043
65	.417	2 779	.222	1.450	.540	.088
70	.358	2.612	416	1.342	560	.181
75	.291	2.438	.870	1.271	577	440
80	227	2 337	1 517	1.225	.580	845
85	136	2 689	.780	1 220	.586	490
90	.000	2.790	.000	1 200	588	.371

APPENDIX D

USER MANUAL

This appendix describes the software input and the output specifications for the simulation of wind field and trajectory relating to tornado-propelled objects. The documentation is consistent with the input/output constraints of the simulation software for the UNIVAC Model 1108 Computer System.*

The discussion that follows relies on notational and reference conventions documented in Section II.

A. INPUT/FORMAT SPECIFICATIONS

a. General Program Execution Rules and Default Options. Each simulation or case requires at most six categories of input information. The possible input categories for a simulation project are:

1) Case identifier (required for each simulated case)
2) Parameter read configuration control (required for each simulated case)
3) Tornado description parameters (required for first simulated case; optional on subsequent cases)
4) Rigid body description parameters (required for first simulated case; optional on subsequent cases)
5) Integration function parameters (optional; may be included for any desired case)
6) End execution flag (required at end of simulation packets/packet)

*This user manual for the computer program for tornado-propelled objects was prepared by Barnett C. Fletcher and revised by John R. Radbill.

Specific information regarding the form and content of each of the above categories is contained in paragraphs b. through o.

Input for each case simulation can be regarded as a data packet containing combinations of parameter inputs to be considered. As many case simulation packets as desired will be executed until the end execution flag is encountered.

Each case simulation packet must contain a case identifier and parameter read configuration control.

The first case simulation of each independent program execution must be initialized. Therefore, the first case packet must contain information parameters for the tornado and rigid body specifications. Subsequent case simulations of a particular execution will continue to use the tornado and rigid body parameters until the program is told to read new parameters via the configuration control image.

Default options are provided for the integration parameters used during the simulation. Therefore, the integration parameters need not be included in any data packet. Change in the integration parameters may be accomplished for any case by changing the read configuration control and including the data in that particular data packet. These integration parameters will continue to be used until the user supplies the next desired change.

The total data input for a particular program execution will then consist of one or more data packets; one packet is required for each case simulation to be considered. The end of execution flag is included only after the last simulation packet.

The following discussion will explain in detail each data input card comprising a simulation case data packet. These input cards are discussed in the order necessary for program execution.

b. Case Documentation Header Card. This card is required for each case simulation packet to be executed.

Function: To provide output documentation reference for each simulation case

Format: Any combination of FORTRAN readable print characters desired in a field comprising colums (1-72)

Example: CASE 503, 12IN PIPE, YAW=90, PITCH=45, ROLL=0, DATE, ETC.

c. Read Configuration Control Card. This card is required for each case simulation packet to be executed.

Function: Provide a logical variable string: this card controls input of subsequent card images, and certain optional output and therefore should contain a logical true (T) to obtain the listed action. A logical false (F) should be set for cards not provided and actions not desired.

Format: L1, T, or F in card columns 9, 18, 27, 36, 45, 54, 63, 72.

Example:

Card Column	Internal Mnemonic	Input Value	Action Obtained
9	RDTORN	T	Read tornado parameters
18	RDBDYP	T	Read body dimensions
27	RDINRT	T	Read and compute weight c.g. and inertia tensor
36	RDAERO	T	Print aerodynamic coef-ficients and sign data
45	RDINTG	T	Read integration parameters
54	RDABER	T	Read state variable accuracy
63	RDINIT	T	Read initial conditions for rigid body

72	PLOT	T	Write state variables on FORTRAN file 3 at each print step for plotting by other programs

d. Option Control Card. This card is required for each case simulation packet to be executed.

Function: Provide a logical variable string; this card controls input/computation and print options

Format: L1, T, or F in card columns 9, 18, 27.

Example:

Card Column	Internal Mnemonic	True Control
9	CYLNDR	Read aerodynamic data in format for cylinders. Compute aerodynamic forces and moments using cylinder formules
18	PRTORN	Print intermediate variables in tornado wind field computation
27	PRINTV	Print internal variables in trajectory computation

*e. Tornado Parameter Cards.[1]

Function: Provide a floating point value string for the following variables.

Card Columns	Format	Echo Print Mnemonic	Description	Units
First Card				
(1-8)	F8.6	R1MILE	The radius of maximum velocity	mi
(9-16)	F8.6	LATDEG	Latitude	deg

[1] This information is required for at least the initial simulation packet of a particular execution. It should be included in any data packet requiring a subsequent change.

(17-24)	F8.6	VMXMPH	Maximum trangential velocity at R1MILE	mph
(25-32)	F8.6	UTCMPH	'x' velocity component of tornado center	mph
(33-40)	F8.6	VTCMPH	'y' velocity component of tornado center	mph
(41-48)	F8.6	XTCMIL	Initial 'x' coordinate of tornado center relative to an arbitrary origin	mi
(49-56)	F8.6	YTCMIL	Initial 'y' coordinate of tornado center relative to an arbitrary origin	mi
(57-64)	F8.6	NUFZPS	Eddy viscosity of ambient air	ft^2/sec
(65-72)	F8.6	ALPHAF	Near-ground vertical scale	ft
(1-8)	F8.6	BETAFT	Upper vertical scale	ft

f. Rigid Body Dimension Card.[1]

Card Columns	Format	Echo Print Mnemonic	Description	Units
(1-8)	F8.6	BDYLFT	Body length, L	ft
(9-16)	F8.6	BDYDFT	Body width, w or diameter d if CYLNDR=T	ft
(17-24)	F8.6	BDYTFT	Body thickness, h (not required if CYLNDR=T)	ft

g. Rigid Body Component Inertial Description (2-10 cards).[1]

Function: Provide a floating point value string for weight, cg location and inertia tensor components about their own axes of 1 to 10 components of the rigid body.

Special Note: Reading of component Inertial Description cards is terminated when 10 cards have been read or when 0. is detected in columns (1-7).

Card Columns	Format	Internal Mnemonic	Description	Units
(1-7)	F7.1	WP	Body component weight	lb
(8-28)	3F7.1	RCG	Body component center of gravity location relative to Body reference location (3 component vector)	ft
(29-35)	F7.1	ITPF2(1, 1)	'xx' element of component inertia tensor relative to component cg	$lb*ft^2$
(36-42)	F7.1	ITPF2(1, 2)	'xy' element	$lb*ft^2$
(43-49)	F7.1	ITPF2(1, 3)	'xz' element	$lb*ft^2$
(50-56)	F7.1	ITPF2(2, 2)	'yy' element	$lb*ft^2$
(57-63)	F7.1	ITPF2(2, 3)	'yz' element	$lb*ft^2$
(64-70)	F7.1	ITPF2(3, 3)	'zz' element	$lb*ft^2$

h. Aerodynamic Coefficient Label Card.[1]

Function: Provide a value string for the following alphanumeric, integer and real variables of types specified by the formats.

Card Columns	Format	Internal Mnemonic	Description
(1-48)	8A6	MODEL	Alphanumeric description of aerodynamic form
(49-51)	13	NA	Number of pitch angle entries in coefficient table NA $\leq$ 19 = NA default
(52-54)	13	IPA	Number of points used in interpolating in pitch angle table. IPA $\leq$ NA. IPA default = 2.
(55-57)	13	NP	Number of roll angle entries in coefficient table. NP $\leq$ 4 = NP default (not used if CYLNDR=T)
(58-60)	13	IPP	Number of points used in interpolating in pitch angle table. IPP $\leq$ NP IPP default = 2 (not used if CYLNDR=T)
(61-66)	F6.1	CNXZAV	Average normal force coefficient for xy face used in computing damping moment coefficient about y axis (not used if CYLNDR=T)
(67-72)	F6.1	CNXZAV	Average normal force coefficient for xz face used in computing damping moment coefficient about z axis (not used if CYLNDR=T)

h. Aerodynamic Reference Area and Air Density Card.[1]

Function: Provide a floating point value string for the aerodynamic reference area and air density as specified below.

Card Columns	Format	Internal Mnemonic	Description	Units
(1-6)	F6.2	AREFF2	Reference area for aerodynamic coefficients AREFF2 default = L*w	ft^2
(7-12)	F6.2	RHOLF3	Air density. Default RHOLF3 = 8.07223×10^{-2}	lb/ft^2
(13-18)	L6	PRAROF	Print control for intermediate aerodynamic force variables	-----

j. Aerodynamic Coefficients for Cylinder (NA cards) for Case When CYLNDR=.TRUE.[1]

Function: Each of the NA ≤ 19 cards provides a floating point value string for the aerodynamic coefficients specified at the pitch angle specified.

Card Columns	Format	Echo Print Mnemonic	Description	Units
(1-6)	F6.4	ALPHA	Pitch Angle, α	deg
(7-12)	F6.4	CD	Drag Coefficient C_D	unitless
(13-18)	F6.4	CL	Lift Coefficient C_L	unitless
(19-24)	F6.4	CM	Moment Coefficient C_m	unitless
(25-30)	F6.4	CMQ	Damping Moment Coefficient C_{mq}	unitless

k. Aerodynamic Coefficients for Rectangular Parallelpiped (Bodies with Three Perpendicular Planes of Symmetry) (NA*NP Cards) for Case When CYLNDR=.FALSE.[1]

Function: Each of the (NA ≤ 19)*(NP ≤ 4) cards provides a floating point value string for the aerodynamic coefficients specified at the pitch and roll angles specified.

As a group, the cards form a two variable table as a function of pitch (row) and roll (column) angles in FORTRAN order.

Card Columns	Format	Echo Print Mnemonic	Description	Units
(1-10)	F10.3	CL	Lift Coefficient, C_L	unitless
(11-20)	F10.3	CD	Drag Coefficient, C_D	unitless
(21-30)	F10.3	CS	Side Force Coefficients, C_S	unitless
(31-40)	F10.3	CM	Pitching Moment Coefficient, C_m	unitless
(41-50)	F10.3	CN	Yawing Moment Coefficient, C_n	unitless
(51-60)	F10.3	CLL	Rolling Moment Coefficient, C_ℓ	unitless
(73-74)	F2.0	ALPHA	Pitch Angle, α	deg
(76-77)	F2.0	PHI	Roll Angle, ϕ	deg

l. Integration Parameter Card. This card is not required for any particular case simulation packet. Default values are provided internally.

Function: Provide a floating point value string and one integer for the following variables.

Card Columns	Format	Internal Mnemonic	Default Values	Description	Units
(1-8)	F8.6	H	10^{-2}	Initial Step Size	sec
(9-16)	F8.6	DELT	10^{-1}	Output Print Interval	sec
(17-24)	F8.6	TFINAL	10.0	Maximum time	sec
(25-32)	I8	MXSTEP	20	Maximum number of steps before output print	
(38-80)	BLANK				

m. State Variable Accuracy Card. This card is not required in any particular case simulation packet. Default values are provided internally.

Function: Provide a floating point value string for the following variables. These variables represent Absolute Error on integration accuracy.

Card Columns	Format	Internal Mnemonic	Default Values	Description
(1-6)	F6.3	EP (1)	10^{-2}	Absolute error on Linear Velocity
(7-12)	F6.3	EP (2)	10^{-2}	Absolute error on tornado center with respect to orgin
(13-18)	F6.3	EP (3)	10^{-2}	Absolute error for Quaterion Components
(19-24)	F6.3	EP (4)	10^{-2}	Absolute error on 'x' Component of Angular Momentum
(25-30)	F6.3	EP (5)	10^{-2}	Absolute error on 'y' and 'z' Components of Angular Momentum

n. Rigid Body Initial Conditions (2 Cards). (1)

Function: Provide a floating point value string for the following variables.

Card Columns	Format	Internal Mnemonic	Description	Units
(1-8)	F8.6	XFT	'x' Coordinate of Rigid Body injection point	ft
(9-16)	F8.6	YFT	'y' Coordinate of Rigid Body injection point	ft
(17-24)	F8.6	ZFT	'z' Coordinate of Rigid Body injection point	ft
(25-32)	F8.6	UMPH	'x' Component of Rigid Body initial velocity	mph
(33-40)	F8.6	VMPH	'y' Component of Rigid Body initial velocity	mph
(41-48)	F8.6	WMPH	'z' Component of Rigid Body initial velocity	mph
(49-56)	F8.6	PSIDEG	Yaw Angle	deg
(57-64)	F8.6	THETDG	Pitch Angle	deg
(65-72)	F8.6	PHIDEG	Roll Angle	deg

Special Note: Body Reference Axes are parallel to inertial axes.

*** RIGID BODY INITIAL CONDITIONS - CARD 2 ***

(1-8)	F8.6	OMXRPM	'x' Component of Angular Velocity	rpm
(9-16)	F8.6	OMYRPM	'y' Component of Angular Velocity	rpm
(17-24)	F8.6	OMZRPM	'z' Component of Angular Velocity	rpm

o. End of Execution Card. This card is required to terminate program execution. It is to be included only at the end of the desired number of simulation cases provided by the user. (i.e., the last card in a data deck.)

Function: Provide a unique integer value flag to terminate program execution.

Card Columns	Format	Explicit Input Required
(73-77)	I5	99999

B. OUTPUT OF SIMULATION

The initial output for each case simulation of a tornado-driven rigid body may be divided into three subsections.

(1) Input Echo
(2) Rigid Body dynamic parameters at the user specified print interval
(3) Additional interval variables (if PRINTV=.TRUE.)

a. Input Echo. Each case simulation provided by the user is documented on output. The documentation begins with an echo of the header message provided by the user and as documented in paragraph A.b.

The remaining initial value information regarding the tornado, Rigid Body and integration parameters is also printed for user convenience. The variable names associated with the printed values may be cross-referenced with the mnemonic lists contained in paragraphs A.c. through A.k.

b. Rigid Body Dynamics. An example of the rigid body dynamic variable information is shown below. This example is an arbitrary selection from a sample output listing. An actual output would contain a series of these specifications; they would be printed according to the user specified print interval.

```
TSEC=.650000, HSEC=.039954
XFT=4.2, YFT=4.6, ZFT=128.6
UFPS=19.5, VFPS=17.4, WFPS=-3.2
OMXRPS=-.135, OMYRPS=-.421, OMZRPS=-.422
YAW=-134.3, PITCH=39.5, ROLL=9.3, RXYFT=6., SPDFPS=26.4
```

The definitions of the printed variable names are listed below.

Variable Name	Description	Units
TSEC	Time from injection (at intervals of DELT)	sec
HSEC	Interval determined by Step Size	sec
XFT	'x' Coordinate	ft
YFT	'y' Coordinate	ft
ZFT	'z' Coordinate	ft
UFPS	'x' Component of Linear Velocity	ft/sec
VFPS	'y' Component of Linear Velocity	ft/sec
WFPS	'z' Component of Linear Velocity	ft/sec
OMXRPS	'x' Component of Angular Velocity	rev/sec
OMYPRS	'y' Component of Angular Velocity	rev/sec
OMZRPS	'z' Component of Angular Velocity	rev/sec
YAW	Yaw Axis ('z') Angle	deg
PITCH	Pitch Axis ('x') Angle	deg
ROLL	Roll Axis ('y') Angle	deg
RXYFT	Trajectory Ground Distance with respect to orgin	ft
SPDFPS	Velocity of Rigid Body along trajectory	ft/sec

c. Additional Internal Variables Printed if PRINTV=.TRUE. An example of the additional internal variable information which is printed at each time step following the output described in paragraph B.b. is shown below. This example is an arbitrary selection from a sample output listing which follows the output shown in paragraph B.b.

```
VWIND=246.7 31.5 26.9, ALPHAW=.0 65.9 47.7, OMEGAW=.080 .596 -.112
VWREL=233.4 19.6 29.1, FW=11426.7 .0 5709.0, FI=10455.8 4613.7 1105.4
```

The definitions of the printed variable names are listed below.

Variable Name	Description	Units
VWIND	Wind velocity vector	ft/sec
ALPHAW	Angles between body and relative wind direction: yaw, pitch, roll	deg
OMEGAW	Angular velocity vector of body in wind coordinates	rev/sec
VWREL	Relative wind velocity vector	ft/sec
FW	Aerodynamic force vector in wind coordinates	lb
FI	Total force vector in inertial coordinates	lb

d. Instantaneous Aerodynamic Coefficients for Cylinder. Printed if PRINTV=. TRUE. and CYLNDR=. TRUE.

An example of the instantaneous aerodynamic coefficients which are printed at each time step following the output described in section is shown below.

CD=1.045, CL=.021, CM=.004, CMQ=-.174

The definitions of the printed variable names are listed below.

Variable Name	Description	Units
CD	Drag Coefficient, C_D	unitless
	Lift Coefficient, C_L	unitless
	Moment Coefficient, C_m	unitless
	Damping Moment Coefficient, C_{mq}	unitless

e. Instantaneous Aerodynamic Coefficients for Body with Three Perpendicular Planes of Symmetry. Printed if PRINTV=. TRUE. and CYLNDR =. FALSE.

An example of the instantaneous aerodynamic coefficients which are printed at each time step following the output described in paragraph B. e. is shown below.

CD=4.049, CS=.000, CL=2.023, CMROLL=.000, CMPITCH=.523, CMYAW=.000

The definitions of the printed variable names are listed below.

Variable Name	Description	Units
CD	Drag Coefficient, C_D	unitless
CS	Side Force Coefficient, C_S	unitless
CL	Lift Coefficient, C_L	unitless
CMROLL	Rolling Moment Coefficient, C_ℓ	unitless
CMYAW	Yawing Moment Coefficient, C_m	unitless

f. Output for Termination of Trajectory. The output for termination of the trajectory is the same as that obtained at the specified print interval except that the variables correspond to the time when the termination condition is satisfied. The current terminating condition is ZFT = 0. This specification can be modified as desired by changing the subroutine TERMIN.

APPENDIX E

COMPUTER PROGRAM LISTINGS

This appendix contains listings of the computer program for the trajectory model of Section V. The program consists of a main program and a number of subroutines in the FORTRAN V language for the UNIVAC 1108 computer at JPL.

```
(1),MAIN/01-20-77
C     MAIN PROGRAM FOR SIMULATION OF TORNADO DRIVEN MISSILES                    MAIN0010
C     PORTABLE VERSION DESIGNED TO SATISFY PFORT VERIFIER                       MAIN0020
C     CG AND AERO MOMENT CENTER MAY BE DISPLACED BY RCG                         MAIN0030
C       J.R.RADBILL, JPL, SECT.366, MAIL 125-128, PHONE (213) 354-2989          MAIN0040
C       STARTED 5-29-75, LAST CHANGE 01-20-77 1410                              MAIN0050
C     ************************************************************************MAIN0060
      LOGICAL   END, PLOT, PRINTV                                               MAIN0070
      INTEGER   KORD(34), IOPT(15)                                              MAIN0080
      REAL      PADTRN(12), PADCRI(11), PADCIN(6), PADARO(546), XTC(2),         MAIN0090
     *          PADES1(21), PADES2(6), YY(30), Q(4), L(3), TSPEC(4),            MAIN0100
     *          OMEGA(3), EULERA(3), TRNMBI(3,3), INERT(3,3), WK(12),           MAIN0110
     *          ITEMP(3,3), INERTI(3,3), F(144), PADSVD(27), XV(6),             MAIN0120
     *          YN(15), G(5), GT(5)                                             MAIN0130
      COMMON    /TORN/ PADTRN /CRINRT/ PADCRI /CINERT/ INERTI, PADCIN           MAIN0140
     *          /CSTATE/ TSPEC, XV, XTC, Q, L, YN, PRINTV                       MAIN0150
     *          /ESTATE/ OMEGA, EULERA, TRNMBI, PADES1, PLOT, PADES2            MAIN0160
     *          /SAVDAT/ PADSVD /DSTATE/ F /CAEROC/ PADARO                      MAIN0170
      EQUIVALENCE (TSPEC,T), (XV,YY)                                            MAIN0180
      DATA      KORD(16), KORD(17)/ 2, 1/, KORD(18), KORD(19), KORD(20),        MAIN0190
     *          KORD(21), KORD(22)/ 3, 5, 9, 10, 12/, KORD(23), KORD(24)        MAIN0200
     *          KORD(25), KORD(26), KORD(27), KORD(28), KORD(29),               MAIN0210
     *          KORD(30), KORD(31), KORD(32), KORD(33), KORD(34)/ 2, 2,         MAIN0220
     *          2, 1, 1, 1, 1, 1, 1, 1, 1/                                      MAIN0230
      DATA      IOPT(1), IOPT(2)/ 4, 20/, IOPT(3), IOPT(4)/ 6, 5/,              MAIN0240
     *          IOPT(5), IOPT(6), IOPT(7)/ 10, -1, 0/, IOPT(8), IOPT(9)/        MAIN0250
     *          13, 14/, IOPT(10), IOPT(11), IOPT(12)/ 16, 18, 133/,            MAIN0260
     *          IOPT(13), IOPT(14)/ 17, -23/, IOPT(15)/ 0/, NEQ/ 12/            MAIN0270
C     ************************************************************************MAIN0280
C          *** READ AND SCALE DATA ***                                          MAIN0290
     1     CALL RDSCDA ( INERT, IOPT, END )                                     MAIN0300
C       *** TERMINATE RUN IF END OF FILE ***                                    MAIN0310
        IF ( END ) GO TO 99                                                     MAIN0320
C         *** INVERT INERTIA TENSOR ***                                         MAIN0330
          DO 3 I = 1, 3                                                         MAIN0340
            DO 2 J = 1, 3                                                       MAIN0350
              ITEMP(J,I) = INERT(J,I)                                           MAIN0360
              INERTI(J,I) = 0.                                                  MAIN0370
     2      CONTINUE                                                           MAIN0380
            INERTI(I,I) = 1.                                                    MAIN0390
     3    CONTINUE                                                             MAIN0400
          CALL MATINV ( ITEMP, 3, INERTI, 3, D, WK(1), WK(4), WK(10) )          MAIN0410
          WRITE (6,215) INERTI                                                  MAIN0420
C         *** INITIALIZE ANGULAR MOMENTUM FROM ANGULAR VELOCITY ***             MAIN0430
          CALL MVMPY ( INERT, OMEGA, L )                                        MAIN0440
C         *** INITIALIZE TRANSFORMATION MATRIX FROM EULER ANGLES ***            MAIN0450
          CALL TRANME ( EULERA, TRNMBI )                                        MAIN0460
C         *** INITIALIZE QUATERNION FROM TRANSFORMATION MATRIX ***              MAIN0470
C         *** USE EULER ANGLES DIRECTLY FOR SINGULAR CASE YAW=PI ***            MAIN0480
          CALL QUATIN ( TRNMBI, EULERA, Q )                                     MAIN0490
C         *** INITIALIZE INTEGRATOR ***                                         MAIN0500
            T = 0.                                                              MAIN0510
            KORD(1) = 0                                                         MAIN0520
          CALL SODE ( TSPEC, YY, F, KORD, NEQ, D, D, D, IOPT )                  MAIN0530
C         *** INTEGRATOR OPERATING ENTRY ***                                    MAIN0540
     6    CALL SODEA ( TSPEC, YY, F, KORD, D, D )                              MAIN0550
C       ***** FUNCTION SWITCH CONTROLLED BY INTEGRATOR **********              MAIN0560
        IF ( KORD(2) ) 40, 10, 30                                               MAIN0570
C         *** EVALUATION OF DERIVATIVES ***                                     MAIN0580
    10    CALL DERIV                                                          MAIN0590
          GO TO 6                                                             MAIN0600
C         **** OUTPUT AND G-STOP BRANCH ****                                    MAIN0610
    30    IF ( KORD(1).EQ.6 .OR. KORD(1).EQ.7 ) GO TO 90                      MAIN0620
C         *** COMPUTE DEPENDANT STATE VARIABLES AT INTERPOLATED POINT ***       MAIN0630
    35    CALL DERIV                                                          MAIN0640
C         *** COMPUTE EULER ANGLES ***                                          MAIN0650
          CALL CEULER ( TRNMBI, EULERA )                                        MAIN0660
C         *** PRINT CURRENT STATE ***                                           MAIN0670
          IF ( KORD(1).EQ.4 ) WRITE (6,230)                                     MAIN0680
          CALL PRINTS                                                           MAIN0690
          IF ( NSTOP.EQ.1 ) GO TO 92                                            MAIN0700
          GO TO 6                                                               MAIN0710
```

```
C           *** MAX SIMULATED TIME ***                                      MAIN0720
   40        IF ( KORD(1).GT.1 ) GO TO 6                                    MAIN0730
             WRITE (6,220)                                                  MAIN0740
             GO TO 95                                                       MAIN0750
C           *** CHECK FOR TERMINAL CONDITION ( G-STOP ) ***                 MAIN0760
   90        CALL TERMIN ( G )                                              MAIN0770
             CALL SODEG ( TSPEC, YY, F, KORD, IFLAG, NSTOP, G, GT )         MAIN0780
             GO TO ( 6, 30, 6, 90, 91, 91, 91, 6 ), IFLAG                   MAIN0790
C           *** STOPPING CONDITION DETECTED ***                             MAIN0800
   91        WRITE (6,240) NSTOP                                            MAIN0810
             GO TO 35                                                       MAIN0820
C           *** TERMINAL CONDITION DETECTED ***                             MAIN0830
   92        WRITE (6,270)                                                  MAIN0840
                NSTOP = 0                                                   MAIN0850
C        ***** TERMINATE STATE FILE ***************************************MAIN0860
   95     IF ( PLOT ) END FILE 3                                            MAIN0870
          GO TO 1                                                           MAIN0880
C        ******************************************************************MAIN0890
C           *** CLOSE STATE FILE ********                                   MAIN0900
   99 STOP                                                                  MAIN0910
C     ********************************************************************MAIN0920
  215 FORMAT ( 25H0  INVERSE INERTIA TENSOR/( 4X,1P3E15.5 ) )               MAIN0930
  220 FORMAT ( 25H0  MAXIMUM SIMULATED TIME / )                             MAIN0940
  230 FORMAT ( 21H0. PRINT AT MAX STEPS )                                   MAIN0950
  240 FORMAT ( 14H0  *** NSTOP= , I2 )                                      MAIN0960
  270 FORMAT ( 44H0  TERMINAL CONDITION DETECTED IN SIMULATION )            MAIN0970
C     ********************************************************************MAIN0980
      END                                                                   MAIN0990
```

```
.RDSCDA/01-20-77
```

```
(1).RDSCDA/01-20-77
      SUBROUTINE RDSCDA (INERT, IOPT, END )                                 RDSCD010
C     READ AND SCALE DATA                                                   RDSCD020
C       J.P.RADDILL, JPL, SEC.366, MAIL 125-128, PHONE (213) 354-2989       RDSCD030
C         STARTED 5-29-75, LAST CHANGE 01-20-77 1419                        RDSCD040
C     ********************************************************************RDSCD050
      LOGICAL   PLOT, PDERIV, RDTORN, RDINRT, CYLNDR, RDINTG, RDABER,       RDSCD060
     *          RDINIT, RDBDYP, PRTORN, END, PRINTV, RDAERO                 RDSCD070
      INTEGER   IOPT(5)                                                     RDSCD080
      REAL      HEADER(72), INERT(3,3), INERTI(3,3), TSPEC(4), RUF2PS,      RDSCD090
     *          EULERA(3), TRNMBI(3,3), Q(4), YN(15), DT(10,12), LATDEG,    RDSCD100
     *          RCG(3), L(3), DQDT(4), DLDT(3), LORI, EP(5), EPS(5),        RDSCD110
     *          OMEGA(3), EULERD(3), OMGRPH(3), PADES1(10), PADES2(5),      RDSCD120
     *          XV(6), XFT(3), VMPH(3), D2XDT2(3), PADAPO(535), VTC(2),     RDSCD130
     *          XTC(2), XTCMIL(2), VTCMPH(2), BDYLFT(3)                     RDSCD140
      COMMON    /TORN/    RINIT, LATDEG, VMXMPH, RUF2PS, ALPHAF, BETAFT,    RDSCD150
     *                    ALPHAB, BETAB, GAMMAB, RHO, WBO, PRTORN           RDSCD160
     *          /CINERT/ INERTI, GROVZ, CTAU, RCG, BDYWTP                   RDSCD170
     *          /CAERDC/ CAERO, LORI, PADARO, CYLNDR                        RDSCD180
     *          /CSTATE/ TSPEC, XV, XTC, Q, L, YN, PRINTV                   RDSCD190
     *          /ESTATE/ OMEGA, EULERA, TRNMBI, TCSEC, PDERIV, PADES1,      RDSCD200
     *                   PLOT, PADES2                                       RDSCD210
     *          /DSTATE/ D2XDT2, VTC, DQDT, DLDT, DT, EPS                   RDSCD220
     *          /SAVDAT/ XTCMIL, VTCMPH, BDYLFT, H, DELT, TFINAL, XFT,      RDSCD230
     *                   VMPH, EULERD, OMGRPH                               RDSCD240
      DATA      H0, DELTO, TFINLO, MXSTEP, NEQ, IEND/ .01, .1, 10., 0,      RDSCD250
     *          12, 99999/, INTEXP, PDERIV/ 0, .FALSE./                     RDSCD260
      DATA      DGPRAD, PI, FTPMIL, GOMPH2/ 57.295780, 3.1415927, 5280.,    RDSCD270
     *          7.8670SE4/                                                  RDSCD280
      DATA      EP(1), EP(2), EP(3), EP(4), EP(5)/ 1.E-2, 1.E-2, 1.E-3,     RDSCD290
     *          1.E-2, 1.E-2/                                               RDSCD300
C     ********************************************************************RDSCD310
C           *** READ AND WRITE HEADER ***                                   RDSCD320
    1      READ (5,100) HEADER, I                                          RDSCD330
             END = -1 .EQ. IEND                                             RDSCD340
           IF (END) GO TO 90                                                RDSCD350
           WRITE(6,200) HEADER                                              RDSCD360
           *** READ AND WRITE INPUT CONTROL FLAGS ***                       RDSCD370
           READ (5,10) RDTORN, RDBDYP, RDINRT, RDAERO, RDINTG, RDABER,      RDSCD380
     *                 RDINIT, PLOT, CYLNDR, PRTORN, PRINTV                 RDSCD390
           WRITE(6,201) RDTORN, RDBDYP, RDINRT, RDAERO, RDINTG, RDABER,     RDSCD400
     *                 RDINIT, PLOT, CYLNDR                                 RDSCD410
```

```
C           *** READ AND WRITE TORNADO PARAMETERS ***                          RDSCD420
            IF (RDTORN) READ (5,105) RIMILE, LATDEG, VMXMPH, VTCMPH,           RDSCD430
     *                               XTCMIL, NUF2PS, ALPHAF, BETAFT            RDSCD440
            WRITE (6,202) RIMILE, LATDEG, VMXMPH, VTCMPH, XTCMIL, NUF2PSRDSCD450
     *                  , ALPHAF, BETAFT                                       RDSCD460
               TCSEC = RIMILE * 3600. / VMXMPH                                 RDSCD470
               RIFT = RIMILE * FTPMIL                                          RDSCD480
               GROV2 = GOMPH2 * RIMILE / VMXMPH**2                             RDSCD490
C           *** INITIALIZE TORNADO WIND SPEED COMPUTATION ***                  RDSCD500
               GAMMAB = 0.                                                     RDSCD510
C           *** READ AND WRITE BODY PARAMETERS ***                             RDSCD520
            IF (RDBDYP) READ (5,105) BDYLFT                                    RDSCD530
            WRITE (6,203) BDYLFT                                               RDSCD540
               LOR1 = BDYLFT(1) / RIFT                                         RDSCD550
               CTAU = GROV2 / LOR1                                             RDSCD560
C           *** READ AND/OR COMPUTE WEIGHT, CG, AND INERTIA TENSOR ***         RDSCD570
            CALL RCINRT ( BDYLFT, BDYWTP, RCG, INERT, RDINRT )                 RDSCD580
C           *** READ/WRITE AERODYNAMIC COEFFICIENTS, COMPUTE SCALE FACTORRDSCD590
            CALL RDAROC ( RDAERO )                                             RDSCD600
            WRITE (6,207) GROV2, LOR1, CTAU, CAERO, TCSEC                      RDSCD610
C           *** READ AND WRITE INTEGRATION PARAMETERS ***                      RDSCD620
            IF (RDINTG) READ (5,106) H, DELT, TFINAL, MXSTEP, INTEXP,          RDSCD630
     *                               PDERIV                                    RDSCD640
            IF (H.EQ.0.) H = H0                                                RDSCD650
            IF (DELT.EQ.0.) DELT = DELT0                                       RDSCD660
            IF (TFINAL.EQ.0.) TFINAL = TFINL0                                  RDSCD670
               TSPEC(2) = H / TCSEC                                            RDSCD680
               TSPEC(3) = DELT / TCSEC                                         RDSCD690
               TSPEC(4) = TFINAL / TCSEC                                       RDSCD700
               IF (MXSTEP.NE.0) IOPT(2) = MXSTEP                               RDSCD710
               IF (INTEXP.NE.0) IOPT(6) = INTEXP                               RDSCD720
            WRITE (6,206) H, DELT, TFINAL, MXSTEP, INTEXP                      RDSCD730
            IF (RDABER) READ (5,115) EPS                                       RDSCD740
              DO 4 I = 1, 5                                                    RDSCD750
    4            IF ( EPS(I).LE.0. ) EPS(I) = EP(I)                          RDSCD760
            WRITE (6,216) EPS                                                  RDSCD770
C           *** READ AND WRITE INITIAL CONDITIONS ***                          RDSCD780
            IF (RDINIT) READ (5,105) XFT, VMPH, EULERD, OMGRPM                 RDSCD790
            WRITE(6,208) XFT, VMPH, EULERD, OMGRPM                             RDSCD800
               OMSCAL = 2. * PI * TCSEC / 60.                                  RDSCD810
C           *** SCALE INITIAL CONDITIONS ***                                   RDSCD820
            DO 10 I = 1, 3                                                     RDSCD830
               EULERA(I) = EULERD(I) / DGPRAD                                  RDSCD840
               OMEGA(I)  = OMGRPM(I) * OMSCAL                                  RDSCD850
               XV(2*I-1) = XFT(I) / RIFT                                       RDSCD860
               XV(2*I  ) = VMPH(I) / VMXMPH                                    RDSCD870
             IF (I.EQ.3) GO TO 10                                              RDSCD880
               XTC(I) = XTCMIL(I) / RIMILE                                     RDSCD890
               VTC(I) = VTCMPH(I) / VMXMPH                                     RDSCD900
   10       CONTINUE                                                           RDSCD910
   90 RETURN                                                                   RDSCD920
C     ***************************************************************RDSCD930
  100 FORMAT ( 72A1, I5 )                                                      RDSCD940
  101 FORMAT ( 8(8X,L1) )                                                      RDSCD950
  105 FORMAT ( 9F8.6 )                                                         RDSCD960
  106 FORMAT ( 3F8.6, 2I8, L8 )                                                RDSCD970
  115 FORMAT ( 12E6.3 )                                                        RDSCD980
  200 FORMAT ( 3H1  , 72A1/ )                                                  RDSCD990
  201 FORMAT ( 2X, 7HRDTORN=, L1, 9H, RDBDYP=, L1, 9H, RDINRT=, L1,            RDSC1000
     *         9H, RDAERO=, L1, 9H, RDINTG=, L1, 9H, RDABER=, L1,            RDSC1010
     *         9H, PDINIT=, L1/ 9H  PLOT  =, L1, 9H, CYLNDR=, L1/ )          RDSC1020
  202 FORMAT ( 2X, 7HRIMILE=, 1P1E9.2, 9H, LATDEG=, E9.2, 9H, VMXMPH=,       RDSC1030
     *         E9.2, 9H, VTCMPH=, E9.2/ 9H  VTCMPH=, E9.2, 9H, XTCMIL=,      RDSC1040
     *         E9.2, 9H, YTCMIL=, E9.2/ 9H  NUF2PS=, E9.2, 9H, ALPHAF=,      RDSC1050
     *         E9.2, 9H, BETAFT=, E9.2/ )                                    RDSC1060
  203 FORMAT ( 2X, 7HBDYLFT=, 1P1E9.2, 9H, BDYOFT=, E9.2, 9H, BDYTFT=,       RDSC1070
     *         E9.2 / )                                                      RDSC1080
  206 FORMAT ( 2X, 2HH=, 1P1E9.2, 7H, DELT=, E9.2, 9H, TFINAL=, E9.2,        RDSC1090
     *         9H, MXSTEP=, I8, 9H, INTEXP=, I4 )                            RDSC1100
  207 FORMAT ( 2X, 6HGROV2=, 1P1E9.2, 7H, LOR1=, E9.2, 7H, CTAU=, E9.2,      RDSC1110
     *         8H, CAERO=, E9.2/ 8H  TCSEC=, E9.2/ )                         RDSC1120
  208 FORMAT ( 2X, 6HXFT  =, 1P1E9.2, 8H, YFT  =, E9.2, 6H, ZFT=, E9.2/ )    RDSC1130
```

```
     *          7H  UMPH=, E9.2, 7H, VMPH=, E9.2, 7H, WMPH=, E9.2/          RDSC1140
     *          9H  PSIDEG=, E9.2, 9H, THETDG=, E9.2, 9H, PHIDEG=, E9.2/    RDSC1150
     *          9H  OMXRPM=, E9.2, 9H, OMYRPM=, E9.2, 9H, OMZRPM=, E9.2/)   RDSC1160
   216 FORMAT ( 27H0 ABSOLUTE ERROR TOLERANCES/ 7H   EPS=, 1P5E6.0/ )       RDSC1170
C     ***************************************************************     RDSC1180
      END                                                                   RDSC1190

*PCINRT/01-17-77

(1),RCINRT/01-17-77
      SUBROUTINE RCINRT ( BDYLFT, BDYWTP, RCG, IT, RDINRT )                 RINRT000
C     READ AND/OR COMPUTE WEIGHT, CG, AND INERTIA TENSOR                    RINRT010
C       J.R.RADBILL, JPL, SECT.914, 125/128B, PHONE (213) 354-2989          RINRT020
C         STARTED 7-9-76, LAST CHANGE 01-17-77 0900                         RINRT030
C     ***************************************************************     RINRT040
      LOGICAL  RDINRT                                                       RINRT050
      REAL     RCG(3), RCGBFT(3), RCGFT(3), IT(3,3), ITBPF2(3,3),           RINRT060
     *         ITPF2(3,3)                                                   RINRT070
      COMMON   /CRINRT/ RCGBFT, ITBPF2                                      RINRT080
C     ***************************************************************     RINRT090
         IF ( .NOT.RDINRT ) GO TO 45                                        RINRT100
C          *** ZERO ACUMULATED ARRAYS ***                                   RINRT110
           DO 5 I = 1, 3                                                    RINRT120
              RCGBFT(I) = 0.                                                RINRT130
              DO 5 J = I, 3                                                 RINRT140
                 ITBPF2(I,J) = 0.                                           RINRT150
    5      CONTINUE                                                         RINRT160
C        *** LOOP UNTIL ZERO WEIGHT IS READ, UP TO 10 PARTS MAXIMUM ***     RINRT170
           BDYWTP = 0.                                                      RINRT180
           DO 30 IBPART = 1, 10                                             RINRT190
C            *** READ BODY COMPONENT DESCRIPTION ***                        RINRT200
             READ (5,100) WP, RCGFT, ITPF2(1,1), ITPF2(1,2), ITPF2(1,3),    RINRT210
     *                    ITPF2(2,2), ITPF2(2,3), ITPF2(3,3)                RINRT220
             IF ( WP.EQ.0. ) GO TO 35                                       RINRT230
             WRITE(6,200) IBPART, WP, RCGFT, ITPF2(1,1), ITPF2(1,2),        RINRT240
     *                    ITPF2(1,3), ITPF2(2,2), ITPF2(2,3), ITPF2(3,3)    RINRT250
             BDYWTP = BDYWTP + WP                                           RINRT260
             DO 15 J = 1, 3                                                 RINRT270
   15        RCGBFT(J) = RCGFT(J) * WP + RCGBFT(J)                          RINRT280
C            *** TRANSFORM INERTIA TENSOR OF COMPONENT TO ORIGIN AND SUM *** RINPT290
             WR2 = DOT ( RCGFT, RCGFT ) * WP                                RINRT300
             DO 25 I = 1, 3                                                 RINRT310
                DO 20 J = I, 3                                              RINRT320
                   ITBPF2(I,J) = ITPF2(I,J) -RCGFT(I)*RCGFT(J)*WP           RINRT330
     *                         + ITBPF2(I,J)                              RINRT331
   20           CONTINUE                                                    RINRT340
                ITBPF2(I,I) = ITBPF2(I,I) + WR2                             RINRT350
   25        CONTINUE                                                       RINRT360
   30      CONTINUE                                                         RINRT370
C          *** COPY SYMMETRICAL OFF-DIAGONAL ELEMENTS ***                   RINRT380
   35        ITBPF2(2,1) = ITBPF2(1,2)                                      RINRT390
             ITBPF2(3,1) = ITBPF2(1,3)                                      RINRT400
             ITBPF2(3,2) = ITBPF2(2,3)                                      RINRT410
             DO 40 I = 1, 3                                                 RINRT420
   40        RCGBFT(I) = RCGBFT(I) / BDYWTP                                 RINRT430
C                                                                           RINRT440
C            *** PRINT BODY INERTIAL DESCRIPTION IN DIMENSIONAL FORM ***    RINRT450
   45        WRITE (6,220) BDYWTP, RCGBFT                                   RINRT460
             DO 50 I = 1, 3                                                 RINRT470
   50        WRITE (6,225) ( ITBPF2(I,J), J = I, 3 )                        RINRT480
C          *** NONDIMENSIONALIZE AND PRINT CG AND INERTIA TENSOR ***        RINRT490
             WL2I = 1. /( BDYWTP * BDYLFT**2 )                              RINRT500
             DO 55 I = 1, 3                                                 RINRT510
   55        RCG(I) = RCGBFT(I) / BDYLFT                                    RINRT520
             WRITE (6,230) RCG                                              RINRT530
             DO 65 I = 1, 3                                                 RINRT540
                DO 60 J = I, 3                                              RINRT550
   60           IT(I,J) = ITBPF2(I,J) * WL2I                                RINRT560
                WRITE (6,240) ( IT(I,J), J = I, 3 )                         RINRT570
   65        CONTINUE                                                       RINRT580
      RETURN                                                                RINRT590
```

```
C     ***********************************************************************RINRT600
  100 FORMAT ( 10F7.1 )                                                       RINRT610
  200 FORMAT (-2X, I2,, F7.1, 3F5.1, 6F8.0 )                                  RINRT620
  220 FORMAT (/2X, 7HBDYWTP=, F7.1, 9H, RCGFT =, 3F7.1// 2X,                  RINRT630
     *        24HINERTIA TENSOR (LBM-FT2) )                                   RINRT640
  225 FORMAT ( 2X, 3F9.2 )                                                    RINRT650
  230 FORMAT ( 2X, 4HRCG=, 3F7.4// 2X, 29HINERTIA TENSOR(DIMENSIONLESS))      RINRT660
  240 FORMAT ( 2X, 3F9.5 )                                                    RINRT670
C     ***********************************************************************RINRT680
      END                                                                     RINRT690

ORXIS.DOT

ORHIS(1).DOT
      FUNCTION DOT ( X, Y )                                                   DOT00001
C     FORM DOT PRODUCT OF VECTORS X AND Y                                     DOT00002
C       J.R.RADBILL, JPL, SECT.914, MAIL 125-109A, PHONE (213) 354-6552       DOT00007
C         STARTED 6-07-75, LAST CHANGE 8-07-75 1000                           DOT00008
C     ***********************************************************************DOT00009
      REAL     X(3), Y(3)                                                     DOT00030
C     ***********************************************************************DOT00090
           SUM = 0.                                                           DOT00100
         DO 1 I = 1, 3                                                        DOT00110
    1       SUM = X(I) * Y(I) + SUM                                           DOT00120
           DOT = SUM                                                          DOT00130
      RETURN                                                                  DOT00140
C     ***********************************************************************DOT00997
      END                                                                     DOT00998

1.RDARO2/01-14-77

(1).RDAROC/01-14-77
      SUBROUTINE RDAROC ( RDAERO )                                            RDAR0010
C     READ/WRITE AERODYNAMIC COEFFICIENTS, COMPUTE AERO SCALE FACTORS         RDAR0020
C       WRITTEN INITIALLY BY B.W.MAYCUMBER CSC/JPL                            RDAR0030
C       MODIFIED BY J.R.RADBILL, JPL, SECT.346, MC 125/125, 354-2989          RDAR0040
C         STARTED 6-4-76, LAST CHANGE 01-14-77 0945                           RDAR0050
C     ***********************************************************************RDAR0060
      LOGICAL  CYLNDR, PRAROF, RDAERO                                         RDAR0070
      REAL     LORI, MODEL( 8), ALFTAB(19), PHITAB(4), COFTAB(19,4,6),        RDAR0080
     *         CTD(3), SGNA(4,6), SGNP(4,6), CIN(6), PADI(14), PADTI(2),      RDAR0090
     *         PADT2(9), PADSD1(4), PADSD2(20)                                RDAR0100
      COMMON   /CAEROC/ CAERO, LORI, ALFTAB, NA, IPA, PHITAB, NP, IPP,        RDAR0110
     *                  COFTAB, CTD, SGNA, SGNP, PRAROF, CYLNDR, MODEL        RDAR0120
     *         /CINERT/ PADI, BDYWTP                                          RDAR0130
     *         /TORN/   PADTI, VMXMPH, PADT2                                  RDAR0140
     *         /SAVDAT/ PADSD1, BDYLFT, BDYDFT, BDYTFT, PADSD2, AREFF2,       RDAR0150
     *                  RHOLFC                                                RDAR0160
      DATA      GONPH2, RHOLF3/7.86705E+4, 8.07223E-2/, FTPHIL / 5280./       RDAR0170
C     ***********************************************************************RDAR0180
      IF (.NOT.RDAERO) GO TO 50                                               RDAR0190
           READ (5,100) MODEL, NA, IPA, NP, IPP, CNXYAV, CNXZAV,              RDAR0200
     *                  AREFF2, RHOLFC, PRAROF                                RDAR0210
           IF (NA .EQ.0) NA = 19                                              RDAR0220
           IF (IPA.EQ.0) IPA=  2                                              RDAR0230
           IF (NP .EQ.0) NP =  4                                              RDAR0240
           IF (IPP.EQ.0) IPP=  2                                              RDAR0250
           IF (AREFF2.EQ.0.) AREFF2 = BDYLFT * BDYDFT                         RDAR0260
           IF (RHOLFT.EQ.0.) RHOLFC = RHOLF3                                  RDAR0270
        IF (CYLNDR) GO TO 30                                                  RDAR0280
C            *** CALCULATE DAMPING MOMENT COEFFICIENTS ***                    RDAR0290
           CTD(1) = 0.                                                        RDAR0300
           CTD(2) =-ABS(CNXYAV) * LORI / 6.                                   RDAR0310
           CTD(3) =-ABS(CNXZAV) * LORI * BDYTFT /( 6. * BDYDFT )              RDAR0320
C     *** BRANCH FOR BODIES WITH 3 PERPENDICULAR PLANES OF SYMMETRY ***       RDAR0330
        DO 20 J = 1, NP                                                       RDAR0340
           DO 10 I = 1, NA                                                    RDAR0350
C             *** READ YAW/ROLL MEASURED COEFFICIENTS ***                     RDAR0360
              READ (5,120) CIN, ALFTAB(I), PHIIN                              RDAR0370
C             *** MAP YAW/ROLL MEASURED COEFFS INTO PITCH/ROLL COEFFS **       RDAR0380
              COFTAB(I,J,1) = CIN(2)                                          RDAR0390
              COFTAB(I,J,2) = CIN(1)                                          RDAR0400
```

```
                  COFTAB(I,J,3) = CIN(5)                                    RDAR0410
                  COFTAB(I,J,4) = CIN(4)                                    RDAR0420
                  COFTAB(I,J,5) = CIN(6)                                    RDAR0430
                  COFTAB(I,J,6) = CIN(3)                                    RDAR0440
   10          CONTINUE                                                     RDAR0450
               PHITAB(J) = 90. - PHIN                                       RDAR0460
   20       CONTINUE                                                        RDAR0470
            GO TO 50                                                        RDAR0490
C        *** BRANCH FOR CYLINDRICAL SHAPES ***                              RDAR0500
   30          DO 35 I = 1, NA                                              RDAR0510
   35             READ (5,110) ALFTAB(I), ( COFTAB(I,1,K), K = 1, 4 )       RDAR0520
   50             CAERO = AREFF2 *RHOLFC *VMXNPH**2 *FTPHIL * .5 /          RDAR0530
     *                    ( BDYWTP * GONPH2 )                               RDAR0540
C        *** PRINT INPUT AND CALCULATED QUANTITIES ***                      RDAR0550
C             *** PRINT MODEL SHAPE ***                                     RDAR0560
              WRITE (6,200) MODEL, IPA, IFP, CNXYAV, CNXZAV, AREFF2,RHOLFC  RDAR0570
            IF (CYLNDR) GO TO 70                                            RDAR0580
C           *** PRINT STATIC AERODYNAMIC COEFFICIENTS ***                   RDAR0590
            DO 60 J = 1, NP                                                 RDAR0600
               WRITE (6,210) PHITAB(J)                                      RDAR0610
               DO 60 I = 1, NA                                              RDAR0620
                  WRITE (6,220) ALFTAB(I), ( COFTAB(I,J,K), K = 1, 6 )      RDAR0630
   60       CONTINUE                                                        RDAR0640
               WRITE (6,240) CD                                             RDAR0660
            GO TO 90                                                        RDAR0670
C           *** BRANCH FOR CYLINDRICAL SHAPES ***                           RDAR0680
   70          WRITE (6,205)                                                RDAR0690
               DO 75 I = 1, NA                                              RDAR0700
   75             WRITE (6,220) ALFTAB(I), ( COFTAB(I,1,K), K = 1, 4 )      RDAR0710
   90 RETURN                                                                RDAR0720
C     ***************************************************************      RDAR0730
  100 FORMAT ( 8A6, 4I3, 2F6.5/ 2F6.2, L6 )                                 RDAR0740
  110 FORMAT ( 6F6.4 )                                                      RDAR0750
  120 FORMAT ( 6F10.3, 12X, F2.0, 1X, F2.0 )                                RDAR0760
  200 FORMAT (/2X,29HAERODYNAMIC COEFFICIENTS FOR , 8A6 / 5X, 6HALPHA ,     RDAR0780
     *          11HINTERP PTS=, I2, 17H, PHI INTERP PTS=, I2, 9H, CNXYAV=   RDAR0790
     *        , F5.2, 9H, CNXZAV=, F5.2/ 5X, 7HAREFF2=, F6.2, 9H, RHOLF3=   RDAR0800
     *        , F6.2 )                                                      RDAR0810
  205 FORMAT ( 12HO ALPHA(DEG), 3X, 2HCD, 6X, 2HCL, 6X, 2HCH, 6X, 3HCMQ)    RDAR0820
  210 FORMAT (/5X,10HPHI (DEG) , F5.0/5X,10HALPHA(DEG),2X,2HCD,6X,2HCS,     RDAR0830
     *          6X,2HCL,5X,4HCLL,5X,2HCH,6X,2HCN )                          RDAR0840
  215 FORMAT ( 2X, F4.0, 5X, 4F8.4 )                                        RDAR0850
  220 FORMAT ( 5X, F5.0, 5X, 4F8.4 )                                        RDAR0860
  240 FORMAT ( 5X, 24HDAMPING COEFFICIENTS CD=, 3F8.4 )                     RDAR0880
C     ***************************************************************      RDAR0890
      END                                                                   RDAR0900
```

FORMIS.MATINV

```
FORMIS(1).MATINV
      SUBROUTINE MATINV ( A, N, B, M, DETERM, IPIVOT, INDEX, PIVOT )
C     DESIGNED AND PROGRAMMED BY C. LAWSON                                  F4020010
C       MODIFIED BY J. RADBILL, LAST CHANGE 4/8/76 0935                     F4020020
      INTEGER  IPIVOT(N), INDEX(N,2)                                        F4020030
      REAL     A(N,N), B(N,M), PIVOT(N)                                     F4020040
      EQUIVALENCE (IROW,JROW), (ICOLUM,JCOLUM), (AMAX, T, SWAP)             F4020050
C                                                                           F4020060
C     INITIALIZATION                                                        F4020070
C                                                                           F4020080
      DETERM=1.0                                                            F4020090
      DO 20 J=1,N                                                           F4020100
   20 IPIVOT(J)=0                                                           F4020110
      DO 550 I=1,N                                                          F4020120
C                                                                           F4020130
C     SEARCH FOR PIVOT ELEMENT                                              F4020140
C                                                                           F4020150
      AMAX=0.0                                                              F4020160
      DO 105 J=1,N                                                          F4020170
      IF (IPIVOT(J)-1) 60, 105, 60                                          F4020180
   60 DO 100 K=1,N                                                          F4020190
      IF (IPIVOT(K)-1) 80, 100, 740                                         F4020200
   80 IF (ABS (AMAX)-ABS (A(J,K))) 85, 100, 100                             F4020210
```

```
   85 IROW=J                                                              F4020220
      ICOLUM=K                                                            F4020230
      AMAX=A(J,K)                                                         F4020240
  100 CONTINUE                                                            F4020250
  105 CONTINUE                                                            F4020260
      IF (AMAX.NE.0.) GO TO 110                                           F4020270
      DETERM = 0.                                                         F4020280
      RETURN                                                              F4020290
  110 IPIVOT(ICOLUM)=IPIVOT(ICOLUM)+1                                     F4020300
C                                                                         F4020310
C     INTERCHANGE ROWS TO PUT PIVOT ELEMENT ON DIAGONAL                   F4020320
C                                                                         F4020330
      IF (IROW-ICOLUM) 140, 260, 140                                      F4020340
  140 DETERM=-DETERM                                                      F4020350
      DO 200 L=1,N                                                        F4020360
      SWAP=A(IROW,L)                                                      F4020370
      A(IROW,L)=A(ICOLUM,L)                                               F4020380
  200 A(ICOLUM,L)=SWAP                                                    F4020390
      IF(M) 260, 260, 210                                                 F4020400
  210 DO 250 L=1, M                                                       F4020410
      SWAP=B(IROW,L)                                                      F4020420
      B(IROW,L)=B(ICOLUM,L)                                               F4020430
  250 B(ICOLUM,L)=SWAP                                                    F4020440
  260 INDEX(I,1)=IROW                                                     F4020450
      INDEX(I,2)=ICOLUM                                                   F4020460
      PIVOT(I)=A(ICOLUM,ICOLUM)                                           F4020470
      DETERM=DETERM*PIVOT(I)                                              F4020480
C                                                                         F4020490
C     DIVIDE PIVOT ROW BY PIVOT ELEMENT                                   F4020500
C                                                                         F4020510
      A(ICOLUM,ICOLUM)=1.0                                                F4020520
      DO 350 L=1,N                                                        F4020530
  350 A(ICOLUM,L)=A(ICOLUM,L)/PIVOT(I)                                    F4020540
      IF(M) 380, 380, 360                                                 F4020550
  360 DO 370 L=1,M                                                        F4020560
  370 B(ICOLUM,L)=B(ICOLUM,L)/PIVOT(I)                                    F4020570
C                                                                         F4020580
C     REDUCE NON-PIVOT ROWS                                               F4020590
C                                                                         F4020600
  380 DO 550 L1=1,N                                                       F4020610
      IF(L1-ICOLUM) 400, 550, 400                                         F4020620
  400 T=A(L1,ICOLUM)                                                      F4020630
      A(L1,ICOLUM)=0.0                                                    F4020640
      DO 450 L=1,N                                                        F4020650
  450 A(L1,L)=A(L1,L)-A(ICOLUM,L)*T                                       F4020660
      IF(M) 550, 550, 460                                                 F4020670
  460 DO 500 L=1,M                                                        F4020680
  500 B(L1,L)=B(L1,L)-B(ICOLUM,L)*T                                       F4020690
  550 CONTINUE                                                            F4020700
C                                                                         F4020710
C     INTERCHANGE COLUMNS                                                 F4020720
C                                                                         F4020730
      DO 710 I=1,N                                                        F4020740
      L=N+1-I                                                             F4020750
      IF (INDEX(L,1)-INDEX(L,2)) 630, 710, 630                            F4020760
  630 JROW=INDEX(L,1)                                                     F4020770
      JCOLUM=INDEX(L,2)                                                   F4020780
      DO 705 K=1,N                                                        F4020790
      SWAP=A(K,JROW)                                                      F4020800
      A(K,JROW)=A(K,JCOLUM)                                               F4020810
      A(K,JCOLUM)=SWAP                                                    F4020820
  705 CONTINUE                                                            F4020830
  710 CONTINUE                                                            F4020840
  740 RETURN                                                              F4020850
      END                                                                 F4020860
```

```
FORMIS.MAT-VECT-MPY
FORMIS(1).MAT-VECT-MPY
      SUBROUTINE MVMPY ( A, X, Y )                                        MVMPY001
C     MATRIX VECTOR PRODUCT: Y = A X                                      MVMPY002
C       J.R.RADBILL, JPL, SEC 314, MAIL 125-109A, PHONE (213) 354-7097    MVMPY007
```

```
C          STARTED 6-02-75, LAST CHANGE 6-03-75 1430                    MVMPY008
C     ********************************************************************MVMPY009
      REAL     A(3,3), X(3), Y(3)                                         MVMPY030
C     ********************************************************************MVMPY090
               Y(1) = A(1,1)*X(1) +A(1,2)*X(2) +A(1,3)*X(3)               MVMPY100
               Y(2) = A(2,1)*X(1) +A(2,2)*X(2) +A(2,3)*X(3)               MVMPY110
               Y(3) = A(3,1)*X(1) +A(3,2)*X(2) +A(3,3)*X(3)               MVMPY120
      RETURN                                                              MVMPY800
C     ********************************************************************MVMPY997
      END                                                                 MVMPY998
```

\.TRANMP/10-26-76

```
(1).TRANME/10-26-76
      SUBROUTINE TRANME ( EULERA, TRNMIB )                                TRANM000
C     COMPUTE TRANSFORMATION FROM INERTIAL TO BODY COORDINATES USING      TRANM010
C     EULER ANGLES, ANGLES CONFORM TO AIRCRAFT CONVENTIONS, BODY AND      TRANM020
C     INERTIAL SYSTEMS ARE RIGHT HANDED AND COINCIDE AT ZERO ANGLES.      TRANM025
C       J.R.RADBILL, JPL, SECT.366, MC 125-128, PHONE (213) 354-2989      TRANM030
C       STARTED 6-02-75, LAST CHANGE 10-26-76 0930                        TRANM040
C     ********************************************************************TRANM050
      REAL     EULERA(3), TRNMIB(3,3), YAW(3,3), PITCH(3,3), ROLL(3,3),   TRANM060
     *         TEMP(3,3)                                                  TRANM070
      DATA     YAW(1,3), YAW(2,3), YAW(3,1), YAW(3,2), YAW(3,3)/          TRANM080
     *         0., 0., 0., 0., 1./                                        TRANM090
      DATA     PITCH(1,2), PITCH(2,1), PITCH(2,2), PITCH(2,3),            TRANM100
     *         PITCH(3,2)/ 0., 0., 1., 0., 0./                            TRANM110
      DATA     ROLL(1,1), ROLL(1,2), ROLL(1,3), ROLL(2,1), ROLL(3,1)/     TRANM120
     *         1., 0., 0., 0., 0. /                                       TRANM130
C     ********************************************************************TRANM140
C          * YAW,  PSI=EULERA(1), CLOCKWISE ROTATION ABOUT Z AXIS,        TRANM150
C          * POSITIVE THROUGH TOP OF BODY, UP IN ORIGINAL ORIENTATION,    TRANM160
C          * LEFT-HAND SCREW CONVENTION                                   TRANM165
               YAW(1,1) = COS( EULERA(1) )                                TRANM170
               YAW(1,2) =-SIN( EULERA(1) )                                TRANM180
               YAW(2,1) =-YAW(1,2)                                        TRANM190
               YAW(2,2) = YAW(1,1)                                        TRANM200
C          * PITCH, THETA=EULERA(2), CLOCKWISE ROTATION ABOUT            TRANM210
C          * Y AXIS, POSITIVE THROUGH LEFT SIDE OF BODY, NORTHWARD IN    TRANM220
C          * ORIGINAL ORIENTATION, LEFT HAND SCREW,                      TRANM230
               PITCH(1,1) = COS( EULERA(2) )                              TRANM240
               PITCH(1,3) = SIN( EULERA(2) )                              TRANM250
               PITCH(3,1) =-PITCH(1,3)                                    TRANM260
               PITCH(3,3) = PITCH(1,1)                                    TRANM270
C          * ROLL, PHI=EULERA(3), COUNTERCLOCKWISE ROTATION ABOUT         TRANM280
C          * X AXIS, POSITIVE THROUGH FRONT (NOSE) OF BODY,              TRANM290
C          * EASTWARD IN ORIGINAL ORIENTATION, RIGHT HAND SCREW.         TRANM300
               ROLL(2,2) = COS( EULERA(3) )                               TRANM310
               ROLL(2,3) = SIN( EULERA(3) )                               TRANM320
               ROLL(3,2) =-ROLL(2,3)                                      TRANM330
               ROLL(3,3) = ROLL(2,2)                                      TRANM340
C          *** MULTIPLY YAW, PITCH AND ROLL MATRICES TOGETHER ***         TRANM350
            CALL MATMPY ( PITCH, YAW, TEMP )                              TRANM360
            CALL MATMPY ( ROLL, TEMP, TRNMIB )                            TRANM370
      RETURN                                                              TRANM380
C     ********************************************************************TRANM390
      END                                                                 TRANM400
```

\.QUATIN/10-22-76

```
\(1).QUATIN/10-22-76
      SUBROUTINE QUATIN ( TRANSM, EULERA, Q )                             QUAT0001
C     INITIALIZE QUATERNION FROM TRANSFORMATION MATRIX, USE EULER ANGLES  QUAT0010
C     DIRECTLY IF SINGULAR CASE                                           QUAT0011
C       J.R.RADBILL, JPL, SECT.366, MAIL 125/128, PHONE (213) 354-2989    QUAT0020
C         STARTED 6-02-75, LAST CHANGE 10-22-76 1315                      QUAT0030
C     ********************************************************************QUAT0040
      REAL     TRANSM(3,3), Q(4), EULERA(3)                               QUAT0050
C     ********************************************************************QUAT0060
               Q(1) = .5* SQRT( 1.+TRANSM(1,1)+TRANSM(2,2)+TRANSM(3,3) )  QUAT0070
            IF ( Q(1).LT. 1.E-3 ) GO TO 10                                QUAT0075
               FORQ0I = .25 / Q(1)                                        QUAT0080
```

```
                Q(2) = ( TRANSM(3,2) - TRANSM(2,3) ) * FORQ0I          QUAT0090
                Q(3) = ( TRANSM(1,3) - TRANSM(3,1) ) * FORQ0I          QUAT0100
                Q(4) = ( TRANSM(2,1) - TRANSM(1,2) ) * FORQ0I          QUAT0110
                GO TO 90                                               QUAT0120
C           *** BRANCH FOR SINGULAR CASE YAW=PI, ROLL=0 ***            QUAT0190
   10           Q(1) = 0.                                              QUAT0200
                THETO2 = EULERA(2) / 2.                                QUAT0210
                Q(2) = +SIN( THETO2 )                                  QUAT0220
                Q(3) = 0.                                              QUAT0230
                Q(4) = +COS( THETO2 )                                  QUAT0240
   90 RETURN                                                           QUAT0800
C     ***************************************************************QUAT0997
      END                                                              QUAT0998

1.DERIV/10-22-76

A(1),DERIV/10-22-76
      SUBROUTINE DERIV                                                 DERIV000
C     COMPUTE DERIVATIVES FOR INTEGRATOR                               DERIV010
C       J.R.RADBILL, JPL, SEC.366, MAIL 125-128 PHONE (213) 354-2989   DERIV020
C         STARTED 6-02-75, LAST CHANGE 10-22-76 1100                   DERIV030
C     ***************************************************************DERIV040
      LOGICAL  PDERIV                                                  DERIV050
      REAL     INERTI(3,3), X(3), Q(4), V(3), L(3), OMEGA(3), RCG(3),  DERIV060
     *         EULERA(3), TRNMBI(3,3), DV(3), DQ(4), DL(3), XV(6),     DERIV070
     *         XTC(2), DXTC(2), VWIND(3), VWREL(3), ALPHAW(3), VCPROD(3)DERIV080
     *         TRNMWI(3,3), TAUB(3), F(3), FW(3), TAUW(3), OMEGAW(3),  DERIV090
     *         YN(15), DT(120), EPS(5), RCGW(3), ESPAD(5), TAUI(3),    DERIV100
     *         OMEGAI(3)                                               DERIV110
      COMMON   /CINERT/ INERTI, GROV2, CTAU, RCG, BDYWTP               DERIV120
     *         /CSTATE/ T, H, DELTAT, TF, XV, XTC, Q, L, YN            DERIV130
     *         /ESTATE/ OMEGA, EULERA, TRNMBI, TCSEC, PDERIV, VWIND,   DERIV140
     *                  ALPHAW, OMEGAW, VWREL, FW, F, VWRMAG, ESPAD    DERIV150
     *         /DSTATE/ DV, DXTC, DQ, DL, DT, EPS                      DERIV160
      NAMELIST /DERIV1/ X, V, Q, L, OMEGA                              DERIV167
     *         /DERIV2/ OMEGAI, OMEGAW, FW, TAUW, F, TAUI, TAUB        DERIV168
     *         /DERIV3/ VCPROD, DL, DQ                                 DERIV169
C     ***************************************************************DERIV170
C          *** UNPACK POSITION & VELOCITY VECTORS ***                  DERIV180
           DO 1 I = 1, 3                                               DERIV190
              X(I) = XV(2*I-1)                                         DERIV200
              V(I) = XV(2*I)                                           DERIV210
C          *** TRANSFORMATION MATRIX (BODY-INERTIA) FROM QUATERNION *** DERIV220
           CALL TRANMQ ( Q, TRNMBI )                                   DERIV230
C          *** COMPUTE ANGULAR VELOCITY FROM ANGULAR MOMENTUM ***      DERIV240
           CALL MVMPY ( INERTI, L, OMEGA )                             DERIV250
           IF (PDERIV) WRITE (6,DERIV1)                                DERIV255
C          *** COMPUTE WIND VELOCITY OF MOVING TORNADO IN SPACE COORDS *DERIV260
           CALL TOTWND ( XTC, DXTC, X, VWIND )                         DERIV270
C          *** FIND RELATIVE VELOCITY IN SPACE COORDINATES ***         DERIV280
           DO 10 I = 1, 3                                              DERIV290
   10         VWREL(I) = VWIND(I) - V(I)                              DERIV300
C          *** FIND WIND COORDINATES AND BODY ANGLES WRT WIND ***      DERIV310
           CALL WINDCA ( VWREL, TRNMBI, VWRMAG, TRNMWI, ALPHAW )       DERIV320
C          *** TRANSFORM ANGULAR VELOCITY FROM BODY TO WIND COORDINATES DERIV350
           CALL MVMPY ( TRNMBI, OMEGA, OMEGAI )                        DERIV355
           CALL VMMPY ( OMEGAI, TRNMWI, OMEGAW )                       DERIV360
C          *** COMPUTE AERODYNAMIC FORCES & MOMENTS IN WIND COORDINATES DERIV370
           CALL AROFRC ( VWRMAG, ALPHAW, OMEGAW, FW, TAUW )            DERIV380
C          *** TRANSFORM AERODYNAMIC FORCE TO SPACE COORDINATES ***    DERIV390
           CALL MVMPY ( TRNMWI, FW, F )                                DERIV400
C          *** ADD WEIGHT TO AERODYNAMIC FORCE IN INERTIAL COORDINATES *DERIV410
              F(3) = F(3) - 1.                                         DERIV430
C          *** TRANSFORM AERO MOMENT FROM WIND TO BODY COORDINATES ***  DERIV460
           CALL MVMPY ( TRNMWI, TAUW, TAUI )                           DERIV470
           CALL VMMPY ( TAUI, TRNMBI, TAUB )                           DERIV475
           IF (PDERIV) WRITE (6,DERIV2)                                DERIV477
C          *** TORQUE OF WEIGHT ABOUT BODY ORIGIN ***                  DERIV480
           CALL CROSS ( RCG, TRNMBI(1,3), RCGW )                       DERIV510
C          *** COMPUTE DERIVATIVES OF ANGULAR MOMENTUM IN BODY COORD ***DERIV520
C          *** AND LINEAR ACCELERATION IN INERTIAL COORDINATES ***     DERIV525
           CALL CROSS ( OMEGA, L, VCPROD )                             DERIV530
           DO 20 I = 1, 3                                              DERIV540
```

```
                DL(I) = ( TAUB(I) + RCGW(I) ) * CTAU - VCPROD(I)          DERIV550
                DV(I) = GROV2 * F(I)                                      DERIV555
   20         CONTINUE                                                    DERIV557
C            *** COMPUTE DERIVATIVES OF QUATERNION COMPONENTS ***         DERIV560
             CALL QUATD ( OMEGA, Q, DQ )                                  DERIV570
             IF (PDERIV) WRITE (6,DERIV3)                                 DERIV575
      RETURN                                                              DERIV580
C     ******************************************************************DERIV590
      END                                                                 DERIV600

1.TRANMQ/10-22-76

A(1).TRANMQ/10-22-76
      SUBROUTINE TRANMQ ( Q, TRANSM )                                     TRNMQ001
C     COMPUTE TRANSFORMATION MATRIX FROM QUATERNION                       TRNMQ002
C       J.R.RADBILL, JPL, SECT.366, MAIL 125-128,  PHONE (213) 354-2989 TRNMQ007
C         STARTED 6-03-75, LAST CHANGE 10-22-76 1615                      TRNMQ008
C     ******************************************************************TRNMQ009
      REAL     Q(4), TRANSM(3,3)                                          TRNMQ030
C     ******************************************************************TRNMQ090
             TRANSM(1,1) = 1. - 2. * ( Q(3)**2 + Q(4)**2 )               TRNMQ100
             TRANSM(1,2) = 2. * ( Q(2) * Q(3) + Q(1) * Q(4) )            TRNMQ110
             TRANSM(1,3) = 2. * ( Q(2) * Q(4) - Q(1) * Q(3) )            TRNMQ120
             TRANSM(2,1) = 2. * ( Q(2) * Q(3) - Q(1) * Q(4) )            TRNMQ190
             TRANSM(2,2) = 1. - 2. * ( Q(2)**2 + Q(4)**2 )               TRNMQ200
             TRANSM(2,3) = 2. * ( Q(3) * Q(4) + Q(1) * Q(2) )            TRNMQ210
             TRANSM(3,1) = 2. * ( Q(2) * Q(4) + Q(1) * Q(3) )            TRNMQ280
             TRANSM(3,2) = 2. * ( Q(3) * Q(4) - Q(1) * Q(2) )            TRNMQ290
             TRANSM(3,3) = 1. - 2. * ( Q(2)**2 + Q(3)**2 )               TRNMQ300
      RETURN                                                              TRNMQ850
C     ******************************************************************TRNMQ997
      END                                                                 TRNMQ998

1.TOTWND/01-07-77

A(1).TOTWND/01-07-77
      SUBROUTINE TOTWND ( XTC, VTC, X, VWIND )                            TOTWD010
C     COMPUTE MOVING TORNADO TOTAL WIND VELOCITY IN INERTIAL COORDINATESTOTWD020
C       J.R.RADBILL, JPL, SECT.366, MAIL 125-128, PHONE (213) 354-2989  TOTWD030
C         STARTED 6-09-75, LAST CHANGE 01-07-77 1500                    TOTWD040
C     ******************************************************************TOTWD050
      REAL     XTC(2), VTC(2), X(3), VWIND(3), VWINDC(3), PAD1(6),       TOTWD060
     *         PAD2(3)                                                    TOTWD070
      COMMON   /TORN/ PAD1, ALPHAB, BETAB, GAMMAB, PAD2                   TOTWD080
C     ******************************************************************TOTWD090
C          *** COMPUTE LOCATION OF BODY RELATIVE TO TORNADO CENTER ***   TOTWD100
             XR = X(1) - XTC(1)                                           TOTWD110
             YR = X(2) - XTC(2)                                           TOTWD120
             R  = SQRT( XR**2 + YR**2 )                                   TOTWD130
C          *** FORM UNIT VECTOR ALONG RADIUS FROM STORM CENTER TO POINT  TOTWD140
             IF ( R.GT.0. ) GO TO 1                                       TOTWD150
             URX = 0.                                                     TOTWD160
             URY = 0.                                                     TOTWD170
             GO TO 2                                                      TOTWD180
   1         URX = XR / R                                                 TOTWD190
             URY = YR / R                                                 TOTWD200
C          *** COMPUTE WIND VELOCITY IN CYLINDRICAL COORDINATES FOR      TOTWD210
C          *** STATIONARY TORNADO. COMPONENTS ARE RADIAL, TANGENTIAL(CC)TOTWD220
C          *** AND VERTICAL                                              TOTWD230
   2         CALL TORNAD ( R, X(3), VWINDC )                             TOTWD240
C          *** FACTOR TO FORCE TRANSLATIONAL VELOCITY TO 0 AT Z=0 ***    TOTWD250
             F = 1. - EXP(-BETAB * GAMMAB * X(3) / ALPHAB )               TOTWD260
C          *** TRANSFORM WIND VELOCITY FROM CYLINDRICAL TO RECTANGULAR   TOTWD270
C          *** COORDINATES AND ADD TRANSLATIONAL VELOCITY OF STORM CENTR TOTWD280
             VWIND(1) = VWINDC(1) *URX -VWINDC(2) *URY +VTC(1) * F       TOTWD290
             VWIND(2) = VWINDC(1) *URY +VWINDC(2) *URX +VTC(2) * F       TOTWD300
             VWIND(3) = VWINDC(3)                                        TOTWD310
      RETURN                                                              TOTWD320
C     ******************************************************************TOTWD330
      END                                                                 TOTWD340

1.TORNAD/12-14-76-D
```

```
:1).TORNAD/12-14-76-0
      SUBROUTINE TORNAD ( RB, ZB, VBW )                                  TORN0001
C     STATIONARY TORNADO WIND VELOCITY VECTOR VBW=V/VMAX FROM POSITION   TORN0002
C     RELATIVE TO CENTER, RB=R/R1, ZB=Z/R1 WHERE R1 IS RADIUS FOR VMAX.  TORN0003
C     EDDY VISCOSITY DEFINED BY PARAMETERS ALPHAF, BETAFT, NU            TORN0004
C     MODEL BY P. BERGARABEDIAN, AND F. FENDEL, TRW. PROGRAMMED BY       TORN0005
C       J.R.RADBILL, JPL, SECT.366 MAIL 175/128, PHONE (213) 354-2989    TORN0007
C         STARTED 5-23-75, LAST CHANGE 12-14-76 1300                     TORN0008
C     ***************************************************************** TORN0009
      LOGICAL  PRTORN                                                    TORN0010
      INTEGER  ZLORET, UVWRET                                            TORN0015
      REAL     LATDEG, NU, VBW(3)                                        TORN0030
      COMMON   /TORN/ RIMILE, LATDEG, VMXMPH, NU, ALPHAF, BETAFT, ALPHAB TORN0050
     *              , BETAB, GAMMAB, RBO, WBO, PRTORN                    TORN0051
      DATA     DGPRAD, FTPMIL, PI04, OMEGAE, SECPHR/ 57.295778, 5280.,   TORN0060
     *         .78539816, 7.2722052E-5, 3600./                           TORN0061
      NAMELIST /INITAL/ RIFT, OMEGA,RBO, ALPHAB, BETAB, GAMMAB, WB,      TORN0080
     *                  WBT, WBO                                         TORN0081
     *         /COMP/   RB, ZB, PSIOR, PSIROR, ZFT, POWER, WBT, UB, VB,  TORN0085
     *                  WB, VBW                                          TORN0086
C     ***************************************************************** TORN0090
      IF ( ZB.LE.0. ) GO TO 90                                           TORN0095
      IF ( GAMMAB.GT.0.) GO TO 11                                        TORN0100
C           *** DEFAULT VALUES FOR EDDY VISCOSITY PARAMETERS ***         TORN0105
            IF ( NU    .EQ.0. ) NU = 1.                                  TORN0107
            IF ( ALPHAF.EQ.0. ) ALPHAF = 3.5                             TORN0110
            IF ( BETAFT.EQ.0. ) BETAFT = 270.                            TORN0112
            RIFT   = RIMILE * FTPMIL                                     TORN0120
C           *** LOCAL VORTICITY IN RADIANS / SECOND ***                  TORN0124
            OMEGA = OMEGAE * SIN( LATDEG / DGPRAD )                      TORN0125
C           *** OUTER RADIUS OF TORNADO DIMENSIONLESS ***                TORN0130
            RBO = SQRT( 1.5 *VMXMPH /( OMEGA *RIMILE *SECPHR ) )         TORN0135
            ALPHAB = ALPHAF / RIFT                                       TORN0150
            BETAB  = BETAFT / RIFT                                       TORN0160
            GAMMAB = RIFT * SQRT( 5. *OMEGA/( 3. * NU ) )                TORN0170
C     *** COMPUTE LOWER LIMIT OF INTEGRAL FOR WB(Z), Z.GT.ALPHA ***      TORN0200
C        *** CALL PROCEDURE ZLO ***                                      TORN0205
            ASSIGN 5 TO ZLORET                                           TORN0210
            ZBT = ALPHAB                                                 TORN0220
          GO TO 20                                                       TORN0240
C         *** CALL PROCEDURE UVW ***                                     TORN0245
 5          ASSIGN 10 TO UVWRET                                         TORN0250
            POWER = ALPHAB + BETAB                                       TORN0260
          GO TO 80                                                       TORN0270
10          WBO = WB - WBT                                               TORN0280
          IF (PRTORN) WRITE (6,INITAL)                                   TORN0290
C     *** COMPUTATION SECTION ********************************************TORN0300
C       *** RADIAL DEPENDANCE ***                                        TORN0310
11        IF ( RB.GT.1. ) GO TO 12                                       TORN0320
C         *** CORE, RB .LT. 1 ***                                        TORN0315
            PSIOR  = RB                                                  TORN0330
            PSIROR = 2.                                                  TORN0340
          GO TO 15                                                       TORN0350
C         *** POTENTIAL VORTEX, 0 .LT.RB.LT.RBO ***                      TORN0360
12        IF ( RB.GT.RBO ) GO TO 13                                      TORN0370
            PSIOR  = ( RBO**2 - RB**2 )/(( RBO**2 - 1. ) * RB )          TORN0380
            PSIROR = -2./( RBO**2 -1. )                                  TORN0390
          GO TO 15                                                       TORN0400
C         *** OUTSIDE TORNADO, RB.GT.RBO ***                             TORN0410
13          VBW(1) = 0.                                                  TORN0420
            VBW(2) = 0.                                                  TORN0430
            VBW(3) = 0.                                                  TORN0440
          GO TO 70                                                       TORN0450
C       *** VERTICAL DEPENDANCE ***                                      TORN0490
C         *** NEAR-GROUND REGION ***                                     TORN0500
C           *** CALL PROCEDURE ZLO ***                                   TORN0505
15        IF ( ZB.GT.ALPHAB ) GO TO 27                                   TORN0510
            ASSIGN 40 TO ZLORET                                          TORN0520
            ZBT = ZB                                                     TORN0530
C         *** PROCEDURE ZLO ***                                          TORN0540
20          POWER = BETAB * ZBT/ ALPHAB                                  TORN0550
C           *** CALL PROCEDURE UVW ***                                   TORN0560
```

```
                ASSIGN 25 TO UVWRET                                    TORN0570
               GO TO 80                                                TORN0580
   25           WB = ( WBT + PTOP / GAMMAB ) * ALPHAB / BETAB          TORN0590
               GO TO ZLORET, ( 5, 40 )                                 TORN0600
C            *** UPPER REGION ***                                       TORN0610
   27           POWER = ZB + BETAB                                      TORN0620
C               *** CALL PROCEDURE UVW ***                             TORN0630
                ASSIGN 35 TO UVWRET                                    TORN0640
               GO TO 80                                                TORN0650
   35           WB = WBT + WBO                                          TORN0660
C            *** FORM VELOCITY COMPONENTS FROM R AND Z DEPENDANT FACTORS *TORN0700
   40           E = EXP(-GAMMAB*(ZB+BETAB)*(1.-EXP(-ZB/ALPHAB)))        TORN0702
                VB = 1. - E                                            TORN0704
                UB = -SQRT( E * VB )                                   TORN0706
                VBW(1) = PSIOR * UB                                    TORN0710
                VBW(2) = PSIOR * VB                                    TORN0720
                VBW(3) = PSIOR * WB                                    TORN0730
                ZFT = RIFT * ZB                                        TORN0732
              IF (PRTORN) WRITE (6,COMP)                               TORN0735
   70 RETURN                                                           TORN0740
C     ******** UNDERGROUND BRANCH ***************************************TORN0750
   90         DO 95 I = 1, 3                                          TORN0760
   95           VBW(I) = 0.                                           TORN0770
               GO TO 70                                                TORN0780
C     ******** PROCEDURE UVW ********************************************TORN0790
   80           E   = EXP( -GAMMAB * POWER )                          TORN0800
                VB  = 1. -E                                            TORN0810
                UB  = -SQRT( E * VB )                                  TORN0820
                WBT = ( UB -.5 * ASIN( E - VB ) ) / GAMMAB             TORN0830
               GO TO UVWRET, ( 10, 25, 35 )                            TORN0840
C     ***************************************************************TORN0900
       END                                                             TORN0998
```

*WINDCA/10-20-76

```
1),WINDCA/10-20-76
       SUBROUTINE WINDCA ( VWREL, TRNMBI, VWRMAG, TRNMWI, ALPHAW )     WNDCA001
C      FIND TRANSFORMATION 'TRNMWI' FROM WIND TO INERTIAL COORDINATES,  WNDCA002
C      PITCH AND ROLL ANGLES OF BODY RELATIVE TO WIND, ALPHAW(2),       WNDCA003
C      ALPHAW(3). 'TRNMBI' IS TRANSFORMATION FROM BODY TO INERTIAL COORDSWNDCA004
C      FOR PITCH=ROLL=0, WIND AXES ARE ROTATED 180DEG ON Z FROM BODY AXESWNDCA005
C        J.R.RADDILL, JPL, SECT.366, M.C.125/120, PHONE (213) 354-2989  WNDCA007
C          STARTED 8-4-75, LAST CHANGE 10-20-76 1330                    WNDCA008
C      ***************************************************************WNDCA009
       LOGICAL  PRINT                                                  WNDCA010
       REAL     VWREL(3), TRNMBI(3,3), TRNMWI(3,3), ALPHAW(3), VT1(3),  WNDCA030
      *         VT2(3), PADES1(16), PADES2(24)                         WNDCA031
       COMMON   /ESTATE/ PADES1, PRINT, PADES2                         WNDCA050
       DATA     PI/ 3.1415927/                                         WNDCA070
       NAMELIST /WNDAN1/ VWREL, VWRMAG, SINA2, COSA2, SINA3, COSA3,    WNDCA080
      *                  ALPHAW                                       WNDCA085
C      ***************************************************************WNDCA090
            IF ( PRINT ) WRITE (6,190) TRNMBI                          WNDCA095
C           *** FIND RELATIVE VELOCITY MAGNITUDE AND UNIT VECTOR TRNMWI1 WNDCA100
            VWRMAG = UNIT ( VWREL, TRNMWI(1,1) )                       WNDCA110
C           *** FORM VECTOR CROSS PRODUCT TO GET BINORMAL WIND AXIS ***  WNDCA120
            CALL CROSS ( TRNMBI(1,1), TRNMWI(1,1), VT1 )               WNDCA130
            SINA2 = UNIT ( VT1, TRNMWI(1,2) )                          WNDCA140
C           *** FORM NORMAL WIND AXIS VECTOR ***                       WNDCA150
            CALL CROSS ( TRNMWI(1,1), TRNMWI(1,2), TRNMWI(1,3) )       WNDCA160
C           *** ALPHAW(1)=YAW=0, ONLY 2 ANGLES REQ TO DEFINE ORIENTATION WNDCA170
            ALPHAW(1) = 0.                                             WNDCA180
C           *** FIND PITCH ANGLE =ALPHAW(2) ***                        WNDCA190
            COSA2 =-DOT ( TRNMBI(1,1), TRNMWI(1,1) )                   WNDCA200
            ALPHAW(2) = ATAN2( SINA2, COSA2 )                          WNDCA210
C           *** FIND ROLL ANGLE = ALPHAW(3) ***                        WNDCA220
            CALL CROSS ( TRNMWI(1,2), TRNMBI(1,2), VT1 )               WNDCA230
            SINA3 = UNIT ( VT1, VT2 )                                  WNDCA240
            COSA3 =-DOT ( TRNMWI(1,2), TRNMBI(1,2) )                   WNDCA250
            ALPHAW(3) = ATAN2( SINA3, COSA3 )                          WNDCA260
          IF ( PRINT ) WRITE (6,WNDAN1)                                WNDCA270
          IF ( PRINT ) WRITE (6,200) TRNMWI                            WNDCA280
```

```
      RETURN                                                            WNDCA800
C     ******************************************************************WNDCA890
  190 FORMAT ( 3X, 'TRNMBI=', 3F10.6/( 12X, 3F10.6 ) )                  WNDCA940
  200 FORMAT ( 3X, 'TRNMWI=', 3F10.6/( 12X, 3F10.6 ) )                  WNDCA950
C     ******************************************************************WNDCA997
      END                                                               WNDCA998

)RMIS.UNIT

)RMIS(1).UNIT
      FUNCTION UNIT ( V, U )                                            UNITO001
C     FIND UNIT VECTOR U AND MAGNITUDE OF UNIT FOR VECTOR V             UNITO002
C       J.R.RADBILL, JPL, SECT.914, MAIL 125-109A, PHONE (213) 354-6552 UNITO007
C         STARTED 6-07-75, LAST CHANGE 8-07-75 1000                     UNITO008
C     ******************************************************************UNITO009
      REAL     U(3), V(3), MAG                                          UNITO030
           MAG = SQRT( DOT ( V, V ) )                                   UNITO100
           DO 1 I = 1, 3                                                UNITO120
         1    U(I) = V(I) / MAG                                         UNITO140
           UNIT = MAG                                                   UNITO160
C     ******************************************************************UNITO090
      RETURN                                                            UNITO800
C     ******************************************************************UNITO997
      END                                                               UNITO998

)RMIS.CROSS

)RMIS(1).CROSS
      SUBROUTINE CROSS ( X, Y, Z )                                      CROSS001
C     VECTOR CROSS PRODUCT                                              CROSS002
C       J.R.RADBILL, JPL, SECT.914, MAIL 125-109A, PHONE (213) 354-7097 CROSS007
C         STARTED 6-09-75, LAST CHANGE 6-09-75 1030                     CROSS008
C     ******************************************************************CROSS009
      REAL     X(3), Y(3), Z(3)                                         CROSS030
C     ******************************************************************CROSS090
           Z(1) = X(2) * Y(3) - X(3) * Y(2)                             CROSS100
           Z(2) = X(3) * Y(1) - X(1) * Y(3)                             CROSS110
           Z(3) = X(1) * Y(2) - X(2) * Y(1)                             CROSS120
      RETURN                                                            CROSS800
C     ******************************************************************CROSS997
      END                                                               CROSS998

)RMIS.VECT-MAT-MPY

)RMIS(1).VECT-MAT-MPY
      SUBROUTINE VMMPY ( X, A, Y )                                      VMMPY001
C     VECTOR MATRIX PRODUCT: Y = X A                                    VMMPY002
C       J.R.RADBILL, JPL, SECT.914, MAIL 125-109A, PHONE (213) 354-7097 VMMPY007
C         STARTED 6-02-75, LAST CHANGE 6-03-75 1430                     VMMPY008
C     ******************************************************************VMMPY009
      REAL     A(3,3), X(3), Y(3)                                       VMMPY030
C     ******************************************************************VMMPY090
           Y(1) = X(1)*A(1,1) +X(2)*A(2,1) +X(3)*A(3,1)                 VMMPY100
           Y(2) = X(1)*A(1,2) +X(2)*A(2,2) +X(3)*A(3,2)                 VMMPY110
           Y(3) = X(1)*A(1,3) +X(2)*A(2,3) +X(3)*A(3,3)                 VMMPY120
      RETURN                                                            VMMPY800
C     ******************************************************************VMMPY997
      END                                                               VMMPY998

,ARDERC/10-27-76

(1),ARDERC/10-27-76
      SUBROUTINE AROFPC ( VWRMAG, ALPHAW, OMEGAW, FW, TW )              AROF0010
C     AERODYNAMIC FORCES AND MOMENTS FOR BODIES WITH 3 PERPENDICULAR    AROF0020
C     PLANES OF SYMMETRY OR CYLINDERS AND FAR FROM GROUND PLANE         AROF0030
C       J.R.RADBILL, JPL, SECT.366, MAIL C 125/128, PHONE (213) 354-2989AROF0040
C         STARTED 6-06-75, LAST CHANGE 10-27-76 1615                    AROF0050
C     ******************************************************************AROF0060
      LOGICAL  PRAROF, CYLNDR                                           AROF0070
      REAL     ALPHAW(3), OMEGAW(3), FW(3), TW(3), LOR1, SGNA(4,6),     AROF0080
     *         SGNP(4,6), CTD(3), ALFTAB(19), PHITAB(4), ESPAD(37),     AROF0081
     *         COFTAB(19,4,6), C(6), SIGNC(4)                           AROF0082
```

```
      COMMON   /CAEROC/ CAERO, LORI, ALFTAB, NA, IPA, PHITAB, NP, IPP,   ARoF0090
     *         COFTAB, CTD, SGNA, SGNP, PRAROF, CYLNDR                   ARoF0091
     *         /ESTATE/ ESPAD, C                                         ARoF0100
      DATA     IDCFT, DGPRAD/ 19, 57.295780/                             ARoF0110
      DATA     SIGNC/ +1., -1., +1., -1./                                ARoF0115
C     ***************************************************************** ARoF0120
            CF = CAERO * VWRMAG**2                                       ARoF0130
            CT = LORI * CAERO * VWRMAG                                   ARoF0140
      IF (CYLNDR) GO TO 40                                               ARoF0145
C     *** SECTION FOR SHAPES WITH THREE PERPENDICULAR PLANES OF SYMMETRY  ARoF0146
C       *** FIND QUADRANT OF PITCH AND YAW ANGLES AND MAP INTO 0-PI/2     ARoF0150
          CALL MANGLE ( ALPHAW(2), ALFWR, IQA )                          ARoF0160
          CALL MANGLE ( ALPHAW(3), PHIWR, IQP )                          ARoF0170
C       *** LOOP TO INTERPOLATE FOR 6 WIND AXIS COEFFICIENTS ***         ARoF0180
            MSRC = 2                                                     ARoF0185
          DO 10 IC = 1, 6                                                ARoF0190
C           *** SET UP 2D INTERPOLATION FOR ICTH COEFFICIENT ***         ARoF0200
            CALL TB2SET ( ALFTAB, NA, IPA, MSRC, PHITAB, NP, IPP, MSRC,  ARoF0210
     *                    COFTAB(1,1,IC), IDCFT, IERR )                  ARoF0211
C           *** INTERPOLATE FOR ICTH COEFFICIENT ***                     ARoF0220
            ALFWD = ALFWR * DGPRAD                                       ARoF0222
            PHIWD = PHIWR * DGPRAD                                       ARoF0224
            C(IC) = TB2GET ( ALFWD, PHIWD )                              ARoF0230
C           *** COMPUTE FORCES ***                                       ARoF0240
            IF (IC.LE.3)   FW(IC) = C(IC) *CF *SGNA(IQA,IC)*SGNP(IQP,IC) ARoF0250
C           *** COMPUTE MOMENTS ***                                      ARoF0260
            IF (IC.GE.4) TW(IC-3) = C(IC) *CF *SGNA(IQA,IC)*SGNP(IQP,IC) ARoF0270
            IF (IC.GE.5) TW(IC-3) = TW(IC-3) +CTD(IC-3) *OMEGAW(IC-3)*CT ARoF0280
            MSRC = 3                                                     ARoF0290
   10     CONTINUE                                                       ARoF0300
          GO TO 90                                                       ARoF0350
C     *** SECTION FOR CYLINDRICAL OBJECTS ***                            ARoF0400
C       *** FIND QUADRANT OF PITCH ANGLE ***                             ARoF0405
   40     CALL MANGLE ( ALPHAW(2), ALFWR, IQA )                          ARoF0410
            ALFWD = ALFWR * DGPRAD                                       ARoF0412
C       *** INTERPOLATE FOR COEFFICIENTS ***                             ARoF0415
          DO 50 IC = 1, 4                                                ARoF0420
            CALL SLOP ( ALFWD, C(IC), CDOT, ALFTAB, COFTAB(1,1,IC), NA,  ARoF0430
     *                  IPA )                                            ARoF0431
   50     CONTINUE                                                       ARoF0440
C         *** COMPUTE FORCES AND MOMENTS ***                             ARoF0445
            FW(1) = C(1) * CF                                            ARoF0450
            FW(2) = 0.                                                   ARoF0460
            FW(3) = C(2) * CF * SIGNC(IQA)                               ARoF0480
            TW(1) = 0.                                                   ARoF0490
            TW(2) = C(3) * CF * SIGNC(IQA) *CT * C(4) * OMEGAW(2)        ARoF0510
            TW(3) = 0.                                                   ARoF0520
   90     IF (PRAROF) WRITE (6,200) VWRMAG, ALPHAW, OMEGAW, IQA,         ARoF0550
     *                  ALFWD, IQP, PHIWD, C, FW, TW                    ARoF0551
      RETURN                                                             ARoF0800
C     ***************************************************************** ARoF0900
  200 FORMAT (/2X, 7HVWRMAG=, F8.5,8H,ALPHAW=, 3F8.5,8H,OMEGAW=,3F8.5/   ARoF0910
     *        2X, 4HIQA=,I2,7H,ALFWD=,F8.5,5H,IQP=,I2,7H,PHIWD=,F8.5,   ARoF0911
     *        4H, C=,6F6.3/ 2X,3HFW=,3F8.5,4H,TW=, 3F8.5 )               ARoF0912
C     ***************************************************************** ARoF0997
      END                                                                ARoF0998
```

```
*MANGLE

C(1),MANGLE
      SUBROUTINE MANGLE ( A, ABAR, IQAD )                                MANGL010
C     MAP ANGLE INTO FIRST QUADRANT AND RECORD SOURCE QUADRANT           MANGL020
C       J.P.RADRILL, JPL SECT 366, MAIL C 125-128, PHONE (213) 354-2989  MANGL030
C         STARTED 8-28-76, LAST CHANGE 8-26-76 1430                      MANGL040
C     ***************************************************************** MANGL050
      DATA     PI, PI02 / 3.1415927, 1.5707964 /                         MANGL060
C     ***************************************************************** MANGL070
C       *** TEST IF ANGLE IS + OR - ***                                  MANGL080
        IF ( A.GT.0 ) GO TO 20                                           MANGL090
C         *** MINUS. TEST IF 3RD OR 4TH QUADRANT ***                     MANGL100
          IF ( A.GT.-PI02 ) GO TO 10                                     MANGL110
C           *** 3RD QUADRANT ***                                         MANGL120
```

```
                ABAR = PI + A                                                  MANGL130
                IQAD = 3                                                       MANGL140
               GO TO 90                                                        MANGL150
C              *** 4TH QUADRANT ***                                            MANGL160
   10           ABAR = -A                                                      MANGL170
                IQAD = 4                                                       MANGL180
               GO TO 90                                                        MANGL190
C            *** PLUS.  TEST IF 1ST OR 2ND QUADRANT ***                        MANGL200
   20         IF ( A.GT.+PIO2 ) GO TO 30                                      MANGL210
C              *** 1ST QUADRANT ***                                            MANGL220
                ABAR = A                                                       MANGL230
                IQAD = 1                                                       MANGL240
               GO TO 90                                                        MANGL250
C              *** 4TH QUADRANT ***                                            MANGL260
   30           ABAR = PI - A                                                  MANGL270
                IQAD = 2                                                       MANGL280
C                                                                              MANGL290
   90 RETURN                                                                   MANGL300
C     ***************************************************************        MANGL310
      END                                                                      MANGL320
```

```
\.QUATD/7-27-76
```

```
(1).QUATD/7-27-76
      SUBROUTINE QUATD ( OMEGA, Q, DQ )                                        QUATD001
C     COMPUTE DQ/DT = -.5*OMEGA&Q, WHERE Q IS A QUATERNION DESCRIBING          QUATD002
C     ORIENTATION OF BODY AXES, DQ/DT ITS TIME DERIVATIVE AND OMEGA THE        QUATD003
C     ANGULAR VELOCITY VECTOR TREATED AS A QUATERNION WITH ZERO SCALAR         QUATD004
C     PART.  OMEGA&Q DENOTES A QUATERNION PRODUCT.                             QUATD005
C       J.R.RADBILL, JPL, SECT.914, MAIL 125-109A, PHONE (213) 354-6552        QUATD007
C         STARTED 6-02-75, LAST CHANGE 7-27-76 1445                            QUATD008
C     ***************************************************************        QUATD009
      REAL     OMEGA(3), Q(4), DQ(4)                                           QUATD030
C     ***************************************************************        QUATD090
C       *** NORMALIZE QUATERNION TO MAINTAIN ORTHOGONALITY OF TR MATRIX       QUATD092
              QMI = 1./ SQRT( Q(1)**2 +Q(2)**2 +Q(3)**2 +Q(4)**2 )             QUATD093
            DO 5 I = 1, 4                                                      QUATD094
    5         Q(I) = Q(I) * QMI                                                QUATD095
C        *** COMPUTE DERIVATIVES OF QUATERNION COMPONENTS ***                  QUATD097
          DQ(1) =  .5 *( +Q(2)*OMEGA(1) +Q(3)*OMEGA(2) +Q(4)*OMEGA(3) )       QUATD100
          DQ(2) =  .5 *( -Q(1)*OMEGA(1) -Q(4)*OMEGA(2) +Q(3)*OMEGA(3) )       QUATD110
          DQ(3) =  .5 *( +Q(4)*OMEGA(1) -Q(1)*OMEGA(2) -Q(2)*OMEGA(3) )       QUATD120
          DQ(4) =  .5 *( -Q(3)*OMEGA(1) +Q(2)*OMEGA(2) -Q(1)*OMEGA(3) )       QUATD130
      RETURN                                                                   QUATD800
C     ***************************************************************        QUATD997
      END                                                                      QUATD998
```

```
.CEULER/10-22-76
```

```
(1).CEULER/10-22-76
      SUBROUTINE CEULER ( TRNMBI, EULERA )                                     CEULR000
C     COMPUTE EULER ANGLES FROM TRANSFORMATION MATRIX                          CEULR010
C       J.R.RADBILL, JPL, SECT.366, MAIL 125-128, PHONE (213) 354-2989         CEULR020
C         STARTED 6-02-75, LAST CHANGE 10-22-76 1500                           CEULR030
C     ***************************************************************        CEULR040
      REAL     TRNMBI(3,3), EULERA(3)                                          CEULR050
C     ***************************************************************        CEULR060
C          *** YAW ANGLE ***                                                   CEULR070
           EULERA(1) = ATAN2(-TRNMBI(2,1), TRNMBI(1,1) )                       CEULR080
C          *** PITCH ANGLE ***                                                 CEULR090
           EULERA(2) = ASIN( +TRNMBI(3,1) )                                    CEULR100
C          *** ROLL ANGLE ***                                                  CEULR110
           EULERA(3) = ATAN2( TRNMBI(3,2), TRNMBI(3,3) )                       CEULR120
      RETURN                                                                   CEULR130
C     ***************************************************************        CEULR140
      END                                                                      CEULR150
```

```
.PRINTS/11-01-76
```

```
(1).PRINTS/11-01-76
      SUBROUTINE PRINTS                                                        PRTS0001
C     PRINT RESULTS OF ONE INTEGRATION STEP                                    PRTS0010
```

```
C       J.R.RADBILL, JPL, SEC.366, MAIL 125-128, PHONE (213) 354-2989  PRTS0020
C         STARTED 6-02-75, LAST CHANGE 11-01-76 1300                   PRTS0030
C     ***************************************************************PRTS0040
      LOGICAL  PDERIV, PLOT, PRINTV, CYLNDR                            PRTS0050
      REAL     XTC(2), Q(4), L(3), OMEGA(3), EULERA(3), TRNMBI(3,3),   PRTS0060
     *         YN(15), INERTI(3,3), PAD1(9), PAD2(5), VWIND(3), XV(6), PRTS0070
     *         ALPHAW(3), OMEGAW(3), VWREL(3), FW(3), FI(3), OMGRPS(3), PRTS0080
     *         VFPS(3), XFT(3), C(6), PADARO(537)                      PRTS0085
      COMMON   /CSTATE/ T, H, DTP, TF, XV, XTC, Q, L, YN, PRINTV       PRTS0090
     *         /ESTATE/ OMEGA, EULERA, TRNMBI, TCSEC, PDERIV, VWIND,   PRTS0100
     *         ALPHAW, OMEGAW, VWREL, FW, FI, VWRMAG, PLOT, C          PRTS0110
     *         /CAEROC/ PADARO, CYLNDR                                 PRTS0120
     *         /TORN/   RIMILE, LATDEG, VMXMPH, PAD1                   PRTS0130
     *         /CINERT/ INERTI, PAD2, BDYWTP                           PRTS0140
      DATA     DEGPP / 57.295780 /, FTPMIL/ 5280. /, FTPMS / 1.4666667/PRTS0150
     *       , RADPRV / 6.283185 /                                     PRTS0160
C     ***************************************************************PRTS0170
               RIFT = RIMILE * FTPMIL                                  PRTS0180
               VMXFPS = VMXMPH * FTPMS                                 PRTS0190
               RVPRTC = 1. / ( RADPRV * TCSEC )                        PRTS0200
               TSEC = T * TCSEC                                        PRTS0210
               HSEC = H * TCSEC                                        PRTS0220
               SUM = 0.                                                PRTS0225
            DO 2 I = 1, 3                                              PRTS0230
               XFT(I)    = XV(2*I-1) * RIFT                           PRTS0240
               VFPS(I)   = XV(2*I) * VMXFPS                           PRTS0250
               EULERA(I) = EULERA(I) * DEGPR                          PRTS0255
               OMGRPS(I) = OMEGA(I) * RVPRTC                          PRTS0260
               SUM       = VFPS(I)**2 + SUM                           PRTS0265
    2       CONTINUE                                                   PRTS0270
            WRITE (6,200) TSEC, HSEC                                   PRTS0320
            WRITE (6,210) XFT, VFPS, OMGRPS                            PRTS0330
               RXYFT = SQRT( XFT(1)**2 + XFT(2)**2 )                   PRTS0370
               SPDFPS = SQRT( SUM )                                    PRTS0380
            WRITE (6,230) EULERA, RXYFT, SPDFPS                        PRTS0390
C           *** PRINT EXTRA VARIABLES TO STUDY TRIM OF MISSILE ***     PRTS0400
            IF (.NOT.PRINTV) GO TO 10                                  PRTS0410
               ALPHAW(1) = ALPHAW(1) * DEGPR                           PRTS0420
            DO 7 I = 1, 3                                              PRTS0430
               OMEGAW(I) = OMEGAW(I) *RVPRTC                           PRTS0440
               VWIND(I) = VWIND(I) * VMXMPH                            PRTS0450
               VWREL(I) = VWREL(I) * VMXMPH                            PRTS0460
               FW(I)    = FW(I) * BDYWTP                               PRTS0470
               FI(I)    = FI(I) * BDYWTP                               PRTS0480
               ALPHAW(I) = ALPHAW(I) * DEGPR                           PRTS0485
    7       CONTINUE                                                   PRTS0490
            WRITE (6,240) VWIND, ALPHAW, OMEGAW, VWREL, FW, FI         PRTS0500
            IF (CYLNDR) WRITE (6,245) ( C(I), I = 1, 4 )               PRTS0502
            IF (.NOT.CYLNDR) WRITE (6,246) C                           PRTS0504
   10       IF ( PLOT ) WRITE (3,250) TSEC, XFT, OMGRPS, EULERA, VWIND, PRTS0510
     *                  VWREL, FW, FI, VWRMAG, C, RXYFT, SPDFPS        PRTS0520
      RETURN                                                           PRTS0540
C     ***************************************************************PRTS0550
  200 FORMAT ( 7HO TSEC=,F10.4,7H, HSEC=,F9.6 )                        PRTS0560
  210 FORMAT ( 9H  XFT   =, F7.1, 9H, YFT   =, F7.1, 9H, ZFT   =, F7.1/ PRTS0570
     *         9H  VFPS  =, F7.1, 9H, VFPS  =, F7.1, 9H, WFPS  =, F7.1/ PRTS0580
     *         9H  OMXRPS=, F7.3, 9H, OMYRPS=, F7.3, 9H, OMZRPS=, F7.3) PRTS0590
  230 FORMAT ( 6H  YAW=, F6.1, 8H, PITCH=, F6.1, 7H, ROLL=, F6.1,      PRTS0600
     *         8H, RXYFT=, F6.0, 9H, SPDFPS=, F6.1 )                   PRTS0610
  240 FORMAT ( 8H  VWIND =, 3F6.1, 9H, ALPHAW=, 3F6.1, 9H, OMEGAW=,    PRTS0620
     *         3F6.3/ 8H  VWREL=, 3F7.1, 5H, FW=, 3F7.1, 5H, FI=, 3F7.1)PRTS0630
  245 FORMAT ( 5H  CD=, F7.3, 5H, CL=, F7.3, 5H, CH=, F7.3, 6H, CMQ=,  PRTS0631
     *         F7.3 )                                                  PRTS0632
  246 FORMAT ( 5H  CD=,F7.3, 5H, CS=,F7.3, 5H, CL=,F7.3, 9H, CMROLL=,F7.3PRTS0635
     *       , 10H, CMPITCH=,F7.3, 8H, CMYAW=F7.3/ )                   PRTS0636
  250 FORMAT ( 1P6E12.6 )                                              PRTS0640
C     ***************************************************************PRTS0650
      END                                                              PRTS0660

.TERMIN/01-07-77
```

```
(1).TERMIN/01-07-77
      SUBROUTINE TERMIN ( G )                                                  TERMN010
C     COMPUTE G-STOP VECTOR, TERMINAL CONDITION AND EXTREMA CONDITIONS         TERMN020
C       J.R.RADBILL, JPL, SECT.366, MAIL 125-128, PHONE (213) 354-2989         TERMN030
C         STARTED 6-02-75, LAST CHANGE 01-07-77 1340                           TERMN040
C     ***************************************************************        TERMN050
      REAL      G(5), TSPEC(4), PAD1(25), PAD2(141)                            TERMN060
      COMMON    /CSTATE/ TSPEC, X, U, Y, V, Z, W, PAD1                         TERMN070
     *          /DSTATE/ DU, DV, DW, PAD2                                      TERMN080
C     ***************************************************************        TERMN090
C           *** CHECK IF WIND CARRIED OBJECT HAS HIT GROUND PLANE ***           TERMN100
            G(1) = Z                                                           TERMN110
C           *** CHECK FOR EXTREMA IN HEIGHT ***                                TERMN120
            G(2) = W                                                           TERMN130
C           *** CHECK FOR EXTREMA IN HORIZONTAL SPEED ***                      TERMN140
            VH2 = U**2 + V**2                                                  TERMN150
            IF (VH2.NE.0.)                                                     TERMN160
     *         G(3) = ( U*DU + V*DV )/ SQRT( VH2 )                             TERMN170
            IF (VH2.EQ.0.) G(3) = 0.                                           TERMN180
C           *** CHECK FOR EXTREMA IN SPEED ALONG TRAJECTORY ***                TERMN190
            V2 = VH2 + W**2                                                    TERMN200
            IF (V2.NE.0.)                                                      TERMN210
     *         G(4) = ( U*DU + V*DV + W*DW )/SQRT( V2 )                        TERMN220
            IF (V2.EQ.0.) G(4) = 0.                                            TERMN230
C           *** CHECK FOR EXTREMA IN HORIZONTAL RANGE ***                      TERMN240
            R2 = X**2 + Y**2                                                   TERMN250
            IF (R2.NE.0.)                                                      TERMN260
     *         G(5) = ( X*U + Y*V )/ SQRT( R2 )                                TERMN270
            IF (R2.EQ.0.) G(5) = 0.                                            TERMN280
      RETURN                                                                   TERMN290
C     ***************************************************************        TERMN300
      END                                                                      TERMN310

.BLOCK DATA/02-28-77

(1).BLOCK-DATA/02-28-77
      BLOCK DATA
      REAL      SGNA(24), SGNP(24), PAD1(488), PAD2(2)
      COMMON    /CAESOC/ PAD1, SGNA, SGNP, PAD2
      DATA      SGNA/+1.,+1.,+1.,+1.,+1.,+1., -1.,-1.,+1.,-1.,+1.,-1.,
     *             +1.,-1.,+1.,-1.,+1.,-1., +1.,-1.,+1.,-1.,+1.,-1./
      DATA      SGNP/+1.,+1.,+1.,+1.,+1.,-1., +1.,-1.,+1.,+1.,+1.,+1.,
     *             +1.,-1.,+1.,-1.,+1.,+1., +1.,+1.,+1.,-1.,+1.,-1./
      END

CTP:.211   SUPS:42.654

                                                                    NIF@
```

APPENDIX F

ENGLISH TO METRIC UNIT CONVERSIONS

To Convert	Into	Multiply by
in.	cm	2.540
ft	m	0.3048
ft^2/sec	m^2/sec	0.09290
mph	m/sec	0.4470
lb/ft^2	N/m^2	47.88
mile	Km	1.609
$lb_m\text{-}ft^2$	kg/m^2	0.04214
lb	kg	0.4536
ft/sec	m/sec	0.3048